Identification and characterization of microtubule-modulating *Chlamydia pneumoniae* proteins

Inaugural dissertation

for the attainment of the title of doctor

in the Faculty of Mathematics and Natural Sciences

at the Heinrich Heine University Düsseldorf

presented by

Carolin Wevers

From Mönchgladbach, Germany

May, 2023

Düsseldorf

from the Institute for Functional Genome Research of Microorganisms, Eukaryotic Microbiology at the Heinrich Heine University Düsseldorf

Published by permission of the
Faculty of Mathematics and Natural Sciences at
Heinrich Heine University Düsseldorf

Supervisor: Prof. Dr. U. Fleig
Co-supervisor: Prof. Dr. J. Hegemann

Date of oral examination: January 25th, 2023

For my family,

the living and the deceased

Life is never completely

without its challenges

-Stan Lee-

Zusammenfassung

Das gram-negative Bakterium *Chlamydia pneumoniae (C. pneumoniae)* ist ein intrazellulärer Krankheitserreger von gesundheitlicher Relevanz für den Menschen. Chlamydien sind Meister in der Manipulation von Wirtszellprozessen durch den Einsatz spezifischer Effektorproteine. Während die Modulation des Aktin-Zytoskeletts für die Infektion von wesentlicher Bedeutung ist, wurde die Rolle des Mikrotubuli (MT)-Zytoskeletts des Wirts während der Chlamydien Infektion bisher kaum untersucht.

In der vorliegenden Arbeit wurden 116 *C. pneumoniae* Proteine anhand von verschiedenen Kriterien ausgewählt und auf ihre MT-regulatorische Funktion untersucht. Dazu wurde ein genetischer Screen mit der Modellhefe *Schizosaccharomyces pombe* (*S. pombe*) durchgeführt. Insgesamt beeinträchtigten 11 % (13/116) der exprimierten Chlamydiengene das MT-Netzwerk der Hefetransformanten und verursachten Wachstumsdefekte und eine Überempfindlichkeit gegenüber MT-Toxinen. Die anschließende mikroskopische Analyse des Interphasen MT-Zytoskeletts zeigte Veränderungen in der MT Struktur und Organisation in allen 13 Hefetransformanten. Insbesondere die *cpn0216* oder *cpn0443* exprimierenden Transformanten wiesen desorganisierte und massiv längere oder kürzere MTs auf, sowie Veränderungen in der MT-Dynamik. Die MT-modulierende Wirkung konnte auf den C-Terminus von CPn0216 und CPn0443 ($CPn0216^{82-145}$, $CPn0443^{164-417}$) zurückgeführt werden. Die funktionelle Charakterisierung von CPn0443 zeigte, dass das Protein partiell entlang von Interphasen-MTs lokalisiert ist und bindet *in vitro* direkt an MTs. Dies deutet auf eine direkte Wirkung auf MTs hin. Darüber hinaus konnte CPn0443 auch mit einem ER-ähnlichen und MT-Phänotyp in der Hefe in Verbindung gebracht werden.

In transfizierten, nicht polarisierten humanen U2OS-Zellen lokalisierte CPn0443 partiell an Interphasen-MTs und verursachte Veränderungen in der MT-Struktur, die zu dicken MT-Kabeln führten, die sich einrollten und eine "Spaghetti"-ähnliche Struktur aufwiesen. Neben der durch CPn0443 verursachten MT-Veränderungen beeinflusst das Chlamydienprotein auch die ER-Architektur der Säugetierzelle.

In dieser Arbeit konnte gezeigt werden, dass *C. pneumoniae* eine hohe Anzahl MT-modulatorischer Proteine besitzt. Durch CPn0216 und CPn0443 konnte ein erster Eindruck verschafft werden, wie *C. pneumoniae* Proteine das MT-Zytoskelett des Wirtes beeinflussen können. Zukünftig bedarf es weiterer Analysen, um die Funktion von CPn0216 und CPn0443 und die Rolle des MT-Zytoskeletts während der *C. pneumoniae* Infektion besser zu verstehen.

Summary

The gram-negative bacterium *Chlamydia pneumoniae* (*C. pneumoniae*) is an intracellular pathogen of human health relevance. *Chlamydia* is a master at manipulating host cell processes by specific effector proteins. While modulation of the host cell actin cytoskeleton is essential for infection, the role of the host microtubule (MT) cytoskeleton during chlamydial infection has been little studied.

In the present thesis, 116 *C. pneumoniae* proteins were selected based on various criteria and screened for their MT-regulatory function. Therefore, a genetic screen was performed using the model yeast *Schizosaccharomyces pombe* (*S. pombe*). In total, 11 % (13/116) of the expressing chlamydial genes affected the MT network of yeast transformants and caused growth defects and hypersensitivity to MT-toxins. Subsequent microscopic analysis of the interphase MT cytoskeleton revealed changes in the MT structure and organization in all 13 yeast transformants. In particular, transformants expressing *cpn0216* or *cpn0443* showed disorganized and massive longer or short MTs, as well as changes in MT dynamics. The MT-modulatory effect could be attributed to the C-terminus of CPn0216 and CPn0443 ($CPn0216^{82-145}$, $CPn0443^{164-417}$). Functional characterization of CPn0443 showed that the protein is partially localized along interphase MTs and binds directly to MTs *in vitro*, suggesting a direct effect on MTs. Additionally, CPn0443 could also be associated with an ER-like and MT phenotype in the yeast.

In transfected non-polarized human U2OS cells, CPn0443 partially co-localized to interphase MTs and caused alterations in MT structure resulting in thick MT cables that curled and exhibited a "spaghetti"-like structure. In addition to CPn0443-induced MT alteration, the chlamydial protein also affects the ER architecture of the mammalian cell.

In this thesis, it was shown that *C. pneumoniae* possesses a high number of MT-modulatory proteins. CPn0216 and CPn0443 provided a first insight into how *C. pneumoniae* proteins may affect the host MT cytoskeleton. Future analyses are necessary to investigate the function of

CPn0216 and CPn0443 in order to better understand the role of the MT cytoskeleton during *C. pneumoniae* infection.

Abbreviations

%	percentage
~	tilde
+TIP	microtubule plus-end tracking proteins
±	plus-minus
Δ	delta
Δ	delta
° C	celsius degree
aa	amino acid
ABPs	actin-binding proteins
ADP	adenosine diphosphate
amp	ampicillin
ARF1/4	ADP-ribosylation factor 1/4
ATP	adenosine triphosphate
bp	base pairs
C.	*Chlamydia*
CAP	community-acquired pneumonia
CCDC146	coiled-coil domain-containing protein 146
CEP170	centrosomal protein 170 kDa
cOMC	chlamydial outer membrane complex
COPD	chronic obstructive pulmonary disease
CopN	chlamydial outer protein N
Cpn	*Chlamydia pneumoniae*
C-terminus	carboxy-terminus
Ctr	*Chlamydia trachomatis*
ddH_2O	double distilled water
dH_2O	distilled water
DNA	deoxyribonucleic acid
dNTPs	deoxy nucleotides
DYNLT1	dynein light chain type 1
E.coli	*Escherichia coli*
EB	elementary body
EB1	end-binding protein 1

ER	endoplasmatic reticulum
et al	*"et alia",* and others
EtOH	ethanol
F-actin	filamentous actin
FF	two phenylalanines
FFAT	two phenylalanines acidic tract
fwd	forward
g	grams
G-actin	globular actin
GAGs	glycosaminoglycans
GFP	green fluorescent protein
GST	glutathione S-transferase
hpi	hours post infection
hrs	hours
IF	intermediate filament
IM	inner membrane
Inc	inclusion membrane
IPAM	inclusion protein acting on microtubules
kan	kanamycin
kb	kilo base pairs
kDa	kilo Dalton
L	liter
LFM	life fluorescent medium
LFM	life fluorescence media
LiAc	lithium acetate
M	molar
mA	milliampere
Mal3	minichromosome altered loss
MAPs	microtubule-associated proteins
MBC	methyl benzimidazol-2-yl-carbamate
mg	milligram
min	minutes
mL	milliliter
mM	millimolar
MM	minimal media

MOI	multiplicity of infection
Momp	major outer membrane protein
MT	microtubule
MTOC	microtubule-organizing center
nm	nanometer
nmt	no message in thiamine
nt	nucleotide
o/n	overnight
OD	optical density
OM	outer membrane
OMC A/B	outer membrane complex A/B
ON	oligonucleotide
ORF	open reading frame
P	pellet
PAGE	polyacrylamide gel electrophoresis
PBS	phosphate-buffered saline
PCR	polymerase chain reaction
PFA	paraformaldehyde
pH	*pondus hydrogenii*
RB	reticulate body
rev	reverse
RNA	ribonucleic acid
rpm	revolutions per minute
RT	room temperature
S	supernatant
SDS	sodium dodecyl sulfate
sec	seconds
SS	signal sequence
T3SS	type-III-secretion system
TarP	translocated actin-recruiting phosphoprotein
TBZ	thiabendazole, 2-(4'-thiazolyl)benzimidazole
Tea1/2/3/4 protein	tip elongation aberrant 1/2/3/4 protein
Thia	thiamine
Tip1	tip-elongation protein 1
TM	transmembrane domain

U	unit
UV	ultraviolet
V	volume
VAPA	vesicle-associated membrane protein A
VAPB	vesicle-associated membrane protein B
x g	acceleration due to gravity
x^R	resistance
α	apha
β	beta
γ	gamma
µg	microgram
µl	microliter
µM	micromolar

Table of content

1 Introduction

1.1 The eukaryotic cytoskeleton

The eukaryotic cytoskeleton is formed by a three-dimensional network of protein filaments that fulfill numerous essential functions such as fixation of cell organelles for internal cell organization, motility, cell division, intracellular material transport, and cell stabilization. This network is composed of three classes of filamentous polymers: actin, intermediate filaments (IFs), and microtubules (MTs) (**Figure 1**). Briefly, the different functions and properties of these protein filaments provide the cell with flexibility without losing cell stability. The structure of actin and MTs are characterized by changing stages of growth (polymerization) and degradation (depolymerization), referred to as dynamic instability, which allows the cell to actively move. In contrast, IFs act as a support scaffold to maintain the cell shape and stabilize the cell (Mitchison and Kirschner, 1984; Desai and Mitchison, 1997; Herrmann et al., 2007).

Actin exists in the eukaryotic cytoskeleton in two forms, either as free globular actin monomers (G-actin) or as polymeric filamentous actin filaments (F-actin), also called microfilaments. The actin filaments are composed of two linear actin polymer microfilaments that wrap around each other to form a double helix (Holmes et al., 1990). Each actin polymer microfilament consists of G-actin monomers polymerized together. In eukaryotic cells, the actin filaments have a diameter of 5 to 9 mm and are loculated below the plasma membrane or at the cell cortex to control the outer shape of the cell. F-actin forms a dense and flexible structure organized in a variety of linear bundles, two-dimensional networks, and three-dimensional gels cross-linked by connecting proteins (**Figure 1**) (Huisman et al., 2007).

The main role of F-actin in eukaryotic cells is to perform various cellular functions in cell structure (shape and stability), transport networks, cell movement (migration), and cell division (formation of the contractile ring). Similarly, F-actin is essential for endocytosis and the formation of cell processes such as microvilli in intestinal epithelial cells (Pollard and Cooper, 2009). F-actin microfilaments are polar structures and therefore possess a highly dynamic plus-end, where actin assembly occurs, and a minus-end where actin is predominantly

released. The formation of F-actin is reversible to G-actin, which implies rapid polymerization and depolymerization of F-actin for the exercise of functions such as active cell movement. Whereas the polymerization of adenosine triphosphate (ATP)-bound G-actin requires ATP hydrolysis adenosine diphosphate (ADP), the release of ADP-bound G-actin at the minus-end is a hydrolysis-independent process (Egelman et al., 1982; Kabsch and Vandekerckhove, 1992). The actin dynamic is regulated by numerous actin-binding proteins (ABPs) (Selve and Wegner, 1986; Pollard et al., 2000). For example, formin supports actin polymerization by binding to the fast-growing plus-end and nucleating actin assembly into parallel bundles. In addition, profilin binds to G-actin monomers to accelerate actin elongation, while cofilin, as an antagonist, promotes actin disassembly at the minus-end (Didry et al., 1998). Thus, actin accessory proteins determine the rates of polymerization and degradation of F-actin, which must be controlled for the active movement of the cell. Extracellular signals can trigger this movement, as in endocytosis. Other proteins such as the adaptor and connector proteins spectrin and ERM proteins (ezrin, radixin, moesin) are responsible for attaching actin to membranes, including cell-cell junctions (Bois et al., 2006).

In contrast, IFs are nonpolar and form a static network, providing mechanical strength to the cell and causing the cell to retain its shape and anchor organelles in the cell (**Figure 1**). IFs are composed of monomers that assemble into dimers. In this process, the heterogeneous and filamentous IF proteins, which share common sequence and structural features, assemble independently of ATP or GTP (Strelkov et al., 2003). Two dimers form a tetramer by antiparallel linkage, of which eight tetramers assemble to form an IF with a diameter of 10 nm (Kirmse et al., 2007). IF protein structures are classified into six types due to the similarities between mammalian cells (Cooper, 2000). The IFs of epithelial cells are called cytokeratins and belong to types I-II, desmin is found in muscle cells (type III), and internexin is present in neuronal cells (type IV). IFs are localized around the nuclear envelope in all eukaryotic cells and are described as nuclear lamins, the type V nuclear IFs while nestin is present in neuroepithelial cells (type VI). Nuclear lamins support nuclear integrity and serve as scaffolds for heterochromatin and protein complexes (Gruenbaum and Aebi, 2014; Parnaik, 2011). In addition, cell-cell connections of the cytoplasmic IF network, which extends to the cell periphery and is

connected to the outer nuclear membrane, ensures tensile strength for the mechanical stability of the cell (Herrmann et al., 2004; Bois et al., 2006).

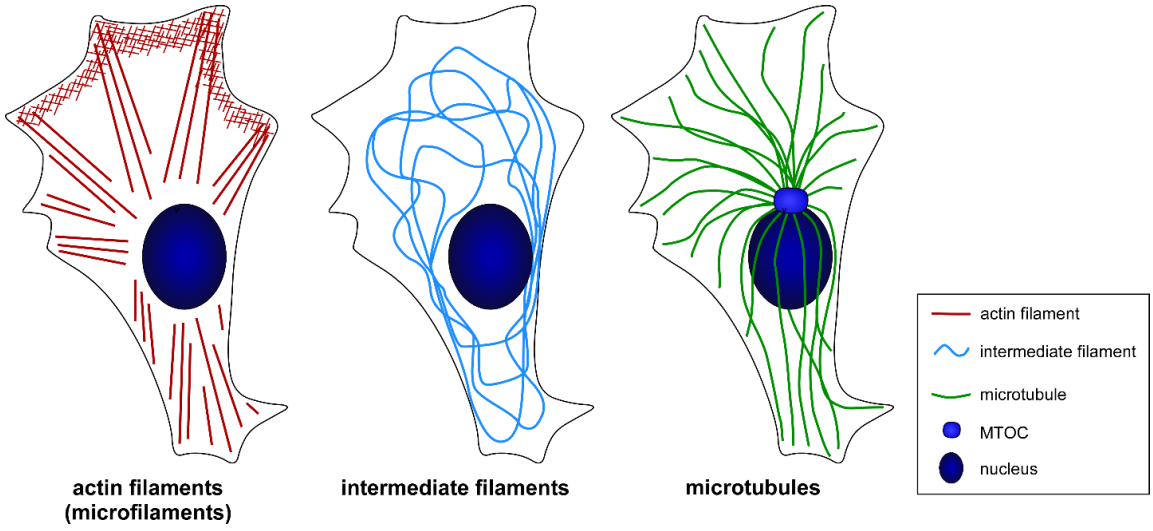

Figure 1: Filaments of the mammalian cytoskeleton.

Schematic illustration of the filaments that form the cytoskeleton of a human non-polarized epithelial cell. The cytoskeleton consisting of actin filaments (red) are organized into linear bundles, two-dimensional networks, and three-dimensional gels, while intermediate filaments (blue) form a meshwork across the cytoplasm and microtubules (MT; green) form a radial structure organized from the MT-organizing center (MTOC).

The MT cytoskeleton in eukaryotic cells represents a highly conserved system as it performs different tasks during the cell cycle. Throughout the cell cycle, eukaryotic cells spend about 90 % of their time in interphase, where interphase MTs form long filaments that span the entire cell (**Figure 1**). In contrast, during mitosis, eukaryotic cells spend approximately 10 % of their time undergoing chromosome segregation by forming a mitotic spindle (Dogterom et al., 2005; Desai and Mitchison, 1997). Accordingly, interphase MTs are essential for intracellular processes such as transport of goods, cell growth, and positioning of the nucleus, while the mitotic spindle is required for cell division.

MTs consist of polar αβ-tubulin hetero-dimers assembled into linear protofilaments. In eukaryotic cells, 13 protofilaments are arranged in a hollow tube with a diameter of approximately 25 nm. The adjacent protofilaments are maintained and stabilized by the MT stabilizing end-binding protein 1 (EB1) by joining the adjacent protofilaments in an A-lattice (longitudinal binding: αβ-tubulin) or a B-lattice (lateral binding: αα-tubulin and ββ-tubulin). In

the B-lattice, structure formation occurs at the α- and β-tubulin subunits of adjacent protofilaments, resulting in a helical structure (Sandblad et al., 2006; Mandelkow et al., 1986). The MT bundles are polarized due to the αβ-tubulin dimers, which is why they each have an MT minus-end where the α-tubulin is exposed and an MT plus-end where the β-tubulin is exposed.

MT nucleation occurs at the major MT-organizing center (MTOC) near the nucleus, with the MT minus-end anchored to the MTOC by the γ-tubulin complex. In contrast, the MT plus-end is highly dynamic reaching into the cell periphery and constantly switching between the stages of MT polymerization and depolymerization (Mitchison and Kirschner, 1984) (**Figure 2**). MT polymerization at the MT plus-end occurs through the binding of free GTP-αβ-tubulin dimers. αβ-tubulin dimers are each associated with a GTP, with a non-hydrolyzable GTP at α-tubulin and a hydrolyzable one at β-tubulin (Nogales et al., 1998; Mitchison, 1993). The binding of the GTP-tubulin dimers leads to interactions between the successively incorporated tubulin dimers and triggers delayed hydrolysis of GTP to GDP. Due to the delayed hydrolysis, the growing MT plus-end forms a GTP-cap. GTP-tubulin is more stable and exhibits a straight conformation. Together with longitudinal and lateral tubulin-binding (A- and B-lattice), it allows MTs to grow straight. In contrast, GDP-bound tubulin has a more curved conformation and is, therefore, more unstable. During rapid MT assembly, the MT lattice is hydrolyzed to GDP-tubulin, whereas the GFP-cap at the MT plus-end is not hydrolyzed until the MT assembly rate decreases. The GDP-rich MT lattice is surrounded by GTP-tubulin islands and stabilized by the MT-stabilizing protein EB1 to ensure straight growth (Drummond and Cross, 2000; Galjart, 2010). As long as the rate of MT assembly exceeds that of hydrolysis of GTP to GDP, the stabilizing GTP-cap is maintained at the growing MT plus-end and MT polymerization continues (Drechsel and Kirschner, 1994). If the rate of MT assembly falls below the GTP-hydrolysis rate, GTP-bound β-tubulin is hydrolyzed to GDP and the GTP-cap at the MT plus-end is lost, resulting in MT instability and the MT catastrophe event.

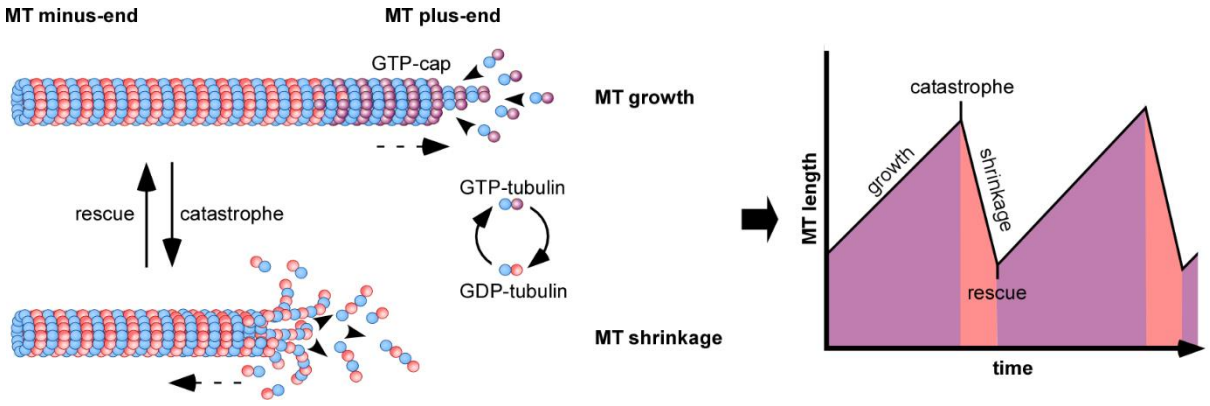

Figure 2: MT dynamic instability of interphase MTs.

Schematic representation of dynamic instability at the microtubule (MT) plus-end and conversion to an MT growth curve. During MT polymerization free GTP-αβ-tubulin binds to the MT plus-end, forming a GTP-cap that stabilizes the MT (rising curve). As long as the rate of MT assembly exceeds that of the hydrolysis, the stabilizing GTP-cap remains at the growing MT plus-end and MT polymerization continues. When the rate of MT assembly falls below the GTP-hydrolysis rate, GTP-cap is hydrolyzed to GDP, resulting in loss of MT stability and the MT catastrophe event occurs (peak). Due to the unstable GDP-tubulin, the lateral tubulin bonds break and the peeling of the protofilaments is triggered. The MT depolymerizes back (falling curve). Once the MT has arrived at the MTOC (lowest peak), a rescue event takes place when the MT begins to polymerize again. The dashed arrows show the growth direction of the MT. Illustration is modified from Janulevicius et al., 2006; Michaels et al., 2020 and Drechsel and Kirschner, 1994.

When the growing MT arrives at the end of the cell, contact of the cell end with the MT plus-end generates compressive forces that interrupt the growth of the MT and cause an MT pause. The reduced MT assembly rate allows GTP-hydrolysis to hydrolyze the stabilizing GTP-cap into GDP-tubulin. The unstable GDP-tubulin breaks the lateral tubulin bonds and protofilament peeling is triggered and the MT depolymerizes back to the MTOC or to the GTP-tubulin island in the tubulin. Recovery of the MT can occur during MT depolymerization by attaching GTP-tubulin to the shrinking end fast enough to form a new GTP-cap. The resulting MT polymerization is termed a rescue event (Drummond and Cross, 2000; Mitchison and Kirschner, 1984; Galjart, 2010).

The multifaceted nature of the complex MT network requires tight regulation of its dynamic behavior and organization within the cell through the involvement of MT-associated proteins (MAPs) (Akhmanova and Steinmetz, 2008; Tran et al., 2001). Although many MAPs are already

known, not much is known about their mechanisms. A subset of MAPs are the MT plus-end tracking proteins (+TIPs), which are localized at the plus-ends of interphase MTs to regulate MT dynamics (van der Vaart et al., 2009). The +TIPs can be subdivided into MT-stabilizing and -destabilizing proteins. MT-stabilizers include the EB proteins and cytoplasmic linker protein-170 (CLIP-170), which are MT catastrophe antagonists that promote MT growth (Perez et al., 1999; Mimori-Kiyosue et al., 2000). In particular, the EB proteins have a high affinity to stabilize the growing MT plus-end and thereby promote MT growth and suppressing MT catastrophe. However, they also bind along the MT lattice to link the adjacent protofilaments together and stabilize the MT (Busch and Brunner, 2004). MT-stabilizers also include polymerases, such as XMAP215, which promote rapid MT growth by binding free αβ-tubulin dimers and thereby causing MT assembly at the MT plus-end (Mimori-Kiyosue et al., 2000; Brouhard et al., 2008). In contrast, MT destabilizers have the effect of increasing the rate of depolymerization, suppressing MT rescue or promoting MT catastrophe. For example, stathmin prevents the incorporation of free αβ-tubulin dimers, thereby slowing MT polymerization. Additionally, serve the MT-separating enzymes katanin and spastin weaken lateral tubulin units, thereby triggering MT catastrophe (Roll-Mecak and McNally, 2010).

Another class of proteins influencing MT dynamics are motor proteins. While kinesin motor proteins are directed to the plus-end in the cell periphery, dynein motor proteins are directed to the minus-end in the direction of the MTOC (Howard and Hyman, 2009; Lawson and Carazo Salas, 2013; Horio and Murata, 2014). The kinesin-13-motor protein MCAK migrates to MT tips and removes the stabilizing GTP-cap, initiating MT catastrophe and acting as an MT catastrophe protagonist to promote MT depolymerization (Howard and Hyman, 2007). Other MAPs such as MAP2, Tau, and MAP65 directly affect MTs by binding along the MT lattice and cross-linking and cross-linking MTs filament into antiparallel bundles (Ichihara et al., 2001; Al-Bassam et al., 2002; Chang-Jie and Sonobe, 1993; Walczak and Shaw, 2010).

1.1.1 Bacterial pathogens modulate the host cytoskeleton

Several bacterial pathogens use the eukaryotic host cytoskeleton for their developmental cycle. Particularly, the host actin cytoskeleton appears to play an essential part in the bacterial entrance and escape. A large number of bacterial pathogens utilize effector proteins, such as

Salmonella, Shigella, Shigella, Listeria, and *Chlamydia*, to manipulate actin dynamics, allowing the pathogen to access the host cell.

Listeria monocytogenes is an example of a bacterial pathogen that uses the effector protein internalin B (InlB) to modulate the actin cytoskeleton of non-phagocytosing cells for its internalization. Seveau et al., 2004 demonstrated that actin polymerization is coordinated by the interaction of InlB with the host cell tyrosine kinase receptor Met. The activation of the c-Met-dependent Akt-phosphorylation and F-actin remodulation triggers the internalization through the zipper-mechanism (Phelps et al., 2018). In addition, *Listeria* uses the host cell actin structure for its movement within the cell and from cell to cell (Seveau et al., 2004).

For its internalization process, *Salmonella* uses the effector proteins SipA, SipC, SopB, SopE, and its homolog SopE2 to remodulate the actin cytoskeleton (Fattinger et al., 2021; Hume et al., 2017). These proteins are secreted directly into the host cell via the type-III secretion system (T3SS) (Zhou and Galán, 2001). SipA and SipC nucleate F-actin polymerization due to the binding directly to F-actin, promoting actin bundling and thereby increasing uptake efficiency and suppressing cofilin-induced F-actin depolymerization (Hayward and Koronakis, 1999; McGhie et al., 2001; McGhie et al., 2004). For RhoGTPases-dependent actin modulation, SopE and SopE2 activate Cdc42 and manipulate Rac1 to trigger polymerization of F-actin and membrane ruffling by recruiting WASP and Arp2/3 (Hänisch et al., 2010; Hänisch et al., 2011; Friebel et al., 2001).

Chlamydia also undergoes actin-induced internalization via the T3SS effector protein translocated actin recruiting phosphoprotein (TarP) (Jewett et al., 2006). TarP orthologs are present in all *Chlamydia* species such as *C. trachomatis, C. pneumoniae, C. muridarium,* and *C. caviae*, which exhibit actin recruitment at the site of entry (Clifton et al., 2005; Clifton et al., 2004). The *C. trachomatis* TarP CT456 and *C. pneumoniae* TarP CPn0572 are known to promote polymerization of the actin cytoskeleton at the entry site to ensure endocytosis of the pathogen (Zrieq et al., 2017; Clifton et al., 2004). CPn0572 co-localizes with actin spots, thick

and elongated actin cables, and stabilizes pre-assembled F-actin by inhibiting the binding of the actin-separating protein cofilin (Zrieq et al., 2017).

Besides the actin-dependent chlamydial entry and exit, actin filaments and dynamics are also restructured to form a vacuole around the pathogen for intracellular development until exit from the cell by extrusion (Kumar and Valdivia, 2008; Hybiske and Stephens, 2007a). Kumar and Valdivia, 2008 monitored in *C. trachomatis* infected cells the formation of an F-actin ring around the inclusion 20 hours post-infection. This F-actin ring is essential for maintaining the integrity of the inclusion. Thereby, the effector protein CT813/InaC supports and promotes the formation of the inclusion and its stability by the surrounding F-actin cage (Kokes et al., 2015). In addition, formin and septin contribute to the nucleation and formation of the actin cage around the *C. trachomatis* inclusion (Volceanov et al., 2014). The F-actin cage around the inclusion promotes Golgi ministack reorganization.

In contrast to the purposes of actin during bacterial infection, not much is known about the functional contribution of the MT cytoskeleton of the host cell. Up to now, bacterial effector proteins participating in MT-induced bacterial invasion or in MT-modulating processes that are part of the infection process are barely identified. Furthermore, the mechanism through which these MT-modulating proteins interfere with MTs is also unknown.

Clostridium difficile is a bacterial pathogen that affects host cell actin cytoskeleton via the actin ADP-ribosylating toxin *Clostridium difficile* transferase (CDT) which causes MT-based protrusion of the pathogen (Schwan et al., 2009; Haglund and Welch, 2011). CDT affects the ADP-ribosylation of actin resulting an actin depolymerization. This leads to a strong reduction of the actin excretion at the plasma membrane whereby MTs remain in the polymerization stage for a longer period of time and thus form MT protrusions. CDT does not affect MTs directly, but its actin-depolymerizing effect leads loss of controlled MT polymerization, resulting in cellular extensions that curl around external bacteria as MT-based protrusions on the host cell plasma membrane (Schwan et al., 2014; Nölke et al., 2016).

Enteropathogenic E. coli (EPEC) utilizes the T3SS secreted effector protein EspG for its host MT cytoskeleton manipulation. EspG disrupts the cell's MT network by directly binding α-tubulin subunit, although the mechanism is unknown (Glotfelty and Hecht, 2012).

A T3SS secreted effector protein has been identified for *C. pneumoniae* that chlamydial outer protein N (CopN) expression in human non-polarized HeLa cells affects the host cell MT network, whereas CopN from *C. trachomatis* does not exhibit this activity on MTs (Huang et al., 2008; Fields and Hackstadt, 2000). CopN of *C. pneumoniae* has an essential function in the infection process of non-polarized HEp2 cells. Huang et al., 2008 demonstrated that CopN has a function in development due to the fact that inhibited CopN activity inhibits *C. pneumoniae* replication. In contrast, this observation is not reported for *C. trachomatis* infected cells, suggesting that CopN is not required for *C. trachomatis* development (Huang et al., 2008). Further ectopic expression analysis of *C. pneumoniae* CopN in human non-polarized HeLa cells showed disruption of the MT network (Huang et al., 2008). CopN from *C. pneumoniae* inhibits MT polymerization by directly binding non-polymerized β-tubulin of an αβ-tubulin dimer, but it does not polymerize MTs or induce MT depolymerization. In this way, CopN inhibits MT assembly by sequestering tubulin and delaying nucleation (Archuleta et al., 2011; Nawrotek et al., 2014; Huang et al., 2008). Experimental studies proved that a mutation-induced loss of function of CopN protein does not allow interaction with tubulin. However, the specific mechanism is not yet defined (Nawrotek et al., 2014). Further expression analysis of CopN in mammalian cells and yeast showed an effect on MT structure formation and prevention of cell division, suggesting that CopN may disrupt the mitotic spindle, leading to defective chromosome segregation and inhibition of cytokinesis (Huang et al., 2008). Furthermore, the question of the role of CopN interaction with the MT network in the *C. pneumoniae* developmental cycle remains unresolved. The second MT modulator of *C. pneumoniae* is the TarP ortholog CPn0572. Braun, 2015 monitored the co-localization of CPn0572 with MTs of yeast and mammalian cells during her master thesis. Furthermore, the expression of CPn0572 triggers the modulation of MTs in yeast and mammalian cells. Thus, CPn0572 is able to control the dynamics of both actin and MTs.

To date, inclusion membrane (Inc) proteins from *C. trachomatis* are known to be involved in *Chlamydia*-induced MT modulations, whereas no Inc protein from *C. pneumoniae* is known. First, *C. trachomatis* hijacks the dynein-motor complex of the host cell for the transport of the inclusion along the MTs to the MOTC. Second, *C. trachomatis* induces the formation of an MT cage around the inclusion, followed by post-translational modification of the MT cage to stabilize the inclusion. Inc proteins modulating the host MT cytoskeleton are described in more detail in section 1.4.

1.2 *Chlamydia* as a pathogen

The genus *Chlamydia* belongs to the order *Chlamydiales* which are obligate intracellular, gram-negative bacteria with a biphasic life cycle that infect a wide range of host organisms and cause various diseases. The order *Chlamydiales* include four families: *Chlamydiaceae*, *Simkaniaceae, Waddliaceae,* and *Parachlamydiaceae* (**Figure 3**).

Chlamydia are contagious to animals and/or humans. Animal pathogenic *Chlamydia* includes *C. abortus* and *C. pecorum,* which are found in various farm animals such as goats, sheep, pigs, and cattle. *C. felis* is found in cats, while *C. psittaci* infects birds such as parrots, cockatoos, budgies, pigeons, ducks, geese, and turkeys. Moreover, *C. caviae* infects rodents such as guinea pigs, and *C. muridarum* infects mice (Nunes and Gomes, 2014; Roulis et al., 2013). In addition, *C. felis, C. abortus,* and *C. psittaci* are classified as potentially zoonotic, whose infection is reported to be transmissible from animals to humans.

The two most important human pathogens are *C. trachomatis* and *C. pneumoniae*. While *C. pneumoniae* infects both humans and animals such as horses, koala bears, amphibians, and iguanas, *C. trachomatis* is exclusively human pathogenic (Nunes and Gomes, 2014; Roulis et al., 2013).

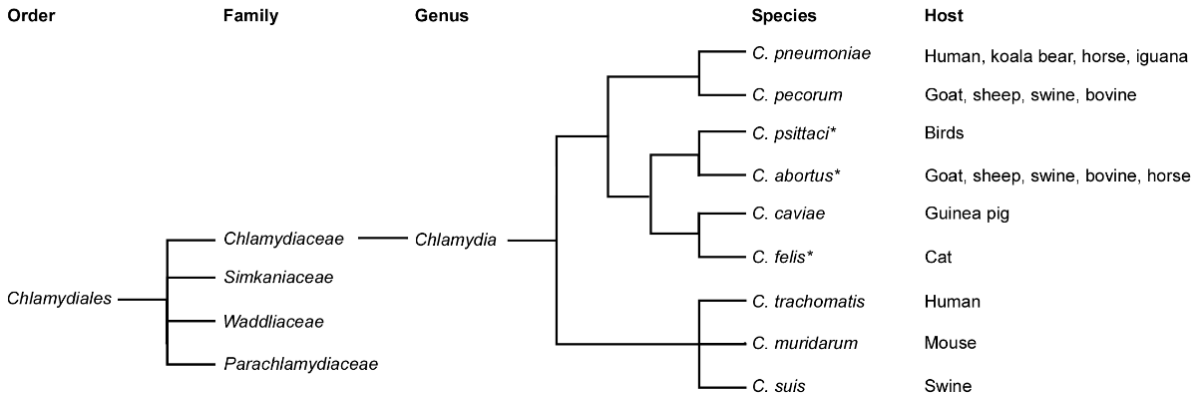

Figure 3: Taxonomic classification of the order *Chlamydiae*.

Representation of order, family, genus, and species is modified from Nunes and Gomes, 2014. Additionally, examples of host organisms of each *Chlamydia* species are listed. Black asterisks denote the *Chlamydia* species with zoonotic potential, meaning the infection can be transmitted from animals to humans.

1.2.1 Human pathogen Chlamydia

In 2020, the World Health Organization (WHO) estimated approximately 129 million new cases of chlamydial infection worldwide among adults and adolescents aged 15 to 49 years (WHO, 2021). Although a *Chlamydia* infection is a serious infectious disease whose consequences may be fatal, it does not receive enough attention to determine the development of the number of cases worldwide each year. In contrast to other sexually transmitted diseases such as HIV, HPV, or syphilis, chlamydial infection is not a notifiable disease in Germany.

1.2.1.1 *Chlamydia pneumoniae*

C. pneumoniae is a pathogenic bacterium with a global presence that causes upper and lower respiratory tract infections. In acute respiratory tract infections with *C. pneumoniae*, 70 % of patients have mild symptoms or are asymptomatic, while 30 % suffer from severe respiratory disease. Diseases of upper respiratory tract infection include pharyngitis or sinusitis, whereas lower respiratory tract infection results in asthma, bronchitis, chronic obstructive pulmonary disease (COPD), or pneumonia (Grayston et al., 1993; Hahn et al., 1991; Hahn et al., 2002). Worldwide, approximately 40 % to 60 % of the adult population has developed antibodies against *C. pneumoniae*, indicating a high prevalence (Peeling and Brunham, 1996). The prevalence of antibodies is age-dependent with approximately 50 % at the age of 20 years and

70 % to 80 % at the age of 60 to 70 years, indicating frequent reinfection with this pathogen with increasing age (Blasi et al., 2009). Approximately 10 % of community-acquired pneumonia (CAP), 4 % to 25 % of patients with asthma, and 5 % of bronchitis and sinusitis cases in adults are diagnosed as a result of *C. pneumoniae* infection due to the positive detection of antibodies (Kuo et al., 1995; Hahn et al., 1991; Blasi et al., 2009). Furthermore, *C. pneumoniae* is also associated with several other chronic diseases such as Alzheimer's disease, atherosclerosis, or multiple sclerosis, as demonstrated by serological detection of antibodies to *C. pneumoniae* or PCR-based detection of bacteria in the affected tissues (Balin et al., 2008; Grayston and Campbell, 1999; Stratton and Wheldon, 2006; Kuo et al., 1995). Additionally, living bacteria were isolated directly from the diseased tissues of patients with Alzheimer's disease or atherosclerosis (Ramirez, 1996; Balin and Appelt, 2001). Nevertheless, it is not clear whether the chlamydial infection is a causal trigger or an innocent bystander.

Moreover, meta-analyses have assessed the association between a *C. pneumoniae* infection and lung cancer risk. Serological detection of *C. pneumoniae*-specific IgA and IgG antibody titers correlates with a 2-fold increased risk of developing lung cancer (Chaturvedi et al., 2010; Zhan et al., 2011; Hua-Feng et al., 2015). Interestingly, in a lung cancer animal model, 15 % of rats that are repeatedly infected with *C. pneumoniae* resulted in lung cancer, while no cases occurred in the control group (Chu et al., 2012).

1.2.1.2 *Chlamydia trachomatis*

C. trachomatis is a human pathogenic *Chlamydia* that is divided into two biovars, trachoma and lymphogranuloma venereum (LGV), which are subdivided into 18 serovars in total. The serovar classification is based on serological typing of specific epitopes of the OmpA-antigen, a major outer membrane protein (Momp) (Elwell et al., 2016; Faris et al., 2019).

The trachoma biovar includes serovars A, B, Ba, and C that infect ocular epithelial cells and cause ocular trachoma that, if untreated, leads to entropion, trichiasis, opacification, and blindness (Burton, 2007; Tabbara, 2001). In addition, this biovar includes the non-disseminating serovars D, Da, E, F, G, H, I, Ia, J, and K . In men and women, these serovars are transmitted sexually (orally, genitally, rectally), infecting the epithelial cells and mucous

membranes of the genitourinary tract (Takahashi et al., 1998). However, 70 % to 80 % of the infected women are asymptomatic, while approximately 50 % in men, causing the majority of *Chlamydia* infections to remain undetected and thus untreated (Stamm, 1999). Particularly for women with untreated *C. trachomatis* infection, 10 % and 40 % of them develop symptomatic pelvic inflammatory disease (PID). As a consequence, this can lead to an increased incidence of ectopic pregnancy or tubal obstruction causing infertility (Rashidi et al., 2013). Studies have shown that 30 % to 40 % of infertile women are due to untreated *C. trachomatis* infection (Darville and Hiltke, 2010; Faris et al., 2019). In men, infection with *C. trachomatis* is the most frequent cause of non-gonorrheal urethritis (NGU). Furthermore, epididymitis, swollen seminal vesicles, and possibly prostatitis may also occur (Darville and Hiltke, 2010; Faris et al., 2019; Redgrove and McLaughlin, 2014).

The LGV biovar includes the disseminating serovars L1, L2, L2a, and L3, which are also sexually transmitted and initially infect genital epithelial cells and macrophages (Stoner & Cohen 2015). However, the pathogen then spreads to deeper tissues up to the lymph nodes and causes disease in the lymphatic system leading to lymphadenopathy, fibrosis, and fistulae if left untreated (Faris et al., 2019; Schaeffer and Henrich, 2008).

Many questions regarding the bacterial pathogens *C. pneumoniae* and *C. trachomatis* remain unknown. So far, no successful vaccination strategy has been generated against a *C. pneumoniae* and *C. trachomatis* infection. Also, not all protein functions of the pathogens are known. Therefore, the characterization of chlamydial proteins with unknown functions is fundamental for a better understanding of the infection process and its prevention.

1.3 Life cycle of *Chlamydia*

The obligate intracellular bacterium *Chlamydia* is characterized by a biphasic developmental cycle. In the life cycle, *Chlamydia* undergoes the phases of adhesion, internalization, differentiation, replication, re-differentiation, and release from the host cell (**Figure 4**). However, the duration of the infection cycle and the individual phases differ among the various chlamydial species. While *C. pneumoniae* completes the infection cycle after 72 to 96 hours, the development of *C. trachomatis* completes after 48 to 72 hours. *Chlamydia* has adapted its

form into elementary bodies (EBs) for extracellular survival and reticulate bodies (RBs) for intracellular replication within the host cell. Importantly, the 0.3 to 0.4 µm EBs are metabolically inactive but infectious, in contrast to the 0.5 to 1 µm noninfectious RBs, which are characterized by their metabolic and replicative activity (Matsumoto and Manire, 1970; Friis, 1972; Wolf et al., 2000; Chi et al., 1987).

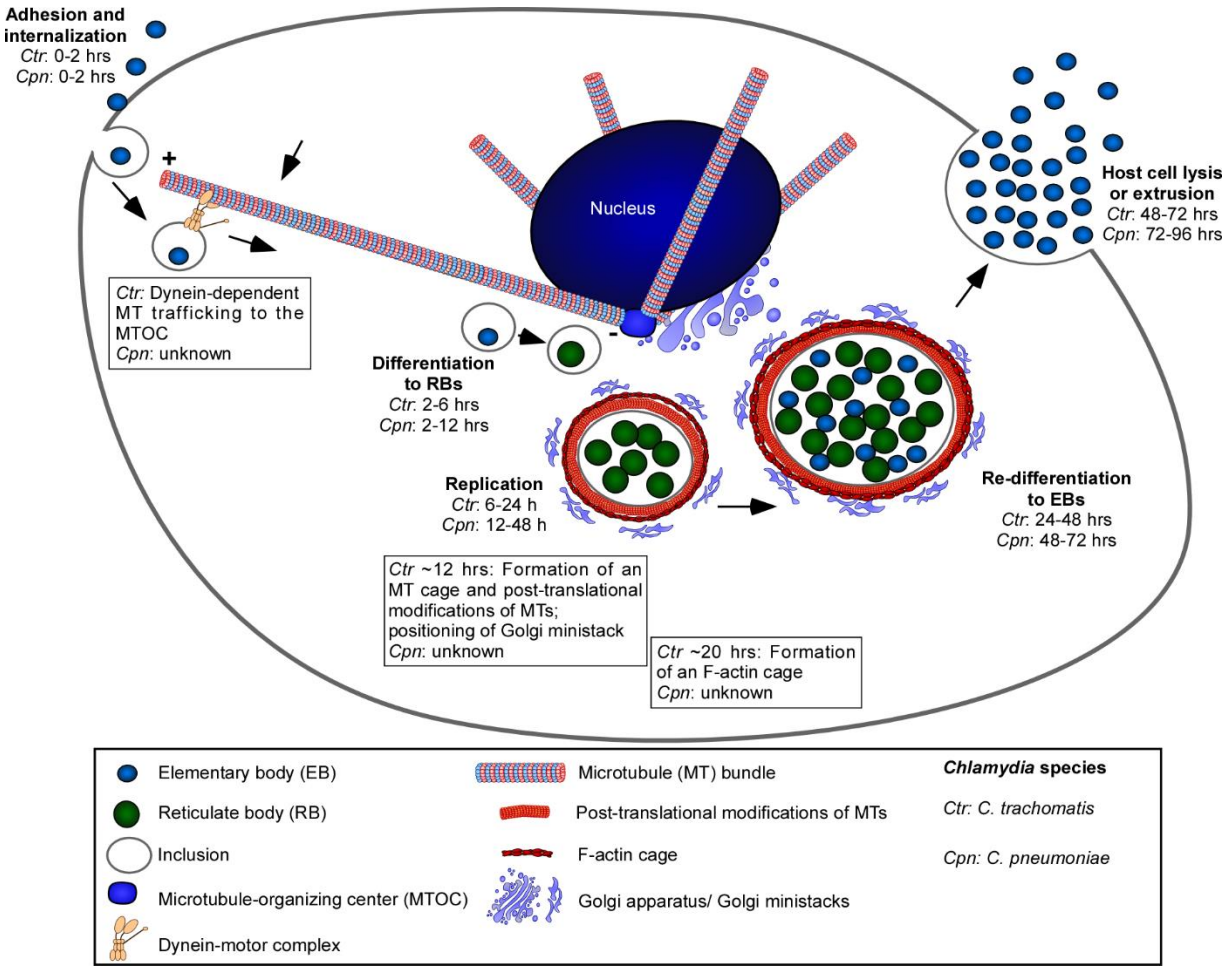

Figure 4: The biphasic life cycle of *C. pneumoniae* and *C. trachomatis.*

Schematic representation of the biphasic life cycle of *C. trachomatis* (*Ctr*) and *C. pneumoniae* (*Cpn*) in a non-polarized cell. Adhesion and internalization: Chlamydial invasion begins the internalization of elementary bodies (EBs) into a membrane-enveloped inclusion. The *Ctr* inclusion migrates along microtubules (MTs) by dynein-dependent transport to the perinuclear region near the cell nucleus to the MT-organizing center (MTOC). Differentiation to RB: EBs inside the nascent inclusion differentiate to reticulate bodies (RBs). Replication: RBs replicate while an MT cage is formed around the inclusion. The MT cage gets post-translationally modified and fragmented Golgi ministacks are repositioned around the inclusion. Later in the process, an F-actin cage is formed around the inclusion. Re-differentiation to EBs: RBs asynchronously differentiate back into EBs. Exit from host

cell: EBs are released by host cell lysis or extrusion (not shown) to infect new cells. Times (hpi: hours post-infection) of the *Cpn* or *Ctr* live cycle are referred from Wolf et al., 2000 and Hammerschlag, 2002. '-' MT minus-end; '+' MT plus-end.

1.3.1 Adhesion and internalization of *Chlamydia*

The chlamydial invasion starts with the adhesion of EBs to the eukaryotic host cell, e.g., mucosal epithelial cells. Subsequently, EBs get internalized by endocytosis to a membrane-bound inclusion within 2 hours.

Gram-negative bacteria such as *Chlamydia* utilize an inner and outer membrane. For stabilization and protection of the EBs against osmotic and environmental stress, the outer bacterial cell wall is achieved through cysteine-rich proteins. Those cysteine-rich proteins are connected by disulfide bridges and to form the chlamydial outer membrane complex (cOMC) (Hatch, 1996). Particularly, the adhesions outer membrane complex proteins A and B (OmcA and OmcB), and the Momp represent key proteins of the cOMC (Hatch, 1996; Feher et al., 2013). In addition, several adhesions and other proteins are required to cooperate with the host cell for receptor-mediated endocytosis of *Chlamydia.*

The initial contact between *C. pneumoniae* and *C. trachomatis* and the host cell occurs through the binding of OmcB to the host cell receptor heparan sulfate proteoglycan (HSPG). HSPG belongs to the negatively charged glycosaminoglycans (GAGs) (Su et al., 1996; Fechtner et al., 2013; Subtil et al., 2005; Stephens et al., 2001).

Studies have shown, that OmcB forms a weak, reversible electrostatic bond to GAGs, whereby the binding requires additional adhesins to stabilize EB-host cell contact (Wuppermann et al., 2001; Beswick et al., 2003). GAG structures are essential for the infection process, as evidenced by a significant reduction in chlamydial infectivity due to the inhibition of GAGs (Wuppermann et al., 2001; Beswick et al., 2003; Moelleken and Hegemann, 2008; Fadel and Eley, 2008). The *C. pneumoniae* and *C. trachomatis* adhesin Momp on the outer bacterial cell wall uses the mannose 6-phosphate receptor (M6PR)/insulin-like growth factor receptor 2 (IGFR2) for host

cell attachment (Puolakkainen et al., 2005; Abdelrahman and Belland, 2005). Studies have demonstrated, that Momp stimulates non-specific electrostatic and hydrophobic interactions with host cells that contribute to the binding of *Chlamydia* to the host (Su et al., 1990). Further adhesions are polymorphic membrane proteins (Pmps). The Pmp21 from *C. pneumoniae* binds and activates the human epidermal growth factor receptor (EGFR) (Mölleken et al., 2013). Mölleken et al., 2013 demonstrated that the binding of the *C. pneumoniae* Pmp21 to EGFR induces the mitogenic signaling via extracellular-signal-regulated kinase 1/2 (Erk1/2) and the phosphatidyl-inositol-3-kinase (PI3K) signal cascade. Inhibition of the ERK1/2 or PI3K activity has been shown a reduction of EB internalization (Coombes and Mahony, 2002; Mölleken et al., 2013). This suggests, that Pmp21 is important for stable adhesion, and is also required for signaling, internalization, and establishment of the *C. pneumoniae* inclusion. In contrast, the host cell interaction partner of the *C. pneumoniae* Pmp6 and Pmp20 are still unknown (Mölleken et al., 2010). Lipopolysaccharides (LPS) also belong to the adhesines and are present on the outer cell wall of *C. trachomatis*. LPS uses the cystic fibrosis transmembrane conductance regulator (CFTR) for the interaction with the host cell for the internationization of *C. trachomatis* (Ajonuma et al., 2010). Moreover, CPn0473, also called lipid internalization promoting protein (LipP) is another identified *C. pneumoniae* adhesin protein with its unique function as a phospholipid translocator (Galle et al., 2019). LipP is also involved in the internalization process by initiating the internalization of EBs in a lipid-raft-associated manner (Fechtner et al., 2016; Galle et al., 2019). However, its human receptor partner is still unknown.

In addition to adhesin proteins, other chlamydial effector proteins, virulence factors, and further proteins are required for the chlamydial life cycle, which are transferred directly from the EBs to the host cell via the T3SS needle apparatus. The T3SS penetrates the host plasma membrane for the injection of bacterial effector proteins such as TarP. TarP is fundamental for the internalization process of EB into the host cell. This protein ensures EB endocytosis by promoting actin polymerization at the entry site and manipulating actin dynamics of the cell (Zrieq et al., 2017; Jewett et al., 2006). Therefore, the actin restructuring causes the formation of microvilli pockets at the site of bacterial invasion. In addition, actin modulation by TarP is also required for exit from the host cell by exocytosis (Zrieq et al., 2017; Clifton et al., 2004;

Carabeo et al., 2002). Studies have shown, that a disrupted actin network negatively affects the internalization of (Kumar and Valdivia, 2008; Hybiske and Stephens, 2007b). After receptor-mediated endocytosis of EBs into the host cell, the EBs are located in a membrane-bound inclusion (Fields and Hackstadt, 2000; Wolf et al., 2000).

Additionally, the Inc proteins CT850 is required to hijack cytoskeletal structures for the intracellular transport of the *C. trachomatis* inclusion along MTs to the MTOC (Bastidas et al., 2013; Kumar and Valdivia, 2008; Grieshaber et al., 2003). The role of the MT cytoskeleton during the *Chlamydia* infection is explained in more detail in section 1.4.

1.3.2 Differentiation of EBs into RBs

After the internaliztaion of EBs into inclusions, the differentiation phase of *C. pneumoniae* occurs between 2 to 12 hours post-infection. Primary EBs differentiate asynchronously into metabolically active RBs through the cooperation of different chlamydial proteins (Wolf et al., 2000).

Within the differentiation from EB to RB, the regular structure of the *Chlamydia* cOMC is rearranged (Hackstadt et al., 1985). By breaking the disulfide bridges, the cross-linked proteins of the complex are reduced. This leads to a more permeable membrane. Additionally, the histone-like proteins Hc1 and Hc2 from the chlamydial DNA get removed by the *Chlamydia*-specific early upstream ORF (EUO) protease. Then, the chlamydial DNA starts to decondense (Kaul et al., 1997; Abdelrahman and Belland, 2005; Clifton et al., 2004). Subsequently, the decondensed DNA is transcribed and early-stage genes are expressed, followed by the secretion of proteins via the T3SS system. Effector proteins and Inc proteins are required to adapt the inclusion membrane to the infection requirements for the further course of the infection, e.g. manipulation of host cell mechanisms for the delivery of nutrients from the host cell secretory vesicles (Bastidas et al., 2013; Kumar and Valdivia, 2008; Grieshaber et al., 2003).

1.3.3 Replication of RBs

Around 12 to 48 hours post-infection, RBs of *C. pneumoniae* begin replication and continue

actively influencing the processes of the eukaryotic host cell to ensure the progression of the infection.

This stage of the chlamydial live cycle is referred to as the most active transcription phase, where mid-stage genes encoding proteins are participating in the growth and division of RBs (Nicholson et al., 2003). Furthermore, mid-stage proteins prevent the fusion of the inclusion with host lysosomes and improve the inhibition of apoptosis of infected cells by degrading pro-apoptotic factors (Rockey et al., 2002; Scidmore et al., 1996; Rajalingam et al., 2001). In this way, C*hlamydia* can escape the host cell defense but is still able to use the cellular transport processes for its growth and development.

During the replication phase, an RB is capable of binary replication approximately 9 to 11 times. The increasing number of replicated RBs leads to an enlargement of the inclusions, in which up to 1,000 new chlamydial particles accumulate during a chlamydial cycle (Hammerschlag, 2002; van Ooij et al., 1998). In addition, the formation of the MT cage and post-translational modification is explained in more detail separately in section 1.4.

1.3.4 Re-differentiation of RBs into EBs

After the replication phase, asynchronous re-differentiation of *C. pneumoniae* RBs begins 48 to 72 hours after infection. While some RBs are still replicating, other RBs are already beginning to re-differentiate into EBs (Wolf et al., 2000).

This stage of the chlamydial life cycle is distinguished by the expression of late-stage genes. These late-stage proteins are involved in chromatin condensation and the formation of cOMC and their cross-links via disulfide bridges to protect the re-differentiated EBs from extracellular stress by the environment. Before RBs complete their re-differentiation into EBs, the expression of early phase genes encoding adhesins, Pmps, and other effector proteins are also required to prepare EBs for the next host cell infection (Nicholson et al., 2003; Abdelrahman and Belland, 2005).

After re-differentiation into metabolically inactive EBs, DNA is condensed into chromatin by association with histone-like proteins, and the transcriptional machinery is shut down. After 72 hours at the latest, chlamydial development is complete and the inclusion is predominantly filled with EBs.

1.3.5 Exit of the cell

Finally, between 72 and 96 hours after infection with *C. pneumoniae*, EBs are released from the enlarged inclusion and the chlamydial cycle is complete. EBs exit the host cell in three different ways: host cell lysis, exocytosis, or extrusion (Wolf et al., 2000; Hybiske and Stephens, 2007a; Moulder, 1991).

1.4 Role of the host cell cytoskeleton during the *Chlamydia* infection

In recent years, the interaction between the host cell MT cytoskeleton and *C. trachomatis* has been studied. The experimental results based on transfected and infected non-polarized human cells, which exhibit a radiating MT orientation from the MTOC, close to the nucleus. In nature, *Chlamydia* infects polarized epithelial cells whose MT orientation differs from non-polarized epithelial cells because their MTs are oriented along the apical-basal axis. Additionally, in those cells, the MTOC is located in the apical, while the nucleus is located in the basal. The differences between the MT organization of polarized and non-polarized cells are described in section 1.5.

So far, the Inc proteins CT850, CT288, CT223, and CT813 have been associated with the modulating host cell MT network (Wesolowski and Paumet, 2017). The prediction of an Inc protein based on the T3SS signal sequence for the T3SS section which is localized in the N-terminus, and the presence of transmembrane domains separating the N-terminus from the C-terminus. Most Inc proteins, such as CT850, CT288, CT223, and CT813 are integrated into the inclusion membrane and their shorter N-terminus and longer C-terminus are located in the host cytosol to extensively modify the inclusion membrane for host cell manipulation (Mital et al., 2013). Studies have shown that the C-terminal region of the Inc protein, in particular, is

essential for interaction with other Inc proteins or with host proteins (Gauliard et al., 2015; Elwell et al., 2017). To date, 107 Inc proteins have been predicted for *C. pneumoniae* and 51 Inc proteins for *C. trachomatis* (Dehoux et al., 2011).

During the life cycle of *C. trachomatis*, four interactions between chlamydial effector proteins and MT-regulatory proteins of the host have been identified: (i) Transport of the nascent inclusion along the MTs to the MTOC using the Inc protein CT850, which is associated with the host cell dynein-motor complex. (ii) Positioning of the inclusion at the MTOC is controlled by the interaction of CT288 with the host cell protein CCDC146. (iii) Formation of the MT cage around the inclusion by CT223/IPAM due to the interaction with the host cell target CEP170. (iv) Post-translational modifications of the MT cage and repositioning of Golgi ministacks around the inclusion induced by the interaction of CT813/Ina with host ARF1 and ARF4 proteins.

(i) The first observed interaction between *C. trachomatis* and the MT cytoskeleton of the host cell occurs at 2 hours post-infection after the EBs are internalized. The inclusion travels along the MTs to the MTOC by the ATP-mediated minus-end-directed dynein motor complex and remains in the perinuclear region of the cell for nutrient uptake from the peri-Golgi region (Clausen et al., 1997; Grieshaber et al., 2003). In mammalian cells, the cytoplasmic dynein motor is the major minus-end directed MT motor, which is subdivided into the dynein complex and the dynactin complex (Grieshaber et al., 2003). For the MT-dependent transporter of the inclusion, in addition to an intact MT network, the effector protein CT850 is required to enable the process (Grieshaber et al., 2003; Al-Zeer et al., 2014). However, CT850 is not localized homogeneously along the entire inclusion membrane. Instead, CT850 is found in high concentrations in patches on the inclusion membrane, also called microdomains. The microdomains of CT850 are identified to interact with the dynein light chain type 1 (DYNLT1) of the dynein motor complex (Mital et al., 2010; Mital et al., 2015) (**Figure 5**). The CT850-DYNLT1 interaction subverts the dynein motor complex to traffick the inclusion along MTs and promote proper positioning at the MTOC (Mital et al., 2010; Mital et al., 2015). Mutation of DYNLT1 inhibits inclusion transport and positioning at the MTOC, suggesting that DYNLT1 is

required for the performance of these functions (Weber et al., 2017; Mital et al., 2015). In addition, inclusion fusion at the large MTOC is a dynein-dependent process, is delayed, and occurs at multiple sites in the cell when either the MTs are not anchored to the MTOC or multiple MTOCs are present (Richards et al., 2013). Overall, the interaction of the DYNLT1 protein of the dynein complex with the Inc protein CT850 is critical for the transport of the inclusion as a cargo-linking complex via the minus-end-directed dynein motor complex along the MTs to the MTOC for further chlamydial development. In other studies, co-localization of the *C. trachomatis* inclusion with the $p150^{Glued}$ subunit of the dynactin complex is observed, although the chlamydial interaction partner is still unknown (Grieshaber et al., 2003).

Dynein-dependent inclusion transport is observed for *C. trachomatis.* To date, no MT-dependent transport of the inclusion has been identified in *C. pneumoniae*, suggesting that the modulation of the cytoskeletal network differs between *C. trachomatis* and *C. pneumoniae* (Clausen et al., 1997; Grieshaber et al., 2003; Mital et al., 2015). So far, it has not been confirmed that *C. pneumoniae* is able to hijack the minus-end-directed dynein motor complexes for the transfer of inclusion along the MT to reach the MTOC, although both *C. trachomatis and C. pneumoniae* are localized at the MTOC (Clausen et al., 1997; Grieshaber et al., 2003; Mital et al., 2015).

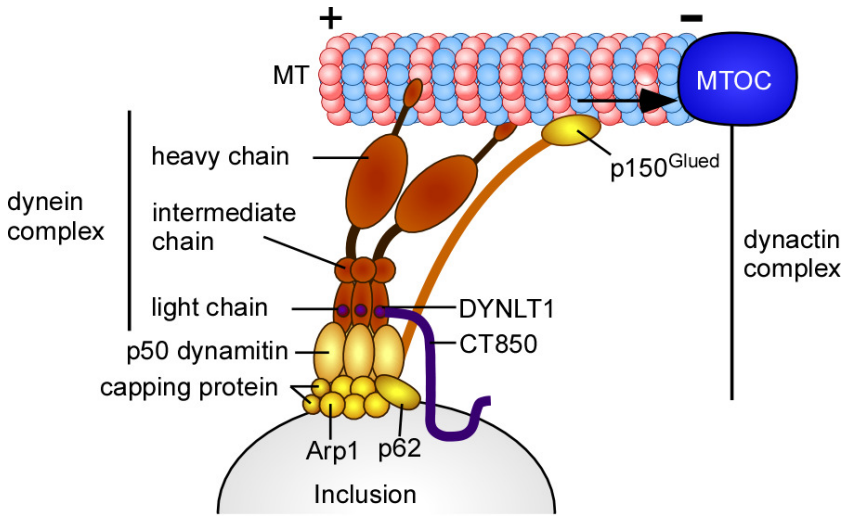

Figure 5: Transport of a *C. trachomatis* inclusion along the MT by hijacking the minus-end directed dynein motor.

The minus-end-directed dynein motor complex consists of a dynein complex (orange part) and a dynactin complex (yellow part) that are connected. The dynein complex is composed of two heavy chains attracted to the

microtubule (MT), intermediate chains, and light-chains including DYNLT1, which are then connected to p50 dynamitin, a component of the dynactin complex. The multi-subunit dynactin complex is responsible for cargo interaction and is structured in a filament of a large subunit $p150^{Glued}$, p50 dynamitin, p62, actin-related protein 1 (Arp1), and actin-capping protein. The inclusion protein CT850 integrated into the *C. trachomatis* inclusion membrane is the chlamydial interaction partner of the dynein light-chain DYNLT1 domain (purple part). Schematic illustration is created by the information from Hirokawa, 1998; Mital et al., 2015; Waterman-Storer et al., 1998. MTOC: MT-organizing center; '+' MT plus-end; '-' MT minus-end.

(ii) At the mid-stage infection at approximately 12 hours post-infection, the inclusion is localized at the MTOC. CT288 is another Inc protein in *C. trachomatis*, which interacts with the C-terminal region of the human centrosomal protein coiled-coil domain-containing protein 146 (CCDC146). In an uninfected host cell, CCDC146 is anchored to the MTOC and interacts with the γ-tubulin complex at the MT minus-end. During chlamydial infection CCDC146 it is recruited for the chlamydial inclusion (Almeida et al., 2018). This recruitment depends on chlamydial protein synthesis but not on the need for intact host MTs or the Golgi complex. Interestingly, mutation of CT288 does not affect recruitment of CCDC146 to inclusion. These data suggest there are other chlamydial proteins participating in the recruitment of host cell CCDC146 to the periphery of bacterial inclusion (Almeida et al., 2018).

(iii) Around 12 hours post-infection, an MT cage is formed around the inclusion by the interaction of the Inc protein CT223/IPAM (inclusion protein acting on MTs) with the host centrosomal protein CEP170. CT223/IPAM is integrated into the inclusion membrane in microdomains to recruit CEP170 to the inclusion. Moreover, CT223/IPAM is necessary for the stimulation of MT organization around chlamydial inclusion (Dumoux et al., 2015; Alzhanov et al., 2009).

(iv) After the MT cage formation, the post-translational modification of the MT cage by detyrosination and acetylation to form a network of stable, post-translationally modified MTs near the inclusion. Therefore, CT813/InaC hijacks and binds the host GTPases ARF1 and ARF4 to enhance post-translational modifications of the MT cage (Kumar and Valdivia, 2008; Wesolowski and Paumet, 2017). A mutation of CT813/InaC leads to loss of recruitment of the GTPases ARF1 and ARF4 (Wesolowski and Paumet, 2017). Additionally, the post-translational

modifications stabilized the MT cage and influences the MT depolymerization rate. However, these stable MTs respond with increased resistance to nocodazole, a substance that induces depolymerization. These results suggest, that *C. trachomatis* exploits the function of stable MTs to support its development (Al-Zeer et al., 2014). Further studies have shown, that the RHO-associated protein kinase (ROCK) is required for the stabilization of MTs (Al-Zeer et al., 2014).

Moreover, post-translationally modified MTs control the positioning of the Golgi ministacks, whose fragmentation of the Golgi complex is promoted by the GTPases Rab6 and Rab11 to enhance nutrient delivery to the inclusion (Rejman Lipinski et al., 2009). Deletion of InaC results in a lack of modified MTs and also consequences a defective Golgi rearrangement (Wesolowski et al., 2017; Kokes et al., 2015). In addition to the repositioning of Golgi ministacks around the inclusion, an intact MT network is required for Golgi stack association to preserve nutrients, e.g., for inclusion development (Al-Zeer et al., 2014).

Furthermore, post-translationally modified MTs are observed to be associated with the endoplasmic reticulum (ER) as the MTs slide along the ER structure. The stabilized MTs surrounding the inclusion cause sections of the ER to be hijacked. For the transfer of lipids into the inclusion, sections of the ER are aligned toward the inclusion to support the formation of ER-inclusion contact sites. The contact sites of the ER with the inclusion are formed by the interaction of IncD/CERT with the host cell ER-resident proteins VAPA/VAPB (Derré et al., 2011). The *C. trachomatis* protein CT005/IncV interacts via its two phenylalanines (FF) in an acidic tract (FFAT)-motifs with the human proteins VAPA/VAPB, but whether the post-translationally modified MTs play a role has not been investigated (Stanhope et al., 2017).

1.5 *S. pombe* as a model organism to identify MT-modulating proteins

Schizosaccharomyces pombe (*S. pombe*) is a rod-shaped haploid fission yeast and a unicellular organism characterized by a short generation time of 2.5 hours in full medium under optimal conditions, making it easy to handle and genetically manipulate (Forsburg and Rhind, 2006).

There are several convincing reasons why *S. pombe* is the optimal choice for both the

identification of bacterial MT-modulating proteins and for detailed studies of chlamydial protein effects on the interphase MT cytoskeleton of the host cell. First, the fundamental regulatory processes of cytoskeletal elements and structures such as tubulin or the interphase MT cytoskeleton are highly conserved in eukaryotes. In addition, the *S. pombe* genome is fully sequenced with approximately 5,000 genes, allowing the genetic interactions obtained in *S. pombe* to be transferred to higher eukaryotes due to the highly conserved processes and components (Forsburg and Rhind, 2006; Yanagida, 2002).

Besides the simple handling of *S. pombe*, the effect of the chlamydial protein on the interphase MT cytoskeleton of the yeast is easy to analyze, because the interphase MT structure has a defined organization. *S. pombe* has 3 to 4 antiparallel MT bundles, each consisting of 3 to 4 individual MTs. MT bundles start at the MTOC close to the nucleus and are directed along the longitudinal axis of the yeast cell toward the cell tips (Tran et al., 2001). *S. pombe* belongs to the non-polarized cells which are characterized by an MT minus-ends anchored to the MTOC, whereas the MT plus-end grows toward the two polarized cell ends (**Figure 6**).

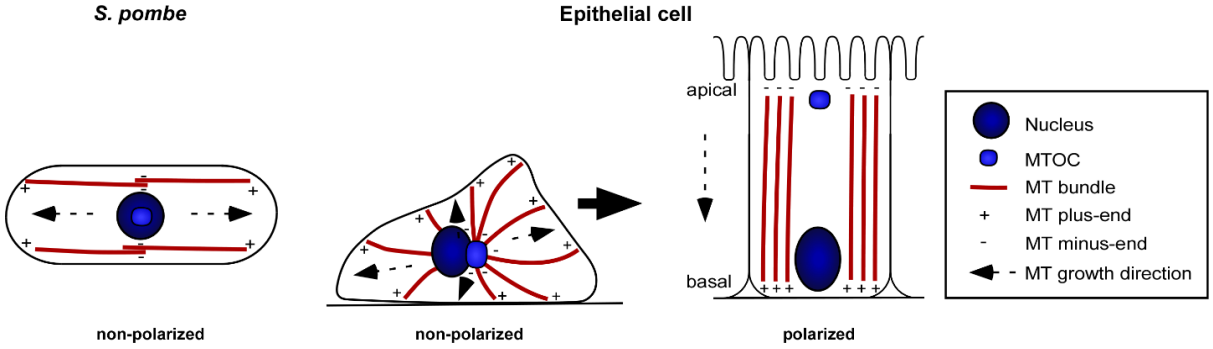

Figure 6: Interphase MT structure of polarized and non-polarized eukaryotic cells. *S. pombe* has a non-polarized microtubule (MT) organization whose MT minus-ends start at the MT-organizing center (MTOC) near the nucleus and are oriented with the growing MT plus-ends along the longitudinal axis of the bent-shaped yeast cell toward the cell ends. Epithelial cells exhibit a non-polarized MT organization *in vivo* assays or a polarized MT organization when epithelial cells are connected by cell-cell junctions. MTs of non-polarized epithelial cells are organized in a radiant structure. Their MT minus-ends originate at the MTOC and the growing MT plus-ends are oriented towards the plasma membrane, while MTs of polarized cells are organized in a uniform MT growth direction along the apical-basal axis. The MT minus-ends start at the apical surface and grow toward the basal surface. Representation is modified from Drubin and Nelson, 1996.

Human epithelial cells are either polarized or non-polarized. Epithelial cells are non-polarized when they are not arranged in a cell cluster as used in the most *in vivo* assays in the laboratory, while polarized epithelial cells are arranged in a cell cluster and are connected by cell-cell junctions (e.g. tight and adherens junctions) as found on external body surfaces (**Figure 6**).
Non-polarized epithelial cells have a similar MT orientation to that of *S. pombe* because their MTs are organized from the MTOC in a radiant structure (Sanchez and Feldman, 2017; Drubin and Nelson, 1996). In those cells, the MT minus-ends are anchored to the MTOC and the MT plus-ends grow oriented toward the plasma membrane. In contrast, MTs of polarized epithelial cells have a uniform MT growth direction along the apical-basal axis, with the MT minus-ends extending from the apical and the MT plus-ends extending to the basal.

In nature, *Chlamydia* infects polarized epithelial cells of the genitourinary or respiratory tract, whereas *S. pombe* or non-polarized epithelial cells are not natural hosts of *Chlamydia* (Resnikoff et al., 2004). The majority of *in vivo* data on *Chlamydia* are based on experiments with non-polarized epithelial cells. The non-polarized epithelial cells and *S. pombe* have in common an MT orientation originating from the MTOC, which makes *S. pombe* an optimal model organism to first identify new MT-modulating chlamydial proteins, and then to analyze the MT-modulating influence in non-polarized epithelial cells in detail.

1.5.1 The interphase MT cytoskeleton and der regulation of MT dynamics

Tubulin, which makes up MTs, is one of the cytoskeletal elements that are highly conserved within eukaryotes. As in eukaryotes, the linear protofilaments in *S. pombe* consist of contiguous αβ-tubulin dimers, of which 13 protofilaments are arranged in a hollow tube of one diameter. In *S. pombe*, the neighboring protofilaments are stabilized by the MT-stabilizing protein Mal3, the homolog of the human EB1, by connecting the neighboring protofilaments in an A- or B-lattice forming the MT (section 1.1). As mentioned in section 1.5, *S. pombe* has 3 to 4 dynamic MT bundles, which for simplicity will be abbreviated as MTs in the following texts (Tran et al., 2001). At the MT plus-ends, MT dynamics are controlled by key regulators: the MT-stabilizing Mal3/Tea2/Tip1 complex and MT-destabilizing Klp5/Klp6/Mcp1 complex (**Figure 7**).

During MT polymerization, the MT plus-end stabilizing GTP-cap is recognized and stabilized by Mal3 via its N-terminal amino-terminal calponin homology (CH)-domain to maintain MT growth and protect the MT against MT catastrophe (Busch and Brunner, 2004) (**Figure 7**). Mal3 binds preferentially at the growing MT plus-end, additionally, it is also distributed throughout the MT to stabilize the MT lattice via its CH-domain between protofilaments (Busch and Brunner, 2004; Sandblad et al., 2006). Although Mal3 decreases MT shrinkage rate and increases MT growth the mechanism of how Mal3 affects MT assembly is not fully understood (Katsuki et al., 2009). Due to the fact, that Mal3 belongs to the EB family, Mal3 and EB1 exhibit a functional homolog. *In vivo* studies showed, that human EB1 can take over the function in *S. pombe* and mimic the interaction with human adenomatous polyposis coli (APC) *in vitro*, although no APC homolog is present in *S. pombe* (Beinhauer et al., 1997; Browning and Hackney, 2005). Both Mal3 and EB1 assume the roles of MT stabilizer and MT plus-end trafficking, which are mechanistically linked.

Furthermore, Mal3 recruits the kinesin motor protein Tea2 to MTs and promotes its motor activity (Browning et al., 2000) (**Figure 7**). Tea2 has an N-terminal motor domain and thus belongs to the kinesin-7 family. The plus-end-directed Tea2 motor protein actively moves along the MTs to the plus-ends and is required for Tip1 transport, as well as transport of the growth factors Tea1 and Tea4 (Brunner and Nurse, 2000; Busch and Brunner, 2004; Martin, 2009; Browning et al., 2000). Tip1 belongs to the CLIP-170 family (human homolog of CLIP-170) and also stabilizes the growing MT plus-end (Beinhauer et al., 1997). *In vitro* studies have shown, that this kinesin-mediated transport is Tip1- and Mal3-dependent (Bieling et al., 2007). Mal3 interacts directly with Tip1 through its CAP-Gly domain (glycerol-rich domain) and associates with Tea2, keeping the Tea2/Tip1/Tea1/Tea4 complex associated at the growing MT plus-end (Busch and Brunner, 2004).

In addition, the cell polarity factors Tea1 and Tea4 are required for signaling the growth zones of the cell ends for polarized cell growth. Tea1 and Tea4 are not involved in MT stabilization, but Tea1 is attributed to be involved in triggering MT catastrophe. For the Tea2-mediated

transport of Tea1 and Tea4, Tea1 interacts with Tea2, Tip1, and Tea4 to form the Tea2/Tip1/Tea1/Tea4 complex (Mata and Nurse, 1997; Browning et al., 2000; Martin, 2009) (**Figure 7**). Tea1 is localized both at the growing MT plus-end and at the growth zones of the cell to regulate the positioning of the growing MT to the growth zones and is thus involved in MT organization (Mata and Nurse, 1997). MTs growing in the direction of the lateral cell cortex instead of the cell ends, reorganize their MT growth direction after contact with the cell cortex. Subsequently, the MT growth direction is reorganized toward the cell ends. Cells with a defect in Tea1 show defective MT organization and a reduction in MT catastrophe events, resulting in MTs growing around the cell end of the yeast (Mata and Nurse, 1997).

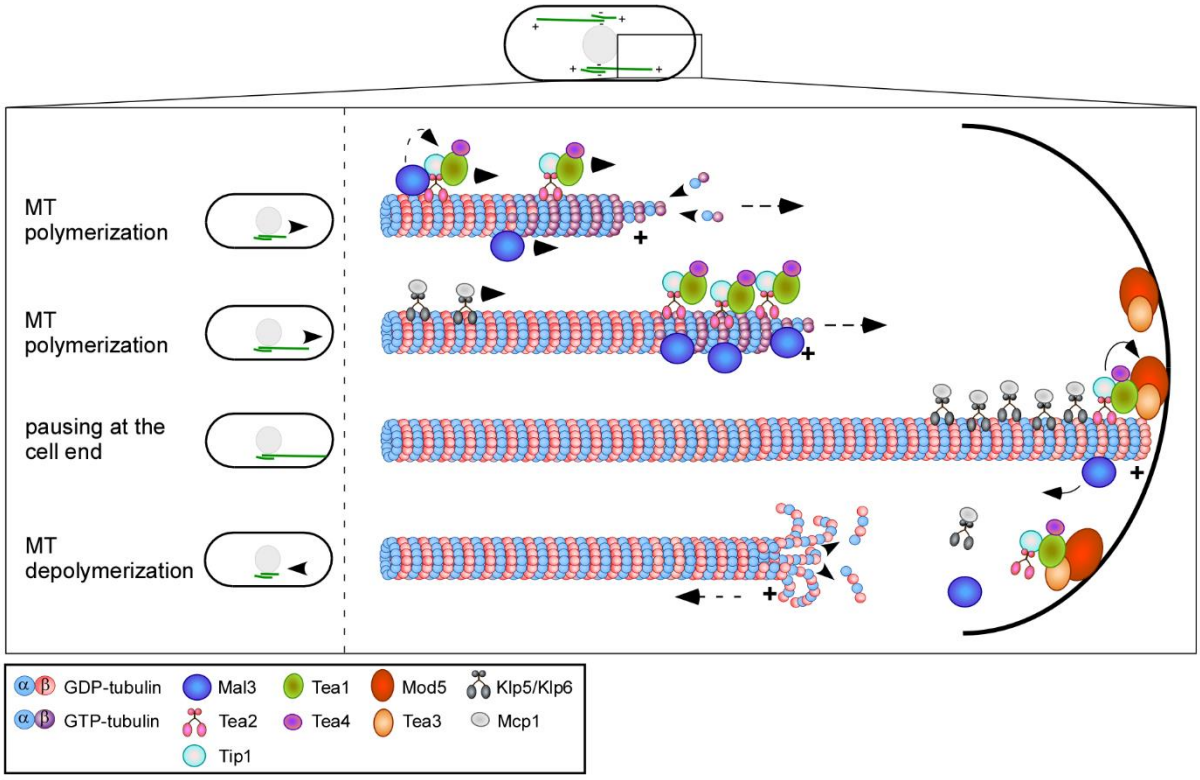

Figure 7: Regulation of MT dynamic dynamics.

Schematic representation of dynamic instability at the MT plus-end. During MT polymerization, the MT plus-end polymerizes by binding free GTP-αβ-tubulin to the MT tip, forming a GTP-cap that stabilizes the MT tip. For the stabilization of the growing MT plus-end are required the MT-stabilizers Mal3 and Tip1. For MT plus-end stabilization, Mal3 moves independently to the growing MT tip, while Tip1 has to be transported by the motor protein Tea2. The motor activity of Tea2 has to be promoted by Mal3 to travel to the MT tip. Tea2 also transports the polarity factors Tea1 and Tea4 as cargos. Together, they form a Tea2/Tip1/Tea1/Tea4 complex. The MT destabilizing Klp5/Klp6/Mcp1 complex accumulated behind the MT stabilizing Tea2/Tip1/Tea1/Tea4 complex.

When the polymerizing MT reaches the cell end, the GTP-cap at the MT tip gets hydrolyzed into GDP-tubulin, and Tea1 anchors Tea4, Tea2, and Tip1 to the plasma membrane-bound Mod5 and Tea3. While the Tea2/Tip1/Tea1/Tea4 complex and Mal3 release the MT tip, the MT-destabilizing Klp5/Klp6/Mcp1 complex reaches the MT tip. The hydrolyzed GDT-tubulin destabilizes the MT structure initiating MT catastrophe. The Klp5/Klp6/Mcp1 complex promotes MT destabilization. Illustration is modified from Janulevicius et al., 2006; Michaels et al., 2020; Meadows et al., 2018 and Drechsel and Kirschner, 1994.

The essential role of the MT stabilizers Mal3, Tea2, and Tip1 in MT growth was confirmed by the analysis of deletion strains, as the absence of the stabilizers has a significant impact on MT organization and dynamics. *In vivo* analyses of Mal3 have shown that Mal3 reduces the rate of MT depolymerization and increases the frequency of rescue (Katsuki et al., 2009). Further experimental evidence showed that nonfunctional MAPs, including Mal3, Tea2, and Tip1 (*tea2Δ, tip1Δ,* and *mal3Δ*), cause massively shorter MTs which are localized to the nuclear region of the cell and affect MT dynamics. The consequence of shorter MTs is abnormal cell morphology, resulting in a T-shaped or bent cell form and a dislocated nucleus (Beinhauer et al., 1997; Browning et al., 2000; Brunner and Nurse, 2000; Behrens and Nurse, 2002).

Another important complex for regulating MT dynamics is the MT destabilizing kinesin-8 Klp5/Klp6/Mcp1 complex, which moves along the MT to the plus-end during MT assembly and accumulates downstream of the Tea2/Tip1/Tea1/Tea4 complex. Klp5/Klp6 complex are co-localized throughout, and their heterodimerization is essential for the destabilizing function of the MT (Unsworth et al., 2008; Meadows et al., 2018).

When the growing MT contacts the cell end, on the one hand, the stabilizing GTP-cap is hydrolyzed to GDP-tubulin. On the other hand, Tea2, Tea4, and Tip1 are transferred from the pausing MT tip to the plasma membrane in a Tea1-dependent manner. Tea1 anchors Tea2, Tea4, and Tip1 to the plasma membrane by interacting with Tea3 and the membrane-associated protein Mod5 (Sawin and Tran, 2006). Tea1, Mod5, and Tea3 are members of the positive feedback-loop, and functionally affect each other (Sawin and Snaith, 2004; Mata and Nurse, 1997). In the following, anchoring of Tea1 and Tea4 leads, on the one hand, to the recruitment of components to promote actin assembly (Martin et al., 2005). On the other hand, with the transfer of the Tea2/Tip1/Tea1/Tea4 complex and the removal of Mal3 from

the MT plus-end, the Klp5/Klp6 complex can advance to the MT tip to promote MT destabilization. *In vivo* studies have proved that the Klp5/Klp6 complex likely functions as a spatial regulator of MT dynamics by registering the slowed MT growth rate and triggering Klp5/Klp6-mediated MT catastrophe to prevent MT overgrowth (Erent et al., 2012). In this regard, the frequency of MT catastrophes depends on the MT length because more Klp5/Klp6 complex accumulates at longer MTs, increasing the probability of MT catastrophe (Tischer et al., 2009). Recent studies showed, that timely shrinkage of MTs requires the protein Mcp1 for the Klp5/Klp6 complex, which is distantly related to the Ase1 family of antiparallel MT binding proteins. Mcp1 is required for association with Klp6 (Meadows et al., 2018). The absence of Klp5 and/or Klp6 (*klp5Δ* and/or *klp6Δ*) leads to hyperstabilized MTs and a reduced frequency of catastrophe events, resulting in overlong MTs that grow around the cell end. Consequently, curling MTs affect MT dynamics (West et al., 2001).

1.6 Aim of work

As masters of actin reorganization for internalization and extrusion through the use of specific bacterial effector proteins, *Chlamydia* has been intensively studied in relation to the actin cytoskeleton. In contrast, the functional role of the host cell microtubule (MT) cytoskeleton during the chlamydial life cycle has hardly been studied. For *C. pneumoniae* in particular, only two effector proteins have been associated with MT modulatory function.

This work aimed to identify new potential MT-modulating proteins of *C. pneumoniae* using the fission yeast *Schizosaccharomyces pombe* (*S. pombe*) to better understand the functional importance of the host MT cytoskeleton during infection. *S. pombe* is not a natural host of *C. pneumoniae,* however, basic regulatory processes of cytoskeletal elements and structures are highly conserved in eukaryotes, and therefore *S. pombe* can be used as a eukaryotic model system.

Of the 1,052 predicted *C. pneumoniae* proteins, corresponding chlamydial genes were to be selected and screened for their effect on wild-type *S. pombe* in the presence or absence of the MT toxin thiabendazole (TBZ). All chlamydial genes whose expression trigger a growth defect

and TBZ-hypersensitivity in yeast, indicating interference with the host cell MT network, should be further investigated. In this context, it should be of interest to analyze the TBZ-hypersensitive yeast transformants for changes in interphase MT structure and organization, and MT dynamics using live-cell imaging microscopy.

Due to the limited time frame, the most promising *C. pneumoniae* proteins should be further characterized. It was the aim to determine the localization of the chosen proteins in *S. pombe* and to narrow down the MT-modulatory domain to a region of the protein by microscopic analysis. Therefore, the proteins of interest were fused to a fluorescent tag. If chlamydial proteins were localized to the MTs, direct binding to MTs would be checked by an *in vitro* MT binding assay. Additionally, potential yeast host cell interaction partners should be identified by immunoprecipitation.

Furthermore, I wanted to investigate the impact of the chlamydial proteins on the human interphase MT cytoskeleton. Therefore, the localization and effect of these chlamydial proteins should be elucidated in transfected, as well as in *C. pneumoniae* infected human epithelial cells to define their functional relevance in the context of the human MT cytoskeleton in the *C. pneumoniae* infection process.

2 Material

2.1 Equipment

Equipment	Manufacture
Blotting	Biometra Fastblot
Cell lysis	Precellys24 Peqlab
Centrifugation	Biofuge pico Hereaus
	Biofuge primoR Hereaus
	Multifuge X3R ThermoFisher Scientific
	Beckmann Optima MAX-E Ultracentrifuge
	Rotanta 460R Hettich
DNA measurements	Nanodrop 2000c Peqlab
DNA Speed-Vac Vacuum-Concentrator	Savant
Electroporation	Gene Pulser Xcell BIO-RAD
Gel documentation	Intas UV System
Incubators	WTC Binder
	Hereaus
	Infors HT Electron
	ThermoFisher Scientific Heraeus
CO_2 Incubators	ThermoFisher Scientific Forma Steri-cycle
Laminar flow cabinet	Clean air
	HERA safe ThermoFisher Scientific
Confocal icroscopy	Nikon Eklipse Ti microscope
Live cell imaging microscopy	Zeiss LSM 880 Airyscan microscope
	Zeiss Spinning Disc-Confocal microscope
OD measurement	Photometer BioEppendorf
PCR Cycler	BIO-RAD C1000 Thermal Cycler
Thermo block	Labnet, Streutronic

2.2 Chemicals

Chemicals	Manufacture
Acrylamid solution Rotiphorese-Gel 30; 37,5:1	ROTH
Adenine	Sigma Aldrich
Agarose	Biozym
Alanine	AppliChem
Ammonium sulfate ($(NH_4)_2SO_4$)	ROTH
Ampicillin	Sigma Aldrich
Arginine	AppliChem
Aspartic acid	ROTH
Aspartic acid	AppliChem
APS	Merck
β-glycerophosphate	BD
Bacto agar	BD
Bacto Malt extract	BD
BCIP	Sigma Aldrich
Biotin	Sigma Aldrich
Carrier DNA	Sigma Aldrich
Complete protease inhibitor	Roche
Coomassie Brilliant Blue	Serva
Cycloheximide	Sigma Aldrich
Cysteine	ROTH
4',6-diamidino-2-phenylindole (DAPI)	Roche
Dimethylformamide (DMF)	Fisher
Dimethylsulfoxide (DMSO)	Merck
Dithiothreitol (DTT)	ROTH
Dorfmanite (Na_2HPO_4 x $2H_2O$)	ROTH
Ethanol	Chemical storage HHU Düsseldorf
Ethylenediaminetetraacetic acid (EDTA)	AppliChem
Ethylene glycol bis-(aminoethyl ether) (EGTA)	Sigma Aldrich
Glucose	ROTH
Glutamic acid	Sigma Aldrich
Glutamine	ROTH
Glycerol	Fisher
Glycine	VWR

Histidine	Sigma Aldrich
Hydrochloric acid (HCl)	Sigma Aldrich
Inositol	Sigma Aldrich
Isoleucine	ROTH
Isopropanol	Chemical storage, HHU Düsseldorf
Kanamycin	Life Technologies
Lanoline	Sigma Aldrich
Leucine	AppliChem
Lithium acetate (LiAc)	ROTH
Lithium chloride (LiCl)	Merck
Lysine	Sigma Aldrich
Manga sulphate ($MnSO_4$)	Sigma Aldrich
Methanol	Chemical storage HHU
Methionine	ROTH
Methyl benzimidazol-2-yl-carbamate	Sigma Aldrich
Milk powder	ROTH
Molbdenum oxide (MoO_3)	Sigma Aldrich
3-(N-morpholino) propanesulfonic acid (MOPS)	Fluka
Nicotinic acid	Sigma Aldrich
Nitro blue tetrazolium chloride (NBT)	Serva
Nonoxynol 40 (NP-40)	Sigma Aldrich
Para amino benzoic acid	Sigma Aldrich
Paraffine	Caeser & Loretz
Peptone	BD
Phenylalanine	TCI
Phenylmethylsulfonyl fluoride (PMSF)	Serva
Polyethylene glycol (PEG)	Sigma Aldrich
Potassium chloride (KCl)	ROTH
Potassium iodide (KI)	Sigma Aldrich
Potassium phthalate monobasic	Sigma Aldrich
Proline	ROTH
Serine	ROTH
Sodium chloride (NaCl)	Fischer
Sodium hydroxate (NaOH)	AppliChem
Sodium lauryl sulfate (SDS)	Sigma Aldrich

Sodium pantothenic acid	Sigma Aldrich
Sodium sulfate (Na_2SO_4)	Merck
Tetramethylethylene diamine (TEMED)	Merck
Thiabendazole	Sigma Aldrich
Thiamine	Sigma Aldrich
Threonine	ROTH
Tris (hydroxymethyl)aminomethane (Tris)	Honeywell
Triton X 100	AppliChem
Tryptone	BD
Tryptophane	ROTH
Tryosine	ROTH
Tween	AppliChem
Uracil	Sigma Aldrich
Valine	ROTH
Vaseline	Caesar & Loretz
Yeast extract	BD
Yeast nitrogen base	BD

2.3 Antibodies and dyes

2.3.1 Unconjugated primary antibodies

Antibody	Application	Dilution	Manufacturer
anti-actin, mouse	Western blot	1:1000	Invitrogen
anti-α-tubulin, mouse	Immunflourecence	1:150	OriGene
anti-α-tubulin, rat	Western blot	1:1000	Santa Cruz
anti-flag, mouse	Western blot	1:1000	Sigma
	Immunofluorescence	1:1000	
anti-GFP, mouse	Western blot	1:1000	Sigma
anti-GFP, rat	Western blot	1:1000	Chromotek
anti-mCherry, mouse	Western blot	1:5000	Invitrogen
anti-momp *Cpn*, mouse	Immunofluorescence	1:100	Wolf et al., 2000
anti-myc, rat	Immunofluorescence	1:500	Chromotek

Antibodies for the application of a Western blot were diluted in a blocking solution of 3 % milk powder and 0.05 % Tween 20 in 1x PBS, or for the application of immunofluorescence they were diluted in 1x PBS.

2.3.2 Fluorescent-conjugated secondary antibodies

Antibody	Application	Dilution	Manufacturer
anti-mouse Alexa488	Immunofluorescence	1:200	Invitrogen
anti-mouse Alexa594	Immunofluorescence	1:200	Invitrogen
anti-mouse IgG	Western blot	1:7500	Promega
anti-rabbit Alexa488	Immunofluorescence	1:200	Invitrogen
anti-rabbit Alexa594	Immunofluorescence	1:200	Life technologies
anti-rabbit IgG	Western blot	1:7500	Promega
anti-rat Alexa488	Immunofluorescence	1:200	Invitrogen
anti-rat IgG	Western blot	1:7500	Sigma

Antibodies for the application of a Western blot were diluted in a blocking solution of 3 % milk powder and 0.05 % Tween 20 in 1x PBS, or for the application of immunofluorescence they were diluted in 1x PBS.

Dye	Application	Dilution	Manufacturer
DAPI	Immunofluorescence	1:500	Sigma

2.4 Enzymes

Enzyme	Application	Manufactures
β-Glucoronidase	Mating	Roche
Proteinase K		AppliChem

2.4.1 Restriction enzymes

Enzyme	Buffer and reaction temperature	Manufactures
BamHI	Unique buffer BamHI, 37 °C	ThermoFisher Scientific
BglI	Buffer O, 37 °C	ThermoFisher Scientific
BglII	Buffer O, 37 °C	ThermoFisher Scientific
EcoRI	Unique buffer EcoRI, 37 °C	ThermoFisher Scientific
HincII	Buffer Tango, 37 °C	ThermoFisher Scientific
HindIII	Buffer R, 37 °C	ThermoFisher Scientific
NotI	Buffer O, 37 °C	ThermoFisher Scientific
PstI	Buffer O, 37 °C	ThermoFisher Scientific

SmaI	Buffer Tango, 30 °C	ThermoFisher Scientific

2.5 Kits

Kit	Manufactures
µMACS GFP Isolation Kit	Miltenyi
QIAGEN Plasmid Midi Kit	Qiagen
Q5 High-Fidelity DNA polymerase	New England Biolabs

2.6 Services

Service	Manufactures
DNA Sequencing	GATC Sanger sequencing
Zeiss Spinning-Disc/ Zeiss LSM 880 Airyscan	Center for Advanced Imaging (CAi), HHU Düsseldorf

2.7 Other material

Materials	Manufactures
Cell culture flasks (25 cm^2, 80 cm^2)	Sarstedt
Cell scraper	ThermoFisher Scientific
Coverslips	Knittel Glas
Electroporation cuvettes	Sarstedt
Eppendorf tubes	Eppendorf
Falcon tubes (15 mL, 50 mL)	Sarstedt
GeneRuler DNA Ladder Mix	ThermoFisher Scientific
Gibco Amphotericin B 250 µg/mL	ThermoFisher Scientific
Gibco DMEM (1x) + GlutaMAX™ -I	ThermoFisher Scientific
Gibco Fetal Bovine Serum (FBS)	ThermoFisher Scientific
Gibco Gentamicin (50 mg/mL)	ThermoFisher Scientific
Gibco HBSS (1x)	ThermoFisher Scientific
Gibco MEM NEAA (100x)	ThermoFisher Scientific
Gibco MEM Vitamin Solution (100X)	ThermoFisher Scientific
Glass beads	ROTH
Immersion oil	Zeiss
PVDF membrane	VWR

Mounting solution Vectashield	Vector
µMAC columns	Miltenyi
Nail polish	Essence cosmetics
Object slides	Diagonal
PageRuler™ Prestained Protein Ladder, 10-180 kDa	ThermoFisher Scientific
PageRuler™ Plus Prestained Protein Ladder, 10-250 kDa	ThermoFisher Scientific
Petri dishes	Sarstedt
Pierce Spin Columns Snap Cap	ThermoFisher Scientific
Pipet tips	Sarstedt
PCR tubes with lids	Applied Biosystems
TC-plate, 6 well, 24 well standard	Sarstedt
Whatman paper	VWR

2.8 Plasmids

Plasmid number	Name, genes, and markers	Origin
270	pJR2-3XL, *LEU2*, *Amp^R*, pREP3X, *nmt1$^+$*-promotor	Beln Moreno et al., 2000
282	pJR2-3XU, *ura4$^+$*, *Amp^R*, pREP3X, *nmt1$^+$*-promotor	Beln Moreno et al., 2000
1287	pJR2-3XU-*cpn0372*, *ura4$^+$*, *Amp^R*, *nmt1$^+$*-promotor, p282 PstI, *Cpn* GiD DNA, ON 2466/2467	This study
1288	pJR2-3XU-*cpn0173*, *ura4$^+$*, *Amp^R*, *nmt1$^+$*-promotor, p282 PstI, *Cpn* GiD DNA, ON 2462/2463	This study
1289	pJR2-3XU-*cpn0308*, *ura4$^+$*, *Amp^R*, *nmt1$^+$*-promotor, p282 PstI, *Cpn* GiD DNA, ON 2468/2469	This study
1292	pJR2-3XU-*cpn0365*, *ura4$^+$*, *Amp^R*, *nmt1$^+$*-promotor, p282 PstI, *Cpn* GiD DNA, ON 2486/2487	This study
1293	pJR2-3XU-*cpn0212*, *ura4$^+$*, *Amp^R*, *nmt1$^+$*-promotor, p282 PstI, *Cpn* GiD DNA, ON 2460/2461	This study
1294	pJR2-3XU-*cpn0648*, *ura4$^+$*, *Amp^R*, *nmt1$^+$*-promotor, p282 PstI, *Cpn* GiD DNA, ON 2506/2507	This study
1295	pJR2-3XU-*cpn0214*, *ura4$^+$*, *Amp^R*, *nmt1$^+$*-promotor, p282 PstI, *Cpn* GiD DNA, ON 2476/2477	This study
1307	pJR2-3XU-*cpn0218*, *ura4$^+$*, *Amp^R*, *nmt1$^+$*-promotor, p282 PstI, *Cpn* GiD DNA, ON 2518/2519	This study

1308	pJR2-3XU-*cpn0065*, *ura4*$^{+}$, *Amp*^{R}, *nmt1*$^{+}$-promotor, p282 PstI, *Cpn* GiD DNA, ON 2494/2495	This study
1309	pJR2-3XU-*cpn0215*, *ura4*$^{+}$, *Amp*^{R}, *nmt1*$^{+}$-promotor, p282 PstI, *Cpn* GiD DNA, ON 2474/2475	This study
1310	pJR2-3XU-*cpn0045*, *ura4*$^{+}$, *Amp*^{R}, *nmt1*$^{+}$-promotor, p282 PstI, *Cpn* GiD DNA, ON 2480/2481	This study
1324	pJR2-3XU-*cpn0512*, *ura4*$^{+}$, *Amp*^{R}, *nmt1*$^{+}$-promotor, p282 PstI, *Cpn* GiD DNA, ON 2510/2511	This study
1325	pJR2-3XU-*cpn0007*, *ura4*$^{+}$, *Amp*^{R}, *nmt1*$^{+}$-promotor, p282 PstI, *Cpn* GiD DNA, ON 2482/2483	This study
1335	pJR2-3XU-mCherry (Hegemann Lab code pCUB1)	J. Hegemann
1384	pJR2-3XU-*cpn0312*, *ura4*$^{+}$, *Amp*^{R}, *nmt1*$^{+}$-promotor, p282 PstI, *Cpn* GiD DNA, ON 2575/2576	This study
1385	pJR2-3XU-*cpn0242*, *ura4*$^{+}$, *Amp*^{R}, *nmt1*$^{+}$-promotor, p282 PstI, *Cpn* GiD DNA, ON 2571/2572	This study
1386	pJR2-3XU-*cpn0292*, *ura4*$^{+}$, *Amp*^{R}, *nmt1*$^{+}$-promotor, p282 PstI, *Cpn* GiD DNA, ON 2649/2650	This study
1387	pJR2-3XU-*cpn0554*, *ura4*$^{+}$, *Amp*^{R}, *nmt1*$^{+}$-promotor, p282 PstI, *Cpn* GiD DNA, ON 2587/2588	This study
1388	pJR2-3XU-*cpn0441*, *ura4*$^{+}$, *Amp*^{R}, *nmt1*$^{+}$-promotor, p282 PstI, *Cpn* GiD DNA, ON 2512/2513	This study
1389	pJR2-3XU-*cpn0753*, ura4^{+}, Amp^{R}, *nmt1*$^{+}$-promotor, p282 PstI, *Cpn* GiD DNA, ON 2496/2497	This study
1390	pJR2-3XU-*cpn0409*, *ura4*$^{+}$, Amp^{R}, *nmt1*$^{+}$-promotor, p282 PstI, *Cpn* GiD DNA, ON 2500/2501	This study
1391	pJR2-3XU-*cpn0518*, *ura4*$^{+}$, *Amp*^{R}, *nmt1*$^{+}$-promotor, p282 PstI, *Cpn* GiD DNA, ON 2514/2515	This study
1392	pJR2-3XU-*cpn0525*, *ura4*$^{+}$, *Amp*^{R}, *nmt1*$^{+}$-promotor, p282 PstI, *Cpn* GiD DNA, ON 2492/2493	This study
1393	pJR2-3XU-*cpn0284*, *ura4*$^{+}$, *Amp*^{R}, *nmt1*$^{+}$-promotor, p282 PstI, *Cpn* GiD DNA, ON 2488/2489	This study
1394	pJR2-3XU-*cpn0166*, *ura4*$^{+}$, *Amp*^{R}, *nmt1*$^{+}$-promotor, p282 PstI, *Cpn* GiD DNA, ON 2490/2491	This study
1395	pJR2-3XU-*cpn0442*, *ura4*$^{+}$, *Amp*^{R}, *nmt1*$^{+}$-promotor, p282 PstI, *Cpn* GiD DNA, ON 2563/2564	This study
1396	pJR2-3XU-*cpn0601*, *ura4*$^{+}$, *Amp*^{R}, *nmt1*$^{+}$-promotor, p282 PstI, *Cpn* GiD DNA, ON 2591/2592	This study

1397	pJR2-3XU-*cpn1046*, *ura4*$^{+}$, *Amp*^{R}, *nmt1*$^{+}$-promotor, p282 PstI, *Cpn* GiD DNA, ON 2712/2713	This study
1398	pJR2-3XU-*cpn0456*, *ura4*$^{+}$, *Amp*^{R}, *nmt1*$^{+}$-promotor, p282 PstI, *Cpn* GiD DNA, ON 2696/2697	This study
1399	pJR2-3XU-*cpn0381*, *ura4*$^{+}$, *Amp*^{R}, *nmt1*$^{+}$-promotor, p282 PstI, *Cpn* GiD DNA, ON 2653/2654	This study
1400	pJR2-3XU-*cpn0067*, *ura4*$^{+}$, *Amp*^{R}, *nmt1*$^{+}$-promotor, p282 PstI, *Cpn* GiD DNA, ON 2623/2624	This study
1401	pJR2-3XU-*cpn0869*, *ura4*$^{+}$, *Amp*^{R}, *nmt1*$^{+}$-promotor, p282 PstI, *Cpn* GiD DNA, ON 2603/2604	This study
1402	pJR2-3XU-*cpn0107*, *ura4*$^{+}$, *Amp*^{R}, *nmt1*$^{+}$-promotor, p282 PstI, *Cpn* GiD DNA, ON 2611/2612	This study
1403	pJR2-3XU-*cpn0291*, *ura4*$^{+}$, *Amp*^{R}, *nmt1*$^{+}$-promotor, p282 PstI, *Cpn* GiD DNA, ON 2579/2580	This study
1404	pJR2-3XU-*cpn0131*, *ura4*$^{+}$, *Amp*^{R}, *nmt1*$^{+}$-promotor, p282 PstI, *Cpn* GiD DNA, ON 2631/2632	This study
1405	pJR2-3XU-cpn0565, *ura4*$^{+}$, *Amp*^{R}, *nmt1*$^{+}$-promotor, p282 PstI, *Cpn* GiD DNA, ON 2585/2586	This study
1406	pJR2-3XU-*cpn0755*, *ura4*$^{+}$, *Amp*^{R}, *nmt1*$^{+}$-promotor, p282 PstI, *Cpn* GiD DNA, ON 2597/2598	This study
1407	pJR2-3XU-*cpn0066*, *ura4*$^{+}$, *Amp*^{R}, *nmt1*$^{+}$-promotor, p282 PstI, *Cpn* GiD DNA, ON 2621/2622	This study
1408	pJR2-3XU-*cpn0288*, *ura4*$^{+}$, *Amp*^{R}, *nmt1*$^{+}$-promotor, p282 PstI, *Cpn* GiD DNA, ON 2567/2568	This study
1409	pJR2-3XU-*cpn0480*, *ura4*$^{+}$, *Amp*^{R}, *nmt1*$^{+}$-promotor, p282 PstI, *Cpn* GiD DNA, ON 2583/2584	This study
1410	pJR2-3XU-*cpn0186*, *ura4*$^{+}$, *Amp*^{R}, *nmt1*$^{+}$-promotor, p282 PstI, *Cpn* GiD DNA, ON 2639/2640	This study
1411	pJR2-3XU-*cpn0658*, *ura4*$^{+}$, *Amp*^{R}, *nmt1*$^{+}$-promotor, p282 PstI, *Cpn* GiD DNA, ON 2508/2509	This study
1412	pJR2-3XU-*cpn0523*, *ura4*$^{+}$, *Amp*^{R}, *nmt1*$^{+}$-promotor, p282 PstI, *Cpn* GiD DNA, ON 2663/2664	This study
1413	pJR2-3XU-*cpn0164*, *ura4*$^{+}$, *Amp*^{R}, *nmt1*$^{+}$-promotor, p282 PstI, *Cpn* GiD DNA, ON 2635/2636	This study
1414	pJR2-3XU-*cpn0241*, *ura4*$^{+}$, *Amp*^{R}, *nmt1*$^{+}$-promotor, p282 PstI, *Cpn* GiD DNA, ON 2569/2570	This study
1415	pJR2-3XU-*cpn0026*, *ura4*$^{+}$, *Amp*^{R}, *nmt1*$^{+}$-promotor, p282 PstI, *Cpn* GiD DNA, ON 2617/2618	This study

1416	pJR2-3XU-*cpn0770*, *ura4*$^{+}$, *Amp*^{R}, *nmt1*$^{+}$-promotor, p282 PstI, *Cpn* GiD DNA, ON 2601/2602	This study
1417	pJR2-3XU-*cpn0830*, *ura4*$^{+}$, *Amp*^{R}, *nmt1*$^{+}$-promotor, p282 PstI, *Cpn* GiD DNA, ON 2667/2668	This study
1418	pJR2-3XU-*cpn0432*, *ura4*$^{+}$, *Amp*^{R}, *nmt1*$^{+}$-promotor, p282 PstI, *Cpn* GiD DNA, ON 2655/2656	This study
1419	pJR2-3XU-*cpn0517*, *ura4*$^{+}$, *Amp*^{R}, *nmt1*$^{+}$-promotor, p282 PstI, *Cpn* GiD DNA, ON 2484/2485	This study
1420	pJR2-3XU-*cpn1003*, *ura4*$^{+}$, *Amp*^{R}, *nmt1*$^{+}$-promotor, p282 PstI, *Cpn* GiD DNA, ON 2607/2608	This study
1421	pJR2-3XU-*cpn0370*, *ura4*$^{+}$, *Amp*^{R}, *nmt1*$^{+}$-promotor, p282 PstI, *Cpn* GiD DNA, ON 2577/2578	This study
1422	pJR2-3XU-*cpn0124*, *ura4*$^{+}$, *Amp*^{R}, *nmt1*$^{+}$-promotor, p282 PstI, *Cpn* GiD DNA, ON 2627/2628	This study
1423	pJR2-3XU-*cpn0041*, *ura4*$^{+}$, *Amp*^{R}, *nmt1*$^{+}$-promotor, p282 PstI, *Cpn* GiD DNA, ON 2619/2620	This study
1424	pJR2-3XU-*cpn0404*, *ura4*$^{+}$, *Amp*^{R}, *nmt1*$^{+}$-promotor, p282 PstI, *Cpn* GiD DNA, ON 2599/2600	This study
1425	pJR2-3XU-*cpn0906*, *ura4*$^{+}$, *Amp*^{R}, *nmt1*$^{+}$-promotor, p282 PstI, *Cpn* GiD DNA, ON 2504/2505	This study
1426	pJR2-3XU-*cpn0912*, *ura4*$^{+}$, *Amp*^{R}, *nmt1*$^{+}$-promotor, p282 PstI, *Cpn* GiD DNA, ON 2502/2503	This study
1427	pJR2-3XU-*cpn0938*, *ura4*$^{+}$, *Amp*^{R}, *nmt1*$^{+}$-promotor, p282 PstI, *Cpn* GiD DNA, ON 2605/2606	This study
1428	pJR2-3XU-*cpn0443*, *ura4*$^{+}$, *Amp*^{R}, *nmt1*$^{+}$-promotor, p282 PstI, *Cpn* GiD DNA, ON 2561/2562	This study
1429	pJR2-3XU-*cpn0126*, *ura4*$^{+}$, *Amp*^{R}, *nmt1*$^{+}$-promotor, p282 PstI, *Cpn* GiD DNA, ON 2629/2630	This study
1430	pJR2-3XU-*cpn0203*, *ura4*$^{+}$, *Amp*^{R}, *nmt1*$^{+}$-promotor, p282 PstI, *Cpn* GiD DNA, ON 2641/2642	This study
1431	pJR2-3XU-*cpn1062*, *ura4*$^{+}$, *Amp*^{R}, *nmt1*$^{+}$-promotor, p282 PstI, *Cpn* GiD DNA, ON 2716/2717	This study
1432	pJR2-3XU-*cpn0366*, *ura4*$^{+}$, *Amp*^{R}, *nmt1*$^{+}$-promotor, p282 PstI, *Cpn* GiD DNA, ON 2464/2465	This study
1433	pJR2-3XU-*cpn0829*, *ura4*$^{+}$, *Amp*^{R}, *nmt1*$^{+}$-promotor, p282 PstI, *Cpn* GiD DNA, ON 2665/2666	This study
1434	pJR2-3XU-*cpn1008*, *ura4*$^{+}$, *Amp*^{R}, *nmt1*$^{+}$-promotor, p282 PstI, *Cpn* GiD DNA, ON 2764/2765	This study

1435	pJR2-3XU-*cpn0524*, *ura4*$^{+}$, *Amp*^{R}, *nmt1*$^{+}$-promotor, p282 PstI, *Cpn* GiD DNA, ON 2754/2755	This study
1436	pJR2-3XU-*cpn0834*, *ura4*$^{+}$, *Amp*^{R}, *nmt1*$^{+}$-promotor, p282 PstI, *Cpn* GiD DNA, ON 2758/2759	This study
1437	pJR2-3XU-*cpn0537*, *ura4*$^{+}$, *Amp*^{R}, *nmt1*$^{+}$-promotor, p282 PstI, *Cpn* GiD DNA, ON 2756/2757	This study
1438	pJR2-3XU-*cpn0813*, *ura4*$^{+}$, *Amp*^{R}, *nmt1*$^{+}$-promotor, p282 PstI, *Cpn* GiD DNA, ON 2700/2701	This study
1439	pJR2-3XU-*cpn0481*, *ura4*$^{+}$, *Amp*^{R}, *nmt1*$^{+}$-promotor, p282 PstI, *Cpn* GiD DNA, ON 2661/2662	This study
1440	pJR2-3XU-*cpn1029*, *ura4*$^{+}$, *Amp*^{R}, *nmt1*$^{+}$-promotor, p282 PstI, *Cpn* GiD DNA, ON 2766/2767	This study
1441	pJR2-3XU-*cpn0815*, *ura4*$^{+}$, *Amp*^{R}, *nmt1*$^{+}$-promotor, p282 PstI, *Cpn* GiD DNA, ON 2702/2703	This study
1442	pJR2-3XU-*cpn0157*, *ura4*$^{+}$, *Amp*^{R}, *nmt1*$^{+}$-promotor, p282 PstI, *Cpn* GiD DNA, ON 2633/2634	This study
1443	pJR2-3XU-*cpn0440*, *ura4*$^{+}$, *Amp*^{R}, *nmt1*$^{+}$-promotor, p282 PstI, *Cpn* GiD DNA, ON 2657/2658	This study
1444	pJR2-3XU-*cpn0255*, *ura4*$^{+}$, *Amp*^{R}, *nmt1*$^{+}$-promotor, p282 PstI, *Cpn* GiD DNA, ON 2645/2646	This study
1445	pJR2-3XU-*cpn1055*, *ura4*$^{+}$, *Amp*^{R}, *nmt1*$^{+}$-promotor, p282 PstI, *Cpn* GiD DNA, ON 2675/2676	This study
1446	pJR2-3XU-*cpn1060*, *ura4*$^{+}$, *Amp*^{R}, *nmt1*$^{+}$-promotor, p282 PstI, *Cpn* GiD DNA, ON 2714/2715	This study
1447	pJR2-3XU-*cpn0850*, *ura4*$^{+}$, *Amp*^{R}, *nmt1*$^{+}$-promotor, p282 PstI, *Cpn* GiD DNA, ON 2704/2705	This study
1448	pJR2-3XU-*cpn1027*, *ura4*$^{+}$, *Amp*^{R}, *nmt1*$^{+}$-promotor, p282 PstI, *Cpn* GiD DNA, ON 2671/2672	This study
1449	pJR2-3XU-*cpn0930*, *ura4*$^{+}$, *Amp*^{R}, *nmt1*$^{+}$-promotor, p282 PstI, *Cpn* GiD DNA, ON 2669/2670	This study
1450	pJR2-3XU-*cpn0357*, *ura4*$^{+}$, *Amp*^{R}, *nmt1*$^{+}$-promotor, p282 PstI, *Cpn* GiD DNA, ON 2651/2652	This study
1451	pJR2-3XU-*cpn0169*, *ura4*$^{+}$, *Amp*^{R}, *nmt1*$^{+}$-promotor, p282 PstI, *Cpn* GiD DNA, ON 2637/2638	This study
1452	pJR2-3XU-*cpn0556*, *ura4*$^{+}$, *Amp*^{R}, *nmt1*$^{+}$-promotor, p282 PstI, *Cpn* GiD DNA, ON 2589/2590	This study
1453	pJR2-3XU-*cpn0147*, *ura4*$^{+}$, *Amp*^{R}, *nmt1*$^{+}$-promotor, p282 PstI, *Cpn* GiD DNA, ON 2498/2499	This study

1454	pJR2-3XU-*cpn0132*, *ura4*$^{+}$, *Amp*^{R}, *nmt1*$^{+}$-promotor, p282 PstI, *Cpn* GiD DNA, ON 2478/2479	This study
1455	pJR2-3XU-*cpn0285*, *ura4*$^{+}$, *Amp*^{R}, *nmt1*$^{+}$-promotor, p282 PstI, *Cpn* GiD DNA, ON 2647/2648	This study
1456	pJR2-3XU-*cpn1070*, *ura4*$^{+}$, *Amp*^{R}, *nmt1*$^{+}$-promotor, p282 PstI, *Cpn* GiD DNA, ON 2718/2719	This study
1457	pJR2-3XU-*cpn0909, ura4*$^{+}$, *Amp*^{R}, *nmt1*$^{+}$-promotor, p282 PstI, *Cpn* GiD DNA, ON 2795/2796	This study
1458	pJR2-3XU-*cpn0879*, *ura4*$^{+}$, *Amp*^{R}, *nmt1*$^{+}$-promotor, p282 PstI, *Cpn* GiD DNA, ON 2799/2800	This study
1459	pJR2-3XU-*cpn0491*, *ura4*$^{+}$, *Amp*^{R}, *nmt1*$^{+}$-promotor, p282 PstI, *Cpn* GiD DNA, ON 2801/2802	This study
1460	pJR2-3XU-*cpn0592*, *ura4*$^{+}$, *Amp*^{R}, *nmt1*$^{+}$-promotor, p282 PstI, *Cpn* GiD DNA, ON 2807/2808	This study
1461	pJR2-3XU-*cpn0544*, *ura4*$^{+}$, *Amp*^{R}, *nmt1*$^{+}$-promotor, p282 PstI, *Cpn* GiD DNA, ON 2811/2812	This study
1462	pJR2-3XU-*cpn0488*, *ura4*$^{+}$, *Amp*^{R}, *nmt1*$^{+}$-promotor, p282 PstI, *Cpn* GiD DNA, ON 2813/2814	This study
1463	pJR2-3XU-*cpn0729*, *ura4*$^{+}$, *Amp*^{R}, *nmt1*$^{+}$-promotor, p282 PstI, *Cpn* GiD DNA, ON 2817/2818	This study
1464	pJR2-3XU-*cpn0844*, *ura4*$^{+}$, *Amp*^{R}, *nmt1*$^{+}$-promotor, p282 PstI, *Cpn* GiD DNA, ON 2839/2840	This study
1465	pJR2-3XU-*cpn0061*, *ura4*$^{+}$, *Amp*^{R}, *nmt1*$^{+}$-promotor, p282 PstI, *Cpn* GiD DNA, ON 2841/2842	This study
1466	pJR2-3XU-*cpn0262*, *ura4*$^{+}$, *Amp*^{R}, *nmt1*$^{+}$-promotor, p282 PstI, *Cpn* GiD DNA, ON 2843/2844	This study
1467	pJR2-3XU-*cpn0821*, *ura4*$^{+}$, *Amp*^{R}, *nmt1*$^{+}$-promotor, p282 PstI, *Cpn* GiD DNA, ON 2805/2801	This study
1468	pJR2-3XU-*cpn0671*, *ura4*$^{+}$, *Amp*^{R}, *nmt1*$^{+}$-promotor, p282 PstI, *Cpn* GiD DNA, ON 2809/2810	This study
1469	pJR2-3XU-*cpn0467*, *ura4*$^{+}$, *Amp*^{R}, *nmt1*$^{+}$-promotor, p282 PstI, *Cpn* GiD DNA, ON 2698/2699	This study
1470	pJR2-3XU-*cpn0216*, *ura4*$^{+}$, *Amp*^{R}, *nmt1*$^{+}$-promotor, p282 PstI, *Cpn* GiD DNA, ON 2472/2473	This study
1471	pJR2-3XU-*cpn0966*, *ura4*$^{+}$, *Amp*^{R}, *nmt1*$^{+}$-promotor, p282 PstI, *Cpn* GiD DNA, ON 2708/2709	This study
1472	pJR2-3XU-*cpn0371*, *ura4*$^{+}$, *Amp*^{R}, *nmt1*$^{+}$-promotor, p282 PstI, *Cpn* GiD DNA, ON 2470/2471	This study

1474	pJR2-3XU-*cpn0994*, *ura4*$^{+}$, *Amp*^{R}, *nmt1*$^{+}$-promotor, p282 PstI, *Cpn* GiD DNA, ON 2762/2763	This study
1475	pJR2-3XU-*cpn0431*, *ura4*$^{+}$, *Amp*^{R}, *nmt1*$^{+}$-promotor, p282 PstI, *Cpn* GiD DNA, ON 2581/2582	This study
1476	pJR2-3XU-*cpn0602*, *ura4*$^{+}$, *Amp*^{R}, *nmt1*$^{+}$-promotor, p282 PstI, *Cpn* GiD DNA, ON 2516/2517	This study
1477	pJR2-3XU-*cpn0746*, *ura4*$^{+}$, *Amp*^{R}, *nmt1*$^{+}$-promotor, p282 PstI, *Cpn* GiD DNA, ON 2516/2517	This study
1478	pJR2-3XU-*cpn1051*, *ura4*$^{+}$, *Amp*^{R}, *nmt1*$^{+}$-promotor, p282 PstI, *Cpn* GiD DNA, ON 2673/2674	This study
1479	pJR2-3XU-*cpn0129*, *ura4*$^{+}$, *Amp*^{R}, *nmt1*$^{+}$-promotor, p282 PstI, *Cpn* GiD DNA, ON 2565/2566	This study
1481	pJR2-3XU-*cpn0216-mCherry*, *ura4*$^{+}$, *Amp*^{R}, *nmt1*$^{+}$-promotor, p1335 BamHI, p1470 ON 2895/2896	This study
1482	pJR2-3XU-*cpn0443-mCherry*, *ura4*$^{+}$, *Amp*^{R}, *nmt1*$^{+}$-promotor, p1335 BamHI, p1428 ON 2966 /2967	This study
1484	pJR2-3XL-*cpn0216*, *LEU2*, *Amp*^{R}, *nmt1*$^{+}$-promotor, p270 NotI, p1470 ON 2472/2473	This study
1485	pJR2-3XL-*cpn0216-mCherry*, *LEU2*, *Amp*^{R}, *nmt1*$^{+}$-promotor, p270 NotI, p1481 ON 2472/3163	This study
1486	pJR2-3XL-*cpn0443-mCherry*, *LEU2*, *Amp*^{R}, *nmt1*$^{+}$-promotor, p270 NotI, p1482 ON 3040/3163	This study
1500	EB3-tdTomato Addgene 50708 from Erik Dent in tdTomato-N1	U. Fleig
1509	pJR2-3XL-*cpn0216*$^{82\text{-}145}$, *LEU2*, *Amp*^{R}, *nmt1*$^{+}$-promotor, p270 NotI, p1470 ON 3095/2473	This study
1510	pJR2-3XL-*cpn0216*$^{82\text{-}145}$*-mCherry*, *LEU2*, *Amp*^{R}, *nmt1*$^{+}$-promotor, p270 NotI, p1481 ON 3095/3163	This study
1511	pJR2-3XL-*cpn0443*$^{164\text{-}417}$, *LEU2*, *Amp*^{R}, *nmt1*$^{+}$-promotor, p270 NotI, p1428 ON 3096/3041	This study
1512	pJR2-3XL-*cpn0443*$^{164\text{-}417}$*-mCherry*, *LEU2*, *Amp*^{R}, *nmt1*$^{+}$-promotor, p270 NotI, p1482 ON 3096/3163	This study
1513	pJR2-3XL-*cpn0443*, *LEU2*, *Amp*^{R}, *nmt1*$^{+}$-promotor, p270 NotI, p1428 ON 3040/3041	This study
1518	*gst-tev-cpn0443*$^{164\text{-}417}$, *TRP1*, Amp^{R}, *lac* promoter, p1360 EcoRI, p1428 ON 3143/3144	This study
1523	pKM55-*gfp*, *Kan*^{R}*, TRP1*, CMV promoter	J. Hegemann
1524	pAE67-*gfp*, *Kan*^{R}*, TRP1*, CMV promoter	J. Hegemann

1525	pAE67-*gfp-cpn0443*, *Kan^R, TRP1*, CMV promoter, p1524 BamHI, p1428 ON 2946/2947	This study
1526	pAE67-*gfp-cpn0443$^{164-417}$*, *Kan^R*, *TRP1*, CMV promoter, p1524 BamHI, p1526 ON 3018/2947	This study
1527	pKM55-*cpn0443$^{164-417}$-gfp*, *Kan^R*, *TRP1*, CMV promoter, p1523 BamHI, p1526 ON 3019/2957	This study
1532	pAE67-*gfp-cpn0443$^{164-236}$*, *Kan^R*, *TRP1*, CMV promoter, p1524 BamHI, p1526 ON 3018/3137	This study
1533	pAE67-*gfp-cpn0443$^{237-331}$*, *Kan^R*, *TRP1*, CMV promoter, p1524 BamHI, p1526 ON 3138/3139	This study
1534	pAE67-*gfp-cpn0443$^{332-417}$*, *Kan^R*, *TRP1*, CMV promoter, p1524 BamHI, p1526 ON 3140/2947	This study
1546	pKM290-*cpn0443-flag*, *CAT, TRP1, NmPro* promoter, p2999 SmaI, p1526 ON 3209/3210, (isolated from XL_1 blue bacteria = methylated)	This study
1549	pKM290-*cpn0443-flag*, *CAT, TRP1, NmPro* promoter, p2999 SmaI, p1526 ON 3209/3210, (isolated from GM48 bacteria = non methylated)	This study
1554	pJR2-3XU-*cpn0474*, *ura4$^+$*, *Amp^R*, *nmt1$^+$*-promotor, p282 PstI, *Cpn* GiD DNA, ON 2305/2306	This study
1586	pJR2-3XU-*cpn0150*, *ura4$^+$*, *Amp^R*, *nmt1$^+$*-promotor, p282 PstI, *Cpn* GiD DNA, ON 2307/2308	This study
1587	pJR2-3XU-*cpn0350*, *ura4$^+$*, *Amp^R*, *nmt1$^+$*-promotor, p282 PstI, *Cpn* GiD DNA, ON 2295/2296	This study
1588	pJR2-3XU-*cpn0465*, *ura4$^+$*, *Amp^R*, *nmt1$^+$*-promotor, p282 PstI, *Cpn* GiD DNA, ON 2297/2298	This study
1589	pJR2-3XU-*cpn0585*, *ura4$^+$*, *Amp^R*, *nmt1$^+$*-promotor, p282 PstI, *Cpn* GiD DNA, ON 2293/2294	This study
1590	pJR2-3XU-*cpn0852*, *ura4$^+$*, *Amp^R*, *nmt1$^+$*-promotor, p282 PstI, *Cpn* GiD DNA, ON 2302/2327	This study
1591	pJR2-3XU-*cpn0998*, *ura4$^+$*, *Amp^R*, *nmt1$^+$*-promotor, p282 PstI, *Cpn* GiD DNA, ON 2833/2834	This study
1592	pJR2-3XU-*cpn1054*, *ura4$^+$*, *Amp^R*, *nmt1$^+$*-promotor, p282 PstI, *Cpn* GiD DNA, ON 2303/2304	This study
1596	pKM55-*cpn0443-gfp*, *Kan^R*, *TRP1*, CMV promoter, p1523 BamHI, p1526 ON 2956/2957	This study
1598	pAE67-*gfp-cpn0443$^{1-163}$*, *Kan^R*, *TRP1*, CMV promoter, p1524 BamHI, p1526 ON 2946/3273	This study

1600	pAE67-*gfp-cpn0443*$^{54-417}$, *Kan*^{R}, *TRP1*, CMV promoter, p1524 BamHI, p1526 ON 3274/2947	This study
1601	pJR2-3XL-*mCherry*, *LEU2, Amp*^{R}, *nmt1*$^{+}$-promotor, p270 NotI, (*mCherry*-BamHI restriction site) p1335 ON 3230/3163	This study
1657	pAE67-*gfp-ct005*, *Kan*^{R}, *TRP1*, CMV promoter, p1524 BamHI, *C. trachomatis LGV* L2 ON 3167/3168	This study
1658	pAE67-*gfp-ct005*$^{146-363}$, *Kan*^{R}, *TRP1*, CMV promoter, p1524 BamHI, *C. trachomatis LGV* L2 ON 3169/3168	This study
2999	pKM290-*flag*, *CAT, TRP1, NmPro* promoter (Hegemann lab code p2999)	J. Hegemann

2.9 Strains and cell lines

2.9.1 *S. pombe* strains

Plasmid number	Name, genes, and markers	Origin
#135	*mal3Δ::his3*$^{+}$, *leu1-32, ura4-D18, his3Δ, ade6-M210, h*$^{+}$	U. Fleig
#605	*his3-D1, ade6-M210, leu1-32, ura4-D18, h*$^{-}$	K. Gould
#224	*nda3-KM311, ade6-M210, leu*$^{-}$, *ura*$^{-}$, *h*$^{-}$	S. Sazer
#742	*tip1-pk-gfp::ura4*$^{+}$, *ade6-M210, ura4-D18, leu1-32, his3Δ, h*$^{-}$	U. Fleig
#880	*kan*^{R}*::nmt81::GFP-atb2*$^{+}$, *mal3Δ::ura4*$^{+}$, *ade6-M210, ura4-D18, leu1-32, his3Δ, h*$^{-}$	U. Fleig
#1318	*kan*^{R}*::nmt81::gfp-atb2*$^{+}$, *ade6-M210, his3D1, leu1-32, ura4-D18, h*$^{+}$	U. Fleig
#1309	*mal3-pk-gfp::ura4*$^{+}$, *ade6-M216, ura4-D18, leu1-32, his3-D1, h*$^{+}$	U. Fleig
#1478	*tea2Δ::his3*$^{+}$, *ade6-M210, his3-D1, leu1-32, ura4-D18, h*$^{-}$	McIntosh
#1495	*tea2-gfp::kan*^{R}, *ade6-M210, his3D1, leu1-32, ura4-D18, h*$^{-}$	U. Fleig
#1785	*tea1-gfp::ura4*$^{+}$, *ade6-M210, leu1-32, ura4-D18, h*$^{-}$	U. Fleig
#2023	*tea1Δ::ura4*$^{+}$, *ura4-D18, leu1-32, his3-D1, ade6-M216, h*$^{-}$	U. Fleig
#2087	*tip1Δ::ura4*$^{+}$, *ura4-D18, leu1, ade6-M210, h*^{90}	U. Fleig
#2129	*tea4-GFP::ura4+, leu1-32, ade6-M210, ura4-D18, his3-D1, h-*	U. Fleig
#2421	*klp5::kan*^{R}, *leu1, ura4, h*$^{-}$	T. Toda
#2422	*klp6::kan*^{R}, *leu1, ura4, his2/7, h*$^{+}$	T. Toda
#3091	*nda2-KM52, his3-D1, ade6-M216, leu1-32, ura4-D18, h*$^{+}$	This study

#3242	*cdc25-22 kan^R::nmt81::gfp-atb2$^+$, leu1-32, ura4-D18, h$^-$*	This study

2.9.2 *S. cerevisiae* strains

Strain number	Genotype	Origin
Cen.PK2	*Mata, leu2-3, 112, ura3-52, trp1-289, his3Δ1, MAL2-8c, SUC2*	Entian et al., 1999

2.9.3 *E. coli* strains

Strain	Genotype	Origin
XL_1-blue	*recA1, lac$^-$, endA1, gyrA46, thi, hsdR17, supE44, relA1,*	Stratagene, manufactured by the Fleig
BL21	*F ompT hsdSB* (rB-mB-) *gal dcm* (DE3)	Invitrogen, manufactured by the Fleig
Rossetta (DE3)	F$^-$ *ompT hsdS*$_B$(r_B^- m_B^-) *gal dcm* (DE3) pLysSRARE (Cam^R)	Novagen
GM48	F- LM- *thr-1, araC14, leuB6*(Am), *fhuA31, lacY1, tsx-78, glnX44*(AS), *galK2*(Oc), *galT22, λ$^-$, dcm-6, dam-3, thiE1*	Marinus, 1973

2.9.4 Adherent cell lines

Strain		Origin
HEp2	Epithelial laryngeal carcinoma cell line of human origin, HeLa morphology, 46 chromosomes	ECACC Nr.: 86030501;
U2OS	Epithelial adherent bone osteosarcoma cells of human origin	ATCC Nr.: CCL-23 ATCC Nr.: HTB-96

2.9.5 *Chlamydia*

Strain		Origin
C. pneumoniae GiD	Giessener isolate of a patient infected with acute broncitis	Jantos et al., 1997
C. trachomatis LGV L2/434/Bu	Bubo from human with LGV	ATCC Nr.: VR-902B

Koala *C. pneumoniae*	Nasal swab of a captive koala showing signs of respiratory illness	Myers et al., 2009

2.10 Media and cultivation

2.10.1 *S. pombe* media

Full medium (YE5S)	
Yeast extract	10 g
Adenine (2.7 mg/mL adenine hemisulfate)	150 mL
Uracil (2 mg/mL)	75 mL
Histidine (7.5 mg/mL)	20 mL
Leucine (7.5 mg/mL)	20 mL
Lysine (7.5 mg/mL)	20 mL
dH_2O	1515 mL
total	2 L

The prepared media and the separately prepared glucose were autoclaved. Solid media additionally contain 20 g/L Bacto agar. Glucose was then added to the autoclaved media at a final concentration of 3 %.

Minimal Medium (MM)	
Potassium phthalate monobasic	6 g
Na_2HPO_4 x $2H_2O$	5.5 g
50x Salt stock	40 mL
1000x Vitamine stock	2 mL
10000x Mineral stock	0.2 mL
dH_2O	1760 mL
total	2 L

The prepared media and the separately prepared glucose were autoclaved. Solid media additionally contain 20 g/L Bacto agar. Glucose was then added to the autoclaved media at a final concentration of 4 %. For the application of MM media, amino acids (arginine, leucine, lysine, histidine, uracil, and adenine) were added to a final concentration of 75 µg/mL (Moreno et al., 1991). If required, thiamine, TBZ, or MBC were added to the media after autoclaving when the media had cooled to ~50 °C. MM media plates containing TBZ or MBC were stored

at 4 °C.

50x Salt stock	
$MgCl_2$ x 6 H_2O	42,8 g
KCl	40.0 g
Na_2SO_4	1.6 g
$CaCl_2$ x 2 H_2O	0.58 g
dH_2O	800.0 mL

The salt stock solution was autoclaved and stored at 4 °C.

1000x Vitamin stock	
Nicotinic acid	10.0 g
Inositol	10.0 g
Sodium pantothenic acid	1.0 g
Biotin	10.0 mg
dH_2O	1 L

The vitamin stock solution was autoclaved and stored at 4 °C.

10000x Mineral stock	
Citric acid	10 g
H_3BO_3	5 g
$CuSO_4$ x $5H_2O$	4 g
MoO3	4 g
$MnSO_4$	4 g
$ZnSO_4$ x $7H_2O$	4 g
$FeCl_2$ x $6H_2O$	2 g
KI	1 g
dH_2O	1 L

The mineral stock solution was autoclaved and stored at 4 °C.

For the regulation of gene expression under the control of *nmt*$^+$-promoters:

Thiamine	**Stock**
5 µg/mL	10 mg/mL in dH_2O

Thiamine was added to MM media after autoclavation when the media had cooled to ~50 °C

(Beln Moreno et al., 2000). Thiamine was stored at RT.

For the screening for TBZ/MBC-sensitivity:

Tiabendazole (TBZ)	**Stock**
1.5 to 12 µg/mL	10 mg/mL in DMF

TBZ was added to MM media after autoclavation when the media had cooled to ~50 °C (Beln Moreno et al., 2000). TBZ was stored at -20 °C.

Methyl-benzimidazole (MBC)	**Stock**
0.5 to 4.5 µg/mL	5 mg/mL in DMSO

MBC was added to MM media after autoclavation when the media had cooled to ~50 °C (Beln Moreno et al., 2000). MBC was stored at -20 °C.

Malt medium (solid)	
Bacto malt extract	30.0 g
Histidine	75.0 mg
Leucine	75.0 mg
Adenine	75.0 mg
Uracil	75.0 mg
Bacto agar	20.0 g
H_2O	1 L
total	1 L

The media have to be adjusted to a pH of 5.5 with 10 M NaOH. The prepared media and the separately prepared glucose were autoclaved.

Life fluorescent medium (FLM)	
Pre-mix	20 mL
Gluscose	20 mL
50x salt stock	8 mL
100x vitamin stock	400 µL
10000x mineral stock	40 µL
Adenine (2.7 mg/mL adenine hemisulfate)	15 mL

Arginine (7.5 mg/mL)	4 mL
Histidine (7.5 mg/mL)	4 mL
Lysine (7.5 mg/mL)	4 mL
dH_2O	300 mL
Bacto agar	20.0 g
H_2O	1 L

The prepared medium was sterile filtrated. LFM-agar includes additionally 2 % agarose (0.4 g in 20 mL FLM). Depending on the plasmid-selective conditions, either 15 mL uracil (2 mg/mL) or 4 mL leucine (7.5 mg/mL) was required.

Pre-mix	
Na_2HPO_4 x 2 H_2O	5,5 g
Potassium phthalate monobasic	6.0 g
Glutamic acid	2.0 g
dH_2O	100.0 mL

The pre-mix was sterile filtrated and stored at 4 °C.

Glucose	
Glucose	40,0 g
dH_2O	100.0 mL

The glucose solution was sterile filtrated and stored at 4 °C.

2.10.2 *S. cerevisiae* media

Synthetic defined media (SD)	
Ammonium sulfate	5 g
Drop-out mix	2 g
Yeast nitrogen base	1.7 g
dH_2O	900 mL
total	1 L

The media have to be adjusted to a pH of 5.5 with 10 M NaOH. The prepared media and the separately prepared glucose were autoclaved. Solid media additionally contain 20 g/L Bacto agar. Glucose was then added to the autoclaved media at a final concentration of 2 %.

Drop-out mix			
Adenine	0.5 g	Lysine	2 g
Alanine	2 g	Methionine	2 g
Arginine	2 g	Para aminobenzoic acid	0.2 g
Aspartic acid	2 g	Phenylalanine	2 g
Cysteine	2 g	Proline	2 g
Glutamic acid	2 g	Serine	2 g
Glutamine	2 g	Tryptophan	2 g
Histidine	2 g	Tyrosine	2 g
Inositol	2 g	Uracil	2 g
Isoleucine	2 g	Valine	2 g
Leucine	2 g		

The drop-out mix was mixed well and stored at 4 °C. Depending on the application, the corresponding amino acid must be left out of the mixture.

Full medium (YPD)	
Peptone	20.0 g
Bacto yeast extract	10.0 g
Tryptophane (5 mg/mL)	4.0 mL
Adenine (2.7 mg/mL adenine hemisulfate)	2.0 mL
dH_2O	1 L
total	1 L

The prepared media and the separately prepared glucose were autoclaved. Solid media additionally contain 27 g/L Bacto agar. Glucose was then added to the autoclaved media at a final concentration of 4 % (Kaiser et al., 1994).

2.10.3 *E. coli* media

Lysogeny broth medium (LB)	
Tryptone	10.0 g
Bacto yeast extract	5.0 g
NaCl	5.0 g
dH_2O	1 L
total	1 L

The prepared media and the separately prepared glucose were autoclaved. Solid media additionally contain 20 g/L Bacto agar. Glucose was then added to the autoclaved media at a final concentration of 4 %. For selection 50 µg/mL ampicillin, 12.5 µg/mL kanamycin, or 20 µg/mL chloramphenicol were added after autoclavation when the media had cooled to ~50 °C. The LB agar plates containing the antibiotics were stored at 4 °C.

For the screening for antibiotic resistance:

Ampicillin (amp)	**Stock**
50 µg/mL	200 mg/mL in dH_2O

Kanamycin (kan)	**Stock**
12.5 µg/mL	50 mg/mL in dH_2O

Chloramphenicol (CAT)	**Stock**
20 µg/mL	20 mg/mL in 96 % EtOH

The stock solution of amp, kan, or CAT were stored at -20 °C and added to LB media after autoclaving when cooled to ~50 °C. LB agar plates containing the antibiotics were stored at 4 °C.

2.10.4 Mammalian cell media

Full cell culture medium (+/+)	
FKS	50 mL
Amphotericin (200mM)	5 mL
Vitamin	5 mL
Non-essential amino acids	5 mL
Gentamicin 50 µg/mL	500 µL
DMEM GlutaMAX™	500 mL

The +/+ media was stored at 4 °C.

Antibiotic-free cell culture medium (+/-)	
FKS	50 mL
Vitamine	5 mL

Non-essential amino acids	5 mL
DMEM GlutaMAX™	500 mL

The +/- media was stored at 4 °C.

Transfection medium (-/-)	
Vitamine	5 mL
Non-essential amino acids	5 mL
DMEM GlutaMAX™	500 mL

The -/- media was stored at 4 °C.

2.11 Buffers and solutions

2.11.1 Buffers for plasmid isolation

P1 buffer	
Tris/ HCl pH 8	50 mM
EDTA	100 mM
RNase	100 µg/mL

The P1 buffer was prepared without RNase and autoclaved. After autoclaving and cooling, RNase was added to the buffer and stored at 4 °C.

P2 buffer	
NaOH	200 mM
SDS	2 %

The P2 buffer was stored at RT.

P3 buffer	
Potassium acetate pH 5.5 EDTA	3 M

The P3 buffer was stored at RT.

2.11.2 Buffers and solutions for biochemical methods

10x PBS	
NaCl	80 g

Na_2HPO_4	14.4 g
KH_2HPO_4	2.4 g
KCl	2 g
dH_2O	1 L

The 10x PBS buffer has to be adjusted to a pH of 7.4 with 10 M NaOH. The prepared buffer was stored at RT. The 10x PBS buffer was diluted with water to 1x PBS buffer. For the 3 % blocking solution, 0.05 % Tween 20 was added to 1x PBS and stored at RT.

HB15-buffer	
100 mM pNitrophenylp.	7.5 mL
100 mM $MgCl_2$	7.5 mL
100 mM EGTA	7.5 mL
dH_2O	6.5 mL
500 mM ß-Glycerophosphat	6 mL
250 mM Mops	5 mL
1 mM Natriumorthovanate	5 mL
20 % TritonX100	2.5 mL
100 mM PMSF	500 µL
1 M DTT	50 µL
Complete Protease Inhibitor	one tab

The HB15 buffer was stored at 4 °C.

4x resolving buffer	
1.5 M Tris/HCl, pH 8,8	960 mL
10 % SDS	40 mL

The 4x resolving buffer was stored at RT.

4x stacking buffer	
0.5 M Tris/HCl, pH 6,8	960 mL
10 % SDS	40 mL

The 4x stacking buffer was stored at RT.

1x running buffer	
10x running buffer (Tris + Glycin)	100 mL
10 % SDS	10 mL
dH_2O	ad 1 L

The running buffer was stored at RT.

Towbin buffer	
Tris	3.0 g
Glycin	14.4 g
Methanol	200 mL
dH_2O	Ad 1 L

The Towbin buffer must have a pH between 8.1 and 8.5 and was stored at RT.

Detection buffer (DIG P3)	
Tris/ HCl pH 9.5	0.1 M
NaCl	0.1 M
$MgCl_2$	50 mM
dH_2O	ad 1 L

The DIG P3 buffer was stored at 4 °C.

3 % Blocking solution	
Milk powder	15 g
0,05 % Tween 20 in 1 x PBS	500 mL

The blocking solution was stored at RT.

Coomassie solution	
Coomassie Brilliant Blue G-250	60 mg
dH_2O	1 L

The coomassie solution have to be adjusted to 35 mM with 37 % HCl and was stored at RT in the dark.

Lysis buffer	
Tris/ HCl pH 7.5	10 mM

NaCl	150 mM
EDTA	0.5 mM
NP-40	0.5 %

The lysis buffer was stored at 4 °C.

Phosphoysis buffer	
Tris	20 mM
NaCl	150 mM
Na_2SO_4	1 mM
EDTA	2 mM
Triton	1 %
NP-40	1 %

The phosphoysis buffer was stored at 4 °C.

Wash/Dilution buffer	
Tris/ HCl pH 7.5	10 mM
NaCl	150 mM
EDTA	0.5 mM

The wash/dilution buffer was stored at 4 °C.

General tubulin buffer	
0.5 M PIPES pH 7.0	1.6 mL
1 M $MgCl_2$ (filtered)	10 µL
100 mM EGTA	100 µL
dH_2O	8.3 mL

The genal tubulin buffer was stored at 4 °C.

Cushion buffer	
0.5 M PIPES pH 7.0	1.6 mL
1 M $MgCl_2$ (filtered)	10 µL
100 mM EGTA	100 µL
60 % Glycerol	6 mL
dH_2O	2.3 mL

The cushion tubulin buffer was stored at 4 °C.

3 Methods

3.1 Culturing of *S. pombe*

3.1.1 Culturing *S. pombe* cells for live-cell imaging

Transformed *S. pombe* cells were pre-cultured for 24 h at 25 °C in 5 mL MM under selective conditions and the presence 5 µg/mL thiamine. Then, cells were washed three times with dH_2O and then cultured at an OD_{600} of 0.03 in 200 mL LFM without thiamine o/n at 25 °C to an OD_{600} of 1. Cells with an adequate OD concentration (log phase) were used for live-cell imaging.

3.1.2 Culturing *S. pombe* cells for serial dilution patch test analysis

Transformed *S. pombe* cells were cultured o/n at the corresponding temperature in 5 mL MM under selective conditions and the absence or presence 5 µg/mL thiamine.

3.2 Culturing of mammalian cell lines

3.2.1 Culturing of HEp2 and U2OS cells

After thawing, mammalian cells were washed with complete medium (+/+) and then cultured in a 25 cm^2 cell culture flask at 37 °C and 6 % CO_2 in +/+ medium in the presence of 3 µL plasmocin. ~70 % confluent cells were solved from the bottom of the flask with a 0.5x trypsin/EDTA solution, washed, and then transferred to an 80 cm^2 cell culture flask containing +/+ medium and in the presence of plasmocin.

3.2.2 Transfection of mammalian cells

Human U2OS cells were cultured on coverslips in a 24-well plate at 37 °C and 6 % CO_2 in an antibiotic-free cell culture medium (+/-). At least 1 hour before transfection, the medium was changed from ~70 % confluent-grown cells to 500 µL/well +/- medium. The transfection mixture containing 100 µL transfection medium (-/-), 0.5 µg plasmid-DNA, and 2 µL/500 µL well TurboFect was mixed well and incubated at RT for 20 minutes. The transfection mixture was

then added to the confluent cells and incubated at 37 °C and 6 % CO_2 for 18 hours.

3.2.3 Fixation of transfected mammalian cells

U2OS cells were washed three times with HBSS and then fixed by adding 500 µL of fresh and 37 °C pre-warmed 3 % PFA in PBS for 15 minutes at RT. Fixed cells were washed three times with HBSS and then stored in HBSS at 4 °C.

3.3 Culturing of *C. pneumoniae*

3.3.1 Infection of mammalian cells with *Chlamydia*

Human HEp2 cells were cultured on coverslips in a 24-well plate at 37 °C and 6 % CO_2 in cell culture medium (+/+). The medium of ~70% confluent-grown cells was replaced by 500 µL/well +/+ medium containing 1 µL *C. pneumoniae* GiD gradient (MOI of 1). Plates were then centrifuged at 30 °C and 28,000 rpm for 1 hour. The medium was replaced with 1 mL/well +/+ medium containing 12 µL/mL cyclohexamide and incubated for 24 to 48 hours at 37 °C and 6 % CO_2.

3.3.2 Fixation of infected mammalian cells

Infected HEp2 cells were washed three times with HBSS and then fixed by adding 500 µL ice-cold methanol for 15 minutes at RT. Cells were washed three times with HBSS and permeabilized for 15 minutes by adding 500 µL of ice-cold 3 % PFA. Cells were then washed three times with HBSS and then stored in HBSS at 4 °C.

3.4 Molecular biological methods

3.4.1 Generation of a chlamydial gene bank library

The *C. pneumoniae* GiD genome (Jantos et al., 1997) was used to generate a *C. pneumoniae* genebank library. All steps of the generation procedure were briefly listed here and described in more detail in the following sections.

C. pneumoniae GiD genome was used as a template to amplify 116 ORFs encoding the genes of interest by using the Q5 High-Fidelity DNA polymerase (section: 3.4.2). By homolog recombination into the *S. cerevisiae* strain CenPK, the amplified ORFs were transformed and integrated into a linearized thiamine-repressive pJR2-3XU vector under the control of the no-message in thiamine (*nmt1*$^{+}$) promoter under plasmid-selective conditions (Entian et al., 1999) (section: 3.4.3, 3.4.4.1). Successfully transformed *S. cerevisiae* transformants were used to isolate plasmid DNA isolation (section: 3.4.6.1) and then electroporated into *E. coli* XL_1 blue cells (section: 3.4.5.3). Next, plasmid DNA was isolated from selective *E. coli* transformants (section: 3.4.6.2/3.4.6.3). The qualitative restriction was used to control the integration of ORFs. Genes showing the restriction patterns for correct integration were sequenced by GATC-Sanger sequencing (section: 3.4.7).

3.4.1.1 Selection markers

The backbone expression vectors contain yeast selection markers such as uracil, leucine, and tryptophan and bacterial selection markers such as ampicillin, kanamycin, and chloramphenicol to control the transformation of plasmids. The plasmid uptake enables the survival of yeast on MM medium, while the bacterial resistance marker enables the survival of bacterial clones in the presence of antibiotics. The following yeast and bacterial markers were used to verify successful plasmid transformation:

Backbone vector	**Used yeast marker**	**Used bacterial marker**
p282	*ura4*$^{+}$	*Amp*^{R}
p270	*LEU*	*Amp*^{R}
p1335	*ura4*$^{+}$	*Amp*^{R}
p1360	*TRP1*	*Amp*^{R}
p1523	*TRP1*	*Kan*^{R}
p1524	*TRP1*	*Kan*^{R}
p2999	*TRP1*	*CAT*

3.4.2 PCR-reaction (Polymerase Chain Reaction) and gel electrophoresis

The Q5 High-Fidelity DNA Polymerase is characterized by high efficiency and extremely low error rates. Therefore, this high-fidelity polymerase was used for the amplification of chlamydial ORFs.

Q5 High-Fidelity DNA polymerase reaction	
5X Q5 Reaction Buffer	5 µL
10 mM dNTPs (dATP, dCTP, dGTP, dTTP)	0.5 µL
10 µM Forward Primer	1.25 µL
10 µM Reverse Primer	1.25 µL
Template DNA	x µL
Q5 High-Fidelity DNA Polymerase	0.25 µL
5X Q5 High GC Enhancer	5 µL
dH_2O	x µL
total	25 µL

1 ng to 1 µg genomic DNA or 1 pg to 10 ng plasmid DNA was used as a DNA template.

PCR cycler program

PCR Phase	Temp.	Duration	Cycles
Initial Denaturation	98 °C	10 min	
Denaturation	98 °C	1 min	35 cycles
Annealing	T_a °C	2.5 min	
Elongation	72 °C	1 min/kb	
Final Elongation	72 °C	2 min	

The recommended "NEB Tm Calculator v1.13.0" from New England was used to determine the annealing temperature for each DNA construct.

Gel electrophoresis

Amplified PCR fragments were usually visualized on a 0.8 to 1 % agarose gel. By adding ethidiumbromid and separating the DNA fragments using electrophoresis at 100 to 180 V, the DNA fragments were visualized under UV light.

3.4.2.1 Amplification of chlamydial genes for the integration into the expression vector p282

To generate a chlamydial gene bank, selected genes were amplified using Q5 high-fidelity DNA polymerase as described in section 3.4.2. The *C. pneumoniae*GiD genome, a Giessen isolate of a patient infected with acute broncitis, served as the DNA template (Jantos et al., 1997). The oligonucleotides contain homologous sites for the integration into the expression vector p282 (pJR2-3XU) linearized with PstI.

Chlamydial gene	Gene size	Oligonucleotides	Sequenced chlamydial gene differs from the GiD genome
cpn0007*	2895 nt	2482/2483	
cpn0026*	867 nt	2617/2618	
cpn0041	1350 nt	2619/2620	
cpn0045	1725 nt	2480/2481	Insert of 10 nt, changed aa sequence
cpn0061*	678 nt	2841/2842	
cpn0065*	1752 nt	2494/2495	
cpn0066	1734 nt	2621/2622	
cpn0067	1104 nt	2623/2624	
cpn0107	774 nt	2611/2612	
cpn0124*	1458 nt	2627/2628	
cpn0126	2280 nt	2629/2630	
cpn0129*	1185 nt	2565/2566	
cpn0131	1035 nt	2631/2632	
cpn0132*	978 nt	2478/2479	nt and aa exchange
cpn0147	450 nt	2498/2499	
cpn0150*	4614 nt	2307/2308	nt and aa exchange
cpn0157	429 nt	2633/2634	
cpn0164	504 nt	2635/2636	
cpn0166	336 nt	2490/2491	
cpn0169	795 nt	2637/2638	
cpn0173	276 nt	2462/2463	
cpn0186	1173 nt	2639/2640	

cpn0203	798 nt	2641/2642
cpn0212	1182 nt	2460/2461
cpn0214	1215 nt	2476/2477
cpn0215	1260 nt	2474/2475
cpn0216	438 nt	2472/2473
cpn0218	480 nt	2518/2519
cpn0241	1155 nt	2569/2570
cpn0242	435 nt	2571/2572
cpn0255	850 nt	2645/2646
cpn0262*	846 nt	2843/2844
cpn0284	498 nt	2488/2489
cpn0285	1548 nt	2647/2648
cpn0288	1149 nt	2567/2568
cpn0291	531 nt	2579/2580
cpn0292	612 nt	2649/2650
cpn0308	366 nt	2468/2469
cpn0312	456 nt	2575/2576
cpn0350	507 nt	2295/2296
cpn0357	852 nt	2651/2652
cpn0365	1035 nt	2486/2487
cpn0366	468 nt	2464/2465
cpn0370	1116 nt	2577/2578
cpn0371*	360 nt	2470/2471
cpn0372	318 nt	2466/2467
cpn0381	1776 nt	2653/2654
cpn0404	1020 nt	2599/2600
cpn0409	486 nt	2500/2501
cpn0431	336 nt	2581/2582
cpn0432	306 nt	2655/2656
cpn0440	639 nt	2657/2658
cpn0441*	951 nt	2512/2513
cpn0442*	519 nt	2563/2564
cpn0443*	1254 nt	2561/2562

cpn0456*	1209 nt	2696/2697
cpn0465*	345 nt	2297/2298
cpn0467	2805 nt	2698/2699
cpn0474	1770 nt	2305/2306
cpn0480*	657 nt	2583/2584
cpn0481	1661 nt	2661/2662
cpn0488	333 nt	2813/2814
cpn0491	1020 nt	2801/2802
cpn0512	1863 nt	2510/2511
cpn0517*	840 nt	2484/2485
cpn0518	975 nt	2514/2515
cpn0523	528 nt	2663/2664
cpn0524	1080 nt	2754/2755
cpn0525	765 nt	2492/2493
cpn0537	360 nt	2756/2757
cpn0544*	1008 nt	2811/2812
cpn0554	291 nt	2587/2588
cpn0556	591 nt	2589/2590
cpn0565	1101 nt	2585/2586
cpn0585	1956 nt	2293/2294
cpn0592	312 nt	2807/2808
cpn0601	321 nt	2591/2592
cpn0602	1005 nt	2516/2517
cpn0648	1002 nt	2506/2507
cpn0658	717 nt	2508/2509
cpn0671	429 nt	2809/2810
cpn0729	1269 nt	2817/2818
cpn0746	1596 nt	2516/2517
cpn0753	849 nt	2496/2497
cpn0755*	1206 nt	2597/2598
cpn0770*	798 nt	2601/2602
cpn0813	1068 nt	2700/2701
cpn0815	754 nt	2702/2703

cpn0821	1005 nt	2805/2801	
cpn0829	558 nt	2665/2666	
cpn0830*	519 nt	2667/2668	
cpn0834	465 nt	2758/2759	
cpn0844	1464 nt	2839/2840	
cpn0850*	1101 nt	2704/2705	
cpn0852	2301 nt	2302/2327	
cpn0869	747 nt	2603/2604	
cpn0879	798 nt	2799/2800	
cpn0906	429 nt	2504/2505	
cpn0909	333 nt	2795/2796	
cpn0912*	1635 nt	2502/2503	Insert of 27 nt, Insert of 9 aa
cpn0930	477 nt	2669/2670	
cpn0938	477 nt	2605/2606	
cpn0966*	1293 nt	2708/2709	
cpn0994*	2046 nt	2762/2763	
cpn0998*	2733 nt	2833/2834	
cpn1003	708 nt	2607/2608	
cpn1008	1299 nt	2764/2765	
cpn1027*	1584 nt	2671/2672	
cpn1029	840 nt	2766/2767	
cpn1046	1089 nt	2712/2713	
cpn1051	312 nt	2673/2674	
cpn1054*	2436 nt	2303/2304	
cpn1055	831 nt	2675/2676	
cpn1060	1935 nt	2714/2715	
cpn1062*	1665 nt	2716/2717	
cpn1070*	1371 nt	2718/2719	

The *C. pneumoniae* GiD genome served as the DNA template for the amplification of the individual chlamydial genes. The annealing temperature was 55 °C. The asterisk (*) marks the chlamydial genes that have variations in the DNA sequence of the GiD genome and the *C. pneumoniae* CWL029 sequence published in the KEGG database.

The amplified chlamydial genes *cpn0045, cpn0132, cpn0150,* and *cpn0912* of this study contain nucleotide sequence alterations compared to the GiD genome which consequently leads to amino acid changes. A detailed overview of the nucleotide changes is shown in **Supplementary Table 1**.

3.4.2.2 Amplification of chlamydial genes for the integration into the expression vector p1335

Selected genes were amplified as described in section 3.4.2. The oligonucleotides contain homologous sites for the integration into the expression vector p1335 (pJR2-3XU) linearized with BamHI. By using this vector, genes were C-terminally fused with the *mCherry*-fluorescence tag.

Chlamydial gene	Gene size	Oligonucleo-tides	DNA template
cpn0216	435 nt	2895/2896	p1270
cpn0443	1251 nt	2966/2967	p1428

The annealing temperature was 55 °C. No DNA sequence variations occurred.

3.4.2.3 Amplification of chlamydial genes for the integration into the expression vector p270

Selected genes and genes fused to *mCherry* were amplified as described in section 3.4.2. The oligonucleotides contain homologous sites for the integration into the expression vector p270 (pJR2-3XL) plasmid linearized with NotI.

Chlamydial gene	Gene size	Oligonucleo-tides	DNA template
cpn0216	438 nt	2472/2473	p1470
cpn0216-mCherry	1146 nt	2472/3163	p1481
cpn0216$^{82\text{-}145}$	199 nt	3095/2473	p1470

cpn0216$^{82\text{-}145}$*-mCherry*	906 nt	3095/3163	p1481
cpn0443	1254 nt	3040/3041	p1428
cpn0443-mCherry	1962 nt	3040/3163	p1482
cpn0443$^{164\text{-}417}$	768 nt	3096/3041	p1428
cpn0443$^{164\text{-}417}$*-mCherry*	1476 nt	3096/3163	p1482

The annealing temperature was 55 °C. No DNA sequence variations occurred.

3.4.2.4 Amplification of chlamydial genes for the integration into the expression vector p1524

Selected genes were amplified as described in section 3.4.2. The oligonucleotides contain homologous sites for the integration into the expression vector p1524 (pAE67) plasmid linearized with BamHI. By using this vector, genes were N-terminally fused with the *GFP*-fluorescence tag.

Chlamydial gene	**Gene size**	**Oligonucleo-tides**	**DNA template**
cpn0443	1254 nt	2946/2947	p1428
cpn0443$^{164\text{-}417}$	768 nt	3018/2947	p1526
cpn0443$^{164\text{-}236}$	225 nt	3018/3137	p1526
cpn0443$^{237\text{-}331}$	291 nt	3138/3139	p1526
cpn0443$^{332\text{-}417}$	264 nt	3140/2947	p1526
cpn0443$^{1\text{-}163}$	489 nt	2946/3273	p1526
cpn0443$^{54\text{-}417}$	1098 nt	3274/2947	p1526
ct005	1092 nt	3167/3168	*C. trachomatis LGV* serovar L2
ct005$^{146\text{-}363}$	696 nt	3169/3168	*C. trachomatis LGV* serovar L2

The annealing temperature was 55 °C. No DNA sequence variations occurred.

3.4.2.5 Amplification of chlamydial genes for the integration into the expression vector p1523

Selected genes were amplified as described in section 3.4.2. The oligonucleotides contain

homologous sites for the integration into the expression vector p1523 (pKM55) linearized with BamHI. By using this vector, genes were C-terminally fused with the *GFP*-fluorescence tag.

Chlamydial gene	Gene size	Oligonucleo-tides	DNA template
cpn0443	1254 nt	3019/2957	p1526
cpn0443$^{164-417}$	768 nt	2956/2957	p1526

The annealing temperature was 55 °C. No DNA sequence variations occurred.

3.4.2.6 Amplification of chlamydial genes for the integration into the expression vector p1360

Selected genes were amplified as described in section 3.4.2. The oligonucleotides contain homologous sites for the integration into the expression vector p1360 (*gst-tev*) linearized with EcoRI. By using this vector, *cpn0443*$^{164-417}$ was N-terminally fused with the *gst-tev* tag.

Chlamydial gene	Gene size	Oligonucleo-tides	DNA template
cpn0443$^{164-417}$	768 nt	3143/3144	p1428

The annealing temperature was 55 °C. No DNA sequence variations occurred.

3.4.2.7 Amplification of chlamydial genes for the integration into the expression vector p2999

Selected genes were amplified as described in section 3.4.2. The oligonucleotides contain homologous sites for integration into the expression vector p2999 (pKM290) linearized with SmaI. Using this vector, the *cpn0443* was fused C-terminally with the *flag*-tag.

Chlamydial gene	Gene size	Oligonucleo-tides	DNA template
cpn0443	1251 nt	3209/3210	p1526

The annealing temperature was 55 °C. No DNA sequence variations occurred.

3.4.3 Linearization of the expression vector

According to the manufacturer's instructions, 100 ng of vector DNA was digested with the appropriate restriction enzyme and buffer o/n at 37 °C and then tested on an agarose gel. The following plasmids were used for the linearization of the vectors:

Expression vectors	Restriction enzyme	Buffer and reaction temperature
p282	PstI	Buffer O, 37 °C
p270	NotI	Buffer O, 37 °C
p1335	BamHI	Unique buffer BamHI, 37 °C
p1360	EcoRI	Unique buffer EcoRI, 37 °C
p1523	BamHI	Unique buffer BamHI, 37 °C
p1524	BamHI	Unique buffer BamHI, 37 °C
p2999	SmaI	Buffer Tango, 30 °C

3.4.4 Transformation of plasmid DNA into eukaryotes

3.4.4.1 Transformation of *S. cerevisiae* via homolog recombination

Integration of an insert into a linearized expression vector was performed by homologous recombination via transformation in *S. cerevisiae* using the lithium acetate method of Gietz and Woods, 2006. Accordingly, the amplified DNA fragment contained 40 nucleotide overlaps at both sites that were homologous to the target site of the linearized vector. Therefore, *S. cerevisiae* CenPK cells were precultured in 5 mL YPD o/n at 30 °C. At an OD_{600} of 0.1 to 0.2, 50 mL of YPD was cultured for 4 to 5 hours at 30 °C to an OD^{600} of 1 (log phase). Then, the cell culture was centrifuged at 3,500 rpm for 5 minutes and washed with dH_2O. The pellet was then resuspended in 1 mL of 0.1 M LiAc pH 8.4-8.9 and centrifuged at 13,000 rpm for 10 seconds. 2x 10^9 cells/mL were resuspended in 0.1 M LiAc. For each transformation, 50 µL CenPK cells/sample was centrifuged at 13,000 rpm for 10 seconds. The cell pellet was resuspended in: 240 µL 50% PEG 4000, 36 µL 1 M LiAc pH 8.4-8.9, 50 µL boiled carrier DNA (2 mg/mL), and 34 µL DNA/plasmid mix (amplified PCR product and linearized plasmid diluted in dH_2O). The following controls without DNA were used: water control, linearized vector control, and non-

linearized vector control to demonstrate transformation efficiency. Samples and controls were incubated at 30 °C for 30 minutes, heat-shocked at 42 °C for 30 minutes, and after centrifugation at 13,000 rpm for 10 seconds, 10 % and 90 % of the samples and controls were plated on plasmid-selective SD plates in 200 µL dH_2O and cultured at 30 °C.

3.4.4.2 Transformation of *S. pombe*

The lithium acetate method of Okazaki et al., 1990 was used to transform genetically modified plasmids into *S. pombe* cells. *S. pombe* strains were cultured o/n in 100-200 mL YES medium at optimal temperature conditions depending on the cell strain. The cell number of 1x 10^8 cells/transformation was determined and the cells were centrifuged at 3,500 rpm for 3 minutes. The cell pellet was then washed with 2 mL 0.1 M LiAc pH 4.9, centrifuged at 3,500 rpm for 3 minutes, resuspended in 70 µL 0.1 M LiAc/transformation, and incubated for 1 hour. 100 µL LiAc-treated cells were resuspended with: 0.5 µg plasmid DNA and 290 µL 50 % PEG 4000, and incubated for 1 hour. An additional water control without DNA was used to check the efficiency of transformation. All samples were heat-shocked at 43 °C for 15 minutes and centrifuged at 3,500 rpm for 5 minutes. Cell pellets were then resuspended in YE5S media and cultured for at least 1 hour. The transformed cells were washed twice with dH_2O and then resuspended in 1 mL of dH_2O to deliver 1x 50 µL and 1x 100 µL to MM selective plates.

3.4.5 Transformation of plasmid DNA into prokaryotes

3.4.5.1 Transformation of *C. pneumoniae*

Passage 0: 71 µL/transformation of *C. pneumoniae* koala isolate LPCoLN was centrifuged at 15,000 rpm for 20 minutes at 4 °C. The EB pellet was sonicated in 100 µL $CaCl_2$ before adding 15 µg plasmid-DNA (isolated from GM48) for a 30 minutes incubation at RT. 50 % of an 80 cm^2 cell culture flask containing ~70 % confluent HEp2 cells were washed with complete medium (+/+) and resuspended in 100 µL $CaCl_2$. (200 µL/80 cm^2 culture flasks). Then, 100 µL of cells were added to EBs and incubated for 20 minutes at RT on the shaker. 5 mL +/+ media and 12 µL/mL cycloheximide were added to the transformation mixture of HEp2 cells, *C. pneumoniae* EBs, and plasmid-DNA. Then the mixture was transferred to a 25 cm^2 culture

flask for centrifugation at 13,000 rpm for 1 hour at 37 °C. Transformed cells were incubated for 4 days at 37 °C and 6 % CO_2.

Passage 1: HEp2 cells were scraped from the bottom of the flask, sonicated, and centrifuged for 15 minutes at 15,000 rpm and 4 °C. Different dilutions (1:5, 1:10) of the supernatant were added to HEp2 cells grown in a 6-well plate, replacing the medium by 2 mL of +/+ medium. Plates were then centrifuged at 28,000 rpm for 1 hour at 37 °C. The media was then replaced with 2 mL of +/+ media, 5 µL/1mL chloramphenicol, and 12 µL/1mL cycloheximide and incubated for 4 days at 37 °C and 6 % CO_2.

Passage 2: Cells were treated such as for passage 1. Additionally, immunofluorescence microscopy was used to verify whether the transformation into *C. pneumoniae* was successful. Detection of the bacterial surface protein Momp with an anti-momp antibody; detection of the Inc membrane protein CPn0147-myc (located on the inclusion membrane) with an anti-myc antibody; detection of CPn0443-flag with an anti-flag antibody; detection of DNA with DAPI.

Passage 3: Selection pressure was increased by using higher concentrations of chloramphenicol.

3.4.5.2 1-minute transformation into bacteria

The protocol for rapid 1-minute transformation with BL21 DMSO-competent *E. coli* is applicable for plasmids carrying an ampicillin cassette and was modified from Golub, 1988. Plasmids carrying a restriction cassette for kanamycin or chloramphenicol cause low efficiency. XL_1-blue electrocompetent *E. coli* and the electroporation method were used to transform these plasmids (section 3.4.5.3).

1 µL of 0.5 to 1 µg DNA was added to 3 µL of DMSO-competent cells, thawed on ice, and incubated at 42 °C for 1 minute. After 1 minute, the tube was placed on ice as soon as possible and 100 µL of pre-warmed LB media was added. Then, the *E. coli* DNA mixture was plated onto pre-warmed LB plates containing the appropriate resistances and incubated at 37 °C o/n.

3.4.5.3 Electroporation of bacteria

The electroporation method is very efficient and is suitable for the selection of ampicillin, kanamycin, and chloramphenicol. The protocol was derived from Golub, 1988. Different concentrations/volumes were used depending on the resistant cassette and the mini/midi preparation of the plasmid (section: 3.4.6.2/3.4.6.3).

Plasmid and XL_1-blue electrocompetent *E. coli* were thawed, stored, and prepared on ice. LB media and electroporation cuvettes were filled with 200 to 400 µL of dH_2O and stored on ice. 15 to 45 µL of electrocompetent cells were mixed with 1 to 100 µL of the plasmid and transferred to the prepared dH_2O in the electroporation cuvette.

Preparation	Isolated plasmid	*E. coli*	dH_2O
Mini (*Amp^R*)	50 µL	15 µL	200 µL
Mini (*Kan^R, CAP^R*)	100 µL	45 µL	400 µL
Midi (*Amp^R, Kan^R, CAP^R*)	1 µL	15 µL	200 µL

All samples were electroporated at 2.1 kV, 200 Ω, 25 µF. After the electroporation impulse, 1 mL of cold LB medium was added to the samples as soon as possible. Then cells regenerated at 37 °C for 1 hour. Samples were centrifuged at 13,000 rpm for 2 minutes, and 10 % or 90 % were plated onto the pre-warmed LB plates with the appropriate resistances for incubation o/n at 37 °C.

3.4.6 Plasmid Isolation methods

3.4.6.1 *S. cerevisiae* plasmid DNA isolation

The alkaline lysis method for isolation of plasmids from *S. cerevisiae* was adopted from Birnboim and Doly, 1979. Transformed *S. cerevisiae* was cultured in 5 mL SD media lacking relevant amino acids for selection o/n at 30 °C. For each plasmid of interest, three grown *S. cerevisiae* colonies were prepared and tested. 2 mL of cells were transferred to 2 mL screw-cap tubes, centrifuged at 3,500 rpm for 5 minutes, washed with dH_2O, and centrifuged again. Then, pellets were resuspended in 500 µL of P1 buffer including RNase. Additionally, 500 µL of P2 buffer was added and samples were inverted 4-6 times. Next, a volume of a PCR tube

containing acid-treated glass beads was added to the samples. Cells were then lysed in the cell disruption device 2x 2000 U for 20 seconds and then centrifuged at 3,500 rpm for 2 minutes. 1 mL of the supernatant was added to 500 µL of P3 buffer. Samples were inverted 4-6 times and incubated on ice for 10 minutes. Then, samples then centrifuged at 13,000 rpm for 15 minutes. 750 µL of the supernatant was vortexed with 750 µL of isopropanol and then centrifuged at 13,000 rpm for at least 30 minutes. The supernatants were carefully discarded and 750 µL of 70 % EtOH was carefully added to continue centrifugation at 13,000 rpm for at least 30 minutes. Pellets were then air-dried upside down on a tissue and then dried in a heating Speed Vac Vacuum Concentrator until the pellets were dry. DNA from the dried pellets was dissolved in 20 µL dH_2O under heat.

3.4.6.2 *E. coli* plasmid mini-preparation

Mini-preparation is an alkaline lysis method described from Sambrook and Russell, 2001. Transformed *E. coli* were cultured in 2 mL LB media including relevant resistances o/n at 37 °C. For each plasmid of interest, five grown *E. coli* colonies were prepared and tested.

First, cells were centrifuged at 13,000 rpm for 1 minute. Next, pellets were resuspended in 250 µL of P1 buffer including RNase. Additionally, 250 µL P2 buffer was added and samples were inverted 4-6 times for 5-minute incubation at RT. Then, 250 µL of P3 buffer was added and samples were inverted 4-6 times for 5-minute incubation on ice. Then, all samples were centrifuged at 13,000 rpm for 10 minutes. 700 µL of the supernatant was vortexed with 700 µL of isopropanol and then centrifuged at 13,000 rpm for at least 15 minutes. The supernatants were carefully discarded and 750 µL of 70 % EtOH was carefully added to continue centrifugation at 13,000 rpm for at least 15 minutes. Pellets were then air-dried upside down on a tissue and then dried in a heating Speed Vac Vacuum Concentrator until the pellets were dry. DNA from the dried pellets was dissolved in 100 µL dH_2O under heat. 3 µL of dissolved DNA was used for restriction enzyme analysis.

3.4.6.3 *E. coli* plasmid midi-preparation

Midi preparation was performed according to the manufacturer's instructions “QIAGEN

Plasmid Purification" based on an alkaline lysis method according to Sambrook and Russell, 2001.

Transformed *E. coli* were cultured in 50 mL LB media with appropriate resistances at 37 °C o/n. Cells were centrifuged at 46,000 rpm for 15 minutes at 4 °C. All pellets were resuspended in 4 mL of P1 buffer including RNase A and LyseBlue. Then, 4 mL of P2 buffer was added and samples were inverted 4-6 times until the suspension turns clear for 15-minute incubation on ice. Samples were centrifuged for at least 30 minutes at 4 °C and 46,000 rpm. The supernatant was then transferred to a new tube and the centrifugation procedure was repeated. All supernatants were loaded onto the column, which was equilibrated with 10 mL of QBT buffer. Columns were washed twice with 10 mL of QC buffer. Next, DNA was eluted by adding 5 mL of QF buffer. 3.5 mL isopropanol was added to the precipitated DNA, vortexed, and centrifuged at 46,000 rpm for at least 30 minutes, at 4 °C. The supernatant was then carefully discarded and 2 mL of 70 % EtOH was carefully added for another centrifugation of at least 30 minutes at 46,000 rpm and 4 °C. Pellets were air-dried upside down on a tissue and then dried in a heating Speed Vac vacuum concentrator until the pellets were dry. DNA from the dried pellets was dissolved in 100-150 µL of dH_2O under heat. 3 µL of dissolved DNA was used for restriction enzyme analysis and 1.5 µL for quantitative determination and purity of DNA sample.

3.4.6.4 Mating: Random spore analysis

For mating of an h^+ with h^- haploid *S. pombe* strains were cultured on YE5S plates. Equal amounts of h^+ and h^- *S. pombe* cells were added to 15 µL dH_2O. Each outgoing yeast strain and the mating strain were patched onto a malt medium plate and incubated at 25 °C for 2-3 days. The presence of ascii was checked under a light microscope. Cells that showed ascii were added to 980 µL of ddH_2O and 20 µL of a 1:10 dilution of β-glucuronidase and then incubated at 25 °C o/n. Cells were then re-checked under a light microscope to prove if the vegetative cells had degraded ascus walls and exposed spores. The cell-spore mixture was then centrifuged at 13,000 rpm for 1 minute, and the spores were washed twice with ddH_2O before resuspension in 1 mL dH_2O. The number of spores/mL was determined under the microscope to deploy 2x 200 and 2x 1000 spores on YE5S plates and incubate them at the appropriate temperature until colonies were grown. All grown colonies were further characterized with

different selective plates and/or different temperatures to identify genetic markers and/or temperature sensitivity.

3.4.7 Verification of integration of the insert into the expression vector

After plasmid isolation, the qualitative restriction was used to control the integration of the ORFs. For this purpose, the plasmids were digested with the appropriate restriction enzyme and buffer according to the manufacturer's instructions for at least 3 hours and tested on an 0.8 % agarose gel. The digested backbone vector without insert was used as a control. Particularly for ORFs with a short length of less than 500 nt, the comparison of the restriction pattern with the control plasmid was difficult. For improved separation of DNA fragments, gel electrophoresis was performed using a 0.8 % gel at 120 V for approximately 3 hours. Genes that showed the restriction patterns for correct integration were sequenced by GATC-Sanger sequencing. As a control for the successful cloning, the following restriction enzymes were used for digestion and primers for sequencing:

3.4.7.1 Verification of the integration of the insert into the expression vector p282

An illustrative plasmid map of the control vector and a vector cloned with a chlamydial gene is shown in **Supplementary Figure 1A**. The backbone expression vector p282 serves as a control.

Plasmid number	Restriction enzymes and DNA fragment sizes	Sequencing primers (ON)
282	HincII: 6064 bp, 2100 bp, 897 bp HindIII: 5579 bp, 3482 bp	
1287	HincII: 7207 bp, 2100 bp	98
1288	HincII: 7165 bp, 2100 bp	98
1289	HincII: 7255 bp, 2100 bp	98
1292	HincII: 7909 bp, 2100 bp	98, 99
1293	HindIII: 6073 bp, 3482 bp, 519 bp	98, 99
1294	HincII: 6655 bp, 2100 bp, 1236 bp	98, 99
1295	HincII: 8107 bp, 2100 bp	98, 99

1307	HincII: 7372 bp, 2100 bp	98
1308	HindIII: 7238 bp, 3482 bp	98, 99
1309	HincII: 6602 bp, 2100 bp, 1547 bp	98, 99
1310	HindIII: 5872 bp, 3482 bp, 1363 bp	98, 2684, 99
1324	HindIII: 5649 bp, 3482 bp, 1669 bp, 52 bp	98, 2769, 99
1325	HindIII: 6311 bp, 3482 bp, 2091 bp	98, 2692, 2694, 2768, 99
1384	HincII: 7345 bp, 2100 bp	98
1385	HincII: 7324 bp, 2100 bp	98
1386	HincII: 7501 bp, 2100 bp	98
1387	HincII: 7180 bp, 2100 bp	98
1388	HincII: 7840 bp, 2100 bp	98, 99
1389	HincII: 7738 bp, 2100 bp	98, 99
1390	HincII: 7375 bp, 2100 bp	98
1391	HincII: 6772 bp, 2100 bp, 1097 bp	98, 99
1392	HincII: 7654 bp, 2100 bp	98
1393	HincII: 7387 bp, 2100 bp	98
1394	HincII: 7225 bp, 2100 bp	98, 99
1395	HincII: 7408 bp, 2100 bp	98
1396	HincII: 7210 bp, 2100 bp	98
1397	HincII: 7981 bp, 2100 bp	98, 99
1398	HincII: 8089 bp, 2100 bp	98, 99
1399	HincII: 7214 bp, 2100 bp, 1450 bp	98, 99
1400	HincII: 6282 bp, 2100 bp, 1340 bp, 371 bp	98, 99
1401	HincII: 7636 bp, 2100 bp	98
1402	HindIII: 6281 bp, 3482 bp	98
1403	HincII: 7420 bp, 2100 bp	98
1404	HindIII: 5430 bp, 3482 bp, 708 bp, 404 bp	98, 99
1405	HindIII: 6608 bp, 3482 bp	98, 99
1406	HindIII: 6200 bp, 3482 bp, 513 bp	98, 99
1407	HindIII: 7251 bp, 3482 bp	98
1408	HincII: 8038 bp, 2100 bp	98, 99
1409	HindIII: 6164 bp, 3482 bp	98
1410	HindIII: 5647 bp, 3482 bp, 1033 bp	98, 99

1411	HindIII: 6224 bp, 3482 bp	98
1412	HindIII: 5573 bp, 3482 bp, 267 bp	98
1413	HincII: 7318 bp, 2100 bp	98
1414	HindIII: 6662 bp, 3482 bp	98, 99
1415	HincII: 6457 bp, 2100 bp, 1299 bp	98
1416	HincII: 7687 bp, 2100 bp	98
1417	HindIII: 5573 bp, 3482 bp, 456 bp	98
1418	HincII: 7195 bp, 2100 bp	98
1419	HincII: 7729 bp, 2100 bp	98, 99
1420	HincII: 8182 bp, 2100 bp	98
1421	HincII: 8005 bp, 2100 bp	98, 99
1422	HindIII: 6339 bp, 3482 bp, 629 bp	98, 99
1423	HincII: 8242 bp, 2100 bp	98, 99
1424	HincII: 6272 bp, 2100 bp, 1637 bp	98
1425	HincII: 7318 bp, 2100 bp	98
1426	HincII: 6272 bp, 2100 bp, 1211 bp, 1069 bp	98, 99
1427	HincII: 7366 bp, 2100 bp	98
1428	HincII: 8143 bp, 2100 bp	98, 99
1429	HincII: 9172 bp, 2100 bp	98, 2782, 99
1430	HincII: 7687 bp, 2100 bp	98
1431	HincII: 6474 bp, 2100 bp, 2080 bp	98, 99
1432	HincII: 7357 bp, 2100 bp	98
1433	HincII: 7450 bp, 2100 bp	98
1434	HincII: 8188 bp, 2100 bp	98, 99
1435	HincII: 7969 bp, 2100 bp	98, 99
1436	HincII: 7354 bp, 2100 bp	98
1437	HincII: 7249 bp, 2100 bp	98
1438	HincII: 7957 bp, 2100 bp	98, 99
1439	HincII: 7411 bp, 2100 bp	98, 99
1440	HincII: 6671 bp, 2100 bp	98, 99
1441	HincII: 6767 bp, 2100 bp, 1097 bp	98, 2778, 99
1442	HincII: 7318 bp, 2100 bp	98
1443	HincII: 6461 bp, 2100 bp, 1067 bp	98

1444	HincII: 7729 bp, 2100 bp	98, 99
1445	HincII: 7723 bp, 2100 bp	98, 99
1446	HincII: 8824 bp, 2100 bp	98, 2786, 99
1447	HincII: 7990 bp, 2100 bp	98, 99
1448	HincII: 8473 bp, 2100 bp	98, 99
1449	HincII: 7366 bp, 2100 bp	98
1450	HincII: 6820 bp, 2100 bp, 921 bp	98
1451	HincII: 7684 bp, 2100 bp	98, 99
1452	HincII: 7480 bp, 2100 bp	98
1453	HincII: 7339 bp, 2100 bp	98
1454	HincII: 7867 bp, 2100 bp	98, 99
1455	HincII: 7009 bp, 2100 bp, 1431 bp	98, 99
1456	HincII: 8473 bp, 2100 bp	98, 99
1457	HincII: 7222 bp, 2100 bp	98
1458	HincII: 7687 bp, 2100 bp	98
1459	HincII: 7909 bp, 2100 bp	98, 99
1460	HincII: 7201 bp, 2100 bp	98
1461	HincII: 7897 bp, 2100 bp	98, 99
1462	HincII: 7222 bp, 2100 bp	98
1463	HincII: 6577 bp, 2100 bp, 1581 bp	98, 99
1464	HincII: 8353 bp, 2100 bp	98, 99
1465	HincII: 7567 bp, 2100 bp	98
1466	HincII: 7738 bp, 2100 bp	98
1467	HincII: 7894 bp, 2100 bp	98, 99
1468	HincII: 7318 bp, 2100 bp	98
1469	HincII: 8305 bp, 2100 bp, 1434 bp, 12 bp	98, 2779, 2780, 99
1470	HincII: 7327 bp, 2100 bp	98
1471	HincII: 7914 bp, 2100 bp	98, 99
1472	HincII: 7249 bp, 2100 bp	98
1474	HincII: 8935 bp, 2100 bp	98, 99
1475	HincII: 7225 bp, 2100 bp	98
1476	HincII: 7894 bp, 2100 bp	98, 99
1477	HincII: 8485 bp, 2100 bp	98, 99

1478	HindIII: 5819 bp, 3482 bp	98
1479	HincII: 7126 bp, 2100 bp	98
1554	HindIII: 6506 bp, 3482 bp, 710 bp, 61 bp	98, C-622, C-572, C-573, 99
1586	HindIII: 8228 bp, 3482 bp, 1894 bp	98, 2321, 2322, 2323, 2324, 2325, 99
1587	HincII: 6140 bp, 2100 bp, 1256 bp	98
1588	HincII: 7234 bp, 2100 bp	98
1589	HincII: 6826 bp, 2100 bp, 2019 bp	98, C-3111, 99
1590	HindIII: 7811 bp, 3482 bp	98, 2427, 2428, 99
1591	HincII: 7411 bp, 2100 bp, 1167 bp, 1044 bp	98, 2855, 99
1592	HindIII: 6809 bp, 3482 bp, 1134 bp	98, C-896, C-961, 99

3.4.7.2 Verification of the integration of the insert into the expression vector p1335

An illustrative plasmid map of the control vector and a vector cloned with a chlamydial gene is shown in **Supplementary Figure 1B**. The backbone expression vector p1335 serves as a control.

Plasmid number	**Restriction enzymes and DNA fragment sizes**	**Sequencing primers (ON)**
1335	HindIII: 6209 bp, 1759 bp, 1023 bp	
1481	HindIII: 6644 bp, 1759 bp, 1023 bp	98
1482	HindIII: 6610 bp, 1759 bp, 1023 bp, 850 bp	98, 2981, 99

3.4.7.3 Verification of the integration of the insert into the expression vector p270

An illustrative plasmid map of the control vector and a vector cloned with a chlamydial gene is shown in **Supplementary Figure 1C**. The backbone expression vector p270 serves as a control.

Plasmid number	**Restriction enzymes and DNA fragment sizes**	**Sequencing primers (ON)**
270	HincII: 6869 bp, 1043 bp, 849 bp	
1484	HincII: 7327 bp, 1024 bp, 568 bp, 281 bp	98

1485	HincII: 6105 bp, 1920 bp, 1024 bp, 568 bp, 281 bp	98
1486	HincII: 6105 bp, 1823 bp, 1024 bp, 913 bp, 568 bp, 281 bp	98, 2981, 99
1509	HincII: 7086 bp, 1024 bp, 568 bp, 281 bp	98
1510	HincII: 6105 bp, 1680 bp, 1024 bp, 568 bp, 281 bp	98
1511	HincII: 7657 bp, 1024 bp, 568 bp, 281 bp	98
1512	HincII: 6105 bp, 2250 bp, 1024 bp, 568 bp, 281 bp	98, 3083, 1592
1513	HincII: 7230 bp, 1024 bp, 913 bp, 568 bp, 281 bp	98, 99
1601	HincII: 6087 bp, 1774 bp, 1043 bp, 568 bp	98, 99

3.4.7.4 Verification of the integration of the insert into the expression vector p1360

An illustrative plasmid map of the control vector and a vector cloned with a chlamydial gene is shown in **Supplementary Figure 2**. The backbone expression vector p1360 serves as a control.

Plasmid number	**Restriction enzymes and DNA fragment sizes**	**Sequencing primers (ON)**
1360	EcoRI 6330 bp	
1518	EcoRI: 7098 bp	1876

3.4.7.5 Verification of the integration of the insert into the expression vector p1523

An illustrative plasmid map of the control vector and a vector cloned with a chlamydial gene is shown in **Supplementary Figure 3A**. The backbone expression vector p1523 serves as a control.

Plasmid number	**Restriction enzymes and DNA fragment sizes**	**Sequencing primers**
1523	BglI: 3057 bp, 2291 bp, 122 bp, 71 bp	
1527	BglI: 3823 bp, 2291 bp, 122 bp, 71 bp	2976

1596	BglI: 3837 bp, 2291 bp, 472 bp, 122 bp, 71 bp	2976, 2977

3.4.7.6 Verification of the integration of the insert into the expression vector p1524

An illustrative plasmid map of the control vector and a vector cloned with a chlamydial gene is shown in **Supplementary Figure 3B**. The backbone expression vector p1524 serves as a control.

Plasmid number	**Restriction enzymes and DNA fragment sizes**	**Sequencing primers (ON)**
1524	HincII: 5599 bp	
1525	HincII: 5501 bp, 1352 bp	2974, 2981
1526	HincII: 6367 bp	2974
1532	HincII: 5824 bp	C-2125
1533	HincII: 5890 bp	2974
1534	HincII: 5863 bp	2974
1598	HincII: 5501 bp, 590 bp	2974
1600	HincII: 6696 bp	2974, 2981, 3206
1657	HincII: 6124 bp, 569 bp	2974, C-2125, C-1296
1658	HincII: 5726 bp, 569 bp	2974

3.4.7.7 Verification of the integration of the insert into the expression vector p2999

An illustrative plasmid map of the control vector and a vector cloned with a chlamydial gene is shown in **Supplementary Figure 4**. The backbone expression vector p2999 serves as a control.

Plasmid number	**Restriction enzymes and DNA fragment sizes**	**Sequencing primers (ON)**
2999	BglII: 7654 bp, 3153 bp, 81 bp	
1549	BglII: 5034 bp, 3837 bp, 3153 bp, 81 bp	2981, 3235, 3236

3.5 Biochemical methods

3.5.1 Whole-cell lysate isolation of *S. pombe*

Cells were pre-cultured for 24 hours at 25 °C in 5 mL MM under selective conditions and the presence of 5 µg/mL thiamine. Then, cells were washed three times with dH_2O and then cultured at an OD_{600} of 0.03 in 200 mL MM without thiamine o/n at 25 °C to an OD_{600} of 1. Cells with an adequate OD concentration (log phase) were centrifuged at 3,500 rpm for 5 minutes at 4 °C, and washed once with dH_2O. The sample preparation was followed on ice. Then, 500 µL HB15-buffer was added to the cell pellets under the hood. Next, cells were transferred into 2 mL screw-cap tubes and the volume of one PCR tube of acid-treated glass beads was added. Then, cells were lysed in the cell disrupter 1x 5,000 U for 10 seconds, paused for 2 minutes on ice, and were lysed again. A hole was pocked in the bottom of the screw-cap tube with the cell lysate and placed on a fresh tube for centrifugation at 4 °C, 3,500 rpm for 1 minute in the 50 mL centrifuge insert. Then, whole-cell lysate was centrifuged at 15,000 rpm, at 4 °C for 5 minutes, transferred to a fresh tube, and then centrifuged at 15,000 rpm, at 4 °C for 30 minutes twice. Subsequently, whole-cell lysates were aliquoted and stored at -20 °C.

Broadford

The whole-cell lysate levels were determined by Bradford to use the lowest protein level as the standard value for the sample set. 200 µL Bradford solution was added to 10 µL whole cell lysate in 790 µL dH_2O. Then, the mixture was vortexed until the solution had a homogeneous color. Then, the solution was incubated for 10 minutes at RT. The OD was measured at the wavelength of 595 nm. The lowest OD was set as the standard OD for the sample set and all samples with a higher OD were diluted with the HB15-buffer.

SDS sample preparation

100 µL whole cell lysate was resuspended with 38.5 µL 4x SDS loading buffer and 5 µL 1 M DTT and boiled for 10 minutes at 100 °C. Samples were stored at -20 °C.

3.5.2 Protein isolation from *S. pombe*: Fast protein lysate

The fast protein lysate isolation from *S. pombe* was described from Matsuyama et al., 2018. Cells were pre-cultured for 24 hours at 25 °C in 5 mL MM under selective conditions and the presence of 5 µg/mL thiamine. Then, cells were washed three times with dH_2O and cultured in 50 mL MM without thiamine o/n at 25 °C. Next, cell numbers of all samples were determined by OD_{600} and adjusted to the lowest number. Then, samples were centrifuged at 3,500 rpm for 5 minutes. Pellets were resuspended in 700 µL 0.7 M NaOH and incubated for 3 minutes at RT. Next, samples were centrifuged at 500 rpm for 5 minutes. All pellets were resuspended in 300 µL SGS-PAGE buffer (195 µL dH_2O, 75 µL 4x SDS loading buffer, 30 µL 1 M DTT) and boiled for 10 minutes at 100 °C. Samples were stored at -20 °C.

3.5.3 Whole-cell lysate isolation of mammalian cells

Mammalian cells grown ~70 % confluent in a 6-well plate were washed twice with HBSS on ice. Subsequently, cells were scraped from the well bottom in the presence of 100 µL phospholysis buffer including 1:100 PMSF and 1:100 PIC. Then, cells were incubated for 30 minutes on ice with regular intervals of vortexing. The whole-cell lysate was centrifuged at 4 °C and 15,000 rpm for 15 minutes. Then, 100 µL whole-cell lysate was added to 38.5 µL 4x SDS loading buffer and 5 µL 1 M DTT and boiled for 10 minutes at 100 °C. Samples were stored at -20 °C.

3.5.4 Immunoprecipitation of *S. pombe*

For the immunoprecipitation of *S. pombe* the µMACS GFP isolation beads and µMACS columns (Miltenyi) were used. Whole-cell lysates of *S. pombe* were isolated as described in section 3.5.1. From the 500 µL whole-cell lysate, 100 µL was used as input control and 400 µL for immunoprecipitation. 100 µL input was resuspended with 38.5 µL 4x SDS loading buffer and 5 µL 1 M DTT and boiled for 10 minutes at 100 °C. 400 µL whole-cell lysate for immunoprecipitation was added to 100 µL beads and incubated for at least 1 hour on ice. Then, the column was equilibrated with 200 µL HB15-buffer before the cell lysate-bead mix was added. Next, the column was washed 10 times with 200 µL HB15-buffer. For the elution, 20 µL 100 °C pre-warmed elution buffer was added and incubated for 5 minutes. Then, 50 µL

pre-warmed elution buffer was added twice to elute the proteins. Samples were boiled for 10 minutes at 100 °C and stored at -20 °C. Samples were analyzed by western blot or coomassie staining.

3.5.5 SDS-PAGE

SDS gels were used to separate proteins for the analysis via Western blot or coomassie staining. All SDS gels were layered with resolving gel (3/4 of the gel) and with stacking gel. The electrophoresis was set on power with 100-120 V.

Resolving gel (4 gels)	8 %	15 %
H_2O	9.7 mL	5 mL
Resolving buffer (4x)	5 mL	5 mL
Acrylamid solution	5.3 mL	10 mL
10 % APS	200 µL	200 µL
TEMED	35 µL	35 µL

An 8 % gel was used for western blots, while a 15 % gel was used for a coomassie staining.

Stacking gel (4 gels)	
H_2O	6 mL
Stacking buffer (4x)	2.5 mL
Acrylamid solution	1.5 mL
10 % APS	200 µL
TEMED	20 µL

The polymerized gel was stored at 4 °C.

3.5.6 Coomassie staining

The 15 % SDS gel was microwaved for 30 seconds at 600 watts in H_2O and incubated for 5 minutes on the shaker. The procedure was done twice. Then, the gel was microwaved for 30 seconds at 600 watts in coomassie solution and incubated for 10 minutes on the shaker. The gel was microwaved again for 30 seconds and incubated o/n. The high background was washed out by additional shaking in H_2O for a few hours.

3.5.7 Western blotting and transfer

Separated proteins in the 8 % SDS gel were transferred to a PVDF membrane. On top of a Whatman paper soaked with towbin buffer, a methanol equilibrated PVDF membrane was placed. The SDS gel was placed on the PVDF membrane and covered on top with a second Whatman paper soaked with towbin buffer. Next, the transfer was blotted for 20 to 26 minutes at 25 V and 1.0 A. Then, the PVDF membrane was blocked for at least 1 hour in blocking solution at RT. Next, the membrane was incubated in 5 mL of unconjugated-primary antibody diluted in blocking buffer o/n on the wheel at 4 °C. Then, the membrane was washed three times with 1x PBS including 0.05 % Tween for 5 minutes. Next, the membrane was incubated in 5 mL of fluorescent-conjugated secondary antibody diluted in blocking buffer for 1 hour on the wheel at RT. The membrane was washed three times with 1x PBS including 0.05 % Tween 20 for 5 minutes before proteins were detected in dark by the addition 20 mL DIG P3, including 66 µL NBT and 66 µL BCIP.

3.5.8 *in vitro* MT binding assay

MT polymerization was performed according to the manufacturer's instructions (Cytoskeleton Inc). For the *in vitro* MT binding assay, GST and GST-CPn0443$^{164-417}$ were used. Protein samples were centrifuged at 60,000 rpm for 35 minutes at 4 °C. Taxol-stabilized MTs were prepared by incubating 10 µL MTs with 1 µL cushion buffer at 35 °C for 20 minutes. Additionally, pre-warm 100 µL general tubulin buffer at 35 °C. Then, 1 uL (2 mM) taxol solution (taxol diluted in DMSO) and taxol-stabilized MTs were added to the 100 µL pre-warmed general tubulin buffer. From the centrifuged protein samples 6 µL GST and 8.3 µL GST-CPn0443$^{164-417}$ were used twice each (for with and without MTs). To the protein sample set with MTs, 15 µL of taxol-stabilized MTs (equivalent to 4 µM tubulin dimer) and 25 µL general tubulin buffer (incl. taxol solution) were added and to the sample set without MTs 40 µL general tubulin buffer (incl. taxol solution) as added. Then, buffer A was added to the protein samples. 4 µL buffer A was added to the GST samples with/without taxol-stabilized MTs and 1.7 µL buffer A was added to the GST-CPn0443$^{164-417}$ samples. Samples were incubated for 30 minutes at RT. Next, samples

(50 µL each) were layered on 200 µL cushion buffer (incl. taxol solution) and centrifuged at 53,000 rpm for 51 minutes at RT. Then, 50 µL supernatant was carefully collected and resuspended with 10 µL 5x SDS (7,1 µL SDS and 2,9 µL 1 M DTT). Next, the pellet was resuspended in 50 µL 1x SDS (12.5 µL 4x SDS and 5 µL 1 M DTT and 32.5 µL dH_2O).

25 % of each supernatant (15 µL) and pellet (12.5 µL) sample were loaded onto 15 % SDS-PAGE followed by Coomassie gel staining to visualize protein bands for MTs and GST or GST-CPn0443$^{164-417}$. Densitometry of bands in the supernatant and pellet fractions were carried out using Image Lab (BioRad), and values of MTs in pellet fraction were graphed as percentages of total MTs found in the supernatant and pellet fractions

3.5.9 Immunofluorescence staining

3.5.9.1 Lectin staining of *S. pombe* cells

Cells were cultured for 24 h at 25 °C in 5 mL MM under selective conditions. Then, cells were centrifuged at 3,000 rpm and the pellet was resuspended in 20 µL of the left-over medium in the reaction tube. Cells were incubated for 3 minutes at RT with 2 µL of 0.5 mg/mL TRITC-staining, diluted in 1xPBS. Cells were washed two times with 1 mL dH_2O. Stained cells were mixed with non-stained cells in the same ratio. 2 µL of the cell mixture was prepared for live-cell imaging.

3.5.9.2 Immunofluorescence straining of mammalian cells

As described in section 3.3.2, infected mammalian cells were fixed on coverslips with 3 % PFA and permeabilized with methanol. PFA-treated transfected cells need to be permeabilized with saponine. Therefore, transfected mammalian cells were permeabilized with 2 % saponin in 1x PBS for 20 minutes at RT. Next, transfected and/or infected cells were stained with an unconjugated primary antibody for 30 minutes at 30 °C. Then, coverslips were washed three times with 1x PBS and then stained with a fluorescent-conjugated secondary antibody for 30 minutes at 30 °C. Then, coverslips were washed again three times with 1x PBS and stained with DAPI for 10 minutes at RT. Next, coverslips were washed three times with 1x PBS and dried under the airflow. Coverslips with the side of cells were placed on 3 µL mounting solution

on top of an object slide and then sealed with nail polish for microscopic analysis. Coverslips were stored at 4 °C.

3.6 Yeast growth analysis

3.6.1 Serial dilution patch test with TBZ or MBC

For a serial dilution patch test, *S. pombe* strains were cultured in 5 mL MM with plasmid-selective conditions and the absence or presence of 5 µg/mL thiamine at 25 °C o/n. Then, the cell OD_{600} was measured to determine the cell number. The OD_{600} of 0.3 equates to the cell number of 2x 10^6 cells/mL. Samples were diluted to 2x 10^6 cells/mL and then further diluted to 2x 10^5, 2x 10^4, and 2x 10^3 cells/mL. From each cell dilution, 5 µL (corresponding 10^4, 10^3, 10^2, and 10 cells) were plated on each MM plate with plasmid-selective conditions. Yeast growth was also tested for sensitivity to the MT-destabilizing drugs TBZ or MBC. Depending on whether a yeast strain is TBZ/MBC sensitive/resistant, the following ratio of TBZ/MBC concentrations was chosen:

***S. pombe* strain**	**TBZ concentrations**
#135	2.5-12 µg/mL
#605	2.5-12 µg/mL
#1318	2.5-12 µg/mL
#1478	2.5-12 µg/mL
#2023	2.5-12 µg/mL
#2087	2.5-12 µg/mL
#2421	5-15 µg/mL
#2422	5-15 µg/mL

Plates were cultured for 6 days at 25 °C.

***S. pombe* strain**	**MBC concentrations**
#605	0.5-4.5 µg/mL
#1318	0.5-4.5 µg/mL

Plates were cultured for 6 days at 25 °C.

3.6.2 Serial dilution patch test with cold-sensitive strains

Cold-sensitive strains were pre-cultured at 30 °C on plates. For a serial dilution patch test, *S. pombe* strains were cultured in 5 mL MM with plasmid-selective conditions and the presence of 5 µg/mL thiamine o/n at 25 °C. Then, the cell OD_{600} was measured to determine the cell number. The OD_{600} of 0.3 equates to the cell number of 2x 10^6 cells/mL. Samples were diluted to 2x 10^6 cells/mL and then further diluted to 2x 10^5, 2x 10^4, and 2x 10^3 cells/mL. From each cell dilution, 5 µL (corresponding 10^4, 10^3, 10^2, and 10 cells) were plated on each MM plate with plasmid-selective conditions. Plates were cultured for 6 days at the corresponding temperatures:

***S. pombe* strain**	**Temperature**
#224	22 °C, 25 °C, 30 °C
#3091	22 °C, 25 °C, 30 °C

3.7 Microscopy

3.7.1 *S. pombe* sample preparation for live-cell imaging

Transformed *S. pombe* cells were pre-cultured for 24 hours at 25 °C in 5 mL MM under selective conditions and the presence of 5 µg/mL thiamine. Then, cells were washed three times with dH_2O and cultured at an OD_{600} of 0.03 in 200 mL LFM without thiamine 24 h at 25 °C to an OD_{600} of 1. Cells with an adequate OD concentration (log phase) were centrifuged at 3,500 rpm for 5 minutes and resuspended in 50-100 µL dH_2O depending on the cell pellet. An object slide is inserted into the slide frame and 80 µL LFM-agar is added on top to place on top a second object slide to form a 0.5 mm agar patch. 4 µL resuspended cells were added on the agar patch and cells were spread over the patch carefully. After the cell patch was dried, a cove slide was placed on top and sealed with VALAP (vaseline, lanolin, paraffin 1:1:1).

3.7.2 Live-cell imaging of *S. pombe*

Live-cell images of *S. pombe* were performed by using the Zeiss LSM 880 Airyscan (CarlZeiss) microscope with the 63x objective at RT in the FastAiryScan modus.

For quantification of MT dynamics, all samples were cultured and prepared under the same conditions and microscopically analyzed with the same settings. 28 Z-stacks for 40 cycles were created from each image. With an image size of 66.02x66.02 µm, each cycle took 7 seconds. For the images, the 488 nm laser was set to 20 % for GFP. The images were then processed by the Airyscan Processing and displayed as maximum intensity projections (MIPs). Analysis of images and measurements were generated with Zen3.0 blue edition software (Zeiss).
For the analysis of GFP and mCherry fluorescence signals, the 488 nm laser was set to 20 % for GFP and 561 nm laser to 5% for mCherry.

3.7.3 Confocal microscopy of mammalian cells

Microscopic analysis of mammalian cells was performed by using the inverse Nikon TiE Live Cell Confocal C2plus with 100-x TIRF objective and a C2 SH C2 Scanner. All images were displayed as MIPs. Analysis of images and measurements were generated with Nikon Element software.

3.8 Quantification and statistics

3.8.1 Quantification of MT dynamics of *S. pombe*

For quantification of MT dynamics, cells with a length between 9 and 12 µm were analyzed by live-cell imaging microscopy. Interphase MTs with a length of 1.5 to 2 µm from the center of the MT overlap zone at the nucleus were used for analysis. MT lengths were measured starting from the MT overlap zone to determine MT growth and shrinkage rates. From the MT that grew or shrank continuously for 280 seconds in the 7-second inter, the mean MT length was calculated. Then, the mean MT length was divided by 280 seconds and represented one data point of the rate of growth/shrinkage in nm/sec.

3.8.2 Quantification of fluorescence intensity

For quantification of a fluorescence signal, lectin-labeled cells expressing a chlamydial gene and lectin-untreated control cells (section 3.5.9.1) were mixed for measurement. The

fluorescence signals of the lectin-labeled and untreated cells were measured in a specific region of the cell (cell tips or cell center). In addition, the fluorescence of the cell background of these cells was measured. The fluorescence signal measured at the cell tips or cell center was normalized against the background signal. Fluorescence intensity was expressed in a.u. (arbitrary fluorescence unit).

3.8.3 Quantification of relative protein levels

To quantify the relative protein levels, a Western blot analysis of whole-cell lysates (section 3.5.7) was first performed and actin was included as an internal control. The band intensities of the Western blot analysis were measured using the ImageJ software to normalize the band intensities of the proteins against their corresponding actin bands. The normalized value of the (plasmid) control was set to 1. The normalized values of proteins were divided by the control (1) to determine the ratio of protein levels.

3.8.4 Statistics

The two-tailed Student's t-test was used to determine the statistical significance of the two groups. All graphs and their statistical analysis were performed using GraphPad Prism 8. Error bars were represented in ± SEM. The number of experiments and data points measured was reported.

4 Results

4.1 Identification of *C. pneumoniae* MT-modulating proteins in *S. pombe*

The objective of this study was to identify novel MT-modulating proteins of *C. pneumoniae.* Throughout this study, I explored single putative *C. pneumoniae* effector proteins for MT-modulating effects caused by their gene expression in the eukaryotic fission yeast *S. pombe*.

To answer the question, how many MT-affecting *C. pneumoniae* proteins exist, I structured the screen in different phases:

(I) selection of *C. pneumoniae* protein candidates

(II) major screen for proteins causing TBZ-hypersensitivity in *S. pombe*

(III) evaluation of their influence on the yeast interphase MT structure

Those *C. pneumoniae* proteins that caused hypersensitivity to different MT-destabilizing drugs in the yeast and alterations on the interphase MT cytoskeleton were selected for further analysis.

4.1.1 (I) Selection of 116 *C. pneumoniae* protein candidates

As genes encoding chlamydial effector proteins are distributed over the entire chlamydial genome, I focused on proteins that were predicted to be effector proteins based on their sequence or structure. These are Inc proteins or proteins that had been reported to affect the growth of the yeast *Saccharomyces cerevisiae* (*S. cerevisiae*) (Subtil et al., 2000; Noël et al., 2002). The *S. cerevisiae* growth defects were detected under different cellular stress conditions such as temperature or osmotic pressure. Additionally, I assayed a number of randomly chosen proteins.

Overall, the screen included in total 116 selected *C. pneumoniae* proteins, which are categorized into four groups (i-iv) based on their characteristics (**Table 1**).

		protein tested
***C. pneumoniae* proteins selected**		**116**
(i)	Inc proteins[Dehoux et al., 2011; Lutter et al., 2012]	78
(ii)	proteins affecting *S. c.* yeast growth[Sisko et al., 2006]	11
(iii)	proteins affecting *S. c.* yeast growth[Herbst, 2011]	10
(iv)	proteins randomly chosen	17

Table 1: 116 *C. pneumoniae* proteins were used for the screen in *S. pombe*.

The screen included (i) 78 predicted inclusion membrane (Inc) proteins, (ii) 11 *C. pneumoniae* proteins whose *C. trachomatis* homologs affect *S. cerevisiae* (*S.c.*) yeast growth under stress conditions, (iii) 10 proteins affecting *S. c.* yeast growth under phloxin B treatment on solid media, and (iv) 17 randomly chosen proteins (Mäurer et al., 2007).

The screen's largest group (i) encompasses 78 inclusion membrane Inc proteins which were either predicted as Inc proteins by bioinformatics and/or identified as Inc proteins based on the size of the loop between two transmembrane areas identified by *in silico* analysis (Lutter et al., 2012; Dehoux et al., 2011). Inc proteins are considered as potential MT-modulating proteins, because they are presumed to be located in the inclusion membrane due to their transmembrane domains and their C-terminus extends into the host cell cytosol. This positioning would allow interaction between the inclusion and MT structure of the host cell.

In group (ii), 11 *C. pneumoniae* proteins which *C. trachomatis* homologs affected the *S. cerevisiae* yeast growth are selected from the dataset described in Sisko et al., 2006. Successful heterogeneous expression in the yeast system and the influence of bacterial proteins on yeast cellular processes were demonstrated. *C. trachomatis* genes with unknown functions on the growth behavior of *S. cerevisiae* under different cellular stress conditions were investigated. Stress conditions such as sensitivity to extreme temperatures or osmotic stress induced by salt are used to reveal a series of overlapping but distinct defects in cellular signaling pathways that can be used for the characterization of genes with unknown functions (Sisko et al., 2006). In this study, the influence of protein expression on yeast growth was scored via a growth index of 0 to 5 (0= no yeast growth; 5= wild-type yeast growth). From their results, I focused first on *C. trachomatis* proteins that cause a defective yeast growth phenotype and second on those proteins that feature a *C. pneumoniae* homolog. In this way, I selected 11 *C. pneumoniae* proteins whose *C. trachomatis* homolog triggers a growth defect

in *S. cerevisiae* and scored between 0 and 3 in the presence of either extreme temperature and/or osmotic pressure.

Group (iii) is an extension of group (ii), as this study also demonstrated successful heterogeneous expression in the yeast system and the influence of bacterial proteins on yeast cellular processes. The influence of *C. pneumoniae* proteins on yeast growth was determined in a screening done by a former colleague from the Hegemann group, Dr. F. Herbst. In her PhD project, she performed a phloxin B screen on solid minimal media to identify potential *C. pneumoniae* effector proteins in *S. cerevisiae* (Herbst, 2011). Phloxin B staining in a colony indicates the presence of many dead cells and thus a massive growth defect. Based on her results, I chose 10 *C. pneumoniae* proteins that lead to a growth defect in *S. cerevisiae*.

The last group (iv) of 17 randomly selected proteins based from a transcriptome analysis of genes during the acute and persistent *C. pneumoniae* infection. Mäurer et al., 2007 categorized the ectopic expression
of significant genes of an acute infection into expression clusters from 1 to 12. For the identification of MT-modulating proteins, I selected randomly at least one protein from each expression cluster.

4.1.2 (II) Identification of chlamydial proteins that cause TBZ-hypersensitivity in the *S. pombe*

First, the *C. pneumoniae* genes needed to be transferred into the fission yeast *S. pombe* to perform the major screen. Therefore, the full-length open reading frames (ORFs) of the 116 selected chlamydial genes were amplified by PCR from the *C. pneumoniae* GiD genome and cloned into the pJR2-3XU *ura4*$^{+}$ *S. pombe* expression vector flanked by the thiamine repressing *nmt1*$^{+}$-promoter and *nmt1*$^{+}$-terminator (Jantos et al., 1997) (**Figure 8**, **Supplementary Figure 1A**).

Verification of the correct DNA sequence of chlamydial genes integrated into the yeast vector was performed and revealed DNA sequence changes at *cpn0045, cpn0132, cpn0150*, and

cpn0912 (**Supplementary Table 1**).

The genes *cpn0132* and *cpn0150* revealed an exchange of the first nucleotide of a triplet, resulting in a change of the amino acid. In contrast, a nucleotide insertion was registered for *cpn0045* and *cpn0912*. The insertion of 27 nucleotides leads to the insertion of 9 amino acids in the gene *cpn0912* which does not affect the subsequent amino acid sequence. In comparison, the insertion of 10 nucleotides for *cpn0045* disrupts the subsequent amino acid sequence of the protein. Repetitive DNA amplification and new cloning revealed a reproducible DNA deviation of all four genes as in the sequencing before that could not be corrected. Since the DNA sequence of the GiD genome and the *C. pneumoniae* CWL029 sequence published in the KEGG database also show DNA deviation, the DNA changes of the sequenced genes could not be caused by an amplification error (section: 3.4.2.1). Based on the reproducible DNA deviation, *cpn0045, cpn0132, cpn0150*, and *cpn0912* were approved for screening.

Then, plasmids were transformed into a wild-type (WT) *S. pombe* strain (**Figure 8**). A control vector (no chlamydial gene) was used for comparison.

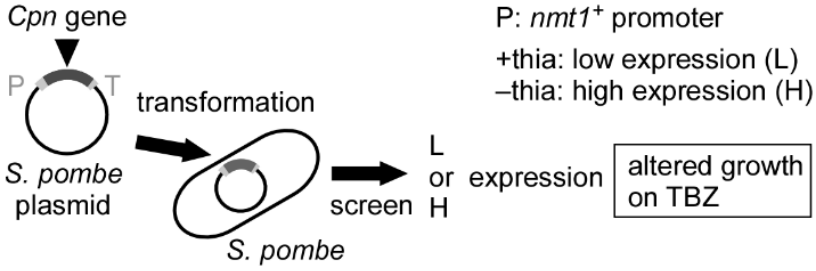

Figure 8: Screening strategy of *C. pneumoniae* genes expressed in *S. pombe*.

Each *C. pneumoniae* gene (*Cpn*, dark grey) was cloned into the *Schizosaccharomyces pombe (S. pombe)* pJR2-3XU *ura4*$^+$ plasmid flanked by the thiamine-regulatable (P) "no message in thiamine" (*nmt1*$^+$)-promoter and (T) *nmt1*$^+$-terminator (light grey). Each of these plasmids carrying a specific *Cpn* gene was transformed into *S. pombe* for reduced growth in the presence of thiabendazole (TBZ). Gene expression was controlled by the presence of thiamine (+thia) to down-regulate the *nmt1*$^+$ promoter for low (L) expression levels or the promoter is de-repressed enabling high (H) gene expression in the absence of thiamine (-thia).

Subsequently, the 116 yeast transformants were analyzed in duplicates via patch test serial dilution assay (10^4-10^1 cells) under different media conditions (**Figure 9A**). The screening conditions included the gene expression controlled by the presence or absence of thiamine

(+thia/-thia) for low (L) or high (H) gene expression. Additionally, *S. pombe* was tested for sensitivity to the MT-destabilizing substance thiabendazole (TBZ) which targets β-tubulin and causes inhibition of MT polymerization (Minagawa et al., 2021). While the control transformant growths unimpaired in the presence or absence of TBZ (+TBZ/-TBZ), *C. pneumoniae* proteins that have an impact on MTs or MT-affecting proteins can be identified by leading to reduced yeast transformant growth in the presence of TBZ.

The outcome of the patch test serial dilution assay revealed different growth defects for the 116 transformants which I categorized into cases 1a, 1b, 2, 3a, 3b, and 4 (**Figure 9B**, **Supplementary Figure 5**, **Supplementary Table 2**).

Case 1a encompasses 67 transformants where expression of the chlamydial gene in question had no negative effect on the growth of the yeast cells (**Figure 9B**). All transformants categorized as case 1a show normal growth under low or high gene expression irrespective of the absence or presence of TBZ.

Case 1b is made up of 18 chlamydial genes which lead to an expression level-dependent growth defect. The reduced yeast growth is observed under high chlamydial gene expression irrespective of the presence/absence of TBZ. Normal yeast growth is detectible for transformants expressing the gene in low levels. This growth pattern demonstrates that high level expression of the chlamydial gene affects general yeast growth but not specifically the MT pathway.

Case 2 has 18 transformants that are lethal to the yeast cell when highly expressed. Death under high level expression is irrespective of the presence/absence of TBZ and the yeast growth is normal under low level gene expression.

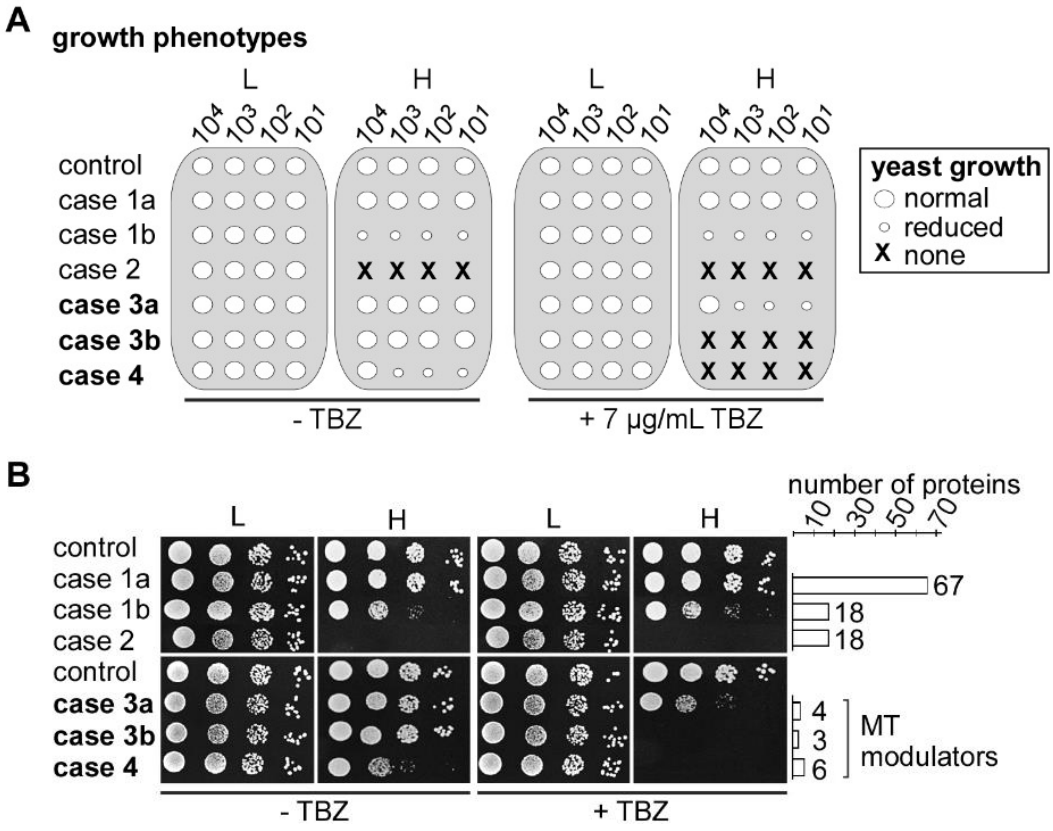

Figure 9: Read-out of patch test serial dilution assay under different conditions. **A** Schematic and **B** representative examples of a serial dilution patch assay (10^4-10^1 cells) showing different growth phenotypes and the numbers of proteins/case under low (L)/high (H) expression of a chlamydial gene in wild-type (WT) *S. pombe* strain. Yeast transformants were incubated on minimal medium under plasmid selective conditions for 6 days at 25 °C in the absence (-TBZ) or presence of 7 µg/mL TBZ (+TBZ). Two yeast transformants were patched. The growth of transformants was compared to a transformant expressing a control plasmid (no chlamydial gene). Normal growth was scored, if growth was very similar (big circle) to control transformant growth, reduced growth (small circle), or no growth (**X**). An explanation of what the different cases imply is found below in the text.

In conclusion, cases 1a, 1b, and 2 are made up of transformants that are either not affected by the chlamydial gene expression (case 1a) or the growth defect/lethality depends on a high expression level irrespective of the MT-destabilizing drug (case 1b and 2). None of these transformants show an increased growth defect in the presence of TBZ. Consequently, transformants categorized in cases 1a, 1b, and 2 were not used for further analysis.

However, all transformants in cases 3a, 3b, and 4 show a TBZ-dependent growth defect which

points out chlamydial proteins that interfere with the MT pathway in *S. pombe* (**Figure 9B**).
Four transformants are categorized for case 3a. Interestingly, transformants highly expressing a specific chlamydial gene in the presence of TBZ display a growth defect, while the yeast growth is normal in the absence of TBZ. Under low gene expression, independent of the absence or presence of TBZ, the yeast growth is not negatively affected by the chlamydial protein. These results show, that high gene expression and the presence of TBZ treatment negatively affect yeast growth.
Three transformants are categorized for case 3b. Transformants highly expressing the chlamydial gene in the presence of TBZ reacted dramatically with lethality on the MT-destabilizing drug treatment, while the yeast growth is not affected in the absence of TBZ. Also, low gene expression is not affecting yeast growth. These results demonstrate, that under high expression of the chlamydial gene, the presence of TBZ in the media is lethal for cell growth.
Additionally, I identified six transformants for case 4 which is highlighted by growth defects under high gene expression that significantly worsens in the presence of TBZ. As a matter of fact, in the presence of TBZ, high level expression of the chlamydial gene is lethal for the yeast transformants.

Taken together, out of the 116 chlamydial proteins I identified 13 proteins, categorized in cases 3a, 3b, and 4, that lead to TBZ-hypersensitivity in the respective yeast transformants. Thus, these proteins appear to disturb the yeast MT pathway and were analyzed further.

4.1.3 Classification of the 13 *C. pneumoniae* proteins causing yeast TBZ-hypersensitivity

Previous to further investigation of the 13 *C. pneumoniae* proteins, I collected the available information for all proteins including:

- protein homolog in other *Chlamydia*?
- presence of a type-III secretion (T3SS) signal in the N-terminal region of the protein?
- predicted protein function?
- protein localization?
- interaction partners?

12/13 proteins are predicted to be Inc proteins. Seven of these proteins have a putative homolog in *C. trachomatis* serovar D, and/or *C. muridarum, C. caviae*, *C. felis*, while five proteins are specific for *C. pneumoniae* (**Figure 10**). Only 1/13 protein (CPn0821) is not an Inc protein but belongs to the group of proteins affecting *S. cerevisiae* yeast growth and has also a homolog in *C. trachomatis* serovar D.

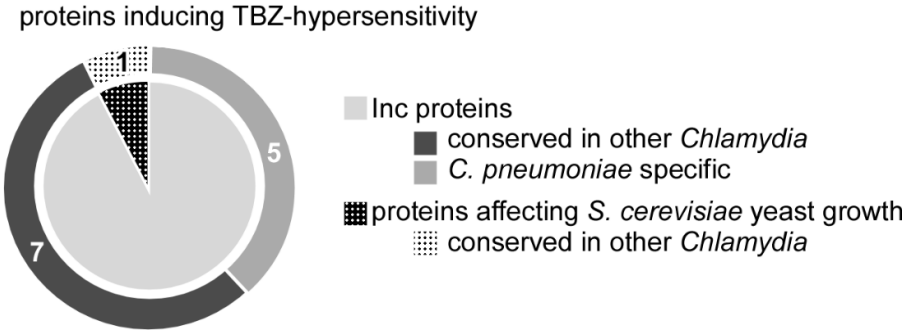

Figure 10: Overview of the 13 *C. pneumoniae* proteins causing TBZ-hypersensitivity in the yeast assay. Proteins were classified previously as either Inc proteins or proteins that cause reduced growth in *S. cerevisiae*. Proteins were further categorized into proteins conserved in other *Chlamydia (*e.g. *C. trachomatis, C. muridarum*, *C. caviae,* and/or *C. felis*) or *C. pneumoniae*-specific proteins.

CPn0821 shares a 51 % homology with the *C. trachomatis* protein CT566, whose gene expression causes a growth defect under stress conditions in *S. cerivisiae* (Sisko et al., 2006) (**Table 2**, **Supplementary Table 3**). Both proteins do not have transmembrane domains (Subtil et al., 2005). Neither the localization nor the predicted function of CPn0821 or CT566 is known.

The following Inc proteins identified in my screen have a *C. trachomatis* homolog (**Table 2**, **Supplementary Table 3**):

C. pneumoniae: **CPn0065**	*C. trachomatis*: CT288
C. pneumoniae: **CPn0186**	*C. trachomatis*: CT119
C. pneumoniae: **CPn0312**	*C. trachomatis*: CT101
C. pneumoniae: **CPn0443**	*C. trachomatis*: CT005
C. pneumoniae: **CPn0565**	*C. trachomatis*: CT449

CPn0065 is classified as a hypothetical Inc protein based on the prediction of four

transmembrane domains. While the function and localization of CPn0065 remains unknown, its *C. trachomatis* homolog CT288 (23.4 % homology) is studied in more detail. Further genomic comparison of *C. pneumoniae*, *C. trachomatis, C. muridarum*, *C. caviae*, and *C. felis* identified, CT288 is a highly conserved Inc protein (Lutter et al., 2012; Dehoux et al., 2011).
In the N-terminus of CT288, the presence of the T3SS-signal was experimentally demonstrated, and further experimental evidence showed that CT288 was detected in the inclusion membrane (Subtil et al., 2001; Subtil et al., 2005; Dehoux et al., 2011). In addition, a yeast two-hybrid (Y2H) and co-immunoprecipitation showed that CT288 binds to the human centrosomal protein coiled coil domain-containing protein 146 (CCDC146), which is recruited to the periphery of the inclusion (Almeida et al., 2018).

CPn0186 is identified as an IncA protein and experimentally showed that CPn0186/IncA is also localized in the ER and co-localizes with the host target protein flotillin-1, a conserved scaffold protein involved in microdomain structuring (Luo et al., 2007; Delevoye et al., 2004; Korhonen et al., 2012).
CPn0186 shares a protein homolog in *C. trachomatis, C. muridarum, C. caviae,* and *C. felis,* which are identified as IncA proteins. Therefore, both CPn0186 and the *C. trachomatis* homolog CT119 proteins (23.4 % homology) have four transmembrane domains and the presence of the T3SS-signal has been demonstrated (Dehoux et al., 2011; Subtil et al., 2001).
CT119 is localized in the inclusion membrane (Hackstadt et al., 1999; Lutter et al., 2012; Dehoux et al., 2011; Bannantine et al., 2000). Further investigations of the *C. trachomatis* protein CT119 showed that the soluble N-ethyl maleimide sensitive-factor attachment protein receptors (SNAREs) Vamp3, Vamp7, and Vamp8 are localized at the inclusion membrane for the interaction with CT119 (Delevoye et al., 2008; Delevoye et al., 2004). These SNARE proteins mediate the fusion of vesicles with the target membrane for exocytosis, as well as the fusion of vesicles with membrane-bound compartments.

CPn0312 is classified as a hypothetical Inc protein and has not been studied to date. CPn0312 has a protein homolog in *C. trachomatis*, *C. caviae*, and *C. felis.* CPn0312 and the *C. trachomatis* protein CT101, also known as MrcAb, are predicted Inc proteins that have two

transmembrane domains and share a homolog of 31.2 % (Lutter et al., 2012; Dehoux et al., 2011). CT101 co-localizes in the inclusion membrane with the host interaction partner inositol-1,4,5-trisphosphate receptor, type 3 (ITPR3), which are responsible for the flux of calcium from the ER (Nguyen et al., 2018).

CPn0357 is classified as a hypothetical Inc protein that exhibits a protein homolog in *C. caviae*, and *C. felis*, but not *C. trachomatis*. Although CPn0357 is localized inside bacteria and a T3SS-signal was detected in the N-terminus of the protein, CPn0357 was not further functionally characterized (Dehoux et al., 2011; Luo et al., 2007).

CPn0443 is a hypothetical Inc protein that has a functional T3SS-sequence in the N-terminus, whereas the intracellular localization remains unknown (Dehoux et al., 2011). CPn0443 shares a homology of 28.4 % with the highly conserved CT005/IncV and is also present in *C. muridarum, C. caviae*, and *C. felis* (Lutter et al., 2012; Dehoux et al., 2011). Despite this conservation and their predictions of four transmembrane domains, there is no further data available about CPn0443, but CT005/IncV is a well characterized protein.

CT005/IncV is localized in the inclusion membrane for the interaction with the host cell integral ER membrane protein VAPA and VAPB (Dehoux et al., 2011; Stanhope et al., 2017). Studies suggest, that VAPs or also called vesicle-associated membrane protein-associated protein, are involved in membrane trafficking by interaction with SNAREs and in the regulation of lipid transport and metabolism (Lev et al., 2008; Weir et al., 2001).

Interestingly, affinity purification-mass spectroscopy analysis revealed that CT005/IncV localizes and interacts with the human MT-associated protein RP/EB family member 1 (MAPRE1), a member of the dynactin complex which regulates the dynamics of the human MT cytoskeleton (Mirrashidi et al., 2015). In addition, mass spectroscopy analysis data and information from various databases were used to predict the function of CT005. In this way, Mirrashidi et al., 2015 proposed that CT005 interacts with proteins of the actin cytoskeleton, centrosome, and endomembrane systems (e.g. ER and Golgi apparatus, endosome, lysosome) including the transport of vesicles and proteins. On the other hand, CT005 is predicted to interact with proteins of cell processes such as endocytosis or lipid binding. With the exception

of its involvement in ER processes, there is no further experimental evidence for the predicted function of CT005 (Mirrashidi et al., 2015; Stanhope et al., 2017).

For the first time, there is evidence from the literature that connects CPn0443 family members to the MT pathway. CPn0443 seems to be the most promising MT-modulating protein concerning its *C. trachomatis* homolog CT005/IncV which is predicted as an MT-associated protein that interacts with the human MAPRE1 protein that regulates the dynamics of the MT cytoskeleton. Concerning this knowledge, CPn0443 will be monitored with particular interest for the further course of this project.

CPn0565 is a hypothetical Inc protein that is 8.8 % homolog to the *C. trachomatis* protein CT449 (full-length comparison). The homology of the full-length proteins is so low because CPn0565 is 366 amino acids (aa) long, while CT449 has only 110 aa. Comparing the entire length of CT449 with the overlapping 117 aa long region of CPn0565, however, reveals 28.2 % identity and 46.2 % similarity, offering the potential for functional homology. CPn0565 and CT449 are both highly conserved Inc proteins that have also homologs in *C. muridarum*, *C. caviae*, and *C. felis* (Lutter et al., 2012; Dehoux et al., 2011). Except for the confirmed secretion of CPn0565 using the T3SS-signal, neither CPn0565 nor CT449 is functionally studied in detail (Dehoux et al., 2011).

In contrast, the *C. trachomatis* protein CT449 is analyzed detailly. For the prediction of the CT449 function, Mirrashidi et al., 2015 used their generated data from affinity purification-mass spectroscopy analysis and information derived from various databases. They hypnotized, that CT449 plays a role in the cell components endomembrane systems (e.g. ER and Golgi apparatus), mitochondria, and cell processes such as apoptosis, antigen processing, or cell cycle and division. Nonetheless, there is no experimental proof for their predictions (Mirrashidi et al., 2015).

CPn1027 exhibits a protein homolog in *C. caviae*, and *C. felis*, but not *C. trachomatis*. CP1027 gets secreted by the T3SS system. Due to the presence of two transmembrane domains, CP1027 is localized in the inclusion membrane of *C. pneumoniae* where it interacts with the host cell proteins activation/proliferation-associated protein 2 (Caprin-2) and glycogen

synthase kinase 3 (GSK3) (Flores et al., 2007; Dehoux et al., 2011). Both host proteins are signaling mediators of the Wnt signaling pathway and GSK3 is involved regulation of MTs (Flores and Zhong, 2015; Dehoux et al., 2011).

Cpn protein	Conserved in *C. trachomatis* D	*Cpn* predicted function	*Cpn* localization
CPn0045	*Cpn* specific	Inc[†, Subtil et al., 2005]	na
CPn0065	CT288[†, *]	Inc[†, Subtil et al., 2005]	na
CPn0186/IncA[Subtil et al., 2001 Delevoye et al., 2004]	CT119/IncA[†,Hackstadt et al., 1999 CCA, CF]	Inc[†, Subtil et al., 2005]	IM[Bannantine et al., 2000] ER[Delevoye et al., 2004]
CPn0216	*Cpn* specific	Inc[†, Subtil et al., 2005]	na
CPn0284	*Cpn* specific	Inc[†, Subtil et al., 2005]	bacteria[Luo et al., 2007]
CPn0312	CT101/MrcAb[†, Mital et al., 2010 CCA, CF]	Inc[†, Subtil et al., 2005]	na
CPn0357	CCA, CF	Inc[†, Subtil et al., 2005]	bacteria[Dehoux et al., 2011]
CPn0365	*Cpn* specific	Inc[†, Subtil et al., 2005]	na
CPn0372	*Cpn* specific	Inc[†, Subtil et al., 2005]	na
CPn0443	CT005/IncV[†, Dehoux et al., 2011,]	Inc[†, Subtil et al., 2005]	na
CPn0565	CT449[†, *]	Inc[†, Subtil et al., 2005]	na
CPn0821	CT566[Subtil et al., 2001]	unknown	na
CPn1027	CCA, CF	Inc[Subtil et al., 2005]	IM[Flores et al., 2007]

Table 2: Characteristics of the 13 *C. pneumoniae* proteins.

Characteristics of the 13 *C. pneumoniae (Cpn)* proteins identified in the screen. Information about *C. trachomatis* serovar D homologs, predicted functions, and localizations are listed for each protein. Detailed characteristics of *C. trachomatis* serovar D homologs are found in **Supplementary Table 3**. Inc: inclusion membrane protein; na:not analyzed; ER: endoplasmic reticulum; *Cpn* specific: no homolog in *C. trachomatis, C. muridarum, C. caviae,* and *C. felis;* * protein is conserved in five *Chlamydia* species: *C. pneumoniae, C. trachomatis, C. muridarum, C. caviae,* and *C. felis* (Lutter et al., 2012). CCA: *C. caviae;* CF: *C. felis*. † my research via pBLAST, homology analysis via EMBOSS needle.

Overview of *C. pneumoniae*-specific proteins: **CPn0045, CPn0216, CPn0284, CPn0365,** and **CPn0372**. Those five proteins have two transmembrane domains that led to their prediction as Inc proteins.

Currently, there is no information available about the proteins CPn0045 and CPn0216. However, the *cpn0045*-induced yeast growth defect may have been caused by the insertion of

the 10 nucleotides due to the amino acid sequence change, resulting in a change in protein function. Whereas the protein CPn0284 has been localized inside bacteria and the presence of a T3SS-signal was detected in the N-terminus of the protein (Dehoux et al., 2011; Luo et al., 2007). In addition, the proteins CPn0365 and CPn0372 are secreted by the T3SS system, demonstrating the presence of a T3SS-signal in the N-terminus of both proteins (Dehoux et al., 2011).

4.1.4 Expression of all 13 *C. pneumoniae* proteins give rise to phenotypes expected for MT pathway modulators

My further investigation focused on the growth phenotypes of the 13 transformants in the presence of another MT-destabilizing drug, methyl benzimidazole-2-yl carbamate (MBC). Both, TBZ and MBC target β-tubulin and inhibit MT polymerization, however, MBC is proposed to be more effective in depolymerizing MTs than TBZ (Minagawa et al., 2021; Walker, 1982). Therefore, a patch test serial dilution assay containing MBC in combination with low or high gene expression was utilized.

As shown in **Figure 11**, all transformants expressing a chlamydial gene are also hypersensitive to MBC (**Supplementary Figure 6A**). I noted that the growth phenotypes of 11/13 transformants are comparable to the growth phenotype scored in the TBZ screening. However, only the transformants highly expressing *cpn0372* and *cpn0565* in the presence of MBC react lethal instead with a strong growth defect such as observed under TBZ treatment. Nevertheless, the outcome of the MBC screening supports the result of the major TBZ screen and confirms the effectiveness and accuracy of the identification of 13 MT-modulating *C. pneumoniae* genes.

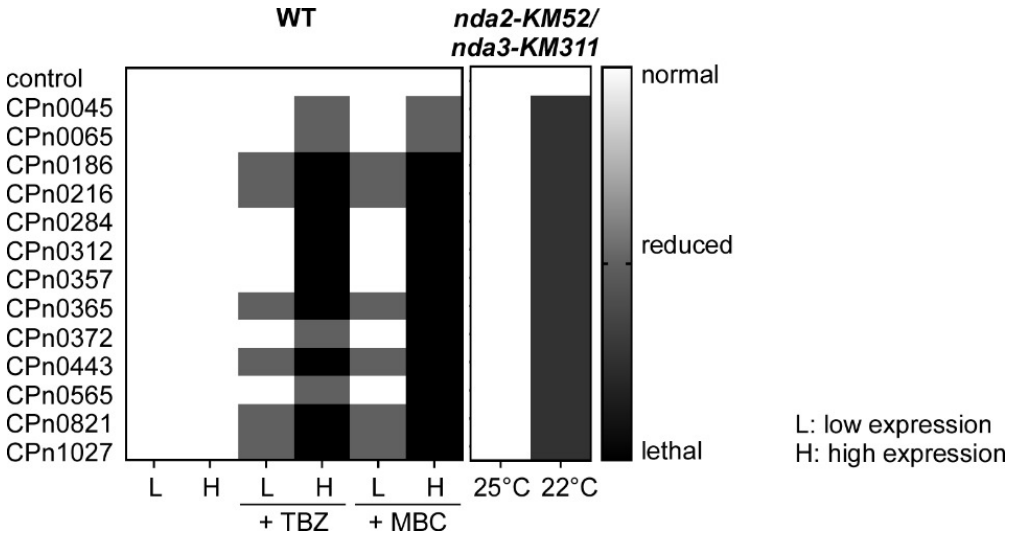

Figure 11: 13 *C. pneumoniae* proteins affect the growth of yeast transformants on MT-destabilizing drugs and the growth of tubulin-mutant strains.

Heatmap of the growth phenotypes of a control transformant strain or transformants expressing one of the indicated 13 MT-modulating chlamydial genes from a plasmid (*pJR2-3XU ura4*$^{+}$) controlled by the thiamine repressing *nmt1*$^{+}$ promoter. Strains analyzed were either wild-type (WT) or the cold-sensitive *nda2-KM52* or *nda3-KM311* mutant strains under plasmid-selective conditions. WT cells were grown at 25 °C for 6 days with/without 7 µg/mL TBZ or 2.5 µg/mL MBC; L: low expression; H: high expression. *nda2-KM52 or nda3-KM311* transformants were incubated at 25 °C or 22 °C for 7 days. L; low expression. Two yeast transformants were patched. The heatmap summarizes the results of the patch test shown in **Supplementary Figure 6A-C**.

Besides the screening for hypersensitivity against two MT-destabilizing drugs, I was interested in whether the expression of these specific *C. pneumoniae* genes showed genetic interaction with the yeast MT pathway. To answer this question, each of the 13 *C. pneumoniae* genes was expressed in two different tubulin-mutant strains *nda2-KM52* (α-tubulin) and *nda3-KM311* (β-tubulin). The mutation of the *nda2* and *nda3* genes cause a nuclear division arrest that leads to cold, TBZ and MBC-hypersensitivity of yeast cells carrying one of the mutations (Umesono et al., 1983). I lowly expressed *C. pneumoniae* genes and cultured the strains at non-permissive 22 °C and 25 °C was used as the control.

Interestingly, all transformants of both cold-sensitive strains, *nda2-KM52* and *nda3-KM311*, showed normal growth at 25 °C, but massive growth defects at 22 °C in comparison to the control plasmid (**Figure 11**, **Supplementary Figure 6B-C**). Thus, all 13 proteins genetically interact with the MT pathway.

In summary, the expression of each of the 13 different chlamydial genes cause (increased) yeast growth defects in the presence of the MT-destabilizing drugs TBZ and MBC. Moreover, the massive growth inhibition seen for the two tubulin-mutant strains when one of the 13 chlamydial genes is expressed clearly demonstrates a perturbation of the MT pathway.

4.1.5 (III) Expression of *C. pneumoniae* proteins leads to alterations of the interphase MT cytoskeleton

With regard to the previous finding, I was interested to determine if the chlamydial gene expression influenced the interphase MT structure of the fission yeast.

The interphase MT cytoskeleton of fission yeast consists of 3 to 4 antiparallel MT bundles, each made up of 3 to 4 individual MTs (Tran et al., 2001). Interphase MT bundles are orientated along the longitudinal axis of the cell, starting from the major MTOC, in close proximity to the nucleus and are directed with their dynamic MT plus-ends towards the end of the cell. For this reason, I examined the effect of expression of the 13 *C. pneumoniae* genes on the interphase MT cytoskeleton via live-cell imaging of the *gfp-α-tubulin* (endogenous *nmt81::gfp-atb2*$^{+}$) expressing yeast strain. In this strain, α-tubulin is tagged with GFP, allowing microscopic visualization of the 6 to 8 MT bundles (Tatebe et al., 2001). For simplicity, MT bundles are abbreviated to MTs in the following texts.

Initially, I tested the growth phenotype of the *gfp-α-tubulin* transformants by patch test serial dilution analysis under lower TBZ conditions (**Supplementary Figure 6D**). Indeed, the growth phenotype outcome of the assay is congruent with the results of the TBZ serial dilution assay from the WT yeast. Subsequently, I microscopically analyzed if each of the 13 highly expressed *C. pneumoniae* genes triggered a change in the interphase MT organization. In all 13 yeast transformants, the influence of the chlamydial gene expression causes various alterations in the interphase MT cytoskeleton compared to the control (**Figure 12A**). These alterations are highlighted by disoriented MT orientation (e.g. CPn0565) and/or the alterations of MT length expressed in massively shorter (e.g. CPn0443) or longer MTs (CPn0216). However, microscopic observation reveals, that the interphase MT phenotype is heterogeneous in the cell population of each transformant and includes abnormal MT structures which differ from MT structures

that are not such impaired. More than 50 % of the cells of each transformant are affected by the altered interphase MT phenotype shown in **Figure 12A** due to the chlamydial gene expression (**Supplementary Figure 7**). To define the alteration of the yeast MT cytoskeleton, the MT cytoskeleton was analyzed according to the following categories: WT-oriented, (i) disoriented MTs, (ii) aberrantly short MTs, and (iii) aberrantly long MTs (**Figure 12B**).

In a WT situation of *S. pombe*, 3 to 4 antiparallel interphase MT are orientated along the long axis and are directed to the cell ends (**Figure 12B**). MTs polymerize from the MTOC near the nucleus (region NN) along the longitudinal axis of the cell to the cell end (region CE). When the plus-ends of these MTs reach the cell end, they pause (neither polymerizing nor depolymerizing) before they depolymerize back to the MTOC and restart the polymerization.

In contrast, the MT cytoskeleton of transformants expressing a chlamydial gene is mostly affected by (i) disoriented MTs. These MTs are not oriented along the long axis of the cell and are not growing in the direction of the cell tip. Instead, disoriented MTs polymerized from the MTOC and are directed to the lateral cell cortex in region NN or CE (**Figure 12B**). All 13 transformants expressing a chlamydial gene gave rise to disoriented MTs structures compared to the control.

Another alteration is transformants with (ii) shorter MTs than the MTs of the control transformant. MTs polymerize and depolymerize predominantly in region NN, close to the nucleus and only a few MTs reach the cell end at the end of region CE.

However, the interphase MT cytoskeleton can also be altered to (iii) aberrantly longer MTs. Some interphase MTs polymerize from the MTOC, orientate along the long axis, and are directed to the cell end in region CE. When these MTs reach the cell tip, they continue to polymerize leading to MTs that grow around the cell end due to physical restraints, rather than undergoing MT catastrophe. Such MTs look like “curved or curled” MTs. These MTs can also depolymerize back to the MTOC.

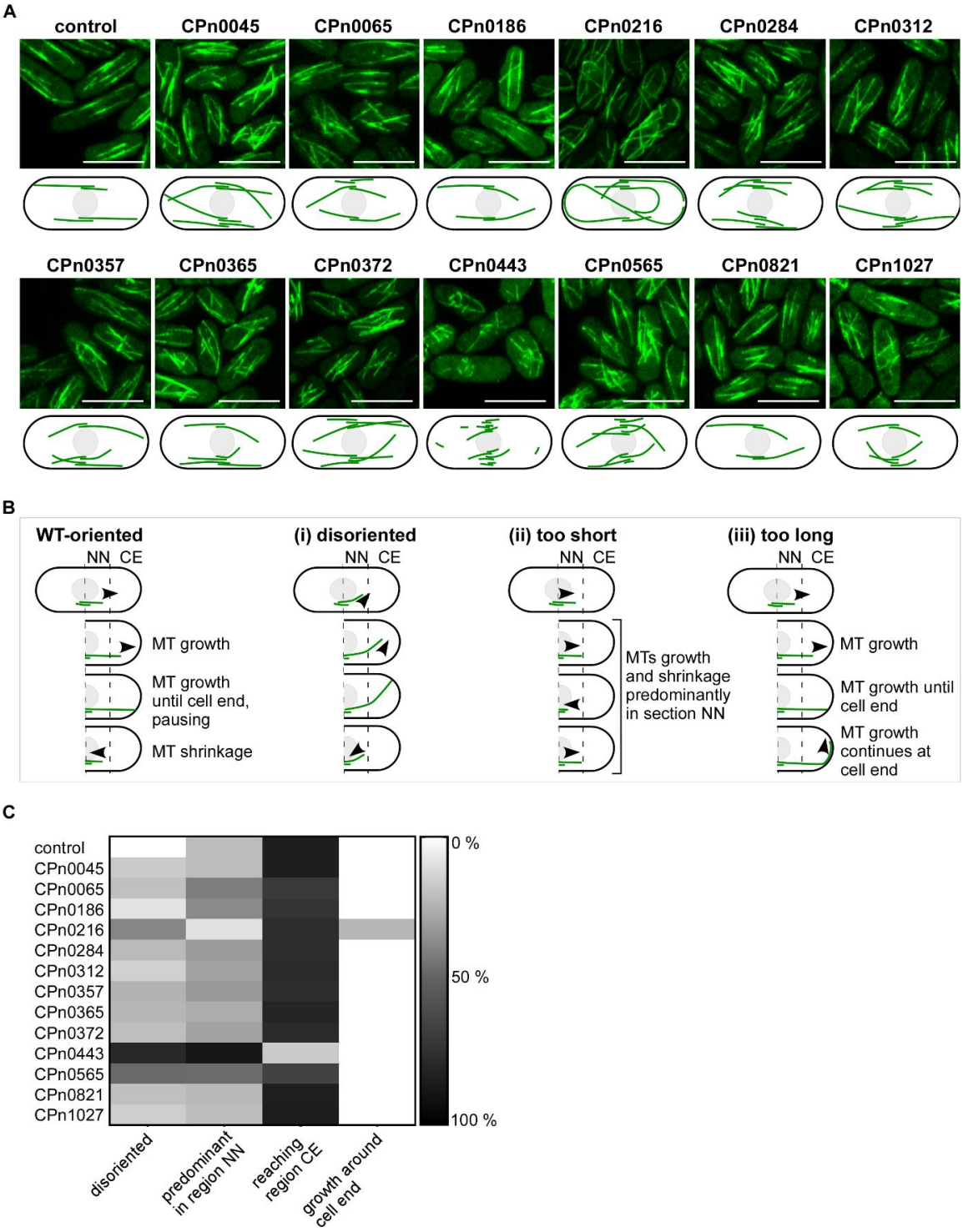

Figure 12: *C. pneumoniae* protein-induced alterations of the interphase MT cytoskeleton. **A** *S. pombe* cells expressing the endogenous *gfp-α-tubulin* (*nmt81::gfp-atb2*$^{+}$, green) were transformed with a control plasmid (pJR2-3XU *ura4*$^{+}$) or plasmids carrying one of the 13 *C. pneumoniae* genes highly expressed from the *nmt1*$^{+}$ promoter under plasmid-selective conditions at 25 °C. Photomicrographs and the relevant schematic

representation of interphase MT structures observed due to *C. pneumoniae* gene expression. Scale bars, 10 µm. Data shown in **A-C** are related to two yeast transformants. **B** Schematic illustration of WT interphase MTs during the cell cycle or alterations of the MT phenotype caused by *C. pneumoniae* gene expression, (i) disoriented MTs; (ii) too short MTs, or (iii) too long MTs. Black arrow heads show the polymerization/depolymerization direction of the MT plus-end, NN: region near the nucleus, CE: region of cell end. **C** Heatmap of the interphase MT phenotypes caused by *C. pneumoniae* proteins (described in B). 100 MTs were counted by: (i) disoriented MTs, (ii) predominant present in region NN (too short MTs), reaching region CE, and (iii)growth around the cell end (too long MTs).

Then, a quantification of the abnormal MT phenotypes was carried out on the following categories: disorganized MTs, predominantly found in region NN, reaching region CE, or MTs which grow around the cell end (**Figure 12C**). The heatmap highlighted, that the expression of all 13 chlamydial genes affects negatively the orientation of MTs and cause a predominant residence in region NN. Though, it is noticeable that the previously observed yeast growth phenotypes on TBZ and MBC are not correlating with the grade of alterations on the interphase MT cytoskeleton.

Interestingly, the gene expressions *cpn0216*, *cpn0443,* and *cpn0565* have a particularly strong influence on the MT cytoskeleton in a way that affects MT length and MT orientation. CPn0216 is the only protein that causes aberrantly long and curling MTs. The opposite effect was scored upon the expression of *cpn0443* and *cpn0565*. The interphase MT cytoskeleton of transformants expressing those genes show mainly massively abnormally short MTs. Although, *cpn0443* and *cpn0565* expression induce similar interphase MT changes, nevertheless, CPn0443 expression leads to even shorter MTs than CPn0565 expression. These shorter MTs are predominantly located in region NN of transformants expressing *cpn0443* and only a few MTs reach region CE of the cell.

Regarding these different MT alterations triggered by the expression of 13 chlamydial genes, I determined if the α-tubulin levels of the transformants were also affected. Therefore, I isolated whole-cell lysates of all transformants and performed Western blot analysis (**Supplementary Figure 8A**). Actin was used as an internal control for the quantification of the α-tubulin levels. The quantification analysis of α-tubulin showed changes between the α-tubulin levels of transformants expressing a chlamydial gene in comparison to the control transformant,

although these changes do not correlate with the interphase MT phenotypes (**Supplementary Figure 8A**-**B**).

In conclusion, the expression of all 13 *C. pneumoniae* genes alters the interphase MT cytoskeleton of the yeast by influencing the MT dynamics such as length or orientation. In particular, CPn0216 and CPn0443 are highlighted by their dramatic influences on the MT structure, encompassing longer and curling MTs for *cpn0216* expressing cells and massively short MTs for *cpn0443* expressing cells. These two types of MT aberrations were analyzed in more detail.

4.2 Expression of *cpn0216* and *cpn0443* caused alterations of MT dynamics in *S. pombe*

4.2.1 CPn0216 and CPn0443 massively affect MT dynamics

The strong alterations of the interphase MTs observed in *cpn0216* and *cpn0443* expressing transformants, propose that MT dynamics are altered. Measuring the rate of MT growth and shrinkage answered the question, if and how the expression of *cpn0216* and *cpn0443* influences MT dynamics.

Live-cell imaging microscopy confirmed that the interphase MTs of control transformants polymerize from the MTOC at the nucleus along the long axis of the cell growing towards the cell tip (**Figure 13A**). MTs reach the cell tip, pause, and start to depolymerize back to the MTOC to restart MT polymerization.

Analysis of transformants expressing *cpn0216* demonstrated, that interphase MTs polymerize from the MTOC along the long axis of the cell to the cell end and do not pause at the cell end. Instead, these MTs continue to grow, resulting in curved MTs around the cell end. At a later time point, these MTs depolymerize.

In contrast, transformants expressing *cpn0443* have massively disorganized interphase MTs which polymerize and depolymerize close to the MTOC. Only a small minority of MTs reach the cell end or lateral cell cortex in these transformants.

For the quantification of MT dynamics, I defined the parameters for the measurement of MTs in these transformants (**Figure 13B**). Firstly, cells ranging in size between 9 to 12 µm length were analyzed in live-cell imaging microscopy. Secondly, only interphase MTs with a length of 1.5 to 2 µm from the middle of the MT overlapping zone at the nucleus were used for the analysis. These MTs were measured to determine the rates of growth and shrinkage. The heterogeneous population of cells expressing *cpn0216* or *cpn0443* was used to measure MT dynamics, regardless of whether the MTs were less or massively aberrant or whether the MT structure was similar to the control.

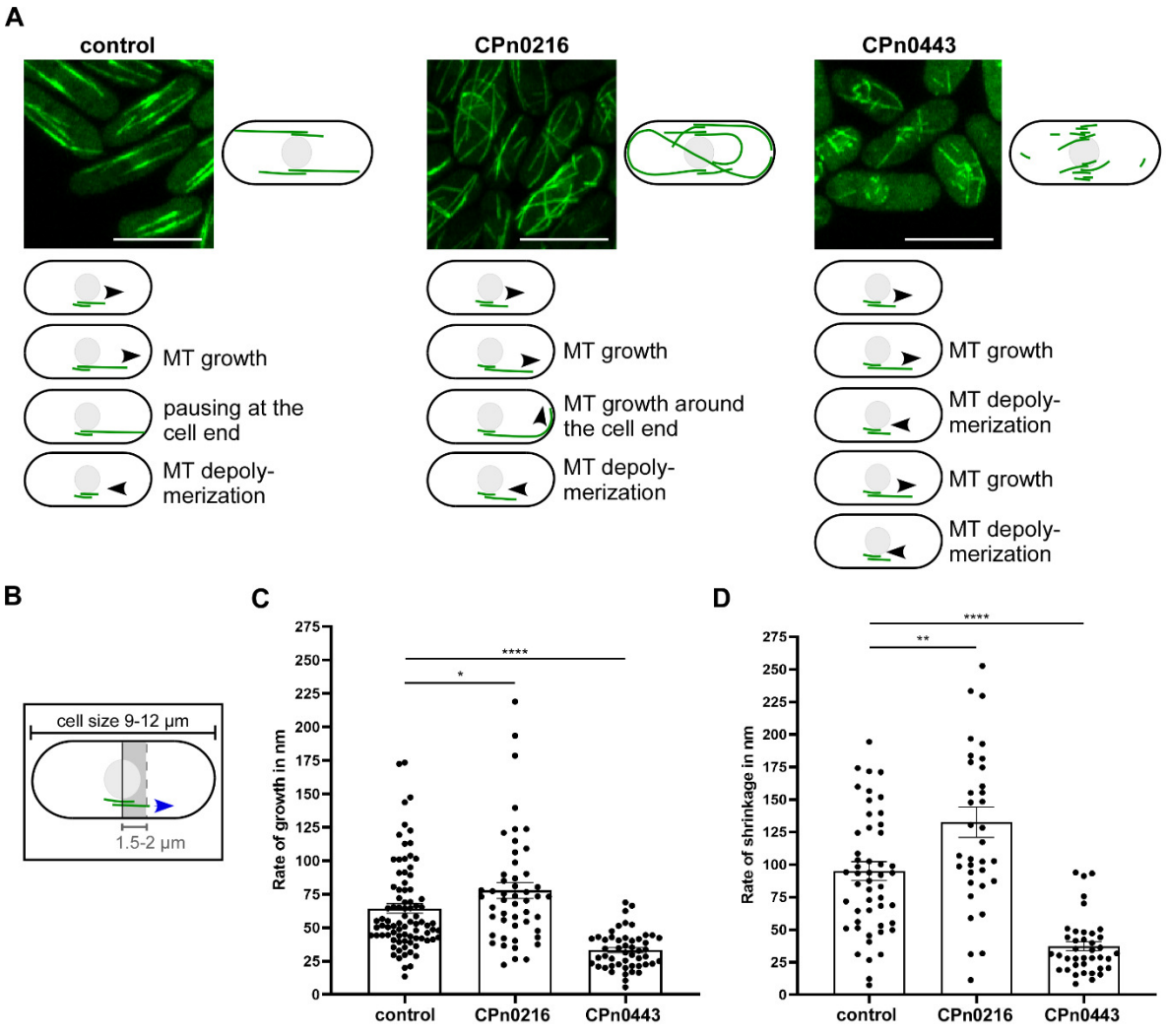

Figure 13: CPn0216 and CPn0443 massively affect MT dynamics.

A Live-cell images and schematic illustrations of interphase MTs dynamics in *gfp-α-tubulin* (*nmt81::gfp-atb2*$^{+}$, green) cells transformed with a control plasmid (pJR2-3XU *ura4*$^{+}$) or plasmids harboring *cpn0216* or *cpn0443*.

Black arrow heads show the direction of MT polymerization/depolymerization. Scale bars, 10 µm. **B** Schematic illustration of the measurement strategy for MT dynamics. Single MTs were measured until they reached the cell end and/or started to depolymerize prematurely. MT dynamics/time starting with MTs of 1.5-2 µm length (green) from the middle of the MT overlapping zone (black line). Blue arrow shows growth direction. **C** Quantification of the MT growth rate. Data points represent the mean of growth rate in nm/sec after at least 21 seconds of growth. Control n= 86 MT (6 cells), CPn0216 n= 49 MT (11 cells) and CPn0443 n= 50 MT (6 cells); p= 0.0275 (*), p <0.0001 (****). **D** Quantification of MT shrinking rate. Data points represent the mean of shrinkage rate in nm/sec of at least 21 seconds. Control n= 51 MT (6 cells), CPn0216 n= 35 MT (11 cells) and CPn0443 n= 39 MT (6 cells); p= 0.0039 (**), p <0.0001 (****). For **C** and **D**, error bars denote ± SEM, two-tailed student's T-test was used to determine statistical significance. Quantitative analysis of time-lapse microscopy, 280 seconds in total, 7 seconds intervals. Data shown in **B-D** are related to two individual experiments.

Microscopic analysis showed that the rates of growth and shrinkage are significantly altered by the expression of one of the chlamydial genes even with respect to the heterogeneous MT structures within the cell population (**Figure 13C**). Cells expressing *cpn0216* have a significantly higher growth rate (p= 0.0275; n= 49 MTs) in comparison to the control transformants (n= 86 MTs). In addition, the MT plus-end catastrophe frequency of MTs touching the cell end is significantly reduced to 74 % compared with control. In contrast, the expression of *cpn0443* leads to a significantly decreased rate of growth (p <0.0001; n= 50 MTs) compared to the control.

A similar pattern was detected for the rate of shrinkage. A significant increased rate of shrinkage was observed in cells expressing *cpn0216* (p= 0.0039; n= 35 MTs) and a significant decreased rate of shrinkage in cells expressing *cpn0443* (p <0.0001; n= 39 MTs) in comparison to control cells (n= 51 MTs) (**Figure 13D**). These results demonstrate that both proteins significantly affect MT dynamics.

Furthermore, the time-lapse series of live-cell images of *gfp-α-tubulin* interphase MTs microcopy offer an insight into the polymerization and depolymerization behavior of *cpn0216* and *cpn0443* expressing cells. To highlight the massive changes in MT dynamics, I represented the dynamic behavior of a single MT from either a control, *cpn0216* or *cpn0443* expressing cells into a graph (**Figure 14A-B**).

MT dynamics of a control transformant (green curve) show polymerization of an MT to the cell

end, followed by pausing (pink triangle) and then MT depolymerization back to the MTOC (blue dot) demonstrated in a graphical illustration (**Figure 14A-B**).

In contrast, MT dynamics of cells expressing *cpn0216* (orange curve) are altered causing aberrantly long and curling MTs that grow around the cell end (red star) (**Figure 14A**). The behavior of one of those MTs is graphically illustrated in **Figure 14B**. The orange curve shows MT growth around the cell tip (red star) without forming a plateau representative for a pausing event, followed by an MT depolymerization. This example clearly highlights MT polymerization is faster in *cpn0216* expressing cells in comparison to control cells which conform with the significantly higher growth rate (p= 0.0275) shown in **Figure 13C**.

The opposite behavior is seen for MTs of cells expressing *cpn0443* in the blue curve. Expression of this chlamydial gene leads to massively shorter interphase MTs. An example is shown in **Figure 14A and B**, where the blue curve demonstrates a permanent switching of MT growth and shrinkage in the area close to the MTOC.

In order to get a better picture of MT dynamics, I summarized the measurement of six individual interphase MTs in one graph (**Figure 14C**). The six individual MTs from control cells represent WT-like MT dynamics of MT polymerization to the cell end, pausing, and depolymerization back to the MTOC.

In contrast to the homogeneous MT structure of control transformants, the MT structure of *cpn0216* and *cpn0443* expressing cells is heterogeneous, highlighted in either abnormal MT structures or MT structures that are not such impaired.

Due to these heterogeneous MT phenotypes of *cpn0216* expressing cells, the two main phenotypes observed are shown: (i) three individual MTs, that curve upon reaching the cell tip without pausing, and (ii) three MTs that grow to the cell end, pause, and then depolymerize (**Figure 14C**). The frequency of (i) i.e. massively longer and curved MTs is 26 %. Although (ii) these MTs behave similarly to MTs of control transformants, MTs growing to the cell end and pausing at the cell tip before shrinking back, the MT growth is interrupted by short events of depolymerization. Similarly, MT depolymerization is interrupted by short polymerization events. This MT behavior clearly differs from control MTs.

MT dynamics measured from cells expressing *cpn0443* could be also separated into two MT

phenotypes. (i) three MTs represent massively short MT constantly switch between MT growth and shrinkage without reaching the cell ends, while (ii) three other MTs reach the cell tips, pause, and shrink back (**Figure 14C**). Within the population of aberrant cells, 88 % of the measured (i) MTs are massively shorter and do not polymerize to the cell tips. Nevertheless, both types of MTs clearly differ from the control curves due to the fact, that MT dynamics switch constantly between growth and depolymerization.

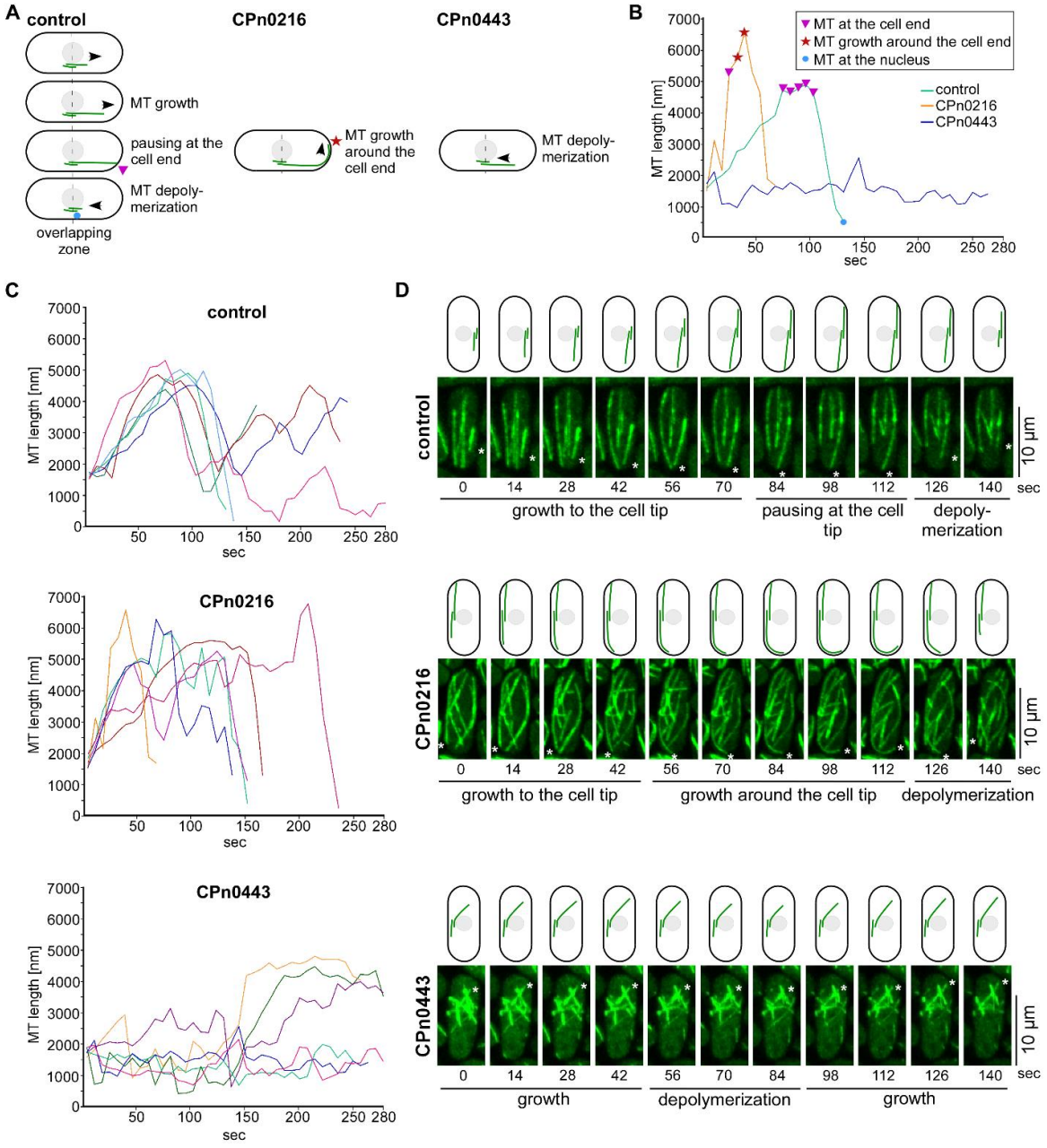

Figure 14: Expression of chlamydial *cpn0216* or *cpn0443* genes results in aberrant MT dynamics. **A** Diagrammatic representation of wild-type MT dynamics of an *S. pombe* interphase cell. Control cells were with

a plasmid not carrying a chlamydial gene (pJR2-3XU *ura4*$^{+}$) or yeast transformants expressing plasmid-borne *cpn0216* or *cpn0443*. Interphase MTs from control cells polymerize from the vicinity of the nucleus in an oriented manner along the long cell axis to the cell end, then pause (pink triangle) and depolymerize back to the nucleus (blue dot). MTs of *cpn0216*-expressing cells do not stop polymerization once the cell end is reached but continue to grow around the cell end resulting in a ”curling” phenotype (red star). On the other hand, MTs of *cpn0443*-expressing cells depolymerize before reaching the cell end. **B** Representative examples of the dynamic behavior of a single MT from either a control, *cpn0216* or *cpn0443* expressing cells. MT dynamics of MTs that were 1.5-2 µm in length (from the middle of the MT overlap zone) were measured via live-cell imaging of *gfp-α-tubulin*. **C** Examples of the dynamic behavior of individual interphase MTs from either control, *cpn0216* or *cpn0443* expressing cells demonstrate the consistently aberrant MT dynamics caused by the expression of these chlamydial proteins. Data shown in **A-C** are related to two individual experiments from **Figure 13**. **D** An example of Live-cell images of *gfp-α-tubulin* (*nmt81::gfp-atb2*$^{+}$, green) interphase MTs of a control cell or *cpn0216* or *cpn0443* highly expressing cells under plasmid selective conditions at 25 °C. White asterisks denote the plus-end of the MT analyzed.

To foreground the aberrant interphase MT phenotypes and their effect on yeast MT dynamics, I visualized photomicrographs of a time-lapse microscopy series of control transformants and transformants expressing either *cpn0216* or *cpn0443* (**Figure 14D**). While the time-lapse series of a control transformant showed MT polymerization, pausing and depolymerization, the MTs of the *cpn0216* expressing cell continue the MT grow and curved around the cell tip before the depolymerization started. No pausing event was monitored. In contrast, the MTs of the *cpn0443* expressing cell demonstrated a permanent switch between MT growth and shrinkage making it impossible for MTs to reach the cell ends.

In conclusion, the expression of *cpn0216* causes significantly increased growth and shrinkage rate, while the expression of *cpn0443* leads to a significantly decreased rate of growth and shrinkage compared to the control. Regardless of whether the MT structure is abnormal or not so impaired, both MT types show a clear influence on MT dynamics compared to the control.

4.2.2 CPn0216 and CPn0443 modulate MTs alterations via their C-terminus

Then, I was interested to determine the protein region of CPn0216 and CPn0443 that cause the massive alterations of the interphase MT cytoskeleton and influence MT dynamics. To

define the subcellular localization of these proteins, live-cell imaging of the *gfp-α-tubulin* expressing yeast strain was used.

The MT-modulating domains of both Inc proteins could be located in the C-terminal region behind the transmembrane domains. This expectation is based on studies that have reported that especially the C-terminal region of Inc proteins is the key player for the interaction with host proteins (Gauliard et al., 2015; Elwell et al., 2017). Importantly, the Inc protein CPn0443 harbors four transmembrane domains, while CPn0216 harbors two transmembrane domains that separate the N-terminal protein region from the C-terminus. For that reason, I generated pJR2-3XL *LEU2* plasmids carrying the C-terminal version of the genes: CPn0216$^{82\text{-}145}$ and CPn0443$^{164\text{-}417}$ (**Figure 15A, B**).

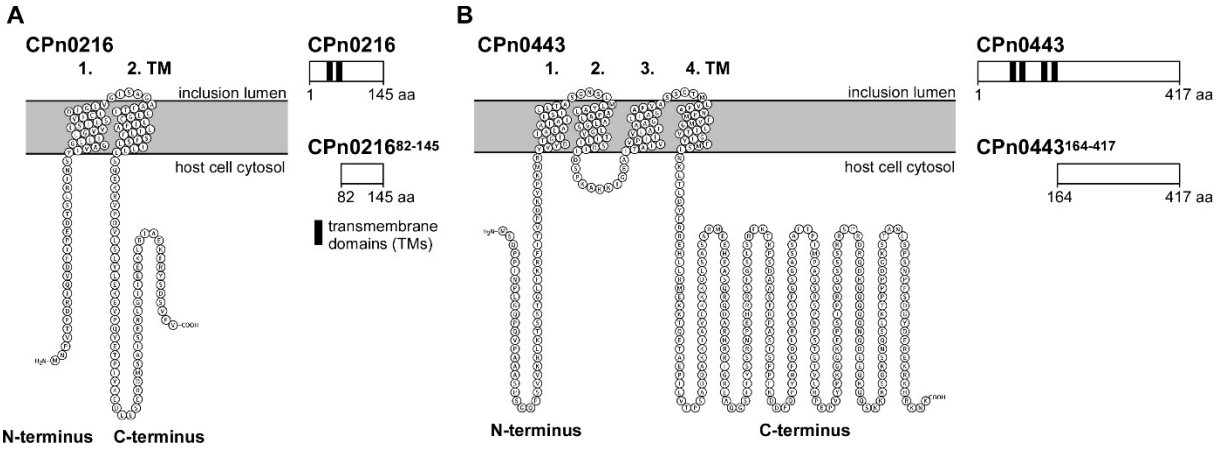

Figure 15: Predicted protein structure of CPn0216 and CPn0443.

A CPn0216 is predicted to be a 145 aa Inc protein that is anchored in the inclusion membrane by two transmembrane domains (TMs). The C-terminal area is comprised of aa 82-145. **B** CPn0443 is predicted to be a 417 aa Inc protein that is anchored in the inclusion membrane by four TMs. The C-terminal area is comprised of aa 164-417. The proteins have a short N-terminal part and longer C-terminus, both located in the host cytosol and connected by a loop. aa: amino acids. Illustrations of predicted protein structures were generated from Protter (https://wlab.ethz.ch/protter/start/).

In order to answer the question, which region of CPn0216 causes the massive alterations of the interphase MT cytoskeleton, I analyzed the influence on the interphase MT cytoskeleton of *cpn0216* and *cpn0216*$^{82\text{-}145}$ expressing yeast cells compared to the control. In case, CPn0216 interacts via its C-terminus with MTs or MT-associated proteins, alterations of the interphase

MT cytoskeleton of *cpn0216* and *cpn0216*$^{82-145}$ expressing cells are comparable.

Microscopic analysis of transformants expressing *cpn0216* or *cpn0216*$^{82-145}$ revealed, that both protein variants function in a similar manner on MTs that cause massively longer MTs which grow around the cell tip and the formation of MT loops (**Figure 16A-B**). While in control transformants, the growing MTs reorganize the growth direction toward the cell end after contact with the lateral cell cortex, MTs of *cpn0216* or *cpn0216*$^{82-145}$ expressing transformants do not correct the MT growth direction toward the cell ends. Microscopic analysis of the single-cell layers of *cpn0216* or *cpn0216*$^{82-145}$ expressing cells revealed the continuous MTs growth along the lateral cell cortex resulting in MT loop formation. For simplicity, the formation of an MT loop of a *cpn0216/cpn0216*$^{82-145}$ expressing transformant is illustrated in **Figure 16C** as a 3D view but I was also able to visualize the formation of an MT loop by using time-lapse microscopy series (**Figure 16D**). The identical alterations of the MT cytoskeleton phenotypes induced by the expression of *cpn0216* or *cpn0216*$^{82-145}$ indicate that the MT-modulating domain has to be located in the C-terminal region of the protein to interact with the MTs or MT-regulating proteins.

Next, I visualized photomicrographs of a time-lapse microscopy series of control transformants and transformants expressing either *cpn0216* or *cpn0443* (**Figure 14D**). While the time-lapse series of a control transformant showed MT polymerization, pausing and depolymerization, the MTs of the *cpn0216* expressing cell continue the MT grow and curved around the cell tip before the depolymerization started. No pausing event was monitored. In contrast, the MTs of the *cpn0443* expressing cell demonstrated a permanent switch between MT growth and shrinkage making it impossible for MTs to reach the cell ends.

To test, if elongated and curling MTs could also be observed in abnormally long fission yeast cells, I used the cell cycle mutant strain *cdc25-22*, which gives rise to highly elongated cells at the G_2/M transition. Therefore, *cpn0216* and *cpn0216*$^{82-145}$ were expressed in the temperature-sensitive yeast mutant strain *cdc25-22 gfp-α-tubulin* (endogenous *cdc25-22 nmt81::gfp-atb2*$^{+}$). By using this yeast strain with longer cells, MT characteristics such as curving MT or the formation of MT loops can be better analyzed.

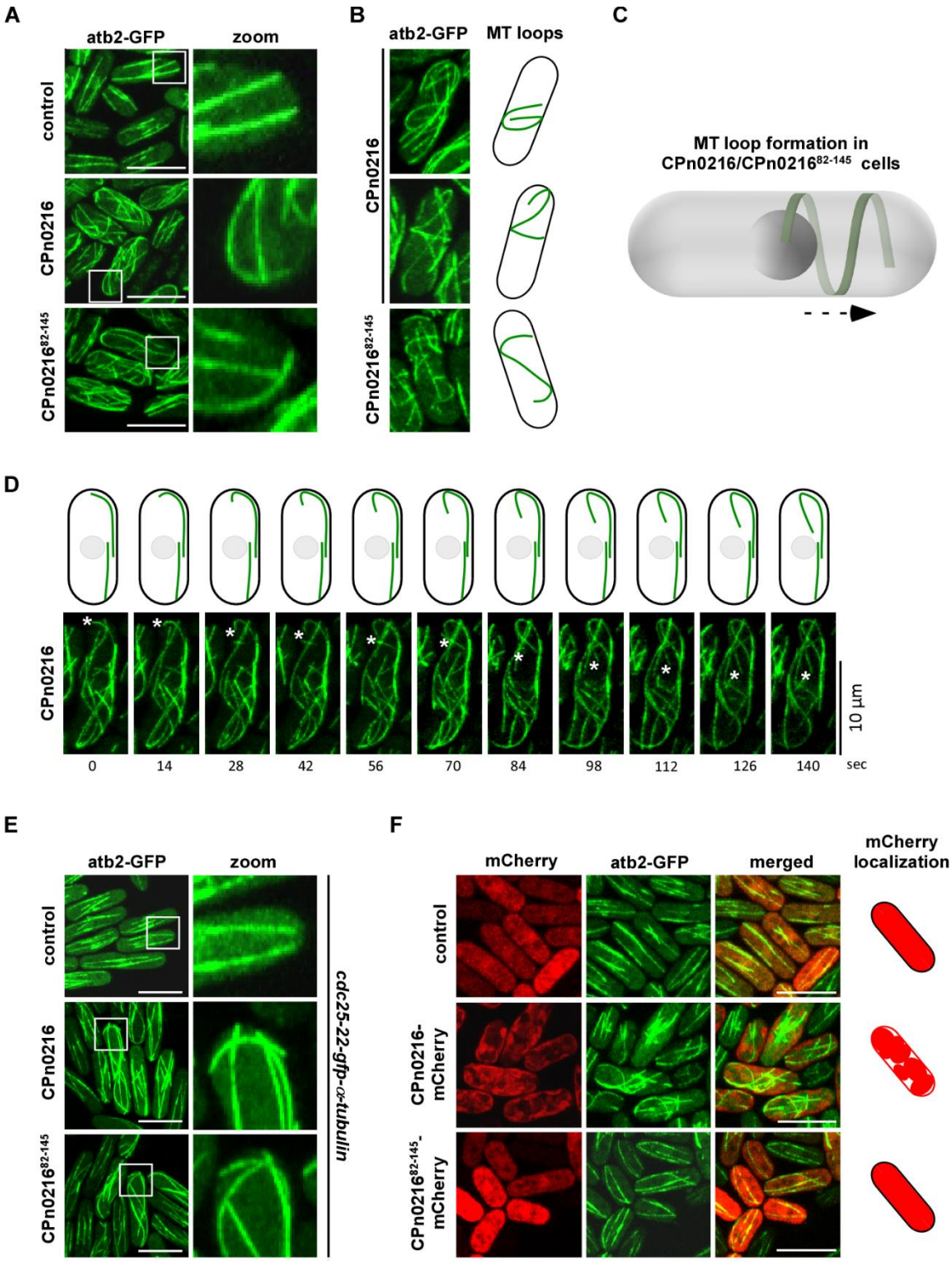

Figure 16: Interphase MT structure and localization analysis of CPn0216.

A-B Photomicrographs of *S. pombe* cells expressing the endogenous *gfp-α-tubulin (nmt81::gfp-atb2⁺,* green) were transformed with a control plasmid (pJR2-3XL *LEU2)* or plasmids carrying either *cpn0216* or *cpn0216*$^{82\text{-}145}$ highly expressed from the *nmt1⁺* promoter under plasmid-selective conditions at 25 °C. **B-C** Photomicrographs and

3D illustration of MT loop formation in *cpn0216* or *cpn0216*$^{82-145}$ expressing cells. **D** An example of Live-cell images of MT loop formation in a *cpn0216* expressing cell. White asterisks denote the plus-end of the MT analyzed. **E** Photomicrographs of *S. pombe* cells expressing the endogenous *cdc25-22-gfp-α-tubulin* (*cdc25-22 nmt81::gfp-atb2*$^{+}$, green) were transformed with a control plasmid (pJR2-3XL *LEU2*) or plasmids carrying either *cpn0216* or *cpn0216*$^{82-145}$ highly expressed from the *nmt1*$^{+}$ promoter under plasmid-selective conditions at 25 °C. **F** Photomicrographs of *gfp-α-tubulin* cells highly expressing a pJR2-3XL *LEU2* plasmid-borne *mCherry* (control, red), *cpn0216-mCherry,* or *cpn0216*$^{82-145}$*-mCherry*. Schematic illustrations represent the localization of mCherry. Scale bars, 10 µm. White boxes show enlargements (zoom). Arrow represents the MT growth direction. Two yeast transformants were analysed.

Live-cell imaging of *cdc25-22 gfp-α-tubulin* cells expressing *cpn0216* and *cpn0216*$^{82-145}$ confirmed that MTs are still elongated and grow around the cell end in comparison to the control (**Figure 16E**). However, in contrast to the WT strain and thus smaller cells, the MTs in the *cdc25-22 gfp-α-tubulin* mutant infrequently grow around the cell ends when the full-length or C-terminus version of *cpn0216* is expressed. These results demonstrate, that *cpn0216* and *cpn0216*$^{82-145}$ expressing cells have longer MTs due to longer phases of polymerization before MT catastrophe.

To answer the question, where CPn0216 or CPn0216$^{82-145}$ are localized in the yeast, I tagged both chlamydial genes C-terminally with a mCherry-tag. As a control, a transformant expressing *mCherry* was used.

The localization analysis revealed, that the previously observed MT phenotype induced by *cpn0216* or *cpn0216*$^{82-145}$ expression is not comparable to the MT phenotype induced by CPn0216-mCherry and CPn0216$^{82-145}$-mCherry (**Figure 16F**). The mCherry-tag negatively influences the functionality of both protein variants. Consequently, the number of cells with massively longer and curved MTs are considerably reduced in the presence of CPn0216-mCherry compared to the cells expressing *cpn0216*, whereas no aberrant MTs are detectible in *cpn0216*$^{82-145}$*-mCherry* expressing cells. Due to the unfunctional protein variants caused by the mCherry-tag, no statement can be made about the localization of CPn0216 or CPn0216$^{82-145}$.

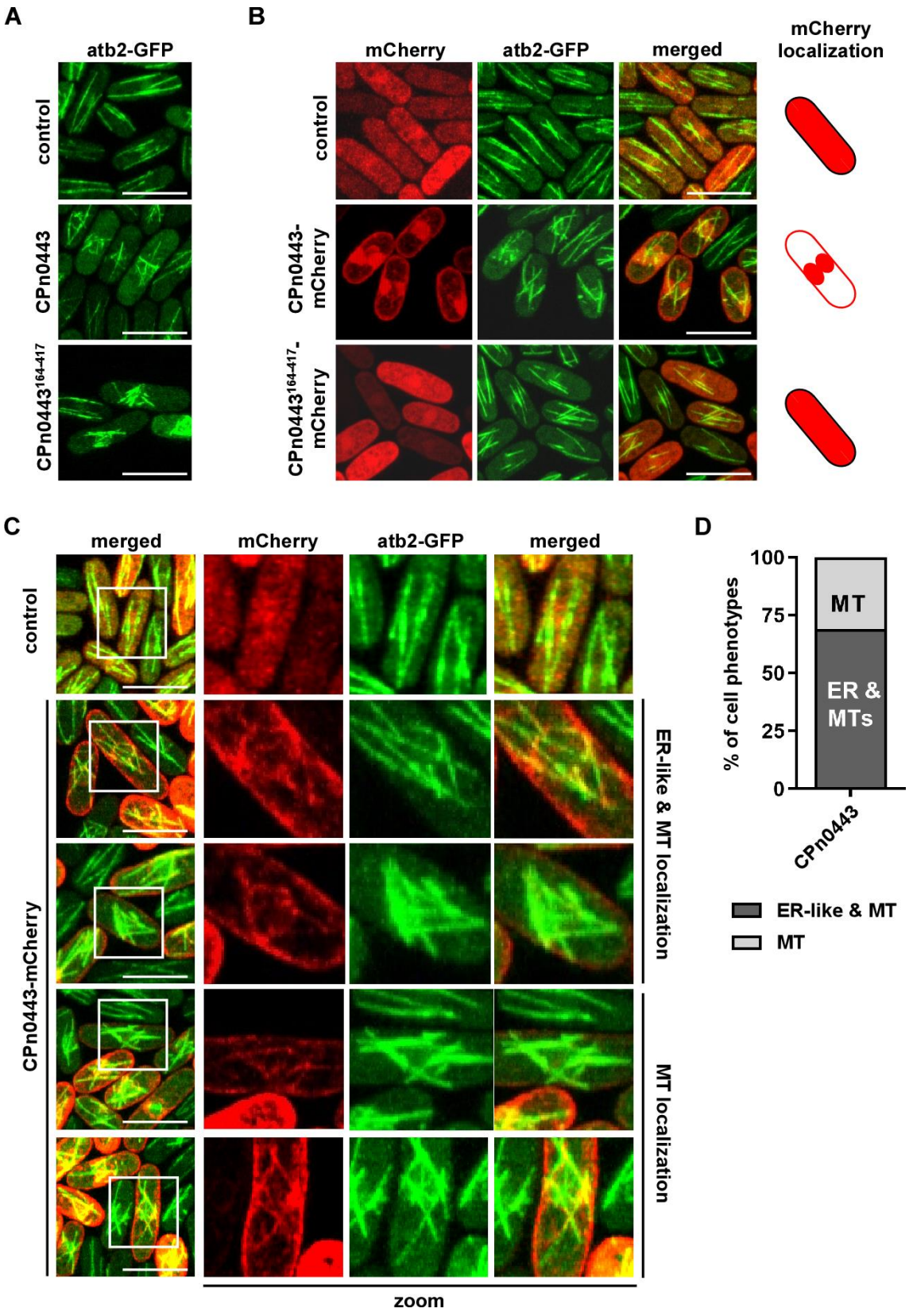

Figure 17: CPn0443 is localized in the region of the nucleus.

A Photomicrographs of *S. pombe* cells expressing the endogenous *gfp-α-tubulin (nmt81::gfp-atb2⁺,* green) were

transformed with a control plasmid (pJR2-3XL *LEU2)* or plasmids carrying either *cpn0443* or *cpn0443*$^{164\text{-}417}$ highly expressed from the *nmt1*$^{+}$ promoter under plasmid-selective conditions at 25 °C. **B** Photomicrographs of *gfp-α-tubulin* cells highly expressing a pJR2-3XL *LEU2* plasmid-borne *mCherry* (control, red), *cpn0443-mCherry,* or *cpn0443*$^{164\text{-}417}$*-mCherry*. Schematic illustrations represent the localization of mCherry. **C-D** Photomicrographic and quantitative analysis overview of cells showing an ER-like and MT localization of CPn0443-mCherry close to the nucleus, or a partial co-localization to the MT structure of the yeast. 50 cells from three independent experiments were analyzed. **A-C** Scale bars, 10 µm.

Next, I was interested to define the region of CPn0443 that causes the massive alterations of the interphase MT cytoskeleton. Therefore, I analyzed the effect on the MT structure of *cpn0443* or *cpn0443*$^{164\text{-}417}$ expressing cells compared to control transformants.

Fluorescence microscopic analysis of transformants expressing *cpn0443* or *cpn0443*$^{164\text{-}417}$ revealed, that the interphase MT phenotype of massively shortened MTs is affected in a similar way by the expression of either *cpn0443*, the full-length protein, or the C-terminal variant of CPn0443 (**Figure 17A**). These comparable alterations of the interphase MT cytoskeleton induce by both CPn0443 variants suggests, that the MT-modulating domain has to be located in the C-terminal region of the protein to interact with the MTs or MT-regulating proteins of the host.

Subsequently, to answer the question, where CPn0443 and CPn0443$^{164\text{-}417}$ are localized in the yeast, I fused both CPn0443 variants with a C-terminal mCherry-tag.

Microscopic analysis showed, that CPn0443-mCherry is predominantly accumulated in close vicinity to the nucleus and is localized at the plasma membrane. Additionally, CPn0443-mCherry negatively affects the formation of the yeast MT cytoskeleton, while the expression of *cpn0443*$^{164\text{-}417}$*-mCherry* caused a significant reduction of cells with massively shorter MTs (**Figure 17B**). The loss of aberrant interphase MT phenotypes in *cpn0443*$^{164\text{-}417}$*-mCherry* expressing cells gives reason to assume that fusion of the mCherry-tag leads to a loss of protein function, thus no statement can be made about the localization of CPn0443$^{164\text{-}417}$-mCherry. Thus, I concentrated on CPn0443-mCherry for further localization analyses.

In addition to the predominantly accumulated CPn0443-mCherry in close proximity to the nucleus and the changes of the MT cytoskeleton observed in **Figure 17B**, it was apparent that

the MT phenotype is not consistent in all *cpn0443-mCherry* expressing cells. Considering to the cloud-like accumulation of MTs co-localizing with the strong accumulation of CPn0443-mCherry in the same region, I tested if CPn0443-mCherry is accumulated by *gfp-α-tubulin* of the yeast strain. For this purpose, *cpn0443-mCherry* was expressed in WT yeast lacking GFP expression. Indeed, the checkup revealed that CPn0443-mCherry continues to accumulate in a cloud-like cluster in the vicinity of the nucleus even in the absence of *gfp-α-tubulin* (**Supplementary Figure 9**).

Besides the strong accumulations of CPn0443 mCherry and MTs in the region of the nucleus, I focused on cells with a less strong CPn0443 mCherry signal to detect co-localization with host cell structures. Less strong CPn0443 mCherry signals provided the identification of the ring-shaped CPn0443-mCherry localization in the middle of the cell (**Figure 17C**). This phenotype in addition to the CPn0443-mCherry detection along the plasma membrane suggests an ER localization such as observed in Zhang et al., 2012 by using the ER marker GFP-AHDL in *S. pombe*. From the ring-like localization of CPn0443-mCherry, I also co-localized CPn0443-mCherry partially along some shorter and disorganized MTs. The second phenotype I observed showed that CPn0443-mCherry partially co-localized with shorter MTs without an ER-like localization. Quantitative analysis of 150 CPn0443-mCherry transfected cells revealed that 68.7 % of the cells showed an ER-like and MT phenotype, whereas 31.3 % of the cells exhibited an MT phenotype only (**Figure 17D**).

Summing up, the massive alterations of the interphase MT cytoskeleton are caused by the C-terminal domains of CPn0216 and CPn0443. Further localization analysis of CPn0216-mCherry was not evaluable, while CPn0443-Cherry is located in close vicinity to the nucleus that suggests ER-like and MT localization or partial MT localization only.

4.2.3 CPn0216 appears to stabilize MTs and reduces the localization of cell end marker proteins

In the further course of the functional characterization of CPn0216, I was interested in discovering whether CPn0216 affects MT structure, organization, and MT dynamics via a direct

effect on MTs or by an interaction with a host cell protein.

MT dynamics and associated MT length are determined by the spatial regulation of the MT-stabilizing Mal3/Tea2/Tip1 complex and the MT-destabilizing Klp5/Klp6 complex. During MT polymerization, the MT-stabilizing Mal3/Tea2/Tip1 complex is localized at the growing MT plus-end and stabilizes the MT tip via Mal3 and Tip1, while the MT-destabilizing Klp5/Klp6 complex accumulates behind it (Bieling et al., 2007). The motor protein Tea2 does not stabilize the MT tip but is essential for Mal3-mediated transport of Tip1 and for the movement of other polarization factors such as Tea1 and Tea4, which are necessary for the maintenance of polarized cell growth (Browning and Hackney, 2005). For movement to the MT plus-end, Tea1 forms a large complex with Tea4, Tea2, and Tip1 while Mal3 is necessary to activate the motor activity. At the growing MT plus-end, Tea1 acts as an "MT growth navigator" regulating the direction of MT growth, while Tea1 anchored at the cell end serves as a cortical landmark (Mata and Nurse, 1997; Behrens and Nurse, 2002). Upon contact of the growing MT plus-end with the cell end, the MT-destabilizing Klp5/Klp6 complex advances to the Tea1/Tea4/Tea2/Tip1 complex. Contact of the MT tip with the cell end slows MT polymerization and the MT-destabilizing Klp5/Klp6 complex replaces the Tea1/Tea4/Tea2/Tip1 complex at the MT plus-end. Tea1 initiates the MT catastrophe event through a Tea1-mediated anchoring of Tea4, Tea2, and Tip1 at the cell end. The release of the Tea1/Tea4/Tea2/Tip1 complex and Mal3 from the MT tip causes MT destabilization and allows the Klp5/Klp6 complex to initiate MT depolymerization (Brunner and Nurse, 2000; Behrens and Nurse, 2002). In the microscope, Tea1-GFP, Tea4-GFP, Tea2-GFP, and Tip1-GFP can be localized as accumulated dots along growing MTs and at the cell ends (Brunner and Nurse, 2000; Sawin and Nurse, 1998).

Considering the long MTs that curl around the cell ends and the disordered MT growth direction that forms MT loops, the question of how CPn0216 affects MTs arises. Therefore, I was focused to answer the following questions:

1. Does CPn0216 and/or CPn0216$^{82-145}$ stabilize MTs in the absence of an MT stabilizer?

2. Does CPn0216 interact with one of the major regulators of MT dynamics or a cell end marker protein?

First, I was interested in clarifying if the reason for the failing MT catastrophe event of the growing MT upon contact with the cell end, and the resulting continued MT growth around the cell end, is a CPn0216 and CPn0216$^{82\text{-}145}$-induced hyperstabilization of the MTs. To determine whether CPn0216 and CPn0216$^{82\text{-}145}$ contribute to MT stabilization, I analyzed the effect of *cpn0216* and *cpn0216*$^{82\text{-}145}$ expression on MT growth in the absence of the MT stabilizer Mal3 in the *mal3Δ gfp-α-tubulin* deletion strain. Since Mal3 is required for stabilization for the polymerizing MT plus-end, the *mal3Δ gfp-α-tubulin* mutant generally has shorter interphase MTs than a WT strain without a mutation.

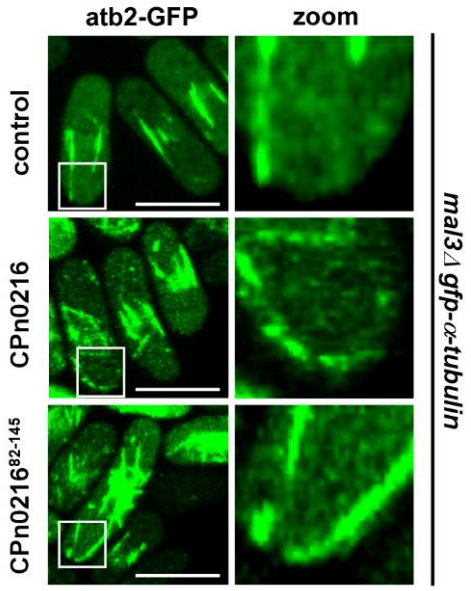

Figure 18: Indications for MT curling at the cell end of *cpn0216* and *cpn0216*$^{82\text{-}145}$ expressing *mal3Δ gfp-α-tubulin* mutants.

Photomicrographs of *S. pombe* cells expressing the endogenous *mal3Δ gfp-α-tubulin (mal3Δ nmt81::gfp-atb2*$^{+}$*,* green) were transformed with a control plasmid (pJR2-3XL *LEU2)* or plasmids carrying either *cpn0216* or *cpn0216*$^{82\text{-}145}$ highly expressed from the *nmt1*$^{+}$ promoter under plasmid-selective conditions at 25 °C. Scale bars, 10 µm. White boxes show enlargements (zoom). Two yeast transformants were analyzed.

Live-cell imaging of the *cpn0216* and *cpn0216*$^{82\text{-}145}$ expressing cells showed massive aberrant MT structures and for some cells MT growth to the cell end with indications of MTs curling

around the cell end despite the absence of host cell MT stabilizer. In contrast, the MT of control cells are organized along the longitudinal axis of the cell toward the cell ends and MTs are predominantly short except for a few MTs that grow to the cell end and shrink again after contact (**Figure 18**). These observations imply that CPn0216 could stabilize MTs even in the absence of Mal3 and cannot undergo MT catastrophe upon contact with the cell end.

To answer the second question, if CPn0216 interacts with one or more major regulators of MT dynamics or a cell polarity factor, I used the deletion strains *tea1Δ, tea2Δ, tip1Δ,* and *mal3Δ*, and the mutant strains *klp5* and *klp6* for the expression of *cpn0216* and performed a serial dilution patch test under TBZ treatment.

In case, CPn0216 interacts with Klp5, Klp6, Tea1, Tea2, Tip1, and/or Mal3, no interaction would be possible in the absence of this host cell interaction partner and the yeast would grow unaffected like the control in the presence of TBZ. If the yeast reacts with a growth defect and TBZ-hypersensitivity to the expression of *cpn0216*, this indicates that CPn0216 continues to influence the MT network by interacting with the host cell target.

Serial dilution patch assays of *cpn0216* expressing *klp5* and *klp6* mutant strains indicated a strong growth defect and TBZ-hypersensitivity (**Figure 19A**). A similar growth defect and TBZ-hypersensitivity is noted for *cpn0216* expressing *tea2Δ, tip1Δ,* and *mal3Δ* deletion strains compared to control transformants, while the expression of *cpn0216* impaired yeast growth *tea1Δ* mutants but does not cause TBZ-hypersensitivity (**Figure 19B**). The TBZ-independent reduced yeast growth of *tea1Δ* mutants caused by high *cpn0216* expression may indicate a possible interaction between CPn0216 and Tea1. However, yeast growth is not rescued suggesting for another host cell interaction partner of CPn0216 is involved in the induction of the growth defect in the absence of Tea1.

Next, I assessed the effect of CPn0216 on the localization of Tea1. For this purpose, I transformed *tea1-gfp* (endogenous *tea1-pk-gfp*) expressing cells with a plasmid carrying the *cpn0216* and documented the localization of Tea1-GFP by live-cell microscopy.

Microscopic analysis of *cpn0216* expressing *tea1-gfp* cells revealed two interesting facts. First, I monitored the tracking of Tea1-GFP signals starting from the MTOC towards the end of the

cell, but I did not notice any signals moving in the direction of the lateral cell cortex (**Figure 19C**). Secondly, the Tea1-GFP fluorescence signal intensity at the cell ends is significantly decreased (p= 0.0045, n= 50) compared to the control (**Figure 19C**).

Considering that Tea1 is essential for anchoring Tea4, Tea2, and Tip1 at the cell end to initiate MT catastrophe, I investigated whether the reduction of Tea1-GFP fluorescence signal intensity also affects the fluorescence signal intensity of Tea4-GFP, Tea2-GFP, and Tip1-GFP. Therefore, I expressed *cpn0216* in *tea4-gfp, tea2-gfp,* and *tip1-gfp (tip1-pk-gfp)* strains and detected significantly reduced fluorescence signal intensity of Tea4-GFP (p= 0.0328, n= 50) and Tip1-GFP (p= 0.0487, n= 50) at the cell ends, while the fluorescence signal intensity of Tea2-GFP is slightly reduced compared to the control (**Figure 19C**). In these strains expressing *cpn0216*, I was able to track the signals from Tea4-GFP, Tea2-GFP, and Tip1-GFP from the MTOC to the end of the cell, but I detected only rarely signals moving towards the lateral cell cortex.

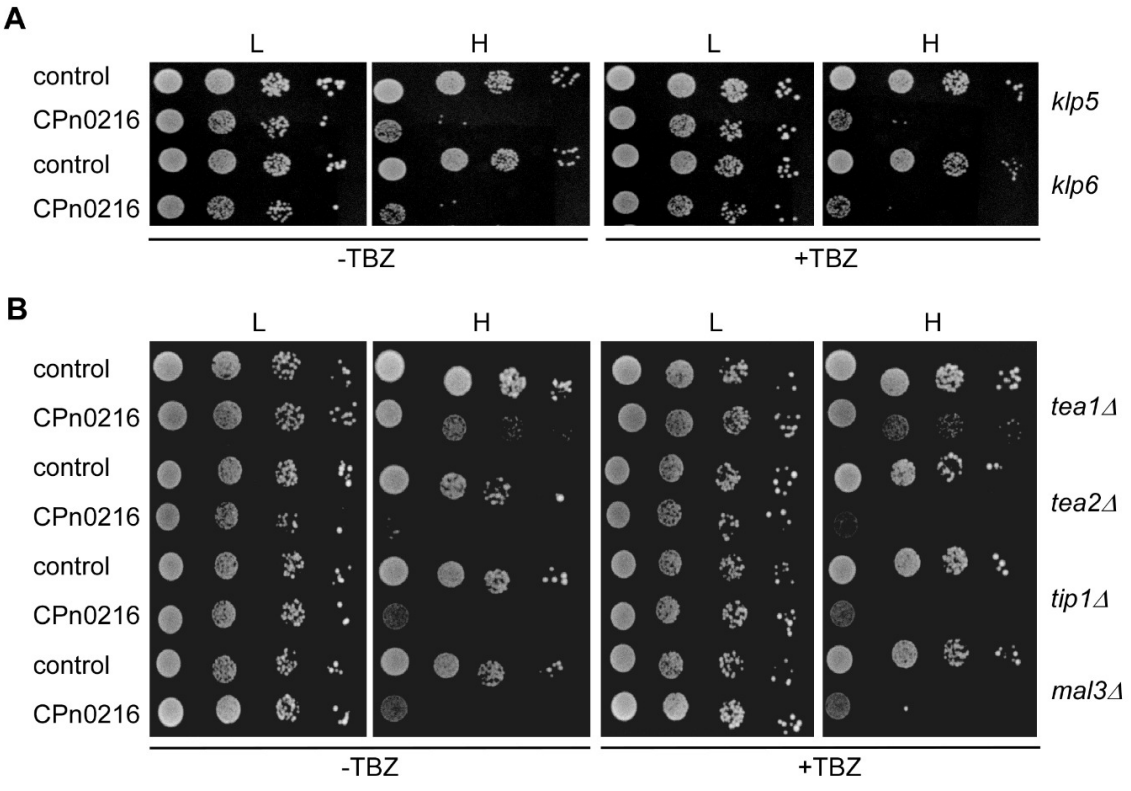

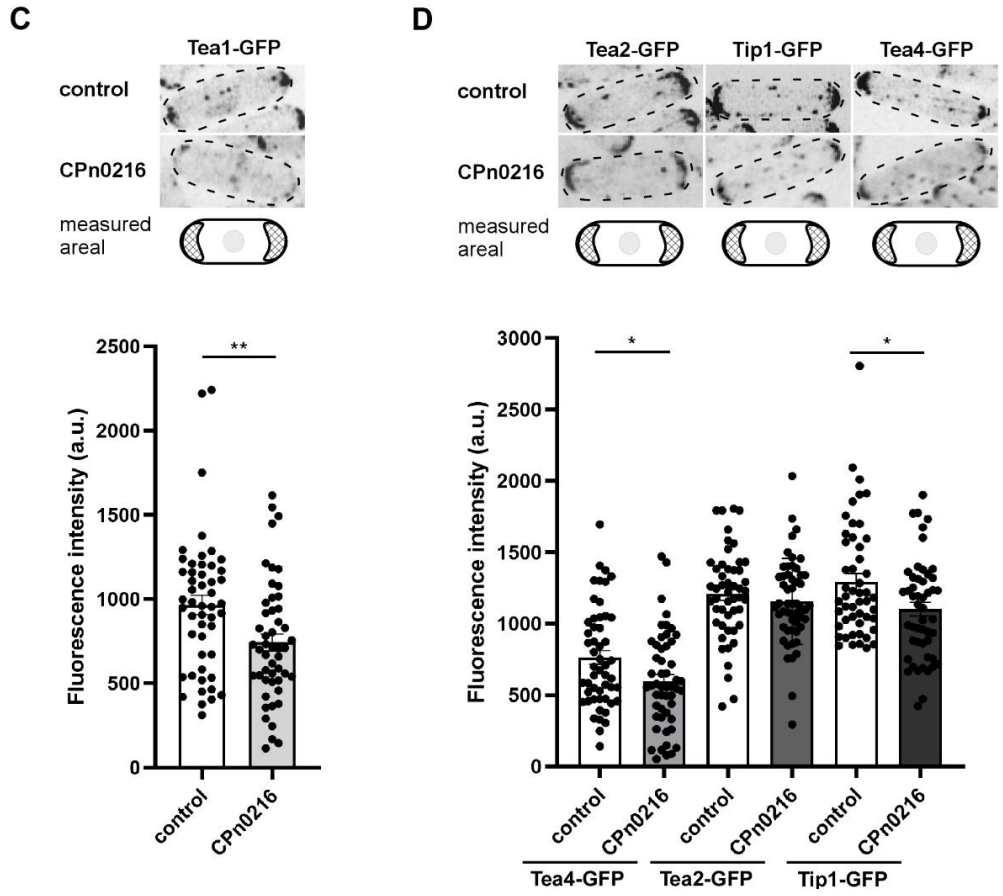

Figure 19: CPn0216 affects the localization of cell end marker proteins.

A-B Serial dilution patch tests (10^4-10^1 cells) of *klp5, klp6,* or *tea1Δ, tea2Δ, tip1Δ,* and *mal3Δ* mutants transformed with a control plasmid (pJR2-3XL *LEU2*) or *cpn0216* expressed on a plasmid under the control of the *nmt1⁺* promoter. Transformants were grown for 6 days at 25 °C on plasmid-selective media without (-TBZ) or with TBZ (+TBZ), L and H: low or high expression. **A** 9 µg/mL TBZ **B;** 6.5 µg/mL TBZ. Two yeast transformants were patched. **C-D** *S. pombe* cells expressing the endogenous *tea1-gfp* (*tea1-pk-gfp*), *tea4-gfp, tea2-gfp*, or *tip1-gfp* (*tip1-pk-gfp*) were transformed with a control plasmid (pJR2-3XL *LEU2*) or plasmid carrying the *cpn0216* and highly expressed from the *nmt1⁺* promoter under plasmid selective conditions at 25 °C. Quantification of Tea1-GFP, Tea4-GFP, Tea2-GFP, and Tip1-GFP fluorescence signal from lectin labeled *cpn0216* expressing cells or lectin-untreated control cells. Schematic cells show the measured area of Tea1-GFP, Tea4-GFP, Tea2-GFP, and Tip1-GFP fluorescence signal normalized against the background. Two-tailed student's t-test was used to determine statistical significance p= 0.0045 (**), Tip1: p= 0.0487 (*), Tea4: p= 0.0328 (*). 50 cells of one experiment were analyzed. Error bars represent ± SEM. a.u. arbitrary fluorescence unit.

This could indicate that Tea1-GFP, Tea4-GFP, Tea2-GFP, and Tip1-GFP signals are only found at correctly oriented MTs toward the cell end, while their loss or reduction results in the incorrect

orientation of MT growth toward the lateral cell cortex and subsequent MT loop formation.

In summary, CPn0216 and CPn0216$^{82-145}$ appear to stabilize MTs that they cannot undergo MT catastrophe and cause elongated MTs curling around the cell ends. In addition, CPn0216 may interact with Tea1 and probably with another host cell protein to affect MTs.

4.2.4 CPn0443$^{164-417}$ binds MTs *in vitro*

Next, I determined if recombinant CPn0443 binds directly to MTs. To determine this, I performed an *in vitro* MT binding assay.

Importantly, for the *in vitro* MT binding assay, a C-terminal version of CPn0443 was required without the four transmembrane domains, as isolation of proteins containing transmembrane domains is extremely problematic. Therefore, *cpn0443$^{164-417}$*, without transmembrane domains, was fused to a glutathione-S-transferase (GST) protein and expressed in *E. coli* for subsequent protein isolation and purification. As a control, purified GST was used for the comparison to test whether GST-CPn0443$^{164-417}$ binds MTs.

Briefly, the *in vitro* MT binding assay was performed using purified GST and GST-CPn0443$^{164-417}$ in the presence/absence of taxol-stabilized MTs. Ultracentrifugation allowed the separation of the sample into supernatant and pellet fractions. If GST-CPn0443$^{164-417}$ binds MTs, two bands, one for GST-CPn0443$^{164-417}$ at 56 kDa and one band for MTs at 50 kDa would be predominantly present in the pellet fraction versus the supernatant fraction. In case GST-CPn0443$^{164-417}$ does not bind MTs, GST-CPn0443$^{164-417}$ would be predominantly present in the supernatant, while MTs would be mainly present in the pellet fraction.

The MT binding assay in the absence of taxol-stabilized MTs showed, that both GST and GST-CPn0443$^{164-417}$ are predominantly present in the supernatant fraction (i, iii) compared to the pellet fraction (ii, iv) **(Figure 20)**. In the presence of taxol-stabilized MTs, GST is mainly present in the supernatant fraction (v) and MTs are mainly present in the pellet fraction (vi), indicating that GST does not bind MTs. In contrast, both taxol-stabilized MTs and

GST-CPn0443$^{164-417}$ are predominantly present in the pellet fraction (viii) compared to the supernatant fraction (vii). This analysis indicated, that GST-CPn0443$^{164-417}$ binds MTs.

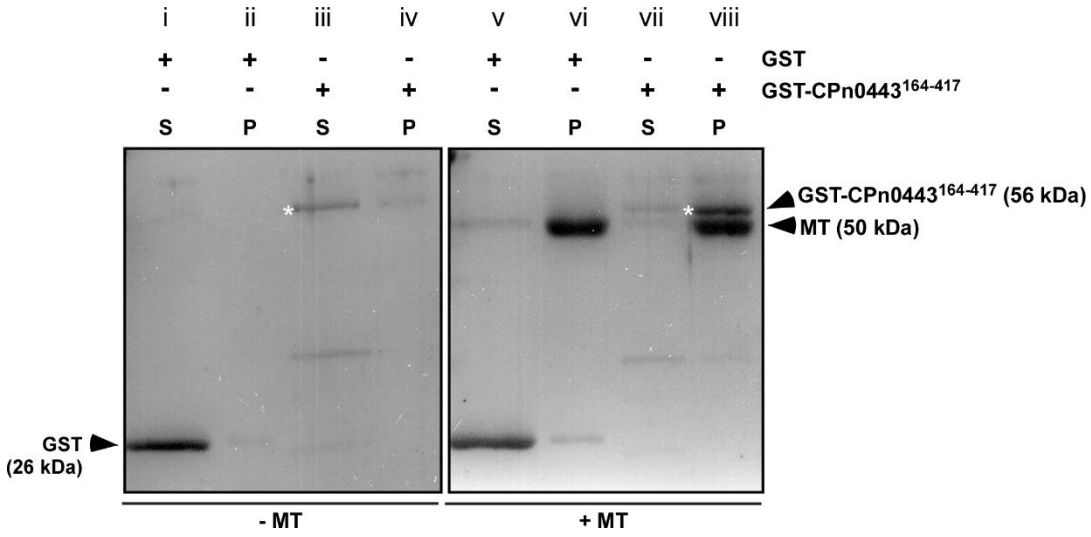

Figure 20: CPn0443$^{164-417}$ binds MTs *in vitro*.

Representative MT co-sedimentation assay showed a direct interaction between GST-CPn0443$^{164-417}$ (56 kDa) and MTs (50 kDa). GST (26 kDa) is used as a control. Bacterially-expressed recombinant GST or GST-CPn0443$^{164-417}$ and taxol-stabilized MTs were incubated at RT followed by high-speed centrifugation. The supernatant (S) and pellet (P) fractions were separated via a 15 % SDS-PAGE followed by Coomassie staining. Left Blot: matching control samples without MTs; right Blot: samples with taxol-stabilized MTs. Asterisks mark the band of GST-CPn0443$^{164-417}$. Two individual experiments were analyzed. The blots shown were reproduced by Dr. Abel Alcázar-Román.

4.3 The MT modulator CPn0443

Based on my studies, CPn0443 has been characterized as an MT co-localizing protein affecting MT structure and MT dynamics. This opens up further possibilities for studying the protein in more detail. Mirrashidi et al., 2015 reported that CT005/IncV, the *C. trachomatis* homolog of CPn0443, interacts with a human MT-regulating protein. Briefly, the authors constructed a *Chlamydia* Inc-human interactome by using affinity purification-mass spectroscopy of HEK293T cells plasmid-transfected with 58 putative Inc *C. trachomatis* ORFs. In this way, CT005/IncV interacted with the human protein MAPRE1/EB1 (Mirrashidi et al., 2015). EB1 belongs to a highly conserved protein family of +TIP proteins that regulate the dynamics of the

MT cytoskeleton (Berrueta et al., 1998).

4.3.1 Mal3 co-localizes with CPn0443 in the nuclear vicinity

The connection between CT005/IncV and EB1 raised the question if CPn0443 has an effect on the +TIP protein Mal3, the *S. pombe* homolog of the human EB1 protein (Beinhauer et al., 1997). The MT stabilizing protein Mal3 is localized along the MT lattice, although it preferentially binds to the growing MT plus-ends. On one hand, Mal3 stabilizes the MT lattice by connecting the neighboring protofilaments in an A-lattice (αβ-tubulin) or a B-lattice (αα-tubulin and ββ-tubulin) (Des Georges et al., 2008). On the other hand, Mal3 stabilizes the growing MT plus-ends for MT assembly to prevent premature MT catastrophe. Mal3 can only bind at the MT plus-ends during MT polymerization and releases its binding before MT catastrophe occurs and MTs are destabilized (La Carbona et al., 2006). The movement of the Mal3-GFP comet with the growing MT plus-end, starting from the MTOC along the longitudinal axis of the cell towards the cell ends, can be analyzed in a *mal3⁺-gfp* expressing yeast strain live-cell imaging.

As Mal3 is a regulator of MT dynamics that are altered under *cpn0443* expression, the question arises whether CPn0443 also affects Mal3. Therefore, I was focused to answer the following questions:

1. Does CPn0443 and/or CPn0443$^{164\text{-}417}$ affect the localization of Mal3-GFP?
2. Does CPn0443-mCherry co-localize with Mal3-GFP?

To determine, if CPn0443 and/or CPn0443$^{164\text{-}417}$ affect the localization of Mal3, I transformed both chlamydial gene variants on plasmids in an endogenously *mal3⁺-gfp* expressing yeast strain and analyzed the influence of Cpn0443 on Mal3-GFP by live-cell imaging.

The microscopic analysis of transformants expressing the control plasmid showed Mal3-GFP comets moving from the overlapping zone at the MTOC near the nucleus (region NN) along the long axis of the cells in the direction of the cell end (region CE) (**Figure 21A-B**).

Analysis of cells expressing *cpn0443* or *cpn0443$^{164\text{-}417}$* revealed a significantly high number of cells with massive Mal3-GFP signals accumulating in region NN as a cause of chlamydial gene

expression leading to massive short MTs and only a few Mal3-GFP tracking signals towards the cell ends (region CE) (**Figure 21A-B**). This accumulation of Mal3-GFP looks like a condensed cloud-like clustering and was observed in 77.8 % of *cpn0443* and 83.5 % of *cpn0443*$^{164\text{-}417}$ transformed cells compared to control transformants (both: $p < 0.0001$; n= 4). Quantification of Mal3-GFP fluorescence signals in the nuclear region of *cpn0443* expressing cells compared to the control revealed significantly higher Mal3-GFP fluorescence signal intensity ($p < 0.0001$, n= 50) (**Supplementary Figure 10A**). Quantification of relative Mal3-GFP levels by Western blot analysis of whole-cell lysates was used to verify this statement. For this purpose, Mal3-GFP band intensity was normalized against actin band intensity, confirming a 2.1-fold increase of Mal3-GFP level in *cpn0443* expressing cells relative to control cells (**Supplementary Figure 10B**). Thus, *cpn0443* expression appears to cause not only predominantly localization of Mal3-GFP in the region of the nucleus but also increased Mal3-GFP levels.

Subsequently, I was interested in determining the localization of CPn0443-mCherry, which was already associated with massive short MTs and could be a possible reason for this Mal3 accumulation. For this purpose, *mal3*$^{+}$*-gfp* cells were transformed with the plasmid-borne *cpn0443-mCherry*.

Live-cell imaging of *mal3*$^{+}$*-gfp* transformants expressing *cpn0443-mCherry* revealed predominant localization of accumulated CPn0443-mCherry fluorescence signals in the region of the nucleus, which partially co-localized with accumulated Mal3-GFP signals (**Figure 21C**). These data suggest that Mal3-GFP accumulation in the region of the nucleus is related to shorter MTs caused by the CPn0443-mCherry expression.

In addition, this microscopic analysis also revealed changes in septal positioning due to *cpn0443-mCherry* expression. Whereas in WT *S. pombe*, the septum is located medially in the middle of the cell and is oriented at a 90° angle to the long axis of the cell to divide the cell into two equal parts, expression of *cpn0443-mCherry* affects the septal positioning of the cell and results tilted septa positioning in the middle of the long axis or asymmetric septa positioning (**Supplementary Figure 10C**). 13 % of the *cpn0443-mCherry* expressing cell population is affected by tilted septa, whereas 14 % is affected by asymmetric septa positioning shifted from

the center of the long axis of the cell, resulting in unequal cell division (**Supplementary Figure 10D**). In contrast, only 2 % of the control transformants showed asymmetric septum positioning. These data indicate that CPn0443 expression affects the positioning of the nucleus and thus the septum.

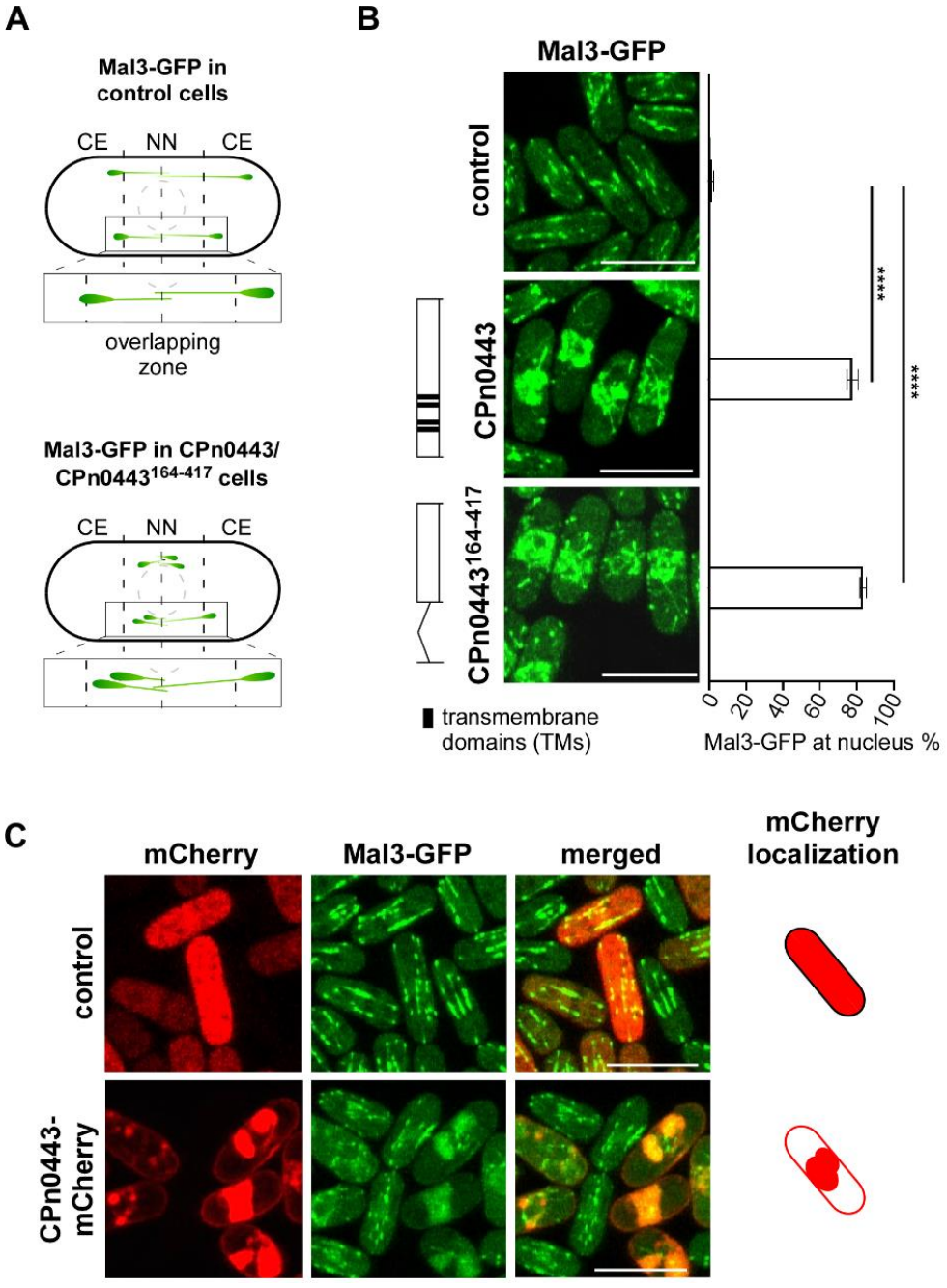

Figure 21: CPn0443 and CPn0443$^{164-417}$ co-localize with Mal3-GFP in the vicinity of the nucleus. A, B Schematic illustration and functional analysis of CPn0443 variant CPn0443$^{164-417}$ in *mal3^{+}-gfp* (endogenous *mal3-pk-gfp,* green) expressing yeast. Full-length *cpn0443* or *cpn0443$^{164-417}$* were highly expressed via

pJR2-3XL *LEU2* plasmids from the *nmt1*$^{+}$ promoter under plasmid selective conditions at 25 °C. The impact of CPn0443 variant CPn0443$^{164\text{-}417}$ on the interphase MT cytoskeleton was determined via live-cell imaging of Mal3-GFP. Photomicrographs demonstrate that both CPn0443 and CPn0443$^{164\text{-}417}$ gave rise to abnormally short MTs as envisaged by the cluster of Mal3-GFP signals around the nucleus. Quantification of cells with strong Mal3-GFP presence in the region near the nucleus (region NN) and only a few Mal3-GFP tracking signals in the direction to the cell ends (region CE). Error bars denote ± SEM. From each of the four individual experiments, 50 cells were analyzed. Two-tailed student's t-test was used to determine statistical significance: p <0.0001 (****). **C** Photomicrographs of pJR2-3XL *LEU2* plasmids carrying *mCherry* or *cpn0443-mCherry* expressing *mal3*$^{+}$*-gfp* transformants.

To determine whether the massively short MTs are caused by CPn0443-induced Mal3 accumulation, I next tested whether Mal3 is the interaction partner of CPn0443. To answer this question, I used a *mal3Δ gfp-α-tubulin* mutant strain whose *mal3* genes are deleted. Since Mal3 is required for stabilization for the polymerizing MT plus-end, the *mal3Δ gfp-α-tubulin* mutant generally has shorter interphase MTs than a WT strain without a mutation. In the case that Mal3 is the host cell interaction partner of CPn0443, the yeast growth and interphase MT structure of *cpn0443* and *cpn0443*$^{164\text{-}417}$ expressing cells should be similar to control cells.
Microscopic analysis of *cpn0443* and *cpn0443*$^{164\text{-}417}$ expressing *mal3Δ* transformants revealed a disorganized MT structure with shorter MTs compared to the control transformant, although the majority of cells exhibited a cloud-like clustering of MTs in the region of the cell nucleus (**Figure 22A**). Interestingly, the interphase MTs of *cpn0443* and *cpn0443*$^{164\text{-}417}$ expressing *mal3Δ* cells are even shorter than the MTs previously observed in the *cpn0443* or *cpn0443*$^{164\text{-}417}$ expressing *mal3*$^{+}$*-gfp* cells. Further localization analysis showed that CPn0443-mCherry is accumulated in the region of the nucleus and co-localized with the cloud-like clustering of MTs (**Figure 22B**). Additionally, a serial dilution patch test of *cpn0443* expressing *mal3Δ* transformants showed, that CPn0443 persists in negatively impacting yeast growth and leads to TBZ-hypersensitivity rather than rescuing growth in the absence of Mal3 (**Figure 22C**).

Since I could not detect any interaction between CPn0443 and Mal3 so far, I performed an immunoprecipitation pull-down assay as the last check to assess whether Mal3-GFP is able to pull down the "prey" protein CPn0443-mCherry. Therefore, the *mCherry* control (negative

control) and *cpn0443-mCherry* were expressed in the *mal3⁺-gfp* yeast strain. In addition, *cpn0443-mCherry* was expressed in a WT yeast strain as a background control for GFP, while a (non-tagged) control was expressed in the *mal3⁺-gfp* strain as a background control for *mCherry*. In case Mal3 and CPn0443 interact directly, Mal3-GFP pulls down CPn0443-mCherry and both proteins would be detected in the immunoprecipitation (IP-) fraction (viii) by Western blot analysis.

The Western blot analysis revealed, that (iv) CPn0443-mCherry and Mal3-GFP are both detected in the input fraction (whole-cell lysate), while in the IP-faction only an enriched signal for (viii) Mal3-GFP was detected, indicating, Mal3-GFP did not pull down CPn0443-mCherry (**Figure 22D**). Additionally, in the input fraction of the controls, (i) CPn0443-mCherry, (ii) Mal3-GFP, or (iii) mCherry and Mal3-GFP could be detected, whereas only enriched Mal3-GFP (vi, vii) could be observed in the IP fraction, accordingly, no (i, v) GFP or (ii, vii) mCherry background was detected. This analysis revealed that CPn0443 is not immunoprecipitating with Mal3.

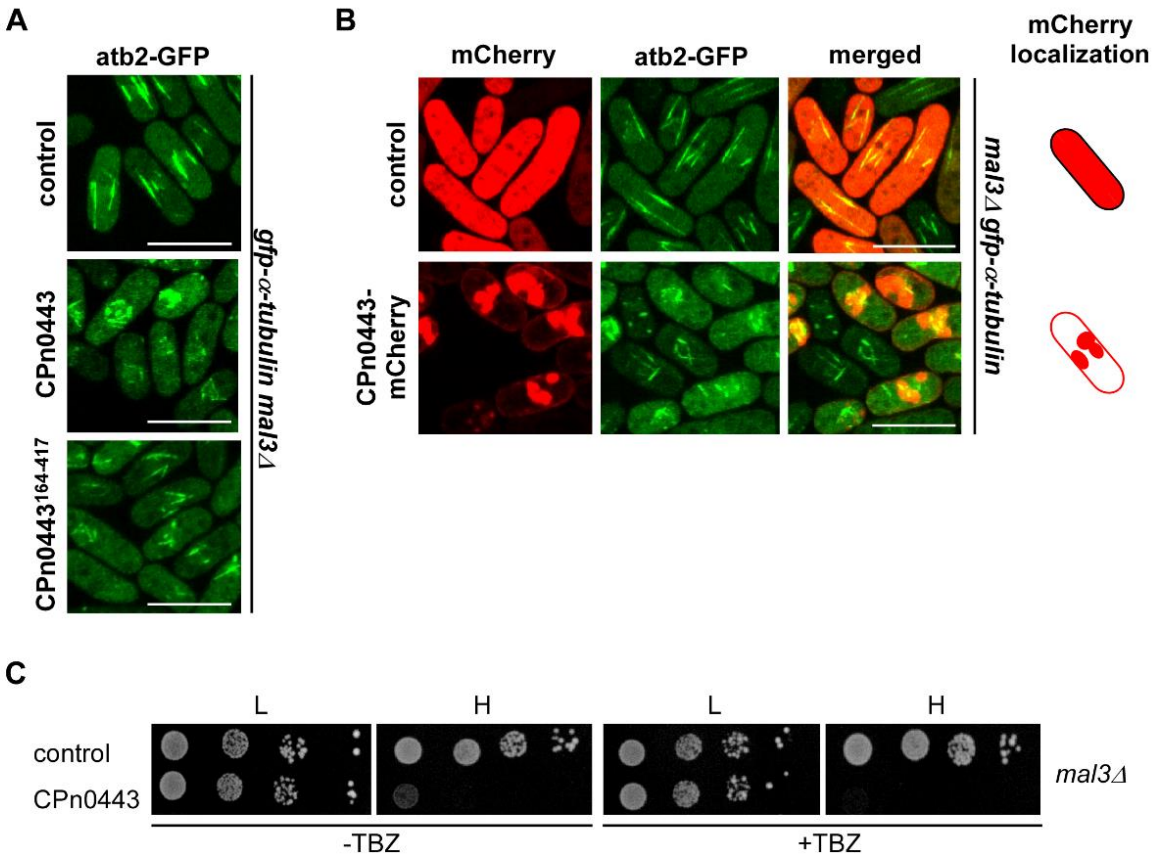

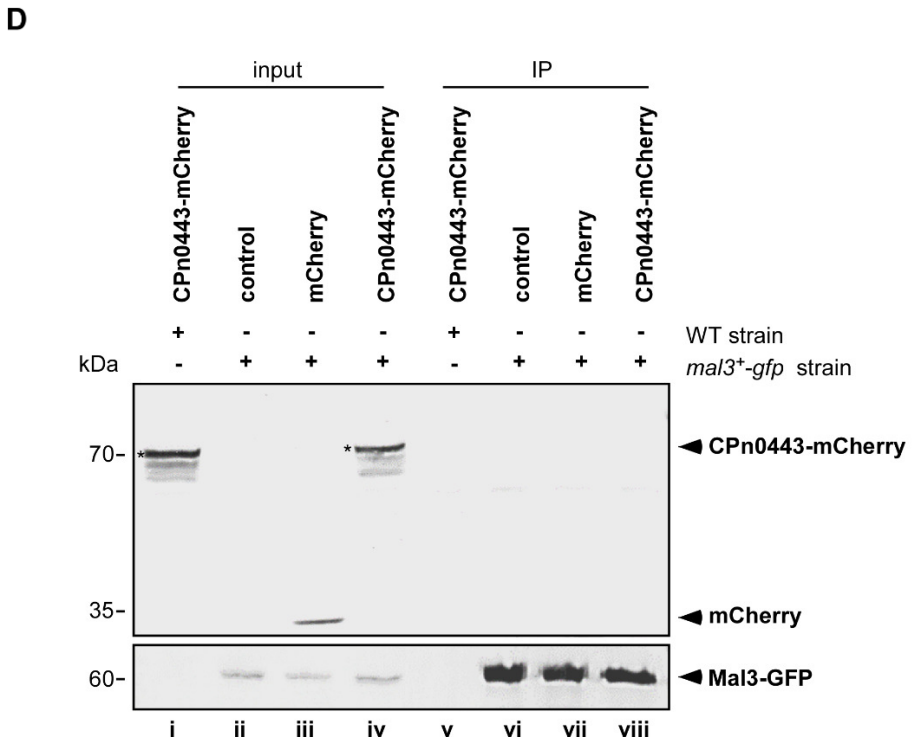

Figure 22: Mal3 is not the direct host cell interaction partner of CPn0443.

A Photomicrographs of *S. pombe* mutants expressing the *mal3Δ gfp-α-tubulin* (*nmt81::gfp-atb2⁺mal3Δ*, green) were transformed with a control plasmid (pJR2-3XL *LEU2)* or plasmids carrying either *cpn0443* or *cpn0443*$^{164\text{-}417}$ highly expressed from the *nmt1⁺* promoter under plasmid selective conditions at 25 °C. **B** Photomicrographs of *mal3Δ gfp-α-tubulin* mutants highly expressing a pJR2-3XL *LEU2* plasmid-borne *mCherry* (control, red), or *cpn0443-mCherry*. Schematic illustrations represent the localization of mCherry. Scale bars, 10 µm. **C** Serial dilution patch tests (10^4-10^1 cells) of *mal3Δ* mutants transformed with a control plasmid (pJR2-3XL *LEU2*) or *cpn0443* expressed on a plasmid under the control of the *nmt1⁺* promoter. Transformants were grown for 6 days at 25 °C on plasmid-selective media without (-TBZ) or with 6.5 µg/mL TBZ (+TBZ); L and H: low or high expression. **D** Western blot analysis of Mal3-GFP immunoprecipitates (GFP-beads) and input (whole-cell lysates) of *S. pombe* cells expressing the endogenous *mal3⁺-gfp* transformed with (non-tagged) control, *mCherry* control, or *cpn0443-mCherry*. As a negative control, *cpn0443-mCherry* was also expressed and immunoprecipitated from the wild-type (WT) *S. pombe* strain. Top: detection of input or IP (immunoprecipitation) fraction of CPn0443-mCherry (72 kDa), non-tagged control, and mCherry control (27 kDa) with an anti-mCherry antibody. Asterisks mark the band of CPn0443-mCherry. Bottom: detection of the Mal3-GFP (63 kDa) with an anti-GFP antibody. **A-D** Two yeast transformants were analyzed.

Considering that none of the analyses confirmed the interaction of CPn0443 and Mal3, it has to be assumed that massively short MTs are not caused by CPn0443-induced Mal3 accumulation. These data imply that the CPn0443 accumulation causes massively short MTs

which consequently results in the accumulation of Mal3.

In summary, the CPn0443-induced MT phenotype is caused Mal3 independently. Rather, Mal3 accumulation near the nucleus appears to be a consequence of the aberrant interphase MT cytoskeleton consisting of massive short MTs.

4.3.2 Further +TIP proteins are affected by CPn0443

For MT plus-end stabilization during MT polymerization, the MT-stabilizer Mal3 and Tip1 are required at the growing MT tip. Briefly, Tip1 binds as cargo to the motor protein Tea2, which moves to the growing MT plus-end after Mal3 activation (Browning and Hackney, 2005; Bieling et al., 2007). When the growing MT reaches the cell end, Tip1 and Tea2 are anchored from the MT tip to the cell end and initiate MT catastrophe. Analysis of a *tip1-gfp* and *tea2-gfp* expressing yeast strain by live-cell imaging reveals localization of Tip1 and Tea2 at the growing MT plus-end and at the cell end.

Considering the localization of short MTs and altered Mal3 localization under the expression of *cpn0443* that accumulates massively in the region of the nucleus, the question arises whether CPn0443 also affects other +TIP proteins such as Tea2 and Tip1. Therefore, I was focused to answer the following questions:

1. Does CPn0443-mCherry co-localize with Tea2-GFP and Tip1-GFP?
2. Does CPn0443 affect the localization of Tea2-GFP and Tip1-GFP and also cause a strong accumulation near the nucleus?

To answer the questions, the yeast strains *tea2-gfp* and *tip1-gfp* were transformed with a control plasmid or a plasmid harboring *cpn0443-mCherry*.

Microscopical analysis of the control transformants of both strains showed, that Tea2-GFP and Tip1-GFP signals moved from the MTOC with the growing MTs toward the cell ends along the long axis of the cell (**Figure 23A-B**). In addition, Tea2-GFP and Tip1-GFP are localized in the growth zones at the end of the cell in both strains.

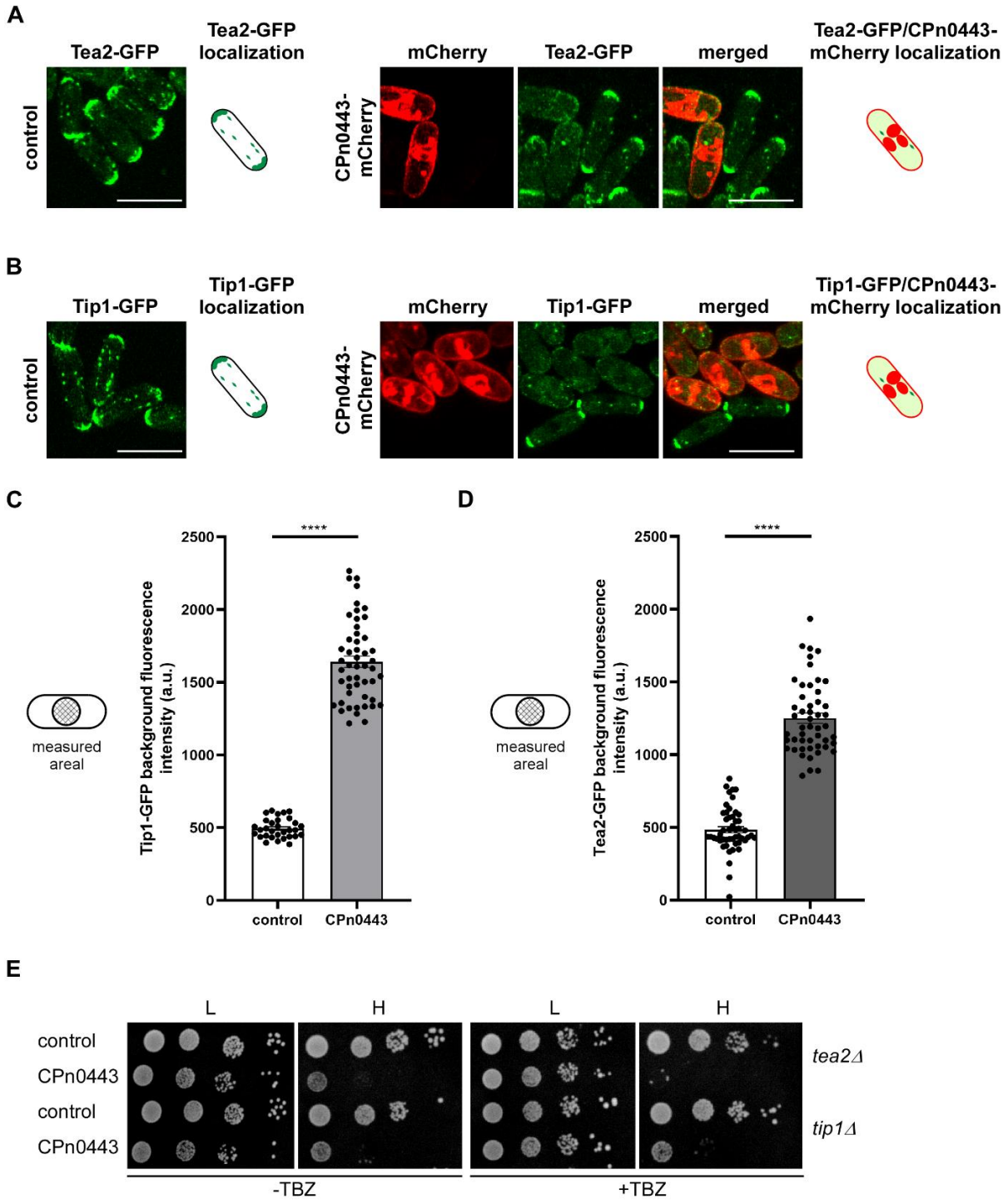

Figure 23: Massively reduces Tea2-GFP or Tip1-GFP signals in *cpn0443-mCherry* expressing cells. **A-B** Microscopic images of *S. pombe* strains expressing the endogenous *tea2-gfp* (green), or *tip1-gfp* (*tip1-pk-gfp,* green) were transformed with a control plasmid (pJR2-3XL *LEU2*) or plasmids harboring *cpn0443-mCherry* (red) and highly expressed from the *nmt1*$^{+}$ promoter under plasmid selective conditions at 25 °C. Schematic illustrations represent the localization of Tea2-GFP or Tip1-GFP and CPn0443-mCherry. Scale bars, 10 µm. **C-D** Quantification of Tea2-GFP and Tip1-GFP fluorescence signal from the background. Schematic cell shows the

measured area of Tea2-GFP and Tip1-GFP fluorescence signal. Two-tailed student's t-test was used to determine statistical significance p<0.0001 (****). 50 cells from one experiment were analyzed. Error bars represent ± SEM. a.u. arbitrary fluorescence unit. **E** Serial dilution patch tests (10^4-10^1 cells) of *tea2Δ* and *tip1Δ* mutants transformed with a control plasmid (pJR2-3XL *LEU2*) or *cpn0443* expressed on a plasmid under the control of the *nmt1⁺* promoter. Transformants were grown for 6 days at 25 °C on plasmid-selective media without (-TBZ) or with 6.5 µg/mL TBZ (+TBZ), L and H: low or high expression. Two yeast transformants were patched.

In contrast, localization analysis of the *cpn0443-mCherry* expressing *tea2-gfp* and *tip1-gfp* cells showed, that CPn0443-mCherry is localized and accumulated in the vicinity of the nucleus (**Figure 23A-B**). Surprisingly, neither a co-localization of Tea2-GFP or Tip1-GFP with CPn0443-mCherry nor an accumulation of Tea2-GFP or Tip1-GFP near the nucleus could be observed. Furthermore, these cells did not appear to have moving Tea2-GFP and Tip1-GFP signals from the MTOC with the growing MT plus-end. However, *cpn0443-mCherry* expressing *tea2-gfp* and *tip1-gfp* cells have a significantly high GFP background compared to control transformants. Quantification of the background GFP-fluorescence signal in the cells revealed a 2.6-fold increase of the GFP background signal in the *tea2-gfp* strain and a 3.3-fold increase in the *tip1-gfp* strain (**Figure 23C-D**). Moreover, based on the short interphase MTs of *cpn0443* expressing cells, Tea2-GFP and Tip1-GFP could not be detected at the growth zones of the end of the cells.

To assess if the alterations of Tea2-GFP and Tip1-GFP localization were caused by an interaction of CPn0443 with Tea2 or Tip1, the growth effect of *cpn0443* expressing *tea2Δ* and *tip1Δ* mutants under TBZ treatment was analyzed. In case Tea2 and/or Tip1 are the interaction partners of CPn0443, CPn0443 would no longer be able to influence MTs in the absence of the interaction partner, resulting in no CPn0443-induced growth defect and TBZ-hypersensitivity, and the yeast growth would be comparable to control transformants.

Serial dilution patch assay of *cpn0443* expressing *tea2Δ* and *tip1Δ* mutants revealed that the expression of the chlamydial gene still causes massive growth defects and TBZ-hypersensitivity compared to the control (**Figure 23E**). Because the absence of Tea2 and Tip1 does not appear to rescue the yeast growth of *cpn0443* expressing transformants, it is improbable that Tea2 or Tip1 are the direct interaction partners of CPn0443.

To sum up, CPn0443 also influences other +TIP proteins of the Tea2/Tip1/Mal3 complex causing a reduction of Tea2-GFP or Tip1-GFP signals in the cells but a strong GFP background signal.

4.3.3 CPn0443 binds and bundles MTs of human U2OS cells

In this study, *cpn0443* expression in *S. pombe* was found to alter MT organization and dynamics, and bind directly to MT in an *in vitro* assay. Next, I was interested in studying the effect of CPn0443 in mammalian cells.

For further characterization of CPn0443, I focused on answering the following questions:

1. Does CPn0443 localize with the human MT cytoskeleton?
2. Where is the MT-binding site located in CPn0443?

To address the question of whether CPn0443 localizes with the human MT cytoskeleton, I generated plasmids carrying CPn0443 C-terminally or N-terminally fused to a GFP-tag under the control of a CMV promoter to transfect U2OS cells (epithelial adherent bone osteosarcoma cells) for 18 hours. As a control, cells were transfected with a GFP-containing plasmid.

However, CPn0443-GFP could not be detected by live-cell imaging or in Western blot analysis of the whole-cell lysate. In contrast, GFP-CPn0443 could be detected by microscopic analysis and ectopic expression analysis of the whole-cell lysate by Western blot. Thus, I switched to N-terminally fused GFP-CPn0443 variants which were expressed (**Supplementary Figure 11A-B**).

U2OS cells are non-polarized epithelial cells whose radial organization of the MT cytoskeleton is directed from the MTOC toward the plasma membrane of the cell which can be observed in cells expressing the GFP-control. In control cells expressing GFP, GFP is localized in the cytosol (**Figure 24A**).

Confocal microscopic analysis of GFP-CPn0443 expression in U2OS cells showed alterations in MT organization and structure, displayed in two distinct MT variants, aberrant or severely aberrant MT structures, depending on the degree of GFP-CPn0443 fluorescence signal

(**Figure 24A**). For both observed aberrant MT variants, GFP-CPn0443 is localized around the nucleus and along the MTs in accumulated punctate patches.

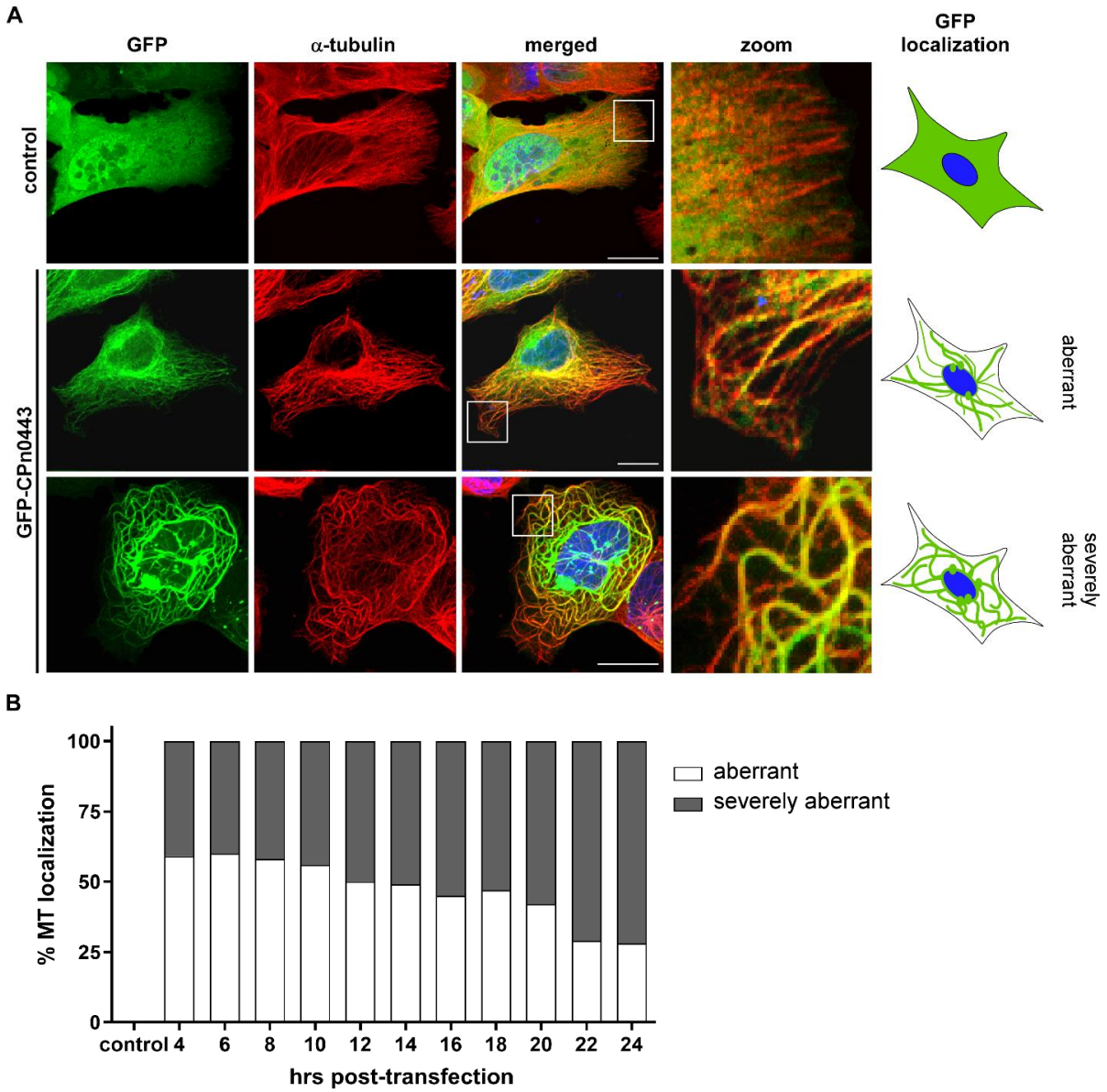

Figure 24: GFP-CPn0443 binds and bundles MTs of the human MT cytoskeleton. **A** Confocal fluorescence images of human U2OS cells were transfected for 18 hours with plasmids expressing GFP (control, green) or GFP-CPn0443. MTs were visualized with anti-α-tubulin antibody (red) and DNA with DAPI (blue). Scale bars, 10 µm. White boxes show enlargements (zoom). Schematic illustrations represent the localization of GFP. **B** Quantification of GFP-CPn0443 expressing cells that show aberrant or severely aberrant MT structures due to co-localization of GFP-CPn0443 with MTs. From each of the three individual experiments, 100 cells were analyzed.

I defined host MT cytoskeleton as aberrant MTs structures when MTs are bundled into thicker

MT cables, but only a few of them curl inside the cell and therefore not oriented toward the plasma membrane. The majority of the bundled MTs are still oriented toward the plasma membrane (**Figure 24A**). In contrast, I defined the mammalian MT cytoskeleton as a severely aberrant MT structure, when most of the MTs are massively bundled into thick MT cables which curl in a “spaghetti-like" structure inside the cell instead of being oriented toward the plasma membrane (**Figure 24A**).

To determine whether the two different MT variants depend on the expression duration of GFP-CPn0443, the alteration of MT interphase structure of U2OS cells expressing GFP-CPn0443 for 4 to 24 hours was documented.
During the first 10 hours, aberrant MT structures are observed in approximately 60 % of transfected cells, characterized by only a few MTs are bundled into thicker MT cables that are not directed toward the plasma membrane (**Figure 24B**). At 12 to 18 hours post-transfection, the ratio of aberrant and severely aberrant MTs is equal at about 50 %, but changes at 20 to 24 hours post-transfection. After 20 hours, up to 70 % of transfected cells showed severely aberrant MT structures characterized by massively thick MT cables organized predominantly in a spaghetti-like structure.

In addition to CPn0443-induced MT modulation and localization of CPn0443-GFP to MTs, I was interested in investigating whether CPn0443 also has an effect on the actin cytoskeleton. In control cells, actin cables are long bundles that are largely arranged in parallel. Both the GFP control and GFP-CPn0443 expressing cells showed long and parallel arranged actin bundles (**Supplementary Figure 12**). Whereas GFP control localized to the cytosol, localization analysis of GFP-CPn0443 revealed that the spaghetti-like structure of GFP-CPn0443 did not co-localize with the actin cables. These data demonstrated, CPn0443 does not co-localize with actin or affect its structure.

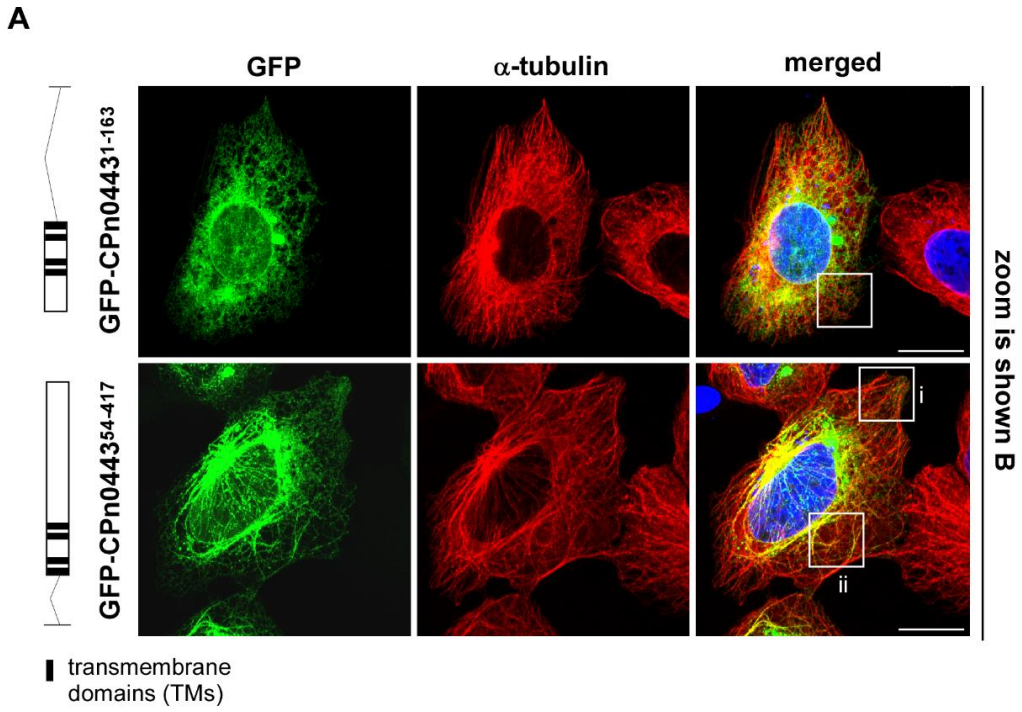

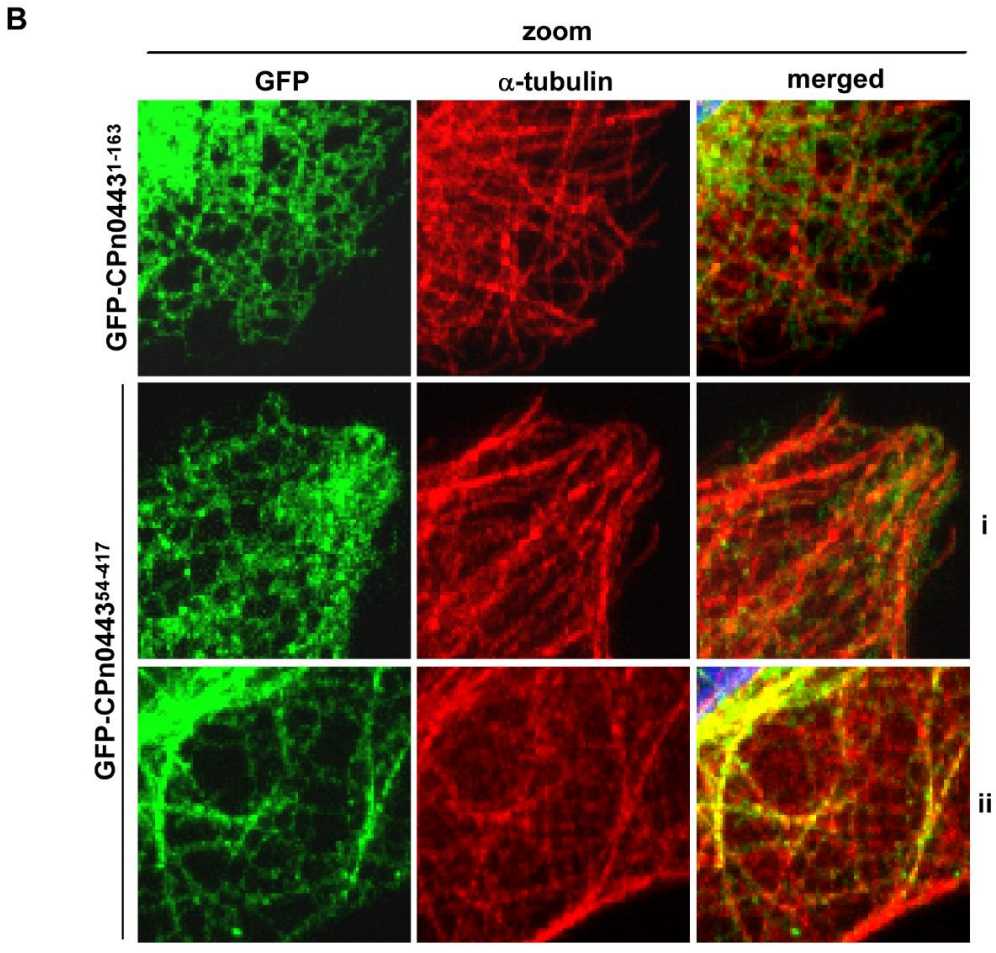

Figure 25: The C-terminal CPn0443 variant GFP-CPn0443$^{54-417}$ co-localizes with MTs.

A-B Confocal fluorescence images of human U2OS cells were transfected for 18 hours with plasmids expressing GFP-CPn0443$^{1-163}$ (green), or GFP-CPn0443$^{54-417}$. White boxes show enlargements (zoom) and zoomed images are shown in **B**. MTs were visualized with anti-α-tubulin antibody (red) and DNA with DAPI (blue). Scale bars, 10 µm. Two individual experiments were analyzed.

To answer the second question, which regions of CPn0443 are essential for MT-binding in human cells, plasmids with different shortened CPn0443 variants were generated. For the first analysis, I was interested in the location of the N-terminal CPn0443 variant (CPn0443$^{1-163}$) and the C-terminal CPn0443 variant (GFP-CPn0443$^{54-417}$). Both shortened CPn0443 variants contain four transmembrane domains.

Microscopic analysis of U2OS cells revealed that GFP-CPn0443$^{1-163}$ is localized around the nucleus in a reticular structure similar to the structure of the ER (**Figure 25A-B**). GFP-CPn0443$^{1-163}$ does not co-localize with MT. In contrast, GFP-CPn0443$^{54-417}$ is localized in an ER-like structure around the nucleus and is also detected along MTs (**Figure 25A-B**). Due to the fact that CT005, the *C. trachomatis* homolog of CPn0443 associates with ER during infection, I used the ER-like localization of GFP-CT005 transfected U2OS cells for comparison for the CPn0443 variants (Stanhope et al., 2017) (**Supplementary Figure 13A**).

Based on these observations, I tested whether GFP-CPn0443$^{1-163}$, GFP-CPn0443$^{54-417}$, and GFP-CPn0443 co-localize with the ER. GFP-CT005 was used as a control for ER localization. For this purpose, U2OS cells were transfected with the CPn0443 variants for 18 hours and co-transfected with a plasmid expressing Sec61β-mCherry that serves as an ER marker (Greenfield and High, 1999).

GFP-CPn0443, GFP-CPn0443$^{1-163}$, GFP-CPn0443$^{54-417}$, and GFP-CT005 show localization with the ER marker Sec61β-mCherry (**Figure 26**, **Supplementary Figure 13B**). While control cells exhibit a reticular ER structure, the ER structure of cells expressing a chlamydial gene was altered. It can be observed that the ER structure appears to be clustered and thickened when the ER co-localizes with strong accumulations of GFP-CPn0443, GFP-CPn0443$^{1-163}$, GFP-CPn0443$^{54-417}$, and GFP-CT005. In particular, the full-length CPn0443 showed alterations of the ER architecture which is similar to the aberrant MT phenotype of GFP-CPn0443

expressing cells. These localization analyses showed on the one hand, that GFP-CPn0443, GFP-CPn0443$^{1-163}$, and GFP-CPn0443$^{54-417}$ co-localize with the ER and change the ER structure, and on the other hand, that GFP-CPn0443 and GFP-CPn0443$^{54-417}$, which contain both the C-terminus of CPn0443, co-localize with MTs (**Figure 26**, **Table 3**). Therefore, it is reasonable to assume that the C-terminus of CPn0443 also plays a crucial role in MT-binding and modulation of the ER architecture in mammalian cells.

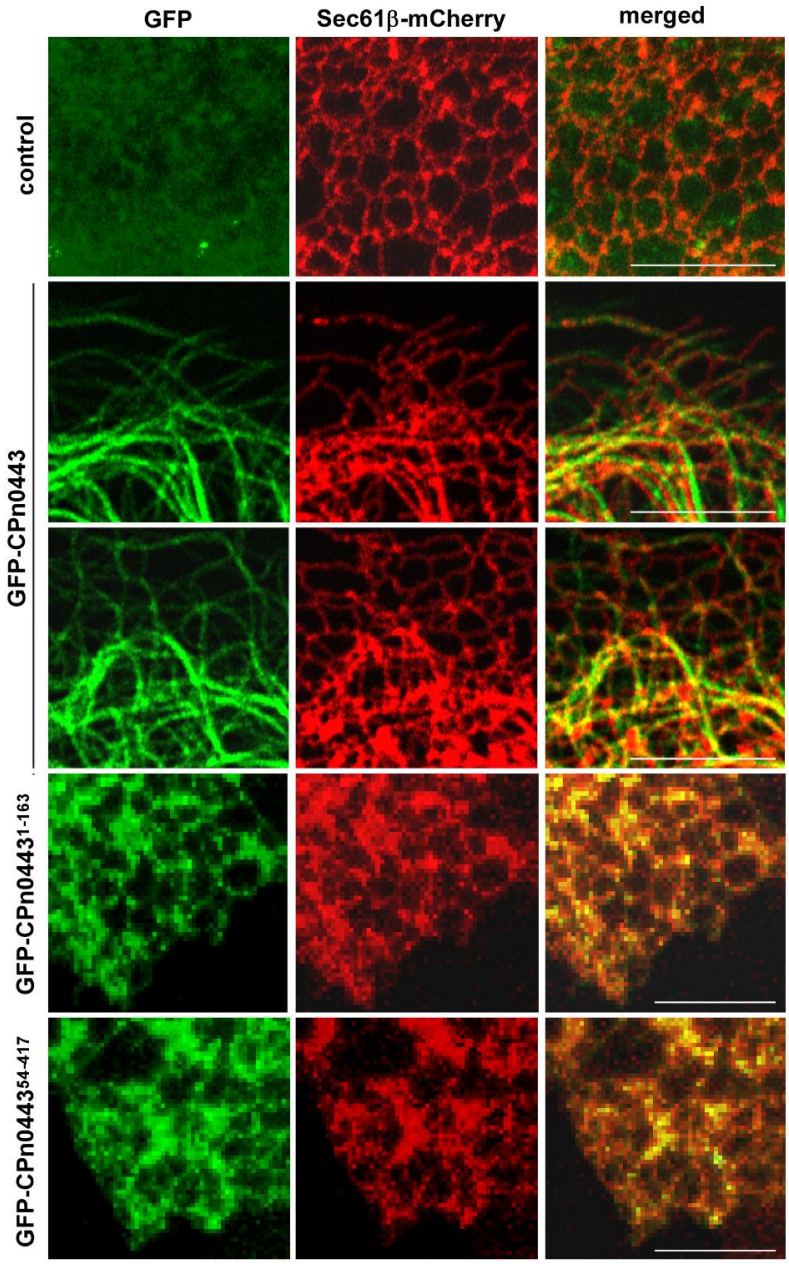

Figure 26: CPn0443 reorganizes the ER architecture of U2OS cells.

Zoomed images of confocal fluorescence microscopy of human U2OS cells were transfected for 18 hours with

plasmids expressing GFP (control, green) or different GFP-CPn0443 variants. In addition, cells were co-transfected with a plasmid expressing Sec61β-mCherry (red, ER marker). Scale bars, 10 µm. One experiment was analyzed.

Next, I was interested in further narrowing down the MT-binding domain in the C-terminus of CPn0443. For this purpose, I generated plasmids with CPn0443 variants: GFP-CPn0443$^{164-417}$, GFP-CPn0443$^{164-236}$, GFP-CPn0443$^{237-331}$, and GFP-CPn0443$^{332-417}$.

However, confocal fluorescence images showed that all CPn0443 variants were localized exclusively in the cytosol of the cells (**Supplementary Figure 11A**). To check for an experimental error, the C-terminal variant of the ER localization control CT005 (CT005$^{146-363}$) was used. Comparable to the shortened CPn0443 variants, CT005$^{146-363}$ is localized to the cytosol and not localized at the ER such as observed for its full-length variant (**Supplementary Figure 13**).

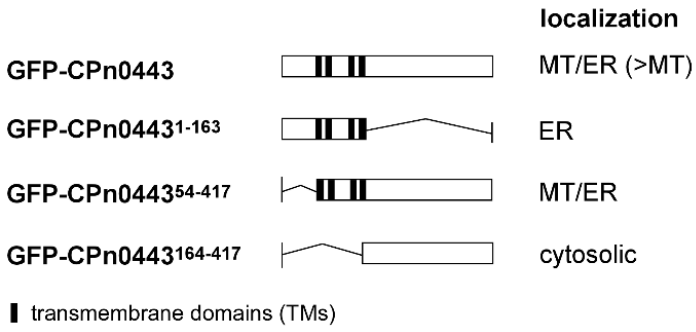

Table 3: Localization of all tested CPn0443 variations in human U2OS cells.

Overview of the localization of the used deletion variants of CPn0443 from transfected human U2OS cells. Microtubule (MT); endoplasmic reticulum (ER).

In conclusion, GFP-CPn0443 and the C-terminal variant GFP-CPn0443$^{54-417}$ co-localize with MTs in human cells, and the ectopic expression of GFP-CPn0443 affects the ER architecture and leads to aberrant MT structures, resulting in thick MT cables organized in a spaghetti-like structure. Thus, the C-terminus of CPn0443 seems to contain the MT-binding domain that is required for MT-binding. Furthermore, GFP-CPn0443, GFP-CPn0443$^{1-163}$, and GFP-CPn0443$^{54-417}$ localize with the ER structure.

4.3.4 CPn0443 localizes to or within *C. pneumoniae* during infection

After investigating the influence and localization of CPn0443 in transfected mammalian cells, it was of interest to determine the impact of CPn0443 during *C. pneumoniae* infection. In the course of further characterization of CPn0443 in mammalian cells, I focused on answering the following questions:

1. Where does CPn0443 localize during a *C. pneumoniae* infection?
2. Does ectopic expression of CPn0443 affect the infection process of *C. pneumoniae*?

C. pneumoniae LPCoLN is a koala isolate that can be genetically manipulated and was established in our laboratory as a strain for plasmid transformation to perform localization analysis during infection (Myers et al., 2009). Therefore, *C. pneumoniae* LPCoLN was transformed with a CPn0443-flag plasmid under the control of the constitutively active *NmPro* promoter followed by infection of non-polarized HEp2 epithelial cells with this transformed *C. pneumoniae* strain for 96 hours (section 3.4.5.1). The second set of HEp2 cells was infected with non-transformed *C. pneumoniae* and used as a control for the comparison of whether CPn0443 has an effect on infection. Furthermore, as a control for localization in the inclusion membrane, the third set of HEp2 cells was infected with CPn0147-myc expressing *C. pneumoniae*, because the predicted Inc protein CPn0443 is assumed to be integrated into the inclusion membrane like most other Inc proteins such as CPn0147 (Luo et al., 2007). Additionally, the major outer membrane protein (Momp) on the bacterial surface was strained of all three sets of infected HEp2 cells to compare the localization of CPn0443 and the controls to assess the effect of CPn0443 on the infection process.

To answer the first question, localization analysis was performed using confocal microscopy. Immunofluorescence analyses for the three sets of infected HEp2 cells showed non-regularly distributed localization of Momp signals co-localized with the bacterial DNA representing *Chlamydia* within the inclusion (**Figure 27A**). In cells infected with CPn0147-myc *C. pneumoniae*, localization of CPn0147-myc to the inclusion membrane is shown as a ring around the inclusion.

Surprisingly, CPn0443-flag *C. pneumoniae* infected cells did not show a ring-like localization of

CPn0443-flag around the inclusion such as observed for CPn0147-myc. Instead, CPn0443-flag is recognized within the inclusion in non-regularly distributed patches which are partially co-localizing with Momp signals. It is not clear from this analysis whether CPn0443-flag co-localizes within *Chlamydia* or on the bacterial cell surface. Besides the localization of CPn0443-flag inside the inclusion, the confocal microscopic images demonstrated no changes in inclusion sizes or their positioning inside the host cell. These data do not suggest a CPn0443-induced effect on the infection process of *C. pneumoniae*.

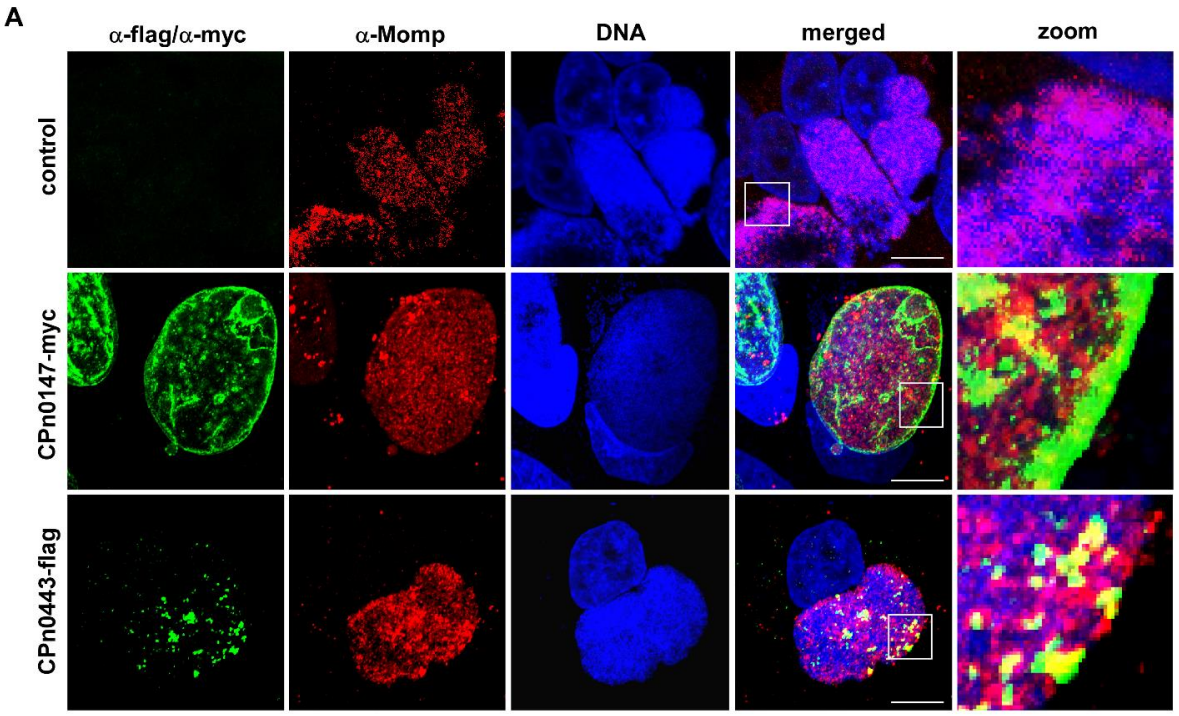

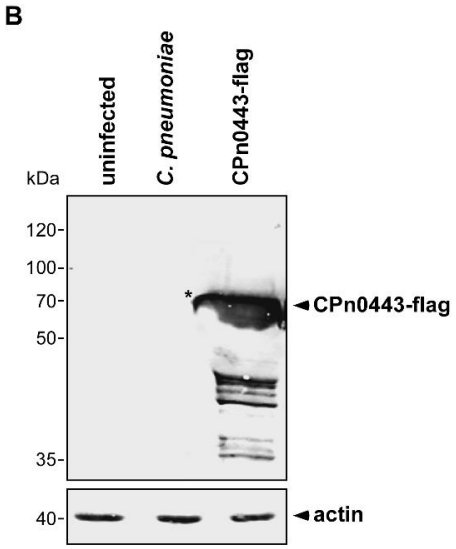

Figure 27: CPn0443 is not localized in the inclusion membrane during a *C. pneumoniae* infection. **A** Confocal fluorescence images of human HEp2 cells infected for 96 hours with (non-transformed) *C. pneumoniae,* CPn0147-myc expressing *C. pneumoniae* (Inc protein: localized on the inclusion membrane), or CPn0443-flag expressing *C. pneumoniae*. CPn0147-myc was visualized with an anti-myc antibody (green), CPn0443-flag with an anti-flag antibody (green), bacterial surface with anti-Momp antibody (red), and DNA with DAPI (blue). White boxes show enlargements (zoom). Scale bars, 10 µm. **B** Western blot analysis of whole-cell lysates of the samples shown in **A**. Top: detection of CPn0443-flag visualized with an anti-flag antibody and marked with an asterisk. The calculated molecular weight of CPn0443-flag is 50 kDa, but the protein band in the blot is present at about 70 kDa. Bottom: detection of the actin (42 kDa) with an anti-actin antibody. Two individual experiments were analyzed.

In addition, Western blot analysis of whole-cell lysate from cells infected with CPn0443-flag *C. pneumoniae* was performed and revealed that CPn0443-flag is not present in the blot at the calculated molecular weight of 50 kDa, instead, the protein is present at approximately 70 kDa (**Figure 27B**).

In this experimental setup, CPn0443-flag is localized on the bacterial surface or within the bacteria without negatively affecting the infection process of *C. pneumoniae*.

5 Discussion

In this thesis, a genetic screen was performed to identify new MT-modulatory proteins of *C. pneumoniae* and I identified 13 proteins with diverse MT regulatory effects. They all triggered a growth defect and TBZ hypersensitivity in the fission yeast *S. pombe* and thus are potentially considered MT-modulating proteins that modulate structures in the host cell. The chlamydial gene expression causes a change in the interphase MT cytoskeleton in all transformants studied. Due to the high number of identified MT modulatory proteins, two proteins, CPn0216 and CPn0443, are selected and analyzed in more detail as a result of their massive changes in the structure and organization of interphase MTs.

5.1 The first screen for MT-modulating proteins of a bacterial pathogen

Until today, the importance of the MT cytoskeleton during the infection process of *C. pneumoniae* is insufficiently established, whereas actin has been proven to play a fundamental role in chlamydial invasion and extrusion. The same is true for other bacterial pathogens, this leads to the fact that only a few bacterial MT-modulating proteins have been identified and functionally characterized. For *C. pneumoniae*, only CopN as MT-destabilizing protein and MT-modulating protein CPn0572 were identified to be associated with the host cell MT cytoskeleton and were investigated in detail (Archuleta et al., 2011; Huang et al., 2008; Braun, 2015).

The genetic screening carried out in this work allowed 116 proteins (about 11 % of all predicted proteins) of the 1,052 predicted proteins for *C. pneumoniae* to be screened for their MT-regulatory function (Dehoux et al., 2011). The screen resulted in the identification of 13 MT-modulating proteins whose chlamydial gene expression triggered a growth defect and TBZ hypersensitivity in the model yeast *S. pombe*. Although numerous genetic studies of various bacterial pathogens using the budding yeast *S. cerevisiae* have identified a variety of effector proteins that interfere with host cell processes, the potential targeting of MT function has not been well investigated so far (Sisko et al., 2006; Herbst, 2011; Popa et al., 2016). In these

previous screens for growth phenotypes triggered by bacterial effectors, the growth defect under selective stress conditions such as temperature or salt could indicate the possible impact of the effector protein on host cell processes. In this way, transformants expressing a *C. trachomatis* gene with unknown function and responding with a growth defect to osmotic stress could be associated with a possible defect in MAPK signaling pathways, nuclear transport, RNA transcription, and translation (Warringer et al., 2003). The genetic screen in this study is the first performed screen to identify a larger number of specific MT-modulating proteins of a bacterial pathogen.

The effectiveness of the powerful screen was already demonstrated by Dr. Corrina Braun characterized both CopN and CPn0572 in *S. pombe* in her master's thesis (Braun, 2015). In the course of her project, she detected a growth defect and TBZ-hypersensitivity in yeast for both CopN and CPn0572 and confirm the MT modulatory functions of the two proteins. For this reason, CopN and CPn0572 were not investigated further in this study. However, CPn1008 was included in the group of 116 *C. pneumoniae* proteins as a potential MT modulator because its *C. trachomatis* homolog CT850 interacts with the host cell dynein-motor-complex to mediate transport of the *C. trachomatis* inclusion along MTs to the MTOC (Grieshaber et al., 2003). CT850 is a highly conserved protein that is present in five chlamydia species and thus appears to play a critical role in infection, although, its functional homology for *C. pneumoniae* remains unknown (Lutter et al., 2012). Interestingly, the expression of *cpn1008* did not result in a growth defect of the yeast. This indicates that there appears to be no functional homology between CPn1008 and CT850. This may suggest, that the MT cytoskeleton of *C. trachomatis* and *C. pneumoniae* are modulated differently and that protein functions differ between the *Chlamydia* species. Additionally, the *C. trachomatis* effector protein CT813 (InaC) also suggests that the MT cytoskeleton is used differently by *C. pneumoniae* and *C. trachomatis*. CT813 is an essential element of the *C. trachomatis* infection and has an MT-modulatory function by inducing post-translational modifications of MT cages around the inclusion, but does not share a homolog in *C. pneumoniae* (Wesolowski et al., 2017).

In this thesis, 13 new MT-modulating proteins of *C. pneumoniae* were identified that

negatively affect the MT structure and organization of the yeast. In this way, the number of previously identified MT modulators of *C. pneumoniae* could be increased from 2 to 15 proteins, representing 1.4 % of the predicted proteins for *C. pneumoniae*. This is the largest number of MT-modulating proteins documented for a bacterial pathogen to date which implies that the MT cytoskeleton must play an essential role during chlamydial infection. Although, the total number of MT-regulating proteins of *C. pneumoniae* is estimated to be higher because 934 predicted *C. pneumoniae* proteins were not tested in this screen. Out of the 13 identified MT-modulating proteins, 12 proteins are characterized as Inc proteins (Lutter et al., 2012; Dehoux et al., 2011). For *C. pneumoniae*, 78 Inc proteins are predicted in total, of which 49 Inc proteins have been tested for MT-modulatory function in this screen, while 29 Inc proteins remain untested (Dehoux et al., 2011). Therefore, it is reasonable to assume that more Inc proteins may cause MT-related growth defects and TBZ-hypersensitivity in yeast. Additionally, it cannot be ruled out that there are other MT-regulatory proteins among the tested proteins whose gene expression triggered the lethality of yeast. Changes in the screen parameters, such as a reduction in gene expression, would possibly identify additional MT-modulating proteins but were not tested due to time constraints. Furthermore, it is possible, that chlamydial proteins with MT-modulating function cannot be identified in this genetic yeast screen because infection-specific post-translational processes do not occur in *S. pombe* as they do in human cells (Wesolowski and Paumet, 2017). Nevertheless, the effectiveness of the powerful screen was demonstrated in several ways, using a second MT-destabilizing toxin MBC to validate the growth defect of the 13 yeast transformants and to confirm the impact of chlamydial proteins in the MT network.

The alterations of the interphase MT structure of the transformants due to the expression of the targeted chlamydial effector proteins confirm that the chlamydial proteins interfere with the host cell MT network. The changes were characterized by disorganized MT structures and changes in MT length that appear to indicate a defect in the regulation of MT dynamics. Interestingly, the expression of the chlamydial gene did not alter cell morphology in any of the transformants, although some MT structures are massively aberrant. Because not all MTs of a cell appear to be affected by the chlamydial proteins, the unaffected MTs may still be involved

in transporting polarity factors for growth zone labeling to maintain the polarized growth and normal rod shape of the cell.

Of the 13 *C. pneumoniae* proteins, three proteins, in particular, caused severe changes in MT phenotype, which could be due to a direct effect of the chlamydial protein on MTs or an interaction with a host cell MT-regulatory protein.

Expression of *cpn0443* and *cpn0565* causes extremely short MTs and a highly disorganized MT structure. This MT phenotype has similarities to that of yeast cells, which have a dysfunctional MT-stabilizing Mal3/Tip1/Tea2 complex that severely limits MT polymerization and keeps MTs short (Brunner and Nurse, 2000; Browning et al., 2000; Browning and Hackney, 2005). Considering these facts, an inhibitory effect induced by CPn0443 and CPn0565 on the MT-stabilizing activity of the Mal3/Tip1/Tea2 complex could be the cause of the short MTs. The opposite effect is observed in transformants expressing *cpn0216*. In yeast, CPn0216 caused extremely long MTs curling around the cell end instead of depolymerizing back to the MTOC. A comparable MT phenotype was observed in *klp5Δ, Klp6Δ,* or *mcp1Δ* mutants, whose MT-destabilizing complex is dysfunctional, resulting in a reduction of MT catastrophe and consequently ongoing MT growth (West et al., 2001; Mata and Nurse, 1997; Zheng et al., 2014; Meadows et al., 2018). This similarity suggests that CPn0216 may reduce the destabilizing function of the Klp5/Klp6/Mcp1 complex through an interaction. In comparison, long and curling MTs are also observed in yeast cells with a defect in the γ-tubulin complex such as *alp14Δ* mutants. Although, the MT phenotype of those mutants differs from that of *klp5Δ, Klp6Δ,* or *mcp1Δ,* as in γ-tubulin complex mutants the number of MT bundles is massively limited (1 to2 MT bundles) compared to the 6 to 8 MT bundle number in the WT *S. pombe* (Sawin et al., 2004; Zimmerman and Chang, 2005; Samejima et al., 2008). The MT bundle number of *cpn0216* expressing cells cannot be accurately defined due to the MT curling, but it appears to be increased rather than to be reduced, which is why the γ-tubulin complex does not seem to act as a host cell interaction partner of CPn0216.

In addition to a possible effect on MT-modulating host cell proteins through an interaction with the bacterial proteins, a direct effect of the bacterial protein on the MT cytoskeleton or tubulin dimers is also conceivable. The *C. pneumoniae* CopN is a representative example of an MT destabilizer that binds non-polymerized αβ-tubulin dimers, efficiently inhibiting MT

polymerization and leading to severe changes in MT structure and mitotic spindles in yeast and mammalian cells (Huang et al., 2008; Archuleta et al., 2011). Although a high number of Inc proteins with MT-modulatory function have been identified in this screen which are predicted to localize in the inclusion membrane during *C. pneumoniae* infection, no bacterial transmembrane protein with direct interaction with MTs is known to date.

Moreover, this screen could also be performed with other bacterial proteins to investigate the functional relevance of the host cell MT cytoskeleton for other bacterial infections. Advantageously, *S. pombe* handling and gene expression can be easily monitored, and interphase changes in the MT cytoskeleton caused by the bacterial protein can be studied in more detail.

All in all, I identify 13 proteins by a genetic screen of 116 *C. pneumoniae* that show both an MT-related yeast growth defect and alteration of the MT cytoskeleton. This allowed me to increase the number of MT-modulating proteins from 2 to 15 proteins, corresponding to 1.4 % of the *C. pneumoniae* genome, indicating that the MT cytoskeleton has to play an essential role during *C. pneumoniae* infection. In addition, I propose that the number of MT-modulating proteins is much higher because approximately 90 % of the *C. pneumoniae* genome has not been tested for MT-modulating functions.
In this study, I investigated CPn0216 and CPn0443 due to their massive influence on the interphase MT structure. Both proteins will be discussed separately in the following chapter 5.2. and 5.3.

5.2 CPn0216, possibly an MT-stabilizer?

The *C. pneumoniae*-specific protein CPn0216 is classified as a hypothetical Inc protein based on the two Inc protein-specific characteristics: two predicted transmembrane domains and a T3SS-sequence prediction in the N-terminus (Dehoux et al., 2011). These predictions have not been studied experimentally, and neither the timing of CPn0216 secretion nor its localization or function during infection has been determined.

Using the yeast-based genetic screen for MT-regulatory proteins, I was able to attribute an MT-modulatory function to CPn216 for the first time. Expression of *cpn0216* in *S. pombe* leads to a severe growth defect and TBZ and MBC-hypersensitivity, suggesting that CPn216 affects MTs or MT-regulatory host cell proteins. Furthermore, CPn0216 causes lethality in α-/β-tubulin mutant strains *nda2-KM52* or *nda3-KM311* and confirmed an impact of CPn0216 in the MT network (Hiraoka et al., 1984; Umesono et al., 1983). Related to the CPn0216-induced growth defect of the various yeast strains is a strongly altered interphase MT cytoskeleton. The MT structure of *cpn0216* expressing *gfp-α-tubulin* cells is characterized by extremely long MTs curling around the cell end. Furthermore, the massive disorganized MT cytoskeleton is characterized by MTs that grow in the direction of the cell cortex instead of in the direction of the cell end. After cell cortex contact, they do not reorganize their direction toward the cell end instead they continue to grow along the cortex in a loop-like manner. These MT loops indicate a misregulation of the growth orientation of the MT plus-end and give reasons to assume that CPn0216 impairs the function of Tea1, the "MT growth navigator" at the MT plus-end (Behrens and Nurse, 2002; Mata and Nurse, 1997). A comparable MT loop formation and MT curling at the cell tips is caused by the loss of the *Aspergillus nidulans* (*A. nidulans*) homolog TeaA (Higashitsuji et al., 2009; Takeshita et al., 2014).

The extra-long and curling MTs lead to the reduction of MT catastrophe events at the cell end, together with an increased rate of growth and shrinkage caused by chlamydial gene expression are characteristic of the activity of an MT stabilizer (Erent et al., 2012; West et al., 2001). The transfer of the CPn0216-specific MT phenotype to the elongated cells of the *cdc25-22 gfp-α-tubulin* yeast strain also argues for an MT-stabilizing function of CPn0216. The development of extremely long and curling MTs due to prolonged polymerization phases before the onset of MT catastrophe confirmed the assumption of CPn0216-induced MT-hyperstability. Surprisingly, the first signs of MT curling at the cell ends are also observed in *cpn0216* expressing *mal3Δ gfp-α-tubulin* mutants. In *mal3Δ gfp-α-tubulin* mutants, the MT-stabilizing complex is dysfunctional resulting in severely restricted MT growth and normally short MTs (Pöhlmann et al., 2014). Despite the loss of MT stabilization by the absence of the MT stabilizer Mal3, these MTs appear to be stabilized by CPn0216, supporting the hypothesis

of CPn0216-induced MT hyperstability. To date, no MT stabilizer with a comparable function is identified for *C. pneumoniae* or *C. trachomatis*. Although, other bacterial pathogens are known to have utilized MT-stabilizing functions in the infection process. *Brucella* modulates MT dynamics using the protein TcpB, which binds MT throughout the MT cytoskeleton, bundling and stabilizing MTs for bacterial transport (Radhakrishnan et al., 2011). In contrast, *Clostridium difficile* causes bacteria internaliztaion by the actin depolymerization-induced formation of MT-based protrusions utilizing CDT (Schwan et al., 2014; Nölke et al., 2016).
Also, *C. trachomatis* uses MTs for CT850-mediated inclusion delivery to the MTOC while CT223/IPAM contributes to the formation of the MT cage surrounding the inclusion and CT813/Ina in its post-translational modification (Wesolowski and Paumet, 2017; Clausen et al., 1997; Grieshaber et al., 2003). As an MT stabilizer, CPn0216 could be considered to have a comparable function, as neither MT-dependent internalization, MT-dependent mobilization of inclusion to MTOC, nor MT cage formation is studied for *C. pneumoniae*. If CPn0216 is an MT stabilizer with MT hyperstabilizing function, CPn0216 should resist cells to cold-induced MT destabilization, similar to what is observed for cold- or nocodazole-treated MTs in the present TcpB (Radhakrishnan et al., 2011). Furthermore, CPn0216 would be expected to localize as a potential MT stabilizer close to MTs and thus could stabilize MTs directly or indirectly via an interaction partner. Both, the MT phenotype and the increased MT growth rate could indicate that CPn0216 binds directly to the MT plus-end to act as an MT capping protein that protects the MT tip from MT destabilization and thereby promotes MT assembly. On the other hand, an indirect MT stabilization via interaction of CPn0216 with an MT plus-end complex would be conceivable. However, localization analysis of CPn0216 had to be avoided because the C-terminal fusion of the mCherry-tag to CPn0216 leads to a reduction in CPn0216-specific MT phenotypes. Possibly, loss of function of CPn0216 occurred due to massively impaired protein folding, which could explain the cause of the partial unaffected of MT structure (Crivat and Taraska, 2012). Using a shorter fusion-taq, such as a flag-taq, could resolve the loss of function and determine the localization of CPn0216.

In the course of a functional characterization, the origin of the MT-modulating effect could be narrowed down to the C-terminus of CPn0216. The similarity of the altered interphase MT

cytoskeletons under expression of the full-length protein or the C-terminus of CPn0216 (CPn0216$^{82-145}$) suggests, that MTs are modulated similarly. Since the C-terminal region plays the key role in the interaction of Inc proteins with host cell proteins, the modulation of the MT cytoskeleton attributed to the CPn0216 C-terminus could be considered as the first indication that CPn0216 is indeed an Inc protein (Elwell et al., 2017; Gauliard et al., 2015).

The direct interaction of CPn0216 with MTs could not be addressed in the current study due to the failure of localization analysis. However, the influence of CPn0216 on the master regulators of MT dynamics and MT organization was investigated in more detail. On the one hand, the CPn0216-specific MT phenotype and changed MT dynamics could be the result of an interference of the regulation of the MT destabilizing Klp5/Klp6 complex with the MT-stabilizing Mal3/Tea2/Tip1 complex. On the other hand, CPn0216 may affect Tea1 in its function as an MT plus-ends growth navigator and cell end maker, resulting in over-long MTs and defective MT organization.

Two models are therefore derived, which will be discussed further in the following:

(i) CPn0216 affects the major regulators of MT dynamics

(ii) CPn0216 interacts with the MT growth navigator Tea1

5.2.1 Model i: Does CPn0216 affect the major regulators of MT dynamics?

The documented MT phenotype of cells expressing *cpn0216* suggests a dysfunctional regulation of MT dynamics caused by either increased activity of the MT-stabilizing kinesin-7 Mal3/Tea2/Tip1 complex or reduced activity of the MT-destabilizing kinesin-8 Klp5/Klp6 complex (Erent et al., 2012) *(***Figure 28***).* On the one hand, CPn0216 may increase stabilization of the MT plus-end by interacting with the MT stabilizers Mal3 or Tip1, preventing the MT-destabilizing Klp5/Klp6 complex accumulating behind it from advancing to the MT tip and thus inhibiting the initiation of MT catastrophe, which could explain the overlong MTs (**Figure 28***).* On the other hand, the increased MT growth rate suggests a CPn0216-induced increased motor function of Tea2 to stabilize the MT tip. However, it could also be considered that

CPn0216 interacts with multiple proteins at the same time, since it could act as cargo to support both the mobility of Tea2 and the MT-stabilizing function of Tip1 to promote MT assembly. Similar utilization has already been documented for *C. trachomatis.* Their inclusions are transported as cargos along the MTs by the interaction of the Inc protein CT850 with the host cell the dynein-motor complex (Grieshaber et al., 2003).

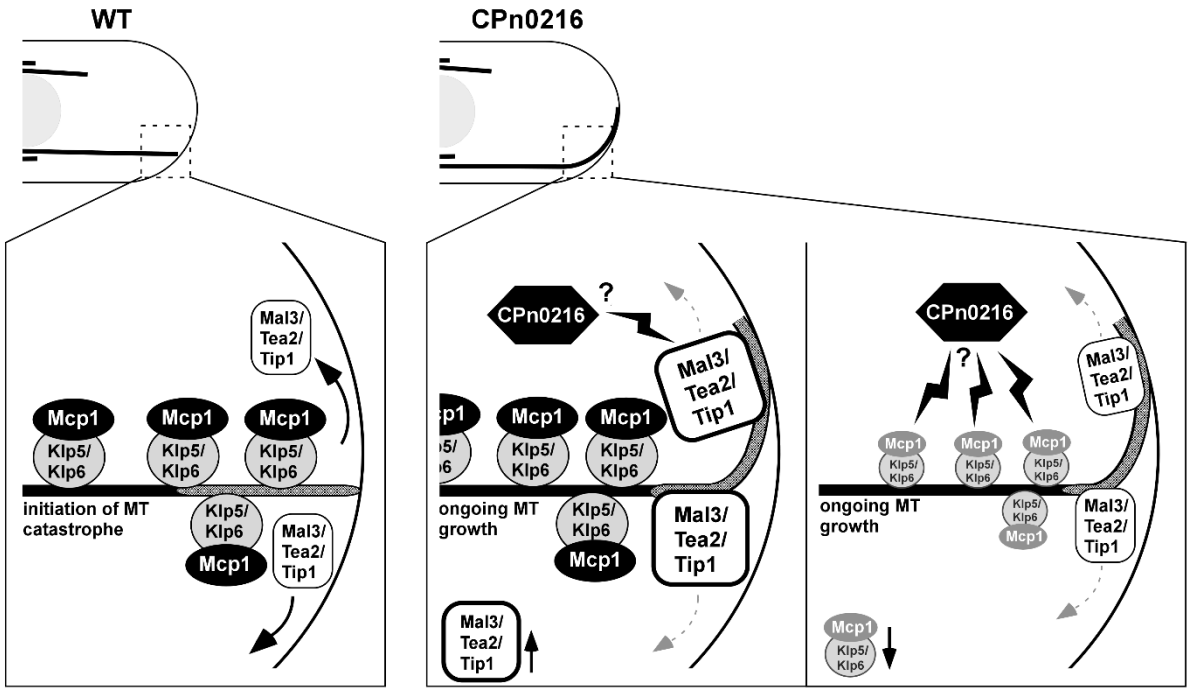

Figure 28: Hypothetical model 1: CPn0216 hyperstabilizes MTs by stimulating the MT-stabilizing function of the Mal3/Tea2/Tip1 complex or by reducing the activity of the Klp5/Klp6/Mcp1 complex. Left: In wild-type (WT) *S. pombe*, MT dynamics, and corresponding MT length are determined by space regulation through the coordination of the MT-stabilizing Mal3-dependent Tea2/Tip1 complex and the MT-destabilizing Klp5/Klp6/Mcp1 complex at the MT plus-end. During MT growth, the Mal3/Tea2/Tip1 complex stabilizes the MT plus-end, whereas the Klp5/Klp6/Mcp1 complex accumulates behind it. Contact of the growing MT tip with the cell end slows MT assembly, allowing the Klp5/Klp6/Mcp1 complex to advance to the MT plus-end (dashed area of the MT), displacing the Mal3/Tea2/Tip1 complex from the MT tip, and triggering MT catastrophe. The release of the Mal3/Tea2/Tip1 complex from the MT plus-end is shown in **Figure 29**. Right: CPn0216 causes a decrease in MT catastrophe and continued MT growth by either stimulating the Tea2/Tip1/Tea1 complex (left side) or decreasing the activity of the Klp5/Klp6/Mcp1 complex (right site) to prevent the MT-destabilizing complex from advancing to the MT plus-end that initiates MT catastrophe.

In view of these considerations, the influence of CPn0216 on yeast growth in the absence of Mal3, Tea2, or Tip1 was analyzed. Although the expression of *cpn0216* in *mal3Δ, tea2Δ*, and

tip1Δ mutants continues to induce lethality and TBZ-hypersensitivity of the yeast, making a single interaction of CPn0216 unlikely, CPn0216 may interact with multiple proteins of Mal3/Tea2/Tip1 complex. First indications for this assumption are longer MTs and signs of MT curling at the cell ends in *cpn0216* expressing *mal3Δ gfp-α-tubulin* mutants, even when the absence of the MT stabilizer protein Mal3 usually negatively affects MT stability and the resulting MT polymerization and causes massively shortened MTs (Busch and Brunner, 2004; Browning and Hackney, 2005). There are two possible explanations for this CPn0216-induced effect. Either, CPn0216 does not interact with the complex and stabilizes directly the MT or CPn0216 directs Tea2 and Tip1. If CPn0216 is able to increase the complex activity of Tip1 and Tea2 in the absence of Mal3, CPn0216 likely affects both Tip1 and Tea2, since Tip1 transport to the MT plus-end is Tea2-dependent and Tea2 does not exert an MT stabilizing function, which could explain the prolonged MTs. Growth analysis of a *cpn0216* expressing *tea2Δ tip1Δ* double-mutants could provide an insight into a potential interaction between CPn0216 and Tea2/Tip1.

As a potential host cell target of CPn0216, the MT-destabilizing Klp5/Klp6 complex could also be considered, since a reduction of the destabilizing activity of the Klp5/Klp6 complex causes overlong and hyperstable MT and suppression of MT catastrophe. The similarity of the MT phenotypes of *klp5Δ* and/or *klp6Δ* mutants, and *cpn0216* expressing cells suggests a common cause, the loss of function of the MT-destabilizing complex (West et al., 2001; Mata and Nurse, 1997). Although the interaction of Klp5 or Klp6 with CPn0216 appears unlikely because expression of *cpn0216* in *klp5Δ* or *klp6Δ* mutants continued to induce lethality and TBZ-hypersensitivity in yeast.

Another actor of the Klp5/Klp6 complex is the binding partner Mcp1. Mcp1 is needed for the accumulation of the Klp5/Klp6 complex at the MT plus-ends and the induction of the MT catastrophe event and MT depolymerization. Similar to the MTmphenotype of *cpn0216* expressing cells, the absence of Mcp1 causes elongated MT curling at the cell ends by reducing MT catastrophe events (Zheng et al., 2014; Meadows et al., 2018). CPn0216 could inhibit the MT destabilization activity of the Klp5/Klp6/Mcp1 complex at the MT plus-end via interaction with Mcp1, which would lead to ongoing MT assembly. Consequently, the MT would

depolymerize with a massive delay.

The question remains whether CPn0216 has a direct influence on MT stability or whether CPn0216 interferes with MT dynamics via interaction with one or more master regulators of MT dynamics and thus inhibits MT catastrophe. In addition to the functionality of the MT-destabilizing Klp5/Klp6/Mcp1 complex at the MT plus-end, the delivery of polymerization factors to the cell ends depends on the MT-stabilizing Mal3/Tea2/Tip1 complex. In particular, Tea1 plays an important role in MT organization, and Tea2 and Tip1 anchoring at the cell end which is a prerequisite for depolymerization. In the following chapter 5.2.2, Tea1 is discussed as a potential host cell target of CPn0216.

5.2.2 Model ii: Does CPn0216 interact with the MT growth navigator Tea1?

The polarity protein Tea1 serves as a cortical landmark for the growing MTs at the cell ends and is localized at the growing MT plus-end to navigate it to the cell end, thereby regulating MT organization (Mata and Nurse, 1997; Behrens and Nurse, 2002). In addition to the overlong MTs curling at the cell ends of *cpn0216* expressing cells, there is also a massive disorganized MT structure. Several MTs are oriented towards the cell cortex and do not reorganize their growth direction towards the cell end after contact, instead, they grow along the cortex and form MT loops. This misalignment of MT could be due to reduced activity of the MT growth navigator Tea1 at the MT plus-end and/or a reduction of Tea1 anchored at the cell end as a landmark. Tea1-GFP cells showed a significant reduction of Tea1-GFP fluorescence intensity at the cell end when *cpn0216* was expressed. On the other hand, Tea1-GFP signals tracking in the direction of the cell end were documented, but not in the direction of the lateral cell cortex. Because the expression of *cpn0216* in the *gfp-α-tubulin* strain resulted in numerous MTs oriented toward the lateral cell cortex, it is reasonable to assume that CPn0216 negatively affects the attachment of Tea1-GFP to the growing MT plus-end. Therefore, the absence of Tea1 at the growing MT tips appears to cause the disorganized MT growth direction, resulting in less Tea1 transported toward the cell end and anchored at the cell end. A mislocalization of Tea1 inside the cell as a possible cause seems rather unlikely since Tea1-GFP was not detected at the cell cortex and thus no new growth zones were created. Rather, the MTs that do not

seem to be influenced by CPn0216 and grow towards the cell end seem to be sufficient for marking the polar growth, which would explain why the cell morphology is not negatively influenced. A similar MT phenotype is found in *A. nidulans* when TeaA, the homolog of Tea1, is absent. This similarity supports the hypothesis that the CPn0216-induced loss of Tea1 at the MT tips causes the disorganized, overlong, and curling MTs of the yeast (Takeshita et al., 2014; Higashitsuji et al., 2009).

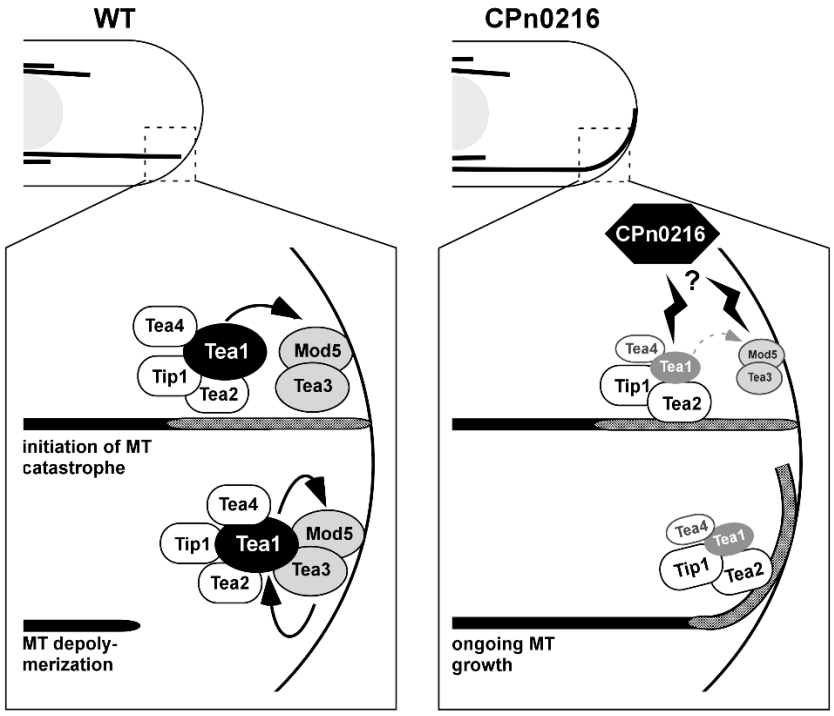

Figure 29: Hypothetical model 2: CPn0216 inhibits MT catastrophe by interrupting the transport and/or anchoring of the Tea1/Tea4/Tea2/Tip1 complex at the cell end.

Left: In wild-type (WT) *S. pombe*, Tea1 forms with Tea4, Tea2, Tip1 a large complex for the transport to growing MT plus-end (dashed area of the MT). After contact of the growing MT plus-end with the cell end, the Tea1/Tea4/Tea/Tip1 complex is anchored to the plasma membrane by the interaction of Tea1 with the membrane-associated protein Mod5 and Tea3. This results in a positive feedback loop of Tea1, Mod5, and Tea3 (double-headed arrow). Through Tea1-mediated anchoring of Tea2 and Tip1 to the cell end, Tea1 initiates the MT catastrophe mechanism as Klp5/Klp6 complex is able to advance to the MT plus-end (shown in **Figure 28**). Right: CPn0216 negatively affects the Tea1/Tea4/Tea/Tip1 complex by inducing a CPn0216-induced reduction of Tea1 at the growing MT plus-end. As a consequence, less Tea1 is transported to the cell end and there is a reduction of Tea1-mediated anchoring of Tea4, Tea2, and Tip1 at the cell end. Tea2 and Tip1 remain at the growing MT plus-end and stabilize it, causing the MT to continue around the cell end without initiating the MT catastrophe.

As a possible reason for the Tea1 reduction at the growing MT tip, several causes could be considered. A degradation of Tea1 could be the explanation for the reduced Tea1 signals at the MT tip and at the cell ends (**Figure 29**). Furthermore, it can be considered that CPn0216 binds Tea1 directly and reduces the binding to the MT tip and the cell end. Alternatively, CPn0216 could occupy the binding site of Tea1 at the Mal3-mediated Tea2/Tip1 complex to be transported as cargo, which could explain the reduction at the MT tip and cell end. The reduced delivery of Tea1 to the cell end also results in less of the cell polarity protein Tea4 being transported to the growth zones of the cell, since the transport of Tea4 is dependent on Tea1. Accordingly, reduced Tea4-GFP fluorescence intensity at the cell ends was also documented. Furthermore, decreased transport of Tea1 to the cell end also has a direct effect on the MT catastrophe mechanism, as Tea1-mediated anchoring of Tea2 and Tip1 at the cell end is required for the MT-destabilizing Klp5/Klp6/Mcp1 complex to initiate MT catastrophe (Browning et al., 2000; Busch et al., 2004). Consequently, loss of Tea1 leads to a reduction in Tea2 and Tip1 release from the MT plus-end that promotes MT growth and inhibits MT catastrophe.

According to growth analysis of *cpn0216* expressing *tea1Δ* mutants, there is reason to assume that Tea1 plays a role in the induction of the MT phenotype, since the chlamydial gene expression in this mutant affects yeast growth less than in the WT strain, and also did not induce TBZ-hypersensitivity. If Tea1 is the only host cell target of CPn0216, yeast growth would be rescued in the absence of Tea1. However, confirmation of the interaction is still required as no immunoprecipitation without CPn0216-mCherry function could be obtained. Since the growth analysis of *cpn0216* expressing *tea1Δ* mutants nevertheless showed an effect on yeast growth, this suggests that there is one or more other host cell target involved in the interaction of CPn0216. Potential interaction partners of CPn0216 are proteins that are either unrelated to Tea1 or proteins whose function is not fully dependent on Tea1. Proteins such as Tea4, whose transport and anchoring are dependent on Tea1, are therefore unlikely to be further interaction partners of CPn0216, as otherwise yeast growth in *cpn0216* expressing *tea1Δ* mutants should no longer be impaired due to loss of function of Tea1 and consequently Tea4 (Higashitsuji et al., 2009). As further interaction partners of CPn0216, the membrane-

associated protein Mod5 and Tea3, with which Tea1 interacts for anchoring, are also rather unlikely, since Tea1, Mod5, and Tea3 are members of a positive feedback loop and affect each other functionally. The absence of Tea1 therefore also has consequences for the localization and function of Mod5 and Tea3. If Mod5 and Tea3 are further interactors of CPn0216, *cpn0216* expression in *tea1Δ* mutants would not negatively affect yeast growth. The Tea2/Tip1 complex represents another potential interaction partner. The anchorage of Tea2 and Tip1 to the plasma membrane is a Tea1-dependent process, but not its transport along the MT to the MT plus-end (**Figure 29***).* Accordingly, the induced growth defect in *cpn0216* expressing *tea1Δ* mutants may be due to an interaction of Tea1 with Tea2 and Tip1. CPn0216, as a possible cargo, could exert a stimulatory effect on the MT-stabilizing complex, thereby hyperstabilizing the MTs and causing overgrowing MTs. Whether the Tea2/Tip1 complex interacts with CPn0216 remains to be clarified by growth analysis of *cpn0216* expressing in *tea2Δ tip1Δ* double mutants. Thus, the question of which other host cell proteins besides Tea1 are involved in host cell interphase MT cytoskeleton modulation remains to be answered.

In summary, CPn0216 is suspected to directly affect MT stability or to influence the major regulators of MT dynamics, either through a reduction of the MT-destabilizing activity of the Klp5/Klp6/Mcp1 complex, and/or through stimulation of the MT-stabilizing Mal3/Tea2/Tip1 complex. I proposed that CPn0216 affects Tea1 and thereby affects the transport and anchoring of the Tea1/Tea4/Tea2/Tip1 complex, explaining the reduction of the MT catastrophe and is the reason for the ongoing MT growth around the cell end.

5.3 Does CPn0443 interact directly with MTs?

CPn0443 is a highly conserved Inc protein with a homolog in *C. trachomatis, C. muridarum, C. caviae*, and *C. felis* and thus appears to be essential for the infection process (Lutter et al., 2012). While the *C. trachomatis* protein CT005, also known as IncV, has been intensively studied, the function and localization of CPn0443 during *C. pneumoniae* infection have not been analyzed.

In this thesis, I was able to link CPn443 to an MT-modulatory function for the first time. In the

genetic screen, expression of *cpn0443* caused severe growth defect and TBZ and MBC-hypersensitivity, and lethality in α-/β-tubulin mutant strains (*nda2-KM52/nda3-KM311*) confirmed the influence of CPn443 in the MT network (Hiraoka et al., 1984; Umesono et al., 1983). Related to the CPn443-induced growth defect of the various yeast strains is a highly altered interphase MT cytoskeleton in *gfp-α-tubulin* cells that was characterized by extremely short and disorganized MTs, whereas only isolated MTs polymerize to the cell end. In addition to cells with massively short MTs, there is also strong MT accumulation near the cell nucleus, which may indicate degraded MT structures. Considering this MT phenotype, functional relevance to MT cage formation during *C. pneumoniae* infection that has not previously been identified in *C. pneumoniae*. Moreover, the CPn0443-induced MT phenotype and reduction of MT growth and shrinkage rate are all characteristics of an MT destabilizer (Zheng et al., 2014). Functional characterization revealed that MT modulatory function appears to be restricted to the C-terminus of CPn0443 since the full-length protein and C-terminus of CPn0443 ($CPn0443^{164-417}$) induced comparable changes in MT structure. The MT-modulating function harbors in the C-terminal region of the protein could be considered the first indication that CPn0443 is an Inc protein (Elwell et al., 2017; Gauliard et al., 2015). The *C. trachomatis* homolog CT005/IncV also interacts with host cell proteins via its C-terminus. On the one hand, CT005/IncV interacts via its FFAT-motifs with the human proteins VAPA/VAPB at the ER, thereby positioning the inclusion close to the ER (Mirrashidi et al., 2015). On the other hand, CT005/IncV is considered to associate with the human MT cytoskeleton. CT005/IncV is predicted to potentially interact with the human MAPRE1, but this interaction is not experimentally verified (Stanhope et al., 2017).

With regard to the short MTs and partial MT accumulation in the region of the cell nucleus, CPn0443 could directly affect MTs by influencing MT dynamics as a capping protein at the MT tip, severing protein along the MTs, or by freely binding free αβ-tubulin dimers such as CopN and thereby inhibiting MT growth (Huang et al., 2008; Archuleta et al., 2011). In localization analysis, in 68.7% of CPn0443-mCherry-expressing cells, the chlamydial protein was detected at the plasma membrane and ring-shaped in the region of the nucleus, indicating ER localization. In *S. pombe*, a large part of the ER is tightly attached to the plasma membrane,

and since ER is continuously connected to the nuclear envelope, the CPn0443-mCherry localization pattern is indicative of ER localization (Ashraf et al., 2021). Nevertheless, a verification of the co-localization of CPn0443-mCherry with the ER using an ER marker such as GFP-AHDL is still required (Zhang et al., 2012). The fact that CT005/IncV interacts with the ER proteins VAPA/VAPB may indicate a functional similarity between CT005 and CPn0443 (Mirrashidi et al., 2015). Most probably, CPn0443 is anchored in the ER by the four transmembrane domains and from there influence the MTs, which would explain the partial localization along the shortened MTs. Based on this localization, it is highly unlikely that CPn0443 acts as a capping protein and blocks the MT plus-end for MT assembly or freely binds αβ-tubulin dimers in the cytosol.

However, it would be possible that along the MT lattice binds localized and severs MTs contributing to early MT destabilization, similar to the like human severing proteins katanin or spatin (Yu et al., 2008). Although no functional domain was previously predicted for CPn0443 in this regard, further analyses would indicate whether CPn0443 possesses enzymatic activity that can lead to the severing of MTs and explain the MT phenotype. Furthermore, the localization of CPn0443-mCherry along MTs suggests direct MT binding. Indeed, direct MT binding was detected *in vitro*, as GST-CPn0443$^{164\text{-}417}$ associates with MTs. CPn0443$^{164\text{-}417}$, whose GST-tag was cleaved, also showed MT association, thus excluding GST-induced MT binding (data not shown). Based on the *in vitro* MT binding of CPn0443$^{164\text{-}417}$ and GST-CPn0443$^{164\text{-}417}$, it is reasonable to assume that the *in vivo* co-localization of CPn0443-mCherry to MTs in yeast is a direct MT binding.

The direct binding of CPn0443 to MTs allows the chlamydial protein to exert a direct influence on MTs and thus modulate MT, or CPn0443 interacts with a host cell protein and thus influences MT. Initially, the major regulators of MT dynamics were considered as potential host cell targets. CPn0443 could stimulate the MT-destabilizing activity of the Klp5/Klp6/Mcp1 complex and thus cause short MTs (Unsworth et al., 2008; West et al., 2001). However, the expression of *cpn0443* in *klp5Δ* and *klp6Δ* mutants triggered a growth defect and TBZ-hypersensitivity. CPn0443 interaction with the Mcp1 protein, which increases the activity of

the Klp5/Klp6 complex, could not yet be verified as a possible host cell target in this study (Zheng et al., 2014).

Considering the massive short MTs of the *cpn0443* expressing cells, the MT-stabilizing Mal3/Tea2/Tip1 complex suggested that the lack of Mal3, Tea2, or Tip1 cause a reduction of MT polymerization, and the MTs are consequently shortened (Busch and Brunner, 2004; Brunner and Nurse, 2000).

First, the MT stabilizer Mal3 was considered, which preferentially binds to the growing MT plus-ends, in addition, Mal3 also stabilizes the MT lattice and could be considered as the host cell target because of the localization of CPn0443 along MTs (Des Georges et al., 2008). Functional characterization of *cpn0443-mCherry* expressing *mal3^{+}-gfp* cells demonstrated Mal3 accumulation in the region of the cell nucleus, which is comparable to the region of MT accumulation of *gfp-α-tubulin* cells. Since CPn0443 co-localizes with both the region of accumulated MTs and the region of accumulated Mal3, it was previously suggested that the interaction of CPn0443 with Mal3 affects MT dynamics and consequently short MTs. However, no direct interaction between Mal3 and CPn0443 could be confirmed. First, Mal3-GFP did not immunoprecipitate with CPn0443-mCherry, and second, expression of *cpn0443* in *mal3Δ* mutants triggered a growth defect and TBZ-hypersensitivity. Third, the effect of *cpn0443* expression in *mal3Δ gfp-α-tubulin* mutants was examined and showed more severely shortened MTs compared to control transplants. Based on three assays, CPn0443 is not expected to interact with Mal3 and be responsible for its accumulation, causing the short MTs. Therefore, CPn0443 may either influence MT polymerization via other major regulators of MT dynamics or CPn0443 directly influences MTs, leading to shortened MTs and the resulting Mal3 accumulation.

Moreover, the loss of Tea2 and Tip1 also has a negative effect on MT polymerization shortened (Busch and Brunner, 2004; Brunner and Nurse, 2000). Because Tea2/Tip1 complex binding to MTs and its stimulation is dependent on Mal3, I expected a similar accumulation of Tea2 and Tip1 in the same region as MTs and Mal3 have already been observed under the expression of *cpn0443* (Browning and Hackney, 2005). Interestingly, in contrast to my expectation, no Tea2-

GFP or Tip1-GFP accumulation was detected in the region of short MTs in *cpn0443-mCherry* expressing *gfp-tea2* and *gfp-tip1* cells. On the contrary, no Tea2-GFP or Tip1-GFP tracking signals could be observed in the cells. Less surprising was the lack of Tea2-GFP or Tip1-GFP localization at the cell end, which can be explained based on short MTs. However, unusually high Tea2-GFP or Tip1-GFP fluorescence intensities were detected in the background, which may indicate, on the one hand, that the absence of Tea2-GFP and Tip1-GFP signals is due to their protein degradation. On the other hand, it is possible that Tea2 and Tip1 are unable to form a complex and therefore cannot be detected on MTs. Initial growth analysis of *cpn0443* expressing *tea2Δ* and *tip1Δ* mutants also revealed a severe growth defect and TBZ-hypersensitivity. Although a direct interaction of CPn0443 with Tea2 and Tip1 seems unlikely, microscopic analyses revealed that CPn0443 affects Tea2 and Tip1 differently than Mal3. Therefore, the relation of CPn0443 with Tea2 and Tip1 should be further investigated in future analyses.

In addition to the massive impact of CPn0443 on the *S. pombe* interphase MT cytoskeleton, ectopic expression of GFP-CPn0443 in non-polarized human U2OS epithelial cells also proved changes in MT organization and structure. GFP-CPn0443 localized around the nucleus and partially along the host cell interphase MTs. The co-localization of CPn0443 to MTs resulted in a GFP-CPn0443 amount-dependent MT change that was expressed in either aberrant or highly aberrant MT structures. Aberrant MT structures, whose MTs are bundled into thicker MT cables primarily radiated from the MTOC to the plasma membrane, are formed predominantly in the first 10 hours after transfection. In contrast, after 20 hours of transfection, the majority of cells exhibited severely aberrant MT structures, characterized by MTs bundled into thick MT cables organized in a spaghetti-like structure instead of being directed toward the plasma membrane of the cell. The development of the severely aberrant MT phenotype with progressive transfection time may indicate that MT structure is affected by increasing amounts of expressed GFP-CPn0443 than at an earlier time point in the aberrant MT phenotype. These aberrant or severely aberrant MT structures were detected in human U2OS cells as well as in human HeLa cells, but not in human HEp2 cells or hamster CHOK1 cells. GFP-CPn0443 was localized exclusively in the cytosol in HEp2 and CHOK1 cells and the protein bands of

GFP-CPn0443 could not be detected at the calculated molecular weight of 72 kDa in the Western blot analysis of whole-cell lysate of these cell lines. One possible reason could be that CPn0443 cannot be correctly post-translationally processed in HEp2 and CHOK1 cells and is therefore non-functional, making binding to MTs impossible. The cause of this "cell line-specific" MT phenotype could not be clarified during the course of this study and therefore remains speculative. One explanation could be that the three predicted N-linked glycosylation motifs and signal sequences in the C-terminus of CPn0443 may indicate multistep protein processing that cannot be correctly performed in HEp2 and CHOK1 cells. In particular, CHOK1 hamster cells, which are not the usual host organism *C. pneumoniae*, might not possess a homolog of the human genes required for N-linked glycosylation of CPn0443 in human cells (Xu et al., 2011; Bryan et al., 2021). In addition, U2OS, HeLa, HEp2, and CHOK1 cells are carcinoma cell lines whose ongoing gene mutation is not controllable or predictable. Therefore, it is possible that in HEp2 and CHOK1 cells, N-linked glycosylation is affected, which is required for the functional modification of CPn0443. It remains to be elucidated why the localization of CPn0443 differs between different cell lines.

In the course of determining the MT-binding domain, the domain could be restricted to the C-terminus of CPn0443, since both the full-length protein and the C-terminal variant GFP-CPn0443$^{54-417}$ exhibited MT localization. While both CPn0443-GFP and GFP-CPn0443$^{54-417}$ partially co-localize with MT structures, CPn0443-GFP induces massive alterations in MT structure of the host cell. Thereby, the ER structure of CPn0443-GFP-expressing cells also exhibits massive restructuring that strongly mimics the aberrant MT cytoskeletons. A potential explanation for this could be that CPn0443 is anchored in the ER and modulates MTs via the C-terminus. This would also explain why the deletion of the transmembrane domains in GFP-CPn0443$^{164-236}$ resulted in exclusively cytosolic localization. A similar observation was made for the ectopically expressed *C. trachomatis* homolog GFP-CT005 and its C-terminal variant GFP-CPn0443$^{164-236}$. While the full-length protein was detected in the ER, GFP-CT005$^{146-363}$ could only be detected in the cytosol. On the one hand, based on the similar ER localization of CPn0443 and CT005, the data suggest that functional homology may be present. On the other hand, the transmembrane domains appear to be essential for

functionality and localization in the host. To rule out that the long GFP-tag (726 aa, 27 kDa) does not affect the intracellular localization of the truncated C-terminal CPn0443 variants, the use of a shorter flag-tag (69 aa, 4 kDa) would be advisable. For even more efficient analysis, the generation and use of a recombinant antibody against CPn0443 would be helpful to study its function and localization without the influence of a fluorescence-tag.

Furthermore, it was of interest to know the influence of CPn0443 and its localization during the *C. pneumoniae* infection. The localization analysis of GFP-CPn0443 failed under the general experimental setup of our laboratory, in which human HEp2 cells were transfected with GFP-CPn0443 or the GFP-control for 18 hours and then infected with *C. pneumoniae* for 30 or 48 hours. GFP-CPn0443 was localized in the cytosol and not along the MTs which may be attributed to the cell line (data not shown). However, changes in individual experimental parameters did not solve the problem. The GFP-CPn0443 analysis also failed when human U2OS cells were transfected with GFP-CPn0443 or GFP-control for 18 hours and then infected with *C. pneumoniae* for 30 or 48 hours. The combination of transfection and infection leads to massive cell death (data not shown). Changing the experimental setup with respect to *C. pneumoniae* concentration or shortening the duration of infection did not solve the problem. Reducing the *C. pneumoniae* concentration massively limited the number of transfected cells, while shortening the duration of infection resulted in too small inclusions for efficient microscopic analysis (data not shown). Therefore, a change in strategy occurred. HEp2 cells were infected with CPn0443-flag ectopic expressing *C. pneumoniae* for 96 hours. Since the majority of Inc proteins, such as CT005/IncV, are integrated into the inclusion membrane, localization of CPn0443 to the inclusion membrane was also expected (Stanhope et al., 2017). Contrary to my expectations, CPn0443-flag is expressed within or on the surface of bacteria in the inclusion during infection. To date, no *C. pneumoniae* protein is known to have a different localization than its *C. trachomatis* homolog, regardless of functional homology. This observation suggests that CPn0443-flag may not be secreted out of the bacteria into the inclusion. Possible causes for this could be that due to the constitutively active *NmPro* promoter, CPn0443 is expressed at the incorrect stage of infection and/or has the incorrect level of expression, and thus protein function does not occur. One possibility for the

correct expression level of CPn0443 and the correct timing during infection would be the use of the endogenous promoter of CPn0443. Nevertheless, the flag-tag could affect secretion. For upcoming experiments, an antibody against CPn0443 is required to identify the correct localization of unlabeled CPn0443 during infection and to determine whether CPn0443 is localized on the bacterial surface, within *C. pneumoniae,* or at the inclusion membrane. If CPn0443 is still detected inside the inclusion and continues to localize on the bacterial surface or within *C. pneumoniae*, the question arises of how CPn0443 can modulate MTs from inside the inclusion. This needs to be addressed in the future.

In summary, CPn0443 negatively affects MTs of both *S. pombe* and human epithelial cells, as well as directly binds to MTs *in vitro*. As a result, I proposed that CPn0443 directly affects MTs by directly binding these MTs. The CPn0443-induced reduced MT dynamics caused shorter MTs, which impairs the localization and function of Tea2 and Tip1 to the growing MTs, which causes their absence. Another consequence of reduced MT dynamics is that Mal3 is detected on growing MTs in the region of short MTs near the nucleus without directly interacting with Mal3. Furthermore, the localization of CPn0443 without the influence of a fluorescent tag during *C. pneumoniae* infection should be investigated to further determine the protein function and its relevance in the infection process. These studies should also address whether CT005 and CPn0443 share functional homology.

6 References

Abdelrahman, Y. M. and Belland, R. J. (2005). The chlamydial developmental cycle. *FEMS microbiology reviews* **29**, 949–959.

Ajonuma, L. C., Fok, K. L., Ho, L. S., Chan, P. K. S., Chow, P. H., Tsang, L. L., Wong, C. H. Y., Chen, J., Li, S., Rowlands, D. K. et al. (2010). CFTR is required for cellular entry and internalization of Chlamydia trachomatis. *Cell. Biol. Int.* **34**, 593–600.

Akhmanova, A. and Steinmetz, M. O. (2008). Tracking the ends: a dynamic protein network controls the fate of microtubule tips. *Nature reviews. Molecular cell biology* **9**, 309–322.

Al-Bassam, J., Ozer, R. S., Safer, D., Halpain, S. and Milligan, R. A. (2002). MAP2 and tau bind longitudinally along the outer ridges of microtubule protofilaments. *The Journal of Cell Biology* **157**, 1187–1196.

Almeida, F., Luís, M. P., Pereira, I. S., Pais, S. V. and Mota, L. J. (2018). The Human Centrosomal Protein CCDC146 Binds Chlamydia trachomatis Inclusion Membrane Protein CT288 and Is Recruited to the Periphery of the Chlamydia-Containing Vacuole. *Frontiers in cellular and infection microbiology* **8**, 254.

Al-Zeer, M. A., Al-Younes, H. M., Kerr, M., Abu-Lubad, M., Gonzalez, E., Brinkmann, V. and Meyer, T. F. (2014). Chlamydia trachomatis remodels stable microtubules to coordinate Golgi stack recruitment to the chlamydial inclusion surface. *Molecular microbiology* **94**, 1285–1297.

Alzhanov, D. T., Weeks, S. K., Burnett, J. R. and Rockey, D. D. (2009). Cytokinesis is blocked in mammalian cells transfected with Chlamydia trachomatis gene CT223. *BMC microbiology* **9**, 2.

Archuleta, T. L., Du, Y., English, C. A., Lory, S., Lesser, C., Ohi, M. D., Ohi, R. and Spiller, B. W. (2011). The Chlamydia effector chlamydial outer protein N (CopN) sequesters tubulin and prevents microtubule assembly. *The Journal of biological chemistry* **286**, 33992–33998.

Ashraf, S., Tay, Y. D., Kelly, D. A. and Sawin, K. E. (2021). Microtubule-independent movement of the fission yeast nucleus. *Journal of cell science*. https://doi.org/10.1242/jcs.253021.

Balin, B. J. and Appelt, D. M. (2001). Role of infection in Alzheimer's disease. *The Journal of the American Osteopathic Association* **101**, S1-6.

Balin, B. J., Little, C. S., Hammond, C. J., Appelt, D. M., Whittum-Hudson, J. A., Gérard, H. C. and Hudson, A. P. (2008). Chlamydophila pneumoniae and the etiology of late-onset Alzheimer's disease. *Journal of Alzheimer's disease : JAD* **13**, 371–380.

Bannantine, J. P., Griffiths, R. S., Viratyosin, W., Brown, W. J. and Rockey, D. D. (2000). A secondary structure motif predictive of protein localization to the chlamydial inclusion membrane. *Cellular microbiology* **2**, 35–47.

Bastidas, R. J., Elwell, C. A., Engel, J. N. and Valdivia, R. H. (2013). Chlamydial intracellular survival strategies. *Cold Spring Harbor perspectives in medicine* **3**, a010256.

Behrens, R. and Nurse, P. (2002). Roles of fission yeast tea1p in the localization of polarity factors and in organizing the microtubular cytoskeleton. *The Journal of Cell Biology* **157**, 783–793.

Beinhauer, J. D., Hagan, I. M., Hegemann, J. H. and Fleig, U. (1997). Mal3, the fission yeast homologue of the human APC-interacting protein EB-1 is required for microtubule integrity and the maintenance of cell form. *The Journal of Cell Biology* **139**, 717–728.

Beln Moreno, M., Durn, A. and Carlos Ribas, J. (2000). A family of multifunctional thiamine-repressible expression vectors for fission yeast. *Yeast* **16**, 861–872.

Berrueta, L., Kraeft, S. K., Tirnauer, J. S., Schuyler, S. C., Chen, L. B., Hill, D. E., Pellman, D. and Bierer, B. E. (1998). The adenomatous polyposis coli-binding protein EB1 is associated with cytoplasmic and spindle microtubules. *Proc Natl Acad Sci USA* **95**, 10596–10601.

Beswick, E. J., Travelstead, A. and Cooper, M. D. (2003). Comparative studies of glycosaminoglycan

involvement in Chlamydia pneumoniae and C. trachomatis invasion of host cells. *The Journal of infectious diseases* **187**, 1291–1300.

Bieling, P., Laan, L., Schek, H., Munteanu, E. L., Sandblad, L., Dogterom, M., Brunner, D. and Surrey, T. (2007). Reconstitution of a microtubule plus-end tracking system in vitro. *Nature* **450**, 1100–1105.

Birnboim, H. C. and Doly, J. (1979). A rapid alkaline extraction procedure for screening recombinant plasmid DNA. *Nucleic acids research* **7**, 1513–1523.

Blasi, F., Tarsia, P. and Aliberti, S. (2009). Chlamydophila pneumoniae. *Clinical microbiology and infection : the official publication of the European Society of Clinical Microbiology and Infectious Diseases* **15**, 29–35.

Bois, P. R. J., O'Hara, B. P., Nietlispach, D., Kirkpatrick, J. and Izard, T. (2006). The vinculin binding sites of talin and alpha-actinin are sufficient to activate vinculin. *Journal of Biological Chemistry* **281**, 7228–7236.

Braun, C. (2015). Der Einfluss von Effektorproteinen aus Chlamydia pneumoniae auf s eukaryotische Mikrotubuli- und Aktinzytoskelett.

Brouhard, G. J., Stear, J. H., Noetzel, T. L., Al-Bassam, J., Kinoshita, K., Harrison, S. C., Howard, J. and Hyman, A. A. (2008). XMAP215 is a processive microtubule polymerase. *Cell* **132**, 79–88.

Browning, H., Hayles, J., Mata, J., Aveline, L., Nurse, P. and McIntosh, J. R. (2000). Tea2p is a kinesin-like protein required to generate polarized growth in fission yeast. *The Journal of Cell Biology* **151**, 15–28.

Browning, H. and Hackney, D. D. (2005). The EB1 homolog Mal3 stimulates the ATPase of the kinesin Tea2 by recruiting it to the microtubule. *The Journal of biological chemistry* **280**, 12299–12304.

Brunner, D. and Nurse, P. (2000). CLIP170-like tip1p Spatially Organizes Microtubular Dynamics in Fission Yeast. *Cell* **102**, 695–704.

Bryan, L., Clynes, M. and Meleady, P. (2021). The emerging role of cellular post-translational modifications in modulating growth and productivity of recombinant Chinese hamster ovary cells. *Biotechnology advances* **49**, 107757.

Burton, M. J. (2007). Trachoma: an overview. *British medical bulletin* **84**, 99–116.

Busch, K. E., Hayles, J., Nurse, P. and Brunner, D. (2004). Tea2p kinesin is involved in spatial microtubule organization by transporting tip1p on microtubules. *Developmental cell* **6**, 831–843.

Busch, K. E. and Brunner, D. (2004). The microtubule plus end-tracking proteins mal3p and tip1p cooperate for cell-end targeting of interphase microtubules. *Current Biology* **14**, 548–559.

Carabeo, R. A., Grieshaber, S. S., Fischer, E. and Hackstadt, T. (2002). Chlamydia trachomatis induces remodeling of the actin cytoskeleton during attachment and entry into HeLa cells. *Infection and immunity* **70**, 3793–3803.

Chang-Jie, J. and Sonobe, S. (1993). Identification and preliminary characterization of a 65 kDa higher-plant microtubule-associated protein. *Journal of cell science* **105 (Pt 4)**, 891–901.

Chaturvedi, A. K., Gaydos, C. A., Agreda, P., Holden, J. P., Chatterjee, N., Goedert, J. J., Caporaso, N. E. and Engels, E. A. (2010). Chlamydia pneumoniae infection and risk for lung cancer. *Cancer epidemiology, biomarkers & prevention : a publication of the American Association for Cancer Research, cosponsored by the American Society of Preventive Oncology* **19**, 1498–1505.

Chi, E. Y., Kuo, C. C. and Grayston, J. T. (1987). Unique ultrastructure in the elementary body of Chlamydia sp. strain TWAR. *Journal of bacteriology* **169**, 3757–3763.

Chu, D.-J., Guo, S.-G., Pan, C.-F., Wang, J., Du, Y., Lu, X.-F. and Yu, Z.-Y. (2012). An experimental model for induction of lung cancer in rats by Chlamydia pneumoniae. *Asian Pacific journal of cancer prevention : APJCP* **13**, 2819–2822.

Clausen, J. D., Christiansen, G., Holst, H. U. and Birkelund, S. (1997). Chlamydia trachomatis utilizes the host cell microtubule network during early events of infection. *Molecular microbiology* **25**, 441–449.

Clifton, D. R., Fields, K. A., Grieshaber, S. S., Dooley, C. A., Fischer, E. R., Mead, D. J., Carabeo, R. A. and Hackstadt, T. (2004). A chlamydial type III translocated protein is tyrosine-phosphorylated at the site of entry and associated with recruitment of actin. *Proceedings of the National Academy of Sciences of the United States of America* **101**, 10166–10171.

Clifton, D. R., Dooley, C. A., Grieshaber, S. S., Carabeo, R. A., Fields, K. A. and Hackstadt, T. (2005). Tyrosine phosphorylation of the chlamydial effector protein Tarp is species specific and not required for recruitment of actin. *Infection and immunity* **73**, 3860–3868.

Coombes, B. K. and Mahony, J. B. (2002). Identification of MEK- and phosphoinositide 3-kinase-dependent signalling as essential events during Chlamydia pneumoniae invasion of HEp2 cells. *Cellular microbiology* **4**, 447–460.

Cooper, G. M. (2000). *The cell. A molecular approach*. Washington, D.C., Sunderland, Mass.: ASM Press.

Crivat, G. and Taraska, J. W. (2012). Imaging proteins inside cells with fluorescent tags. *Trends in biotechnology* **30**, 8–16.

Darville, T. and Hiltke, T. J. (2010). Pathogenesis of genital tract disease due to Chlamydia trachomatis. *The Journal of infectious diseases* **201 Suppl 2**, S114-25.

Dehoux, P., Flores, R., Dauga, C., Zhong, G. and Subtil, A. (2011). Multi-genome identification and characterization of chlamydiae-specific type III secretion substrates: the Inc proteins. *BMC genomics* **12**, 109.

Delevoye, C., Nilges, M., Dautry-Varsat, A. and Subtil, A. (2004). Conservation of the biochemical properties of IncA from Chlamydia trachomatis and Chlamydia caviae: oligomerization of IncA mediates interaction between facing membranes. *The Journal of biological chemistry* **279**, 46896–46906.

Delevoye, C., Nilges, M., Dehoux, P., Paumet, F., Perrinet, S., Dautry-Varsat, A. and Subtil, A. (2008). SNARE protein mimicry by an intracellular bacterium. *PLoS Pathogens* **4**, e1000022.

Derré, I., Swiss, R. and Agaisse, H. (2011). The lipid transfer protein CERT interacts with the Chlamydia inclusion protein IncD and participates to ER-Chlamydia inclusion membrane contact sites. *PLoS Pathogens* **7**, e1002092.

Des Georges, A., Katsuki, M., Drummond, D. R., Osei, M., Cross, R. A. and Amos, L. A. (2008). Mal3, the Schizosaccharomyces pombe homolog of EB1, changes the microtubule lattice. *Nature structural & molecular biology* **15**, 1102–1108.

Desai, A. and Mitchison, T. J. (1997). Microtubule polymerization dynamics. *Annual review of cell and developmental biology* **13**, 83–117.

Didry, D., Carlier, M. F. and Pantaloni, D. (1998). Synergy between actin depolymerizing factor/cofilin and profilin in increasing actin filament turnover. *Journal of Biological Chemistry* **273**, 25602–25611.

Dogterom, M., Kerssemakers, J. W. J., Romet-Lemonne, G. and Janson, M. E. (2005). Force generation by dynamic microtubules. *Current opinion in cell biology* **17**, 67–74.

Drechsel, D. N. and Kirschner, M. W. (1994). The minimum GTP cap required to stabilize microtubules. *Current Biology* **4**, 1053–1061.

Drubin, D. G. and Nelson, W. (1996). Origins of Cell Polarity. *Cell* **84**, 335–344.

Drummond, D. R. and Cross, R. A. (2000). Dynamics of interphase microtubules in Schizosaccharomyces pombe. *Current Biology* **10**, 766–775.

Dumoux, M., Menny, A., Delacour, D. and Hayward, R. D. (2015). A Chlamydia effector recruits CEP170 to reprogram host microtubule organization. *Journal of cell science* **128**, 3420–3434.

Egelman, E. H., Francis, N. and DeRosier, D. J. (1982). F-actin is a helix with a random variable twist. *Nature* **298**, 131–135.

Elwell, C., Mirrashidi, K. and Engel, J. (2016). Chlamydia cell biology and pathogenesis. *Nature reviews. Microbiology* **14**, 385–400.

Elwell, C. A., Czudnochowski, N., Dollen, J. von, Johnson, J. R., Nakagawa, R., Mirrashidi, K., Krogan, N. J., Engel, J. N. and Rosenberg, O. S. (2017). Chlamydia interfere with an interaction between the mannose-6-phosphate receptor and sorting nexins to counteract host restriction. *eLife*. https://doi.org/10.7554/eLife.22709.

Entian, K. D., Schuster, T., Hegemann, J. H., Becher, D., Feldmann, H., Güldener, U., Götz, R., Hansen, M., Hollenberg, C. P., Jansen, G. et al. (1999). Functional analysis of 150 deletion mutants in Saccharomyces cerevisiae by a systematic approach. *Molecular & general genetics : MGG* **262**, 683–702.

Erent, M., Drummond, D. R. and Cross, R. A. (2012). S. pombe kinesins-8 promote both nucleation and catastrophe of microtubules. *PloS one* **7**, e30738.

Fadel, S. and Eley, A. (2008). Differential glycosaminoglycan binding of Chlamydia trachomatis OmcB protein from serovars E and LGV. *Journal of medical microbiology* **57**, 1058–1061.

Faris, R., Andersen, S. E., McCullough, A., Gourronc, F., Klingelhutz, A. J. and Weber, M. M. (2019). Chlamydia trachomatis Serovars Drive Differential Production of Proinflammatory Cytokines and Chemokines Depending on the Type of Cell Infected. *Frontiers in cellular and infection microbiology* **9**, 399.

Fattinger, S. A., Sellin, M. E. and Hardt, W.-D. (2021). Salmonella effector driven invasion of the gut epithelium: breaking in and setting the house on fire. *Current opinion in microbiology* **64**, 9–18.

Fechtner, T., Stallmann, S., Moelleken, K., Meyer, K. L. and Hegemann, J. H. (2013). Characterization of the interaction between the chlamydial adhesin OmcB and the human host cell. *Journal of bacteriology* **195**, 5323–5333.

Fechtner, T., Galle, J. N. and Hegemann, J. H. (2016). The novel chlamydial adhesin CPn0473 mediates the lipid raft-dependent uptake of Chlamydia pneumoniae. *Cellular microbiology* **18**, 1094–1105.

Feher, V. A., Randall, A., Baldi, P., Bush, R. M., La Maza, L. M. de and Amaro, R. E. (2013). A 3-dimensional trimeric β-barrel model for Chlamydia MOMP contains conserved and novel elements of Gram-negative bacterial porins. *PloS one* **8**, e68934.

Fields, K. A. and Hackstadt, T. (2000). Evidence for the secretion of Chlamydia trachomatis CopN by a type III secretion mechanism. *Molecular microbiology* **38**, 1048–1060.

Flores, R., Luo, J., Chen, D., Sturgeon, G., Shivshankar, P., Zhong, Y. and Zhong, G. (2007). Characterization of the hypothetical protein Cpn1027, a newly identified inclusion membrane protein unique to Chlamydia pneumoniae. *Microbiology (Reading, England)* **153**, 777–786.

Flores, R. and Zhong, G. (2015). The Chlamydia pneumoniae Inclusion Membrane Protein Cpn1027 Interacts with Host Cell Wnt Signaling Pathway Regulator Cytoplasmic Activation/Proliferation-Associated Protein 2 (Caprin2). *PloS one* **10**, e0127909.

Forsburg, S. L. and Rhind, N. (2006). Basic methods for fission yeast. *Yeast* **23**, 173–183.

Friebel, A., Ilchmann, H., Aepfelbacher, M., Ehrbar, K., Machleidt, W. and Hardt, W. D. (2001). SopE and SopE2 from Salmonella typhimurium activate different sets of RhoGTPases of the host cell. *Journal of Biological Chemistry* **276**, 34035–34040.

Friis, R. R. (1972). Interaction of L cells and Chlamydia psittaci: entry of the parasite and host responses to its development. *Journal of bacteriology* **110**, 706–721.

Galjart, N. (2010). Plus-end-tracking proteins and their interactions at microtubule ends. *Current biology : CB* **20**, R528-37.

Galle, J. N., Fechtner, T., Eierhoff, T., Römer, W. and Hegemann, J. H. (2019). A Chlamydia pneumoniae adhesin induces phosphatidylserine exposure on host cells. *Nat Commun* **10**, 4644.

Gauliard, E., Ouellette, S. P., Rueden, K. J. and Ladant, D. (2015). Characterization of interactions between inclusion membrane proteins from Chlamydia trachomatis. *Frontiers in cellular and infection microbiology* **5**, 13.

Gietz, R. D. and Woods, R. A. (2006). Yeast Transformation by the LiAc/SS Carrier DNA/PEG Method.

In *Yeast Protocol* (ed. W. Xiao), pp. 107–120. Totowa, NJ: Humana Press Inc.

Glotfelty, L. G. and Hecht, G. A. (2012). Enteropathogenic E. coli effectors EspG1/G2 disrupt tight junctions: new roles and mechanisms. *Annals of the New York Academy of Sciences* **1258**, 149–158.

Golub, E. I. (1988). 'One minute' transformation of competent E. coli by plasmid DNA. *Nucleic acids research* **16**, 1641.

Grayston, J. T., Aldous, M. B., Easton, A., Wang, S. P., Kuo, C. C., Campbell, L. A. and Altman, J. (1993). Evidence that Chlamydia pneumoniae causes pneumonia and bronchitis. *The Journal of infectious diseases* **168**, 1231–1235.

Grayston, J. T. and Campbell, L. A. (1999). The role of Chlamydia pneumoniae in atherosclerosis. *Clinical infectious diseases : an official publication of the Infectious Diseases Society of America* **28**, 993–994.

Greenfield, J. J. and High, S. (1999). The Sec61 complex is located in both the ER and the ER-Golgi intermediate compartment. *Journal of cell science* **112 (Pt 10)**, 1477–1486.

Grieshaber, S. S., Grieshaber, N. A. and Hackstadt, T. (2003). Chlamydia trachomatis uses host cell dynein to traffic to the microtubule-organizing center in a p50 dynamitin-independent process. *Journal of cell science* **116**, 3793–3802.

Gruenbaum, Y. and Aebi, U. (2014). Intermediate filaments: a dynamic network that controls cell mechanics. *F1000prime reports* **6**, 54.

Hackstadt, T., Todd, W. J. and Caldwell, H. D. (1985). Disulfide-mediated interactions of the chlamydial major outer membrane protein: role in the differentiation of chlamydiae? *Journal of bacteriology* **161**, 25–31.

Hackstadt, T., Scidmore-Carlson, M. A., Shaw, E. I. and Fischer, E. R. (1999). The Chlamydia trachomatis IncA protein is required for homotypic vesicle fusion. *Cellular microbiology* **1**, 119–130.

Haglund, C. M. and Welch, M. D. (2011). Pathogens and polymers: microbe-host interactions illuminate the cytoskeleton. *The Journal of Cell Biology* **195**, 7–17.

Hahn, D. L., Dodge, R. W. and Golubjatnikov, R. (1991). Association of Chlamydia pneumoniae (strain TWAR) infection with wheezing, asthmatic bronchitis, and adult-onset asthma. *JAMA* **266**, 225–230.

Hahn, D. L., Azenabor, A. A., Beatty, W. L. and Byrne, G. I. (2002). Chlamydia pneumoniae as a respiratory pathogen. *Frontiers in bioscience : a journal and virtual library* **7**, e66-76.

Hammerschlag, M. R. (2002). The intracellular life of chlamydiae. *Seminars in pediatric infectious diseases* **13**, 239–248.

Hänisch, J., Ehinger, J., Ladwein, M., Rohde, M., Derivery, E., Bosse, T., Steffen, A., Bumann, D., Misselwitz, B., Hardt, W.-D. et al. (2010). Molecular dissection of Salmonella-induced membrane ruffling versus invasion. *Cellular microbiology* **12**, 84–98.

Hänisch, J., Kölm, R., Wozniczka, M., Bumann, D., Rottner, K. and Stradal, T. E. B. (2011). Activation of a RhoA/myosin II-dependent but Arp2/3 complex-independent pathway facilitates Salmonella invasion. *Cell host & microbe* **9**, 273–285.

Hatch, T. P. (1996). Disulfide cross-linked envelope proteins: the functional equivalent of peptidoglycan in chlamydiae? *Journal of bacteriology* **178**, 1–5.

Hayward, R. D. and Koronakis, V. (1999). Direct nucleation and bundling of actin by the SipC protein of invasive Salmonella. *The EMBO journal* **18**, 4926–4934.

Herbst (2011). Identifizierung und Charakterisierung potentieller neuer Effektorproteine aus Chlamydia pneumoniae. *Dissertation*.

Herrmann, H., Kreplak, L. and Aebi, U. (2004). Isolation, Characterization, and In Vitro Assembly of Intermediate Filaments. In *Intermediate filament cytoskeleton* (ed. M. B. Omary and P. A. Coulombe), pp. 3–24. Amsterdam: Elsevier Acad. Press.

Herrmann, H., Bär, H., Kreplak, L., Strelkov, S. V. and Aebi, U. (2007). Intermediate filaments: from cell architecture to nanomechanics. *Nature reviews. Molecular cell biology* **8**, 562–573.

Higashitsuji, Y., Herrero, S., Takeshita, N. and Fischer, R. (2009). The cell end marker protein TeaC is involved in growth directionality and septation in Aspergillus nidulans. *Eukaryotic cell* **8**, 957–967.

Hiraoka, Y., Toda, T. and Yanagida, M. (1984). The NDA3 gene of fission yeast encodes β-tubulin: A cold-sensitive nda3 mutation reversibly blocks spindle formation and chromosome movement in mitosis. *Cell* **39**, 349–358.

Hirokawa, N. (1998). Kinesin and dynein superfamily proteins and the mechanism of organelle transport. *Science (New York, N.Y.)* **279**, 519–526.

Holmes, K. C., Popp, D., Gebhard, W. and Kabsch, W. (1990). Atomic model of the actin filament. *Nature* **347**, 44–49.

Horio, T. and Murata, T. (2014). The role of dynamic instability in microtubule organization. *Frontiers in plant science* **5**, 511.

Howard, J. and Hyman, A. A. (2007). Microtubule polymerases and depolymerases. *Current opinion in cell biology* **19**, 31–35.

Howard, J. and Hyman, A. A. (2009). Growth, fluctuation and switching at microtubule plus ends. *Nature reviews. Molecular cell biology* **10**, 569–574.

Hua-Feng, X., Yue-Ming, W., Hong, L. and Junyi, D. (2015). A meta-analysis of the association between Chlamydia pneumoniae infection and lung cancer risk. *Indian journal of cancer* **52 Suppl 2**, e112-5.

Huang, J., Lesser, C. F. and Lory, S. (2008). The essential role of the CopN protein in Chlamydia pneumoniae intracellular growth. *Nature* **456**, 112–115.

Huisman, E. M., van Dillen, T., Onck, P. R. and van der Giessen, E. (2007). Three-dimensional cross-linked F-actin networks: relation between network architecture and mechanical behavior. *Physical review letters* **99**, 208103.

Hume, P. J., Singh, V., Davidson, A. C. and Koronakis, V. (2017). Swiss Army Pathogen: The Salmonella Entry Toolkit. *Frontiers in cellular and infection microbiology* **7**, 348.

Hybiske, K. and Stephens, R. S. (2007a). Mechanisms of Chlamydia trachomatis entry into nonphagocytic cells. *Infection and immunity* **75**, 3925–3934.

Hybiske, K. and Stephens, R. S. (2007b). Mechanisms of host cell exit by the intracellular bacterium Chlamydia. *Proceedings of the National Academy of Sciences of the United States of America* **104**, 11430–11435.

Ichihara, K., Kitazawa, H., Iguchi, Y., Hotani, H. and Itoh, T. J. (2001). Visualization of the stop of microtubule depolymerization that occurs at the high-density region of microtubule-associated protein 2 (MAP2). *Journal of Molecular Biology* **312**, 107–118.

Jantos, C. A., Heck, S., Roggendorf, R., Sen-Gupta, M. and Hegemann, J. H. (1997). Antigenic and molecular analyses of different Chlamydia pneumoniae strains. *J Clin Microbiol* **35**, 620–623.

Janulevicius, A., van Pelt, J. and van Ooyen, A. (2006). Compartment volume influences microtubule dynamic instability: a model study. *Biophysical Journal* **90**, 788–798.

Jewett, T. J., Fischer, E. R., Mead, D. J. and Hackstadt, T. (2006). Chlamydial TARP is a bacterial nucleator of actin. *Proc Natl Acad Sci USA* **103**, 15599–15604.

Kabsch, W. and Vandekerckhove, J. (1992). Structure and function of actin. *Annual review of biophysics and biomolecular structure* **21**, 49–76.

Kaiser, C., Michaelis, S. and Mitchell, A. (1994). *Methods in yeast genetics. A Cold Spring Harbor Laboratory course manual*. Plainview N.Y: Cold Spring Harbor Laboratory Press.

Katsuki, M., Drummond, D. R., Osei, M. and Cross, R. A. (2009). Mal3 masks catastrophe events in Schizosaccharomyces pombe microtubules by inhibiting shrinkage and promoting rescue. *The Journal of biological chemistry* **284**, 29246–29250.

Kaul, R., Hoang, A., Yau, P., Bradbury, E. M. and Wenman, W. M. (1997). The chlamydial EUO gene

encodes a histone H1-specific protease. *Journal of bacteriology* **179**, 5928–5934.

Kirmse, R., Portet, S., Mücke, N., Aebi, U., Herrmann, H. and Langowski, J. (2007). A quantitative kinetic model for the in vitro assembly of intermediate filaments from tetrameric vimentin. *Journal of Biological Chemistry* **282**, 18563–18572.

Kokes, M., Dunn, J. D., Granek, J. A., Nguyen, B. D., Barker, J. R., Valdivia, R. H. and Bastidas, R. J. (2015). Integrating chemical mutagenesis and whole-genome sequencing as a platform for forward and reverse genetic analysis of Chlamydia. *Cell host & microbe* **17**, 716–725.

Korhonen, J. T., Puolakkainen, M., Häivälä, R., Penttilä, T., Haveri, A., Markkula, E. and Lahesmaa, R. (2012). Flotillin-1 (Reggie-2) contributes to Chlamydia pneumoniae growth and is associated with bacterial inclusion. *Infection and immunity* **80**, 1072–1078.

Kumar, Y. and Valdivia, R. H. (2008). Actin and intermediate filaments stabilize the Chlamydia trachomatis vacuole by forming dynamic structural scaffolds. *Cell host & microbe* **4**, 159–169.

Kuo, C. C., Jackson, L. A., Campbell, L. A. and Grayston, J. T. (1995). Chlamydia pneumoniae (TWAR). *Clinical microbiology reviews* **8**, 451–461.

La Carbona, S., Le Goff, C. and Le Goff, X. (2006). Fission yeast cytoskeletons and cell polarity factors: connecting at the cortex. *Biology of the Cell* **98**, 619–631.

Lawson, J. L. D. and Carazo Salas, R. E. (2013). Microtubules: greater than the sum of the parts. *Biochemical Society transactions* **41**, 1736–1744.

Lev, S., Ben Halevy, D., Peretti, D. and Dahan, N. (2008). The VAP protein family: from cellular functions to motor neuron disease. *Trends in Cell Biology* **18**, 282–290.

Luo, J., Liu, G., Zhong, Y., Jia, T., Liu, K., Chen, D. and Zhong, G. (2007). Characterization of hypothetical proteins Cpn0146, 0147, 0284 & 0285 that are predicted to be in the Chlamydia pneumoniae inclusion membrane. *BMC microbiology* **7**, 38.

Lutter, E. I., Martens, C. and Hackstadt, T. (2012). Evolution and conservation of predicted inclusion membrane proteins in chlamydiae. *Comparative and functional genomics* **2012**, 362104.

Mandelkow, E. M., Schultheiss, R., Rapp, R., Müller, M. and Mandelkow, E. (1986). On the surface lattice of microtubules: helix starts, protofilament number, seam, and handedness. *The Journal of Cell Biology* **102**, 1067–1073.

Marinus, M. G. (1973). Location of DNA methylation genes on the Escherichia coli K-12 genetic map. *Molecular & general genetics : MGG* **127**, 47–55.

Martin, B. R., Giepmans, B. N. G., Adams, S. R. and Tsien, R. Y. (2005). Mammalian cell-based optimization of the biarsenical-binding tetracysteine motif for improved fluorescence and affinity. *Nature biotechnology* **23**, 1308–1314.

Martin, S. G. (2009). Microtubule-dependent cell morphogenesis in the fission yeast. *Trends in Cell Biology* **19**, 447–454.

Mata, J. and Nurse, P. (1997). tea1 and the Microtubular Cytoskeleton Are Important for Generating Global Spatial Order within the Fission Yeast Cell. *Cell* **89**, 939–949.

Matsumoto, A. and Manire, G. P. (1970). Electron Microscopic Observations on the Fine Structure of Cell Walls of Chlamydia psittaci. *Journal of bacteriology* **104**, 1332–1337.

Matsuyama, A., Shirai, A. and Yoshida, M. (2018). Preparation of Cell Lysates of Fission Yeast for Immunoprecipitation. In *Schizosaccharomyces pombe. Methods and protocols* (ed. T. L. Singleton), pp. 125–133. New York: Humana Press.

Mäurer, A. P., Mehlitz, A., Mollenkopf, H. J. and Meyer, T. F. (2007). Gene expression profiles of Chlamydophila pneumoniae during the developmental cycle and iron depletion-mediated persistence. *PLoS Pathogens* **3**, e83.

McGhie, E. J., Hayward, R. D. and Koronakis, V. (2001). Cooperation between actin-binding proteins of invasive Salmonella: SipA potentiates SipC nucleation and bundling of actin. *The EMBO journal* **20**, 2131–2139.

McGhie, E. J., Hayward, R. D. and Koronakis, V. (2004). Control of Actin Turnover by a Salmonella

Invasion Protein. *Molecular Cell* **13**, 497–510.

Meadows, J. C., Messin, L. J., Kamnev, A., Lancaster, T. C., Balasubramanian, M. K., Cross, R. A. and Millar, J. B. (2018). Opposing kinesin complexes queue at plus tips to ensure microtubule catastrophe at cell ends. *EMBO reports*. https://doi.org/10.15252/embr.201846196.

Michaels, T. C., Feng, S., Liang, H. and Mahadevan, L. (2020). Mechanics and kinetics of dynamic instability. *eLife*. https://doi.org/10.7554/eLife.54077.

Mimori-Kiyosue, Y., Shiina, N. and Tsukita, S. (2000). The dynamic behavior of the APC-binding protein EB1 on the distal ends of microtubules. *Current Biology* **10**, 865–868.

Minagawa, M., Shirato, M., Toya, M. and Sato, M. (2021). Dual Impact of a Benzimidazole Resistant β-Tubulin on Microtubule Behavior in Fission Yeast. *Cells*. https://doi.org/10.3390/cells10051042.

Mirrashidi, K. M., Elwell, C. A., Verschueren, E., Johnson, J. R., Frando, A., Dollen, J. von, Rosenberg, O., Gulbahce, N., Jang, G., Johnson, T. et al. (2015). Global Mapping of the Inc-Human Interactome Reveals that Retromer Restricts Chlamydia Infection. *Cell host & microbe* **18**, 109–121.

Mital, J., Miller, N. J., Fischer, E. R. and Hackstadt, T. (2010). Specific chlamydial inclusion membrane proteins associate with active Src family kinases in microdomains that interact with the host microtubule network. *Cellular microbiology* **12**, 1235–1249.

Mital, J., Miller, N. J., Dorward, D. W., Dooley, C. A. and Hackstadt, T. (2013). Role for chlamydial inclusion membrane proteins in inclusion membrane structure and biogenesis. *PloS one* **8**, e63426.

Mital, J., Lutter, E. I., Barger, A. C., Dooley, C. A. and Hackstadt, T. (2015). Chlamydia trachomatis inclusion membrane protein CT850 interacts with the dynein light chain DYNLT1 (Tctex1). *Biochemical and biophysical research communications* **462**, 165–170.

Mitchison, T. and Kirschner, M. (1984). Dynamic instability of microtubule growth. *Nature* **312**, 237–242.

Mitchison, T. J. (1993). Localization of an exchangeable GTP binding site at the plus end of microtubules. *Science (New York, N.Y.)* **261**, 1044–1047.

Moelleken, K. and Hegemann, J. H. (2008). The Chlamydia outer membrane protein OmcB is required for adhesion and exhibits biovar-specific differences in glycosaminoglycan binding. *Molecular microbiology* **67**, 403–419.

Mölleken, K., Schmidt, E. and Hegemann, J. H. (2010). Members of the Pmp protein family of Chlamydia pneumoniae mediate adhesion to human cells via short repetitive peptide motifs. *Molecular microbiology* **78**, 1004–1017.

Mölleken, K., Becker, E. and Hegemann, J. H. (2013). The Chlamydia pneumoniae invasin protein Pmp21 recruits the EGF receptor for host cell entry. *PLoS Pathogens* **9**, e1003325.

Moreno, S., Klar, A. and Nurse, P. (1991). [56] Molecular genetic analysis of fission yeast Schizosaccharomyces pombe. In *Guide to yeast genetics and molecular biology* (ed. C. Guthrie), pp. 795–823. San Diego, Calif. [u.a.]: Acad. Press.

Moulder, J. W. (1991). Interaction of chlamydiae and host cells in vitro. *Microbiological reviews* **55**, 143–190.

Myers, G. S. A., Mathews, S. A., Eppinger, M., Mitchell, C., O'Brien, K. K., White, O. R., Benahmed, F., Brunham, R. C., Read, T. D., Ravel, J. et al. (2009). Evidence that human Chlamydia pneumoniae was zoonotically acquired. *Journal of bacteriology* **191**, 7225–7233.

Nawrotek, A., Guimarães, B. G., Velours, C., Subtil, A., Knossow, M. and Gigant, B. (2014). Biochemical and structural insights into microtubule perturbation by CopN from Chlamydia pneumoniae. *The Journal of biological chemistry* **289**, 25199–25210.

Nguyen, P. H., Lutter, E. I. and Hackstadt, T. (2018). Chlamydia trachomatis inclusion membrane protein MrcA interacts with the inositol 1,4,5-trisphosphate receptor type 3 (ITPR3) to regulate extrusion formation. *PLoS Pathogens* **14**, e1006911.

Nicholson, T. L., Olinger, L., Chong, K., Schoolnik, G. and Stephens, R. S. (2003). Global stage-specific gene regulation during the developmental cycle of Chlamydia trachomatis. *Journal of bacteriology* **185**, 3179–3189.

Noël, L., Thieme, F., Nennstiel, D. and Bonas, U. (2002). Two novel type III-secreted proteins of Xanthomonas campestris pv. vesicatoria are encoded within the hrp pathogenicity island. *Journal of bacteriology* **184**, 1340–1348.

Nogales, E., Downing, K. H., Amos, L. A. and Löwe, J. (1998). Tubulin and FtsZ form a distinct family of GTPases. *Nature structural biology* **5**, 451–458.

Nölke, T., Schwan, C., Lehmann, F., Østevold, K., Pertz, O. and Aktories, K. (2016). Septins guide microtubule protrusions induced by actin-depolymerizing toxins like Clostridium difficile transferase (CDT). *Proc Natl Acad Sci USA* **113**, 7870–7875.

Nunes, A. and Gomes, J. P. (2014). Evolution, phylogeny, and molecular epidemiology of Chlamydia. *Infection, genetics and evolution : journal of molecular epidemiology and evolutionary genetics in infectious diseases* **23**, 49–64.

Okazaki, K., Okazaki, N., Kume, K., Jinno, S., Tanaka, K. and Okayama, H. (1990). High-frequency transformation method and library transducing vectors for cloning mammalian cDNAs by trans-complementation of Schizosaccharomyces pombe. *Nucleic acids research* **18**, 6485–6489.

Parnaik, V. K. (2011). Role of Nuclear Lamins in Nuclear Organization, Cellular Signaling, and Inherited Diseases. In *International Review of Cell and Molecular Biology* (ed. K. W. Jeon), pp. 157–206. Burlington: Elsevier Science.

Peeling, R. W. and Brunham, R. C. (1996). Chlamydiae as pathogens: new species and new issues. *Emerging infectious diseases* **2**, 307–319.

Perez, F., Diamantopoulos, G. S., Stalder, R. and Kreis, T. E. (1999). CLIP-170 Highlights Growing Microtubule Ends In Vivo. *Cell* **96**, 517–527.

Phelps, C. C., Vadia, S., Arnett, E., Tan, Y., Zhang, X., Pathak-Sharma, S., Gavrilin, M. A. and Seveau, S. (2018). Relative Roles of Listeriolysin O, InlA, and InlB in Listeria monocytogenes Uptake by Host Cells. *Infection and immunity*. https://doi.org/10.1128/IAI.00555-18.

Pöhlmann, J., Risse, C., Seidel, C., Pohlmann, T., Jakopec, V., Walla, E., Ramrath, P., Takeshita, N., Baumann, S., Feldbrügge, M. et al. (2014). The Vip1 inositol polyphosphate kinase family regulates polarized growth and modulates the microtubule cytoskeleton in fungi. *PLoS genetics* **10**, e1004586.

Pollard, T. D., Blanchoin, L. and Mullins, R. D. (2000). Molecular mechanisms controlling actin filament dynamics in nonmuscle cells. *Annual review of biophysics and biomolecular structure* **29**, 545–576.

Pollard, T. D. and Cooper, J. A. (2009). Actin, a central player in cell shape and movement. *Science (New York, N.Y.)* **326**, 1208–1212.

Popa, C., Coll, N. S., Valls, M. and Sessa, G. (2016). Yeast as a Heterologous Model System to Uncover Type III Effector Function. *PLoS Pathogens* **12**, e1005360.

Puolakkainen, M., Kuo, C.-C. and Campbell, L. A. (2005). Chlamydia pneumoniae uses the mannose 6-phosphate/insulin-like growth factor 2 receptor for infection of endothelial cells. *Infection and immunity* **73**, 4620–4625.

Radhakrishnan, G. K., Harms, J. S. and Splitter, G. A. (2011). Modulation of microtubule dynamics by a TIR domain protein from the intracellular pathogen Brucella melitensis. *The Biochemical journal* **439**, 79–83.

Rajalingam, K., Al-Younes, H., Müller, A., Meyer, T. F., Szczepek, A. J. and Rudel, T. (2001). Epithelial cells infected with Chlamydophila pneumoniae (Chlamydia pneumoniae) are resistant to apoptosis. *Infection and immunity* **69**, 7880–7888.

Ramirez, J. A. (1996). Isolation of Chlamydia pneumoniae from the coronary artery of a patient with coronary atherosclerosis. The Chlamydia pneumoniae/Atherosclerosis Study Group. *Annals of*

internal medicine **125**, 979–982.

Rashidi, B. H., Chamani-Tabriz, L., Haghollahi, F., Jeddi-Tehrani, M., Naghizadeh, M. M., Shariat, M., Akhondi, M. M., Bagheri, R., Asgari, S. and Wylie, K. (2013). Effects of Chlamydia trachomatis Infection on Fertility; A Case-Control Study. *Journal of Reproduction & Infertility* **14**, 67–72.

Redgrove, K. A. and McLaughlin, E. A. (2014). The Role of the Immune Response in Chlamydia trachomatis Infection of the Male Genital Tract: A Double-Edged Sword. *Frontiers in immunology* **5**, 534.

Rejman Lipinski, A., Heymann, J., Meissner, C., Karlas, A., Brinkmann, V., Meyer, T. F. and Heuer, D. (2009). Rab6 and Rab11 regulate Chlamydia trachomatis development and golgin-84-dependent Golgi fragmentation. *PLoS Pathogens* **5**, e1000615.

Resnikoff, S., Pascolini, D., Etya'ale, D., Kocur, I., Pararajasegaram, R., Pokharel, G. P. and Mariotti, S. P. (2004). Global data on visual impairment in the year 2002. *Bulletin of the World Health Organization* **82**, 844–851.

Richards, T. S., Knowlton, A. E. and Grieshaber, S. S. (2013). Chlamydia trachomatis homotypic inclusion fusion is promoted by host microtubule trafficking. *BMC microbiology* **13**, 185.

Rockey, D. D., Scidmore, M. A., Bannantine, J. P. and Brown, W. J. (2002). Proteins in the chlamydial inclusion membrane. *Microbes and Infection* **4**, 333–340.

Roll-Mecak, A. and McNally, F. J. (2010). Microtubule-severing enzymes. *Current opinion in cell biology* **22**, 96–103.

Roulis, E., Polkinghorne, A. and Timms, P. (2013). Chlamydia pneumoniae: modern insights into an ancient pathogen. *Trends in microbiology* **21**, 120–128.

Sambrook, J. and Russell, D. W. (2001). *Molecular cloning. A laboratory manual*. Cold Spring Harbor, N.Y: Cold Spring Harbor Laboratory Press.

Samejima, I., Miller, V. J., Groocock, L. M. and Sawin, K. E. (2008). Two distinct regions of Mto1 are required for normal microtubule nucleation and efficient association with the gamma-tubulin complex in vivo. *Journal of cell science* **121**, 3971–3980.

Sanchez, A. D. and Feldman, J. L. (2017). Microtubule-organizing centers: from the centrosome to non-centrosomal sites. *Current opinion in cell biology* **44**, 93–101.

Sandblad, L., Busch, K. E., Tittmann, P., Gross, H., Brunner, D. and Hoenger, A. (2006). The Schizosaccharomyces pombe EB1 homolog Mal3p binds and stabilizes the microtubule lattice seam. *Cell* **127**, 1415–1424.

Sawin, K. E. and Nurse, P. (1998). Regulation of cell polarity by microtubules in fission yeast. *The Journal of Cell Biology* **142**, 457–471.

Sawin, K. E., Lourenco, P. C. C. and Snaith, H. A. (2004). Microtubule nucleation at non-spindle pole body microtubule-organizing centers requires fission yeast centrosomin-related protein mod20p. *Current Biology* **14**, 763–775.

Sawin, K. E. and Snaith, H. A. (2004). Role of microtubules and tea1p in establishment and maintenance of fission yeast cell polarity. *Journal of cell science* **117**, 689–700.

Sawin, K. E. and Tran, P. T. (2006). Cytoplasmic microtubule organization in fission yeast. *Yeast* **23**, 1001–1014.

Schaeffer, A. and Henrich, B. (2008). Rapid detection of Chlamydia trachomatis and typing of the Lymphogranuloma venereum associated L-Serovars by TaqMan PCR. *BMC infectious diseases* **8**, 56.

Schwan, C., Stecher, B., Tzivelekidis, T., van Ham, M., Rohde, M., Hardt, W.-D., Wehland, J. and Aktories, K. (2009). Clostridium difficile toxin CDT induces formation of microtubule-based protrusions and increases adherence of bacteria. *PLoS Pathogens* **5**, e1000626.

Schwan, C., Kruppke, A. S., Nölke, T., Schumacher, L., Koch-Nolte, F., Kudryashev, M., Stahlberg, H. and Aktories, K. (2014). Clostridium difficile toxin CDT hijacks microtubule organization and reroutes vesicle traffic to increase pathogen adherence. *Proc Natl Acad Sci USA* **111**, 2313–2318.

Scidmore, M. A., Rockey, D. D., Fischer, E. R., Heinzen, R. A. and Hackstadt, T. (1996). Vesicular interactions of the Chlamydia trachomatis inclusion are determined by chlamydial early protein synthesis rather than route of entry. *Infection and immunity* **64**, 5366–5372.

Selve, N. and Wegner, A. (1986). Rate of treadmilling of actin filaments in vitro. *Journal of Molecular Biology* **187**, 627–631.

Seveau, S., Bierne, H., Giroux, S., Prévost, M.-C. and Cossart, P. (2004). Role of lipid rafts in E-cadherin-- and HGF-R/Met--mediated entry of Listeria monocytogenes into host cells. *The Journal of Cell Biology* **166**, 743–753.

Sisko, J. L., Spaeth, K., Kumar, Y. and Valdivia, R. H. (2006). Multifunctional analysis of Chlamydia-specific genes in a yeast expression system. *Molecular microbiology* **60**, 51–66.

Stamm, W. E. (1999). Chlamydia trachomatis infections: progress and problems. *The Journal of infectious diseases* **179 Suppl 2**, S380-3.

Stanhope, R., Flora, E., Bayne, C. and Derré, I. (2017). IncV, a FFAT motif-containing Chlamydia protein, tethers the endoplasmic reticulum to the pathogen-containing vacuole. *Proc Natl Acad Sci USA* **114**, 12039–12044.

Stephens, R. S., Koshiyama, K., Lewis, E. and Kubo, A. (2001). Heparin-binding outer membrane protein of chlamydiae. *Molecular microbiology* **40**, 691–699.

Stratton, C. W. and Wheldon, D. B. (2006). Multiple sclerosis: an infectious syndrome involving Chlamydophila pneumoniae. *Trends in microbiology* **14**, 474–479.

Strelkov, S. V., Herrmann, H. and Aebi, U. (2003). Molecular architecture of intermediate filaments. *BioEssays : news and reviews in molecular, cellular and developmental biology* **25**, 243–251.

Subtil, A., Blocker, A. and Dautry-Varsat, A. (2000). Type III secretion system in Chlamydia species: identified members and candidates. *Microbes and Infection* **2**, 367–369.

Subtil, A., Parsot, C. and Dautry-Varsat, A. (2001). Secretion of predicted Inc proteins of Chlamydia pneumoniae by a heterologous type III machinery. *Molecular microbiology* **39**, 792–800.

Subtil, A., Delevoye, C., Balañá, M.-E., Tastevin, L., Perrinet, S. and Dautry-Varsat, A. (2005). A directed screen for chlamydial proteins secreted by a type III mechanism identifies a translocated protein and numerous other new candidates. *Molecular microbiology* **56**, 1636–1647.

Su, H., Watkins, N. G., Zhang, Y. X. and Caldwell, H. D. (1990). Chlamydia trachomatis-host cell interactions: role of the chlamydial major outer membrane protein as an adhesin. *Infection and immunity* **58**, 1017–1025.

Su, H., Raymond, L., Rockey, D. D., Fischer, E., Hackstadt, T. and Caldwell, H. D. (1996). A recombinant Chlamydia trachomatis major outer membrane protein binds to heparan sulfate receptors on epithelial cells. *Proc Natl Acad Sci USA* **93**, 11143–11148.

Tabbara, K. F. (2001). Trachoma: a review. *Journal of chemotherapy (Florence, Italy)* **13 Suppl 1**, 18–22.

Takahashi, K., Yoshida, H., Hagiwara, T. and Sato, K. (1998). Serovar Distributions of Genital Chlamydia trachomatis in Japanese Women, and Its Correlation with Clinical Symptoms. *Journal of Infection and Chemotherapy* **4**, 32–35.

Takeshita, N., Manck, R., Grün, N., Vega, S. H. de and Fischer, R. (2014). Interdependence of the actin and the microtubule cytoskeleton during fungal growth. *Current opinion in microbiology* **20**, 34–41.

Tatebe, H., Goshima, G., Takeda, K., Nakagawa, T., Kinoshita, K. and Yanagida, M. (2001). Fission yeast living mitosis visualized by GFP-tagged gene products. *Micron* **32**, 67–74.

Tischer, C., Brunner, D. and Dogterom, M. (2009). Force- and kinesin-8-dependent effects in the spatial regulation of fission yeast microtubule dynamics. *Molecular systems biology* **5**, 250.

Tran, P. T., Marsh, L., Doye, V., Inoué, S. and Chang, F. (2001). A mechanism for nuclear positioning in fission yeast based on microtubule pushing. *The Journal of Cell Biology* **153**, 397–411.

Umesono, K., Toda, T., Hayashi, S. and Yanagida, M. (1983). Two cell division cycle genes NDA2 and

NDA3 of the fission yeast Schizosaccharomyces pombe control microtubular organization and sensitivity to anti-mitotic benzimidazole compounds. *Journal of Molecular Biology* **168**, 271–284.

Unsworth, A., Masuda, H., Dhut, S. and Toda, T. (2008). Fission yeast kinesin-8 Klp5 and Klp6 are interdependent for mitotic nuclear retention and required for proper microtubule dynamics. *Molecular Biology of the Cell* **19**, 5104–5115.

van der Vaart, B., Akhmanova, A. and Straube, A. (2009). Regulation of microtubule dynamic instability. *Biochemical Society transactions* **37**, 1007–1013.

van Ooij, C., Homola, E., Kincaid, E. and Engel, J. (1998). Fusion of Chlamydia trachomatis-containing inclusions is inhibited at low temperatures and requires bacterial protein synthesis. *Infection and immunity* **66**, 5364–5371.

Volceanov, L., Herbst, K., Biniossek, M., Schilling, O., Haller, D., Nölke, T., Subbarayal, P., Rudel, T., Zieger, B. and Häcker, G. (2014). Septins arrange F-actin-containing fibers on the Chlamydia trachomatis inclusion and are required for normal release of the inclusion by extrusion. *mBio* **5**, e01802-14.

Walczak, C. E. and Shaw, S. L. (2010). A MAP for bundling microtubules. *Cell* **142**, 364–367.

Walker, G. M. (1982). Cell cycle specificity of certain antimicrotubular drugs in Schizosaccharomyces pombe. *Journal of general microbiology* **128**, 61–71.

Warringer, J., Ericson, E., Fernandez, L., Nerman, O. and Blomberg, A. (2003). High-resolution yeast phenomics resolves different physiological features in the saline response. *Proc Natl Acad Sci USA* **100**, 15724–15729.

Waterman-Storer, C. M., Desai, A., Chloe Bulinski, J. and Salmon, E. D. (1998). Fluorescent speckle microscopy, a method to visualize the dynamics of protein assemblies in living cells. *Current Biology* **8**, 1227-S1.

Weber, M. M., Lam, J. L., Dooley, C. A., Noriea, N. F., Hansen, B. T., Hoyt, F. H., Carmody, A. B., Sturdevant, G. L. and Hackstadt, T. (2017). Absence of Specific Chlamydia trachomatis Inclusion Membrane Proteins Triggers Premature Inclusion Membrane Lysis and Host Cell Death. *Cell reports* **19**, 1406–1417.

Weir, M. L., Xie, H., Klip, A. and Trimble, W. S. (2001). VAP-A binds promiscuously to both v- and tSNAREs. *Biochemical and biophysical research communications* **286**, 616–621.

Wesolowski, J., Weber, M. M., Nawrotek, A., Dooley, C. A., Calderon, M., St Croix, C. M., Hackstadt, T., Cherfils, J. and Paumet, F. (2017). Chlamydia Hijacks ARF GTPases To Coordinate Microtubule Posttranslational Modifications and Golgi Complex Positioning. *mBio*. https://doi.org/10.1128/mBio.02280-16.

Wesolowski, J. and Paumet, F. (2017). Taking control: reorganization of the host cytoskeleton by Chlamydia. *F1000Research* **6**, 2058.

West, R. R., Malmstrom, T., Troxell, C. L. and McIntosh, J. R. (2001). Two related kinesins, klp5+ and klp6+, foster microtubule disassembly and are required for meiosis in fission yeast. *Molecular Biology of the Cell* **12**, 3919–3932.

WHO (2021). Sexually transmitted infections (STIs). https://www.who.int/news-room/fact-sheets/detail/sexually-transmitted-infections-(stis).

Wolf, K., Fischer, E. and Hackstadt, T. (2000). Ultrastructural analysis of developmental events in Chlamydia pneumoniae-infected cells. *Infection and immunity* **68**, 2379–2385.

Wuppermann, F. N., Hegemann, J. H. and Jantos, C. A. (2001). Heparan sulfate-like glycosaminoglycan is a cellular receptor for Chlamydia pneumoniae. *The Journal of infectious diseases* **184**, 181–187.

Xu, X., Nagarajan, H., Lewis, N. E., Pan, S., Cai, Z., Liu, X., Chen, W., Xie, M., Wang, W., Hammond, S. et al. (2011). The genomic sequence of the Chinese hamster ovary (CHO)-K1 cell line. *Nature biotechnology* **29**, 735–741.

Yanagida, M. (2002). The model unicellular eukaryote, Schizosaccharomyces pombe. *Genome Biology*

3, COMMENT2003.

Yu, W., Qiang, L., Solowska, J. M., Karabay, A., Korulu, S. and Baas, P. W. (2008). The microtubule-severing proteins spastin and katanin participate differently in the formation of axonal branches. *Molecular Biology of the Cell* **19**, 1485–1498.

Zhang, D., Vjestica, A. and Oliferenko, S. (2012). Plasma membrane tethering of the cortical ER necessitates its finely reticulated architecture. *Current biology : CB* **22**, 2048–2052.

Zhan, P., Suo, L., Qian, Q., Shen, X., Qiu, L.-X., Yu, L. and Song, Y. (2011). Chlamydia pneumoniae infection and lung cancer risk: a meta-analysis. *European journal of cancer (Oxford, England : 1990)* **47**, 742–747.

Zheng, F., Li, T., Cheung, M., Syrovatkina, V. and Fu, C. (2014). Mcp1p tracks microtubule plus ends to destabilize microtubules at cell tips. *FEBS letters* **588**, 859–865.

Zhou, D. and Galán, J. (2001). Salmonella entry into host cells: the work in concert of type III secreted effector proteins. *Microbes and Infection* **3**, 1293–1298.

Zimmerman, S. and Chang, F. (2005). Effects of {gamma}-tubulin complex proteins on microtubule nucleation and catastrophe in fission yeast. *Molecular Biology of the Cell* **16**, 2719–2733.

Zrieq, R., Braun, C. and Hegemann, J. H. (2017). The Chlamydia pneumoniae Tarp Ortholog CPn0572 Stabilizes Host F-Actin by Displacement of Cofilin. *Frontiers in cellular and infection microbiology* **7**, 511.

7 Appendix

CPn0045	**Position 1708 nt**	**Position 570 aa**
GiD	-	Tyr-Lys-Ser-Gly-Phe-Arg-Val-Stop
This study	**AGAAGAAACA** (10 nt insert)	Tyr-**Arg-Arg-Asn-Lys-Glu-Arg-Phe-Gln-Ser-Leu**
CPn0132	**Position 748 nt**	**Position 250 aa**
GiD	TCT	Leu-Ser-Glu
This study	**G**CT (nt exchange)	Leu-**Ala**-Glu
CPn0150	**Position 3973 nt**	**Position 1325 aa**
GiD	TGC	Asp-Cys-Asp
This study	**A**GC (nt exchange)	Asp-**Ser**-Asp
CPn0132	**Position 133 nt**	**Position 45 aa**
GiD	-	Ala-Glu
This study	**GATGAGATTCAAGAGCTCCCCTC CCCA** (27 nt insert)	Ala-**Asp-Glu-Ile-Gln-Leu-Pro-Ser-Pro**-Glu

Supplementary Table 1: Deviation of sequenced chlamydial genes compared to the *C. pneumoniae* GiD genome.

The nucleotide (nt) sequence of the chlamydial genes was verified using the Sanger sequencing method and compared with the *C. pneumoniae* GiD genome (DNA template). The DNA and amino acid (aa) sequence alterations are highlighted in red. The exchange of nucleotides leads to amino acid exchange while the insertion of nucleotides leads to amino acid insertion or change in the subsequent amino acid sequence. The nucleotide changes were identified from two individual yeast transformants which were cloned separately.

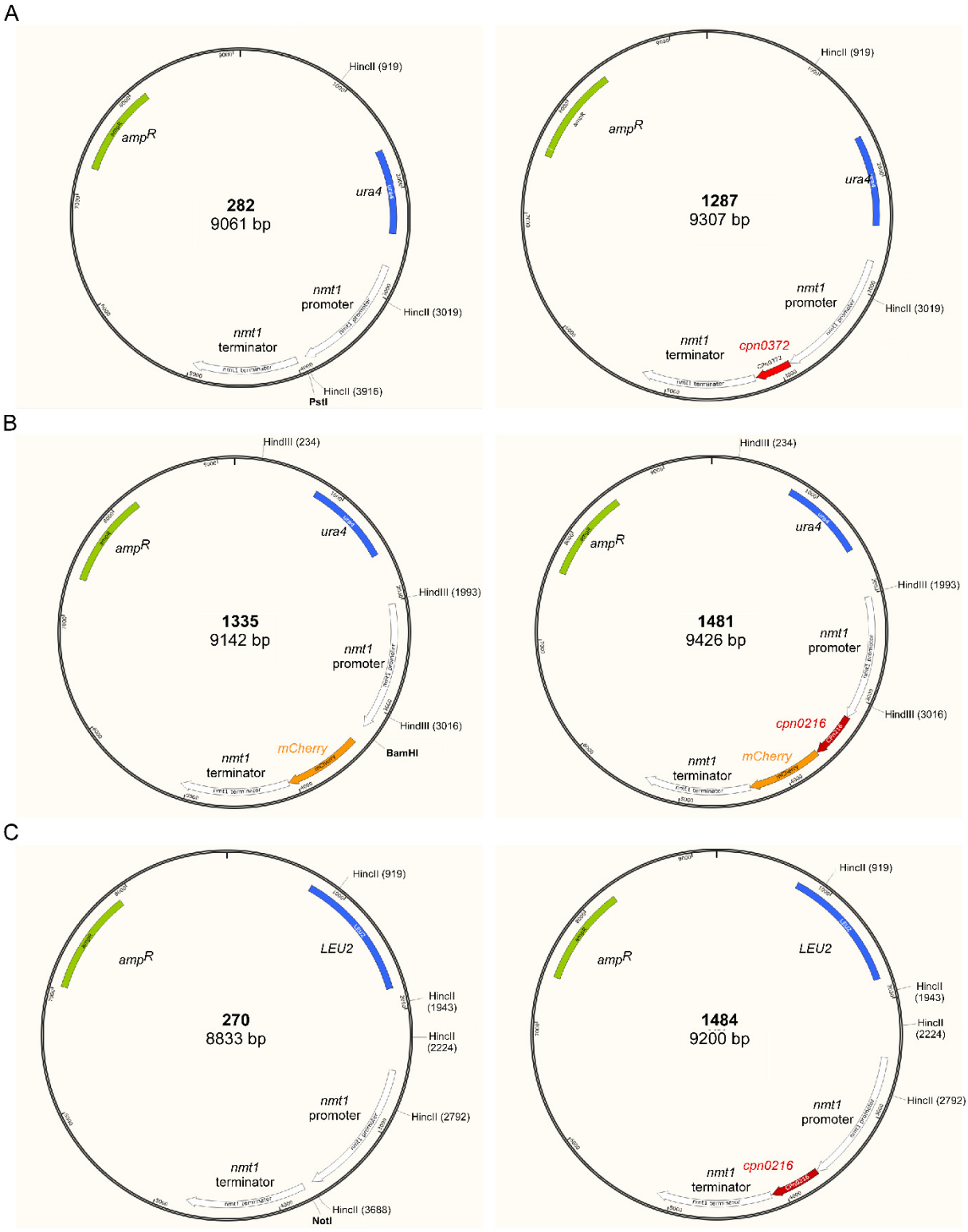

Supplementary Figure 1: Illustrative plasmid maps for chlamydial gene expression in *S. pombe*. **A-C** For gene expression in *S. pombe*, expression vectors p282 (pJR2-3XU), p1335 (pJR2-3XU), and p270 (pJR2-3XL) serve as backbones. Vectors were linearized with (**A**) PstI, (**B**) BamHI, or (**C**) NotI. Gene expression of the control vector (left site without insert) and chlamydial gene (right site with insert, red area) was controlled by the

thiamine-repressive *nmt1*$^{+}$-promoter (white area). The bacterial marker *amp*^{R} (green area) and yeast marker *ura4*$^{+}$ or *LEU2* (blue area) were used for selection. For localization analysis of chlamydial proteins in yeast, genes were C-terminally fused to the *mCherry* fluorescent tag (orange area). Restriction sites HincII or HindIII were used for quantitative digestion.

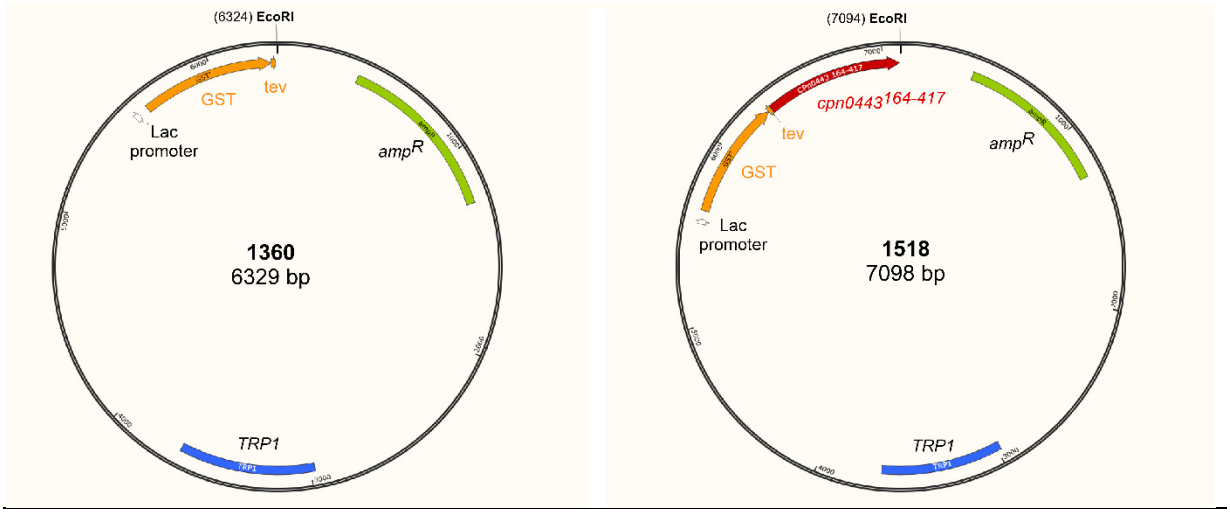

Supplementary Figure 2: Illustrative plasmid maps for the *in vitro* MT binding assay. For the MT binding assay, the expression vector p1360 (*gst-tev*) serves as a backbone and was linearized with EcoRI. Gene expression of the control vector (left site without insert) and the chlamydial gene (right site with insert, red area) was controlled by the *Lac* promoter (white area). The bacterial marker *amp*^{R} (green area) and yeast marker *TRP1* (blue area) were used for selection. For the MT binding analysis, CPn0443$^{164\text{-}417}$ was C-terminally fused to the *gst-tev* tag (orange area). The restriction site EcoRI was used for quantitative digestion.

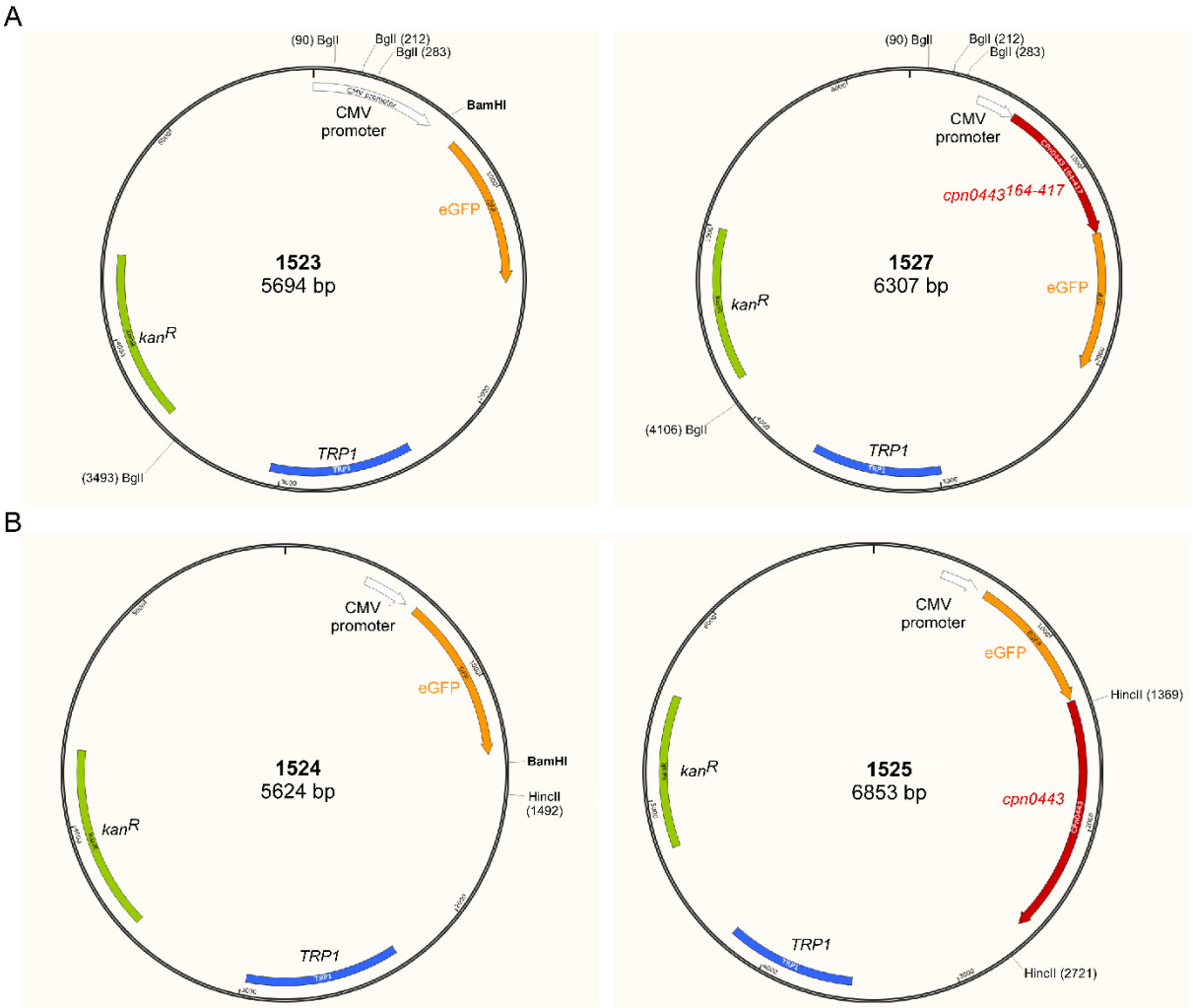

Supplementary Figure 3: Illustrative plasmid maps for chlamydial gene expression in mammalian cells. **A-B** For gene expression in transfected human cells, expression vectors p1523 (pKM55) and p1524 (pAE67) serve as backbones. Vectors were linearized with BamHI. Gene expression of the control vector (left site without insert) and chlamydial gene (right site with insert, red area) was controlled by the *CMV* promoter (white area). The bacterial marker *kan*^{R} (green area) and yeast marker *TRP1* (blue area) were used for selection. For localization analysis of chlamydial proteins in human cells, genes were C-terminally fused to the *GFP*-fluorescent tag (orange area). **A**: Genes were C-terminally fused with the GFP-tag; **B**: Genes were N-terminally fused with the GFP-tag. For quantitative digestion, the restriction sites BglI or HindIII were used.

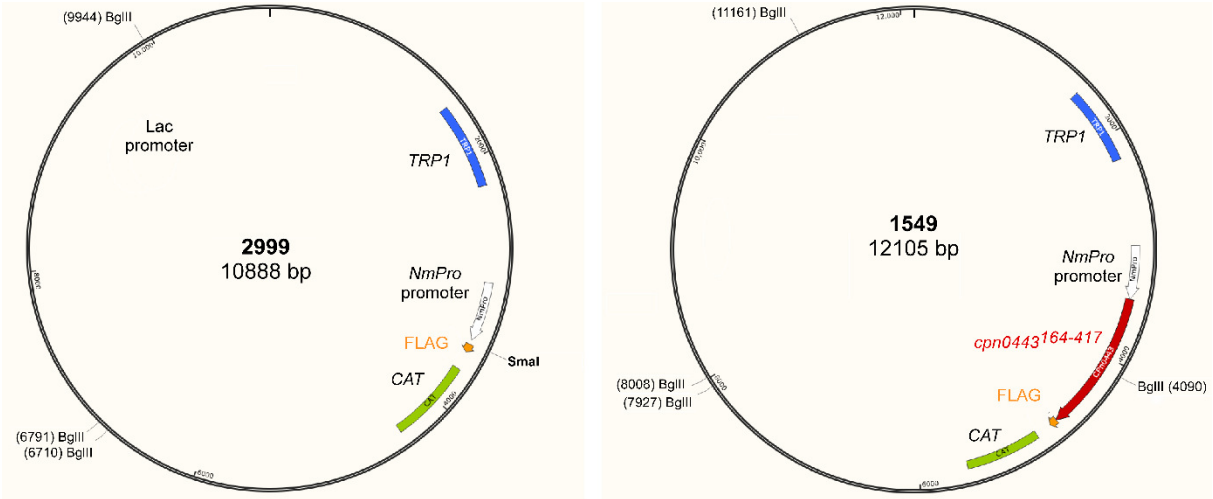

Supplementary Figure 4: Illustrative plasmid maps for the generation of CPn0443-flag expressing *C. pneumoniae*.

For gene expression in *C. pneumoniae*, the expression vector p2999 (pKM290) serves as a backbone and was linearized with SmaI. Gene expression of the control vector (left site without insert) and chlamydial gene (right site with insert, red area) was controlled by the *NmPro* promoter (white area). The bacterial marker *CAT* (green area) and yeast marker *TRP1* (blue area) were used for selection. For localization analysis, CPn0443 was C-terminally fused to the *flag*-tag (orange area). The restriction sites BglII were used for quantitative digestion.

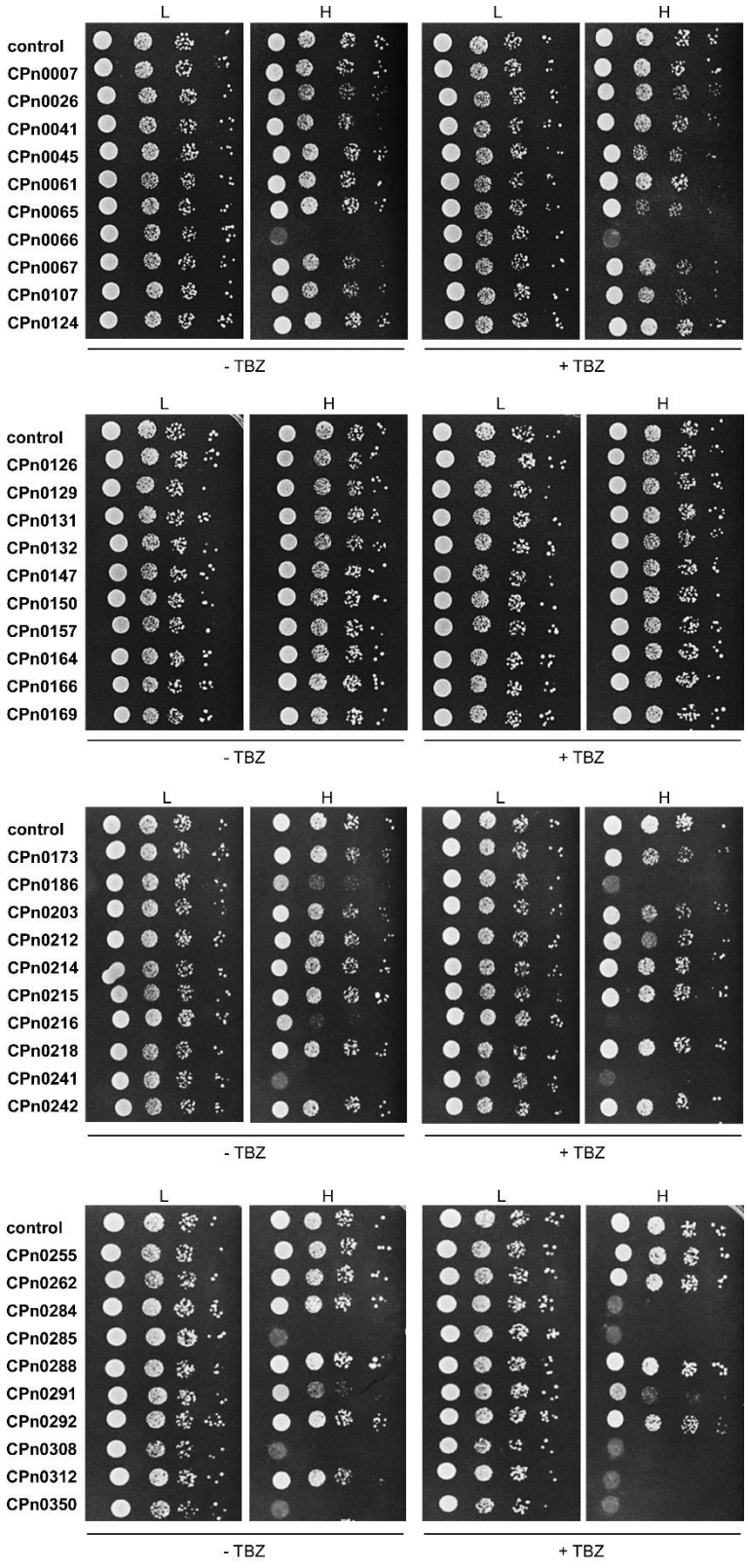
L
H
L
H
control
CPn0007
CPn0026
CPn0041
CPn0045
CPn0061
CPn0065
CPn0066
CPn0067
CPn0107
CPn0124
- TBZ
+ TBZ
L
H
L
H
control
CPn0126
CPn0129
CPn0131
CPn0132
CPn0147
CPn0150
CPn0157
CPn0164
CPn0166
CPn0169
- TBZ
+ TBZ
L
H
L
H
control
CPn0173
CPn0186
CPn0203
CPn0212
CPn0214
CPn0215
CPn0216
CPn0218
CPn0241
CPn0242
- TBZ
+ TBZ
L
H
L
H
control
CPn0255
CPn0262
CPn0284
CPn0285
CPn0288
CPn0291
CPn0292
CPn0308
CPn0312
CPn0350
- TBZ
+ TBZ

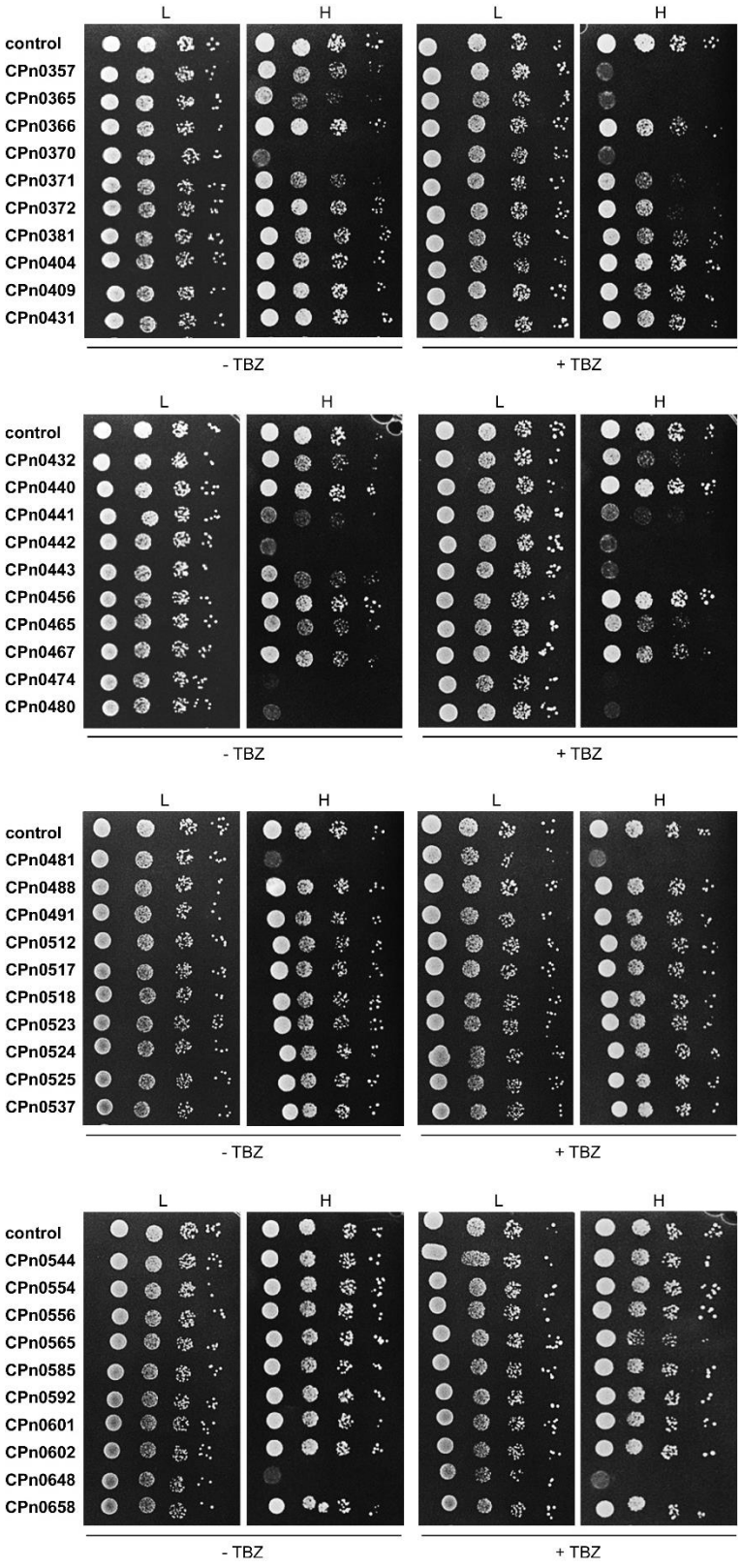
L
H
L
H
control
CPn0357
CPn0365
CPn0366
CPn0370
CPn0371
CPn0372
CPn0381
CPn0404
CPn0409
CPn0431
- TBZ
+ TBZ
control
CPn0432
CPn0440
CPn0441
CPn0442
CPn0443
CPn0456
CPn0465
CPn0467
CPn0474
CPn0480
control
CPn0481
CPn0488
CPn0491
CPn0512
CPn0517
CPn0518
CPn0523
CPn0524
CPn0525
CPn0537
control
CPn0544
CPn0554
CPn0556
CPn0565
CPn0585
CPn0592
CPn0601
CPn0602
CPn0648
CPn0658

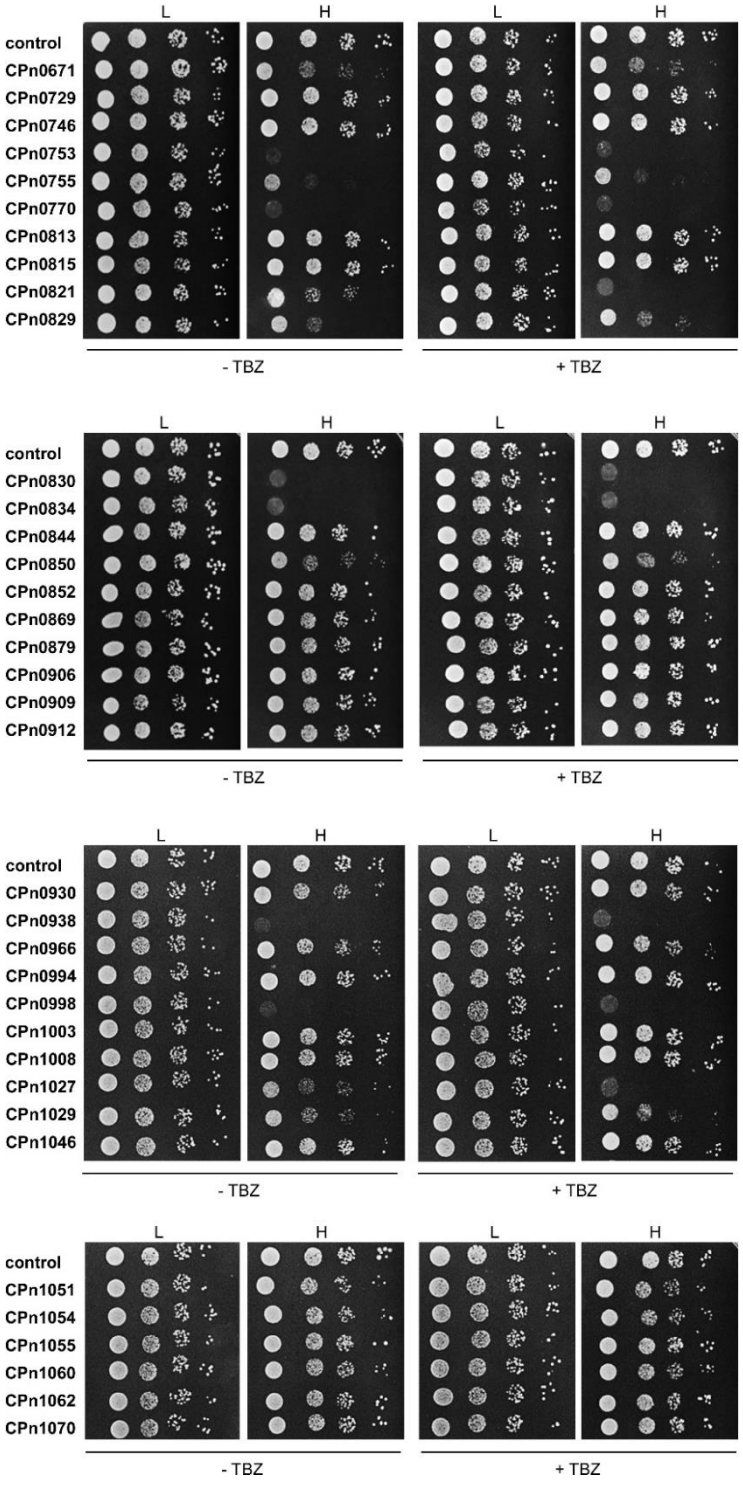

Supplementary Figure 5: Yeast growth phenotypes caused by expression of the 116 *C. pneumoniae* proteins. Serial dilution patch tests (10^4-10^1 cells) of a wild-type (WT) yeast strain expressing either a control plasmid (pJR2-3XU *ura4*$^+$) or one of 116 different plasmids each with one of the selected and indicated *C. pneumoniae* genes. *S. pombe* transformants were grown for 6 days at 25 °C on plasmid-selective media without (-TBZ) or with 7 µg/mL TBZ (+TBZ), L and H: low or high expression of relevant *C. pneumoniae* genes. Two yeast transformants were patched.

Cpn protein	Reference for selection	Case	*Cpn* protein	Reference for selection	Case
CPn0007	i, ii	1a	**CPn0285**	i, ii	2
CPn0026	i, ii	1b	**CPn0288**	i, ii	1a
CPn0041	i, ii	1b	**CPn0291**	i, ii	1b
CPn0045	i, ii	3a	**CPn0292**	i, ii	1a
CPn0061	v	1a	**CPn0308**	i, ii	2
CPn0065	i, ii	3a	**CPn0312**	i, ii	3b
CPn0066	i	2	**CPn0350**	iii	2
CPn0067	i, ii	1b	**CPn0357**	i, ii	3b
CPn0107	v	1b	**CPn0365**	i, ii	4
CPn0124	i, ii	1a	**CPn0366**	i, ii	1a
CPn0126	i, ii	1a	**CPn0370**	i, ii	2
CPn0129	ii	2	**CPn0371**	i, ii	1b
CPn0131	i, ii	1a	**CPn0372**	i, ii	3a
CPn0132	i, ii	1a	**CPn0381**	i	1a
CPn0147	i, ii	1a	**CPn0404**	i	1a
CPn0150	i, ii	1a	**CPn0409**	v	1a
CPn0157	i	1a	**CPn0431**	i, ii	1a
CPn0164	i, ii	1a	**CPn0432**	i, ii	1b
CPn0166	i, ii	1a	**CPn0440**	i, ii	1a
CPn0169	i, ii	1a	**CPn0441**	iii	1b
CPn0173	i, ii	1b	**CPn0442**	i, ii	2
CPn0186	i, ii	4	**CPn0443**	i, ii	4
CPn0203	i	1b	**CPn0456**	iv	1a
CPn0212	i, ii	1b	**CPn0465**	v	1b
CPn0214	i, ii	1a	**CPn0467**	iv	1b
CPn0215	i, ii	1a	**CPn0474**	i, ii	2
CPn0216	i, ii	4	**CPn0480**	i, ii	2
CPn0218	ii	1a	**CPn0481**	i	2
CPn0241	ii	2	**CPn0488**	iii	1a
CPn0242	i, ii	1a	**CPn0491**	iii	1a
CPn0255	iii	1a	**CPn0512**	v	1a
CPn0262	v	1a	**CPn0517**	i, ii	1a
CPn0284	i, ii	3b	**CPn0518**	v	1a

Cpn protein	Reference for selection	Case	*Cpn* protein	Reference for selection	Case
CPn0523	i, ii	1a	**CPn0834**	i	2
CPn0524	i, ii	1a	**CPn0844**	v	1a
CPn0525	iii	1a	**CPn0850**	iv	1b
CPn0537	i	1a	**CPn0852**	v	1a
CPn0544	iii	1a	**CPn0869**	ii	1a
CPn0554	i, ii	1a	**CPn0879**	v	1a
CPn0556	i, ii	1a	**CPn0906**	v	1a
CPn0565	i, ii	3a	**CPn0909**	v	1a
CPn0585	i, ii	1a	**CPn0912**	v	1a
CPn0592	iii	1a	**CPn0930**	i, ii	1a
CPn0601	i, ii	1a	**CPn0938**	i, ii	2
CPn0602	i, ii	1a	**CPn0966**	iv	1a
CPn0648	iii	2	**CPn0994**	i	1a
CPn0658	v	1a	**CPn0998**	v	2
CPn0671	v	1b	**CPn1003**	ii	1a
CPn0729	iii	1a	**CPn1008**	i, ii	1a
CPn0746	v	1a	**CPn1027**	i	4
CPn0753	i, ii	2	**CPn1029**	i, ii	1b
CPn0755	i, ii	1b	**CPn1046**	iv	1a
CPn0770	i, ii	2	**CPn1051**	i, ii	1a
CPn0813	iv	1a	**CPn1054**	i, ii	1a
CPn0815	iv	1a	**CPn1055**	i, ii	1a
CPn0821	iii	4	**CPn1060**	iv	1a
CPn0829	i	1b	**CPn1062**	iv	1a
CPn0830	i	2	**CPn1070**	iv	1a

Supplementary Table 2: Growth phenotypes of *S. pombe* transformants expressing one of the 116 *C. pneumoniae* proteins.

The 116 *C. pneumoniae* proteins chosen for analysis were selected as indicated: Inc proteins[i,ii] (Dehoux et al., 2011; Lutter et al., 2012), proteins affecting *S. cerevisiae* yeast growth[iii,iv] (Sisko et al., 2006; Herbst, 2011) or randomly chosen[v] (Mäurer et al., 2007). Growth phenotypes of transformants expressing one of the 116 *C. pneumoniae* genes.

Ctr protein	Predicted function	Localization	Host cell targets
CT288	Inc[Lutter et al., 2012; Dehoux et al., 2011]	IM[Bannantine et al., 2000]	CCDC146[Almeida et al., 2018]
CT119/ IncA[Hackstadt et al., 1999]	Inc[Lutter et al., 2012; Dehoux et al., 2011]	IM[Hackstadt et al., 1999]	SNARE[Delevoye et al., 2004; Delevoye et al., 2008]
CT101/ MrcAb[Nguyen et al., 2018]	Inc[Lutter et al., 2012; Dehoux et al., 2011]	IM[Nguyen et al., 2018]	ITPR3[Nguyen et al., 2018]
CT005/ IncV[Stanhope et al., 2017]	Inc[Lutter et al., 2012; Dehoux et al., 2011]	IM[Stanhope et al., 2017]	VAPA, VAPB[Stanhope et al., 2017]
CT449	Inc[Lutter et al., 2012; Dehoux et al., 2011]	na	na
CT566	unknown	na	na

Supplementary Table 3: Characteristics of the *C. trachomatis* homologs.

Tabular presentation of the six *C. trachomatis* (*Ctr*) proteins homolog to *C. pneumoniae* which were analyzed in the screen. Information about predicted functions, localizations, and host cell targets are listed for each protein. Inc: inclusion membrane protein; IncA: inclusion membrane protein A; MrcA: myosin regulatory complex subunit A; IncV: inclusion membrane protein V; IM: inclusion membrane; CCDC146: coiled-coil domain-containing protein 146; SNARE: soluble N-ethylmaleimide-sensitive factor-attachment protein receptors; ITPR3: inositol 1,4,5-trisphosphate receptor type 3; VAPA: vesicle-associated membrane protein-associated protein A; VAPB: vesicle-associated membrane protein-associated protein B; na: not analyzed.

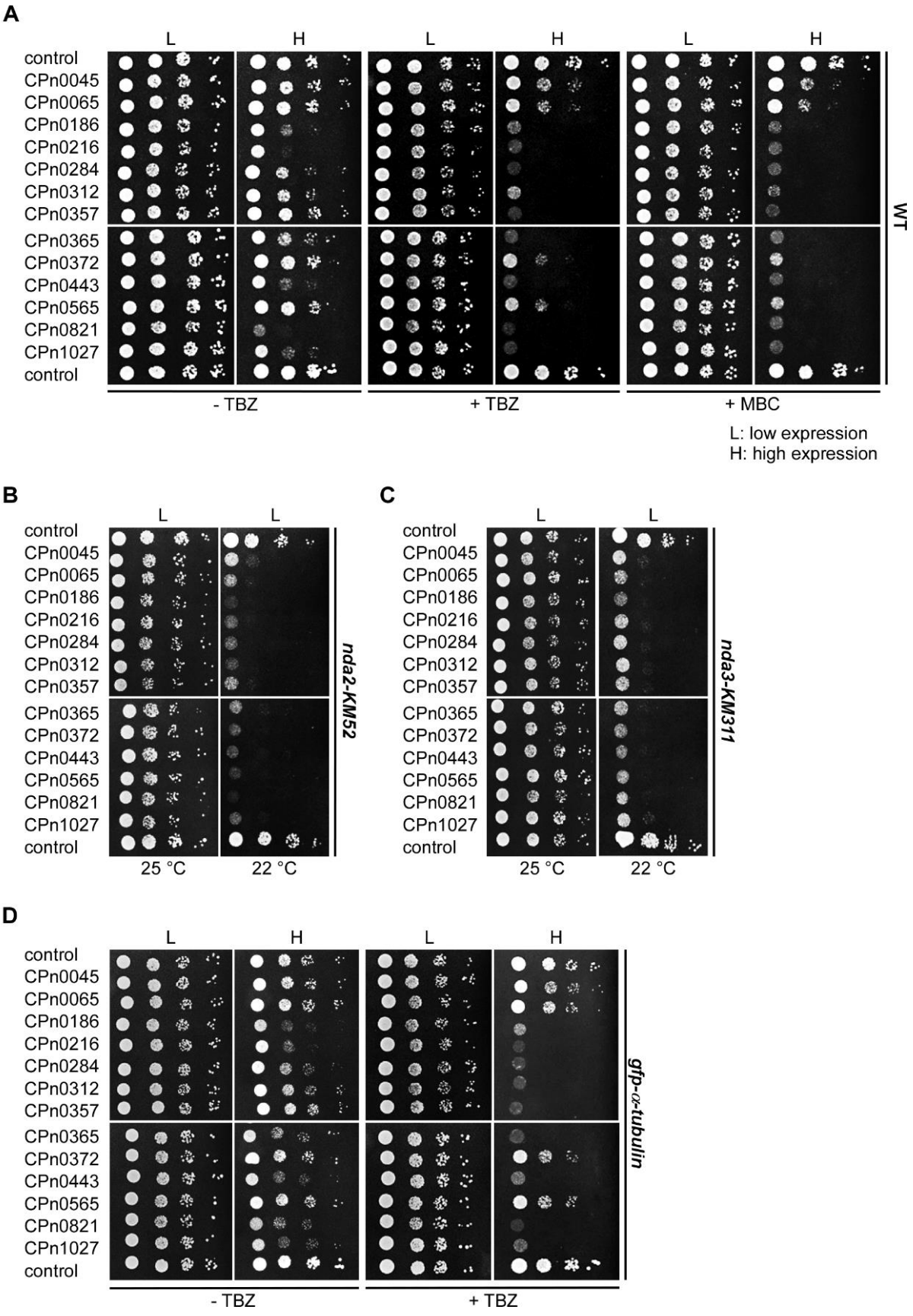
A
L
H
control
CPn0045
CPn0065
CPn0186
CPn0216
CPn0284
CPn0312
CPn0357
CPn0365
CPn0372
CPn0443
CPn0565
CPn0821
CPn1027
control
WT
- TBZ
+ TBZ
+ MBC
L: low expression
H: high expression
B
nda2-KM52
25 °C
22 °C
C
nda3-KM311
D
gfp-α-tubulin

Supplementary Figure 6: Yeast growth phenotypes caused by expression of the 13 *C. pneumoniae* proteins. **A** Serial dilution patch tests (10^4-10^1 cells) of wild-type (WT) yeast strain expressing either a control plasmid (pJR2-3XU *ura4*$^+$) or one of 13 different plasmids each with one of the selected and indicated *C. pneumoniae* genes. *S. pombe* transformants were grown for 6 days at 25 °C on plasmid-selective media without (-TBZ and -MBC) or with 7 µg/mL TBZ or 2.5 µg/ml MBC, L and H: low or high expression of relevant *C. pneumoniae* genes. **B**-**C** Serial dilution patch tests of cold-sensitive *nda2-KM52* or *nda3-KM311* mutants expressing control plasmid (pJR2-3XU *ura4*$^+$) or the indicated *C. pneumoniae* genes. Cells were incubated under plasmid selective conditions at 25 °C or 22 °C for 7 days, L: low expression. **D** Serial dilution patch tests of *gfp-α-tubulin* (*nmt81::gfp-atb2*$^+$) transformants. Cells were incubated under plasmid selective conditions at 25 °C for 6 days without or with 6 µg/mL TBZ, L and H: low or high expression. **A-D** Two yeast transformants were patched.

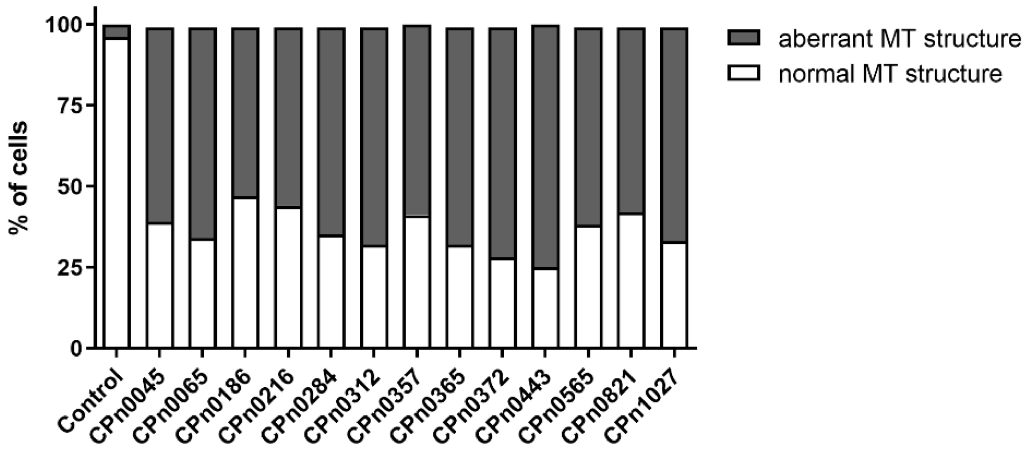

Supplementary Figure 7: Frequency of cells with aberrant interphase MT structures. Quantification of the cell frequency with aberrant interphase MT structures compared to unaffected MT structures which are similar to the control shown in **Figure 12A**. From each of the two individual experiments, 50 cells were analyzed.

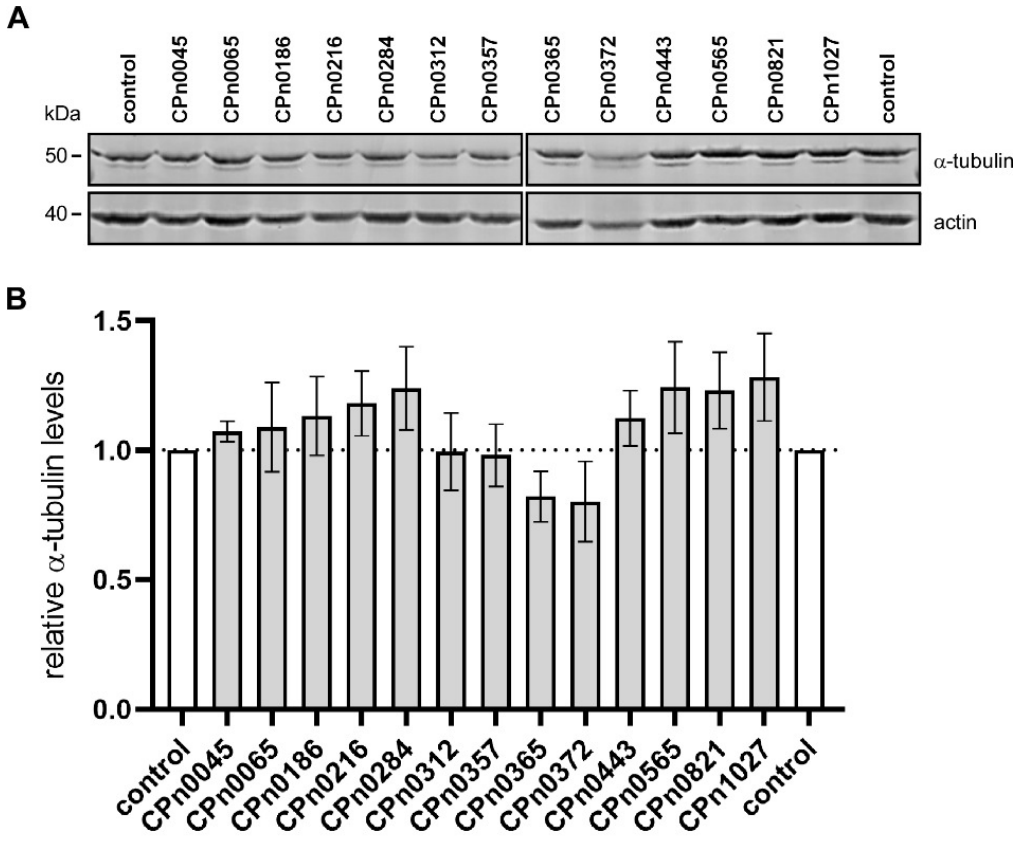

Supplementary Figure 8: The 13 *C. pneumoniae* proteins do not affect α-tubulin levels. **A** Western blot analysis of whole-cell lysates of an *nmt81::gfp-atb2*$^{+}$ (endogenous *gfp-α-tubulin*) yeast strain containing control plasmid (pJR2-3XU *ura4*$^{+}$) or expressing one of the indicated chlamydial genes. Top: detection of α-tubulin (52 kDa) with an anti-α-tubulin antibody. Bottom: detection of actin (42 kDa) with anti-actin antibody as an internal control to normalize the expression of the *C. pneumoniae* gene **B** Quantification of relative α-tubulin levels detected in Western blot analysis. The band intensity of α-tubulin were normalized against the actin bands. The measurement from control transformants were set to 1. n= 2 independent experiments; error bars represent ± SEM.

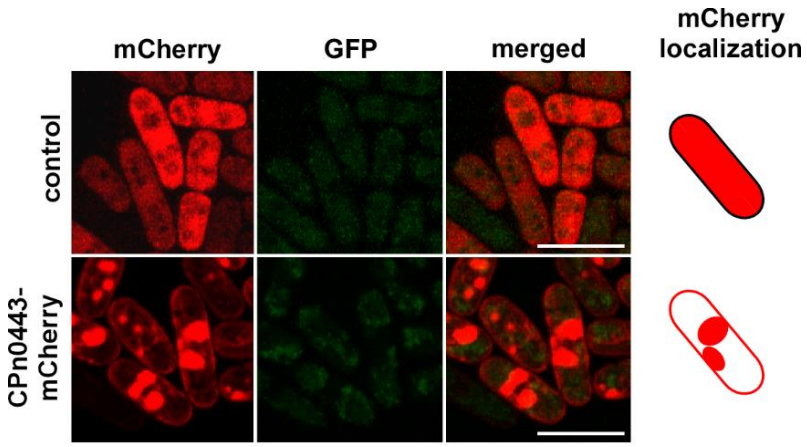

Supplementary Figure 9: Localization of CPn0443-mCherry in WT *S. pombe*.

Photomicrographs of wild-type *S. pombe* cells were transformed with a control plasmid (pJR2-3XL *LEU2*) or plasmid carrying the *cpn0443-mCherry* (red) and highly expressed from the *nmt1*$^{+}$ promoter under plasmid selective conditions at 25 °C. Scale bars, 10 µm. Two yeast transformants were analyzed.

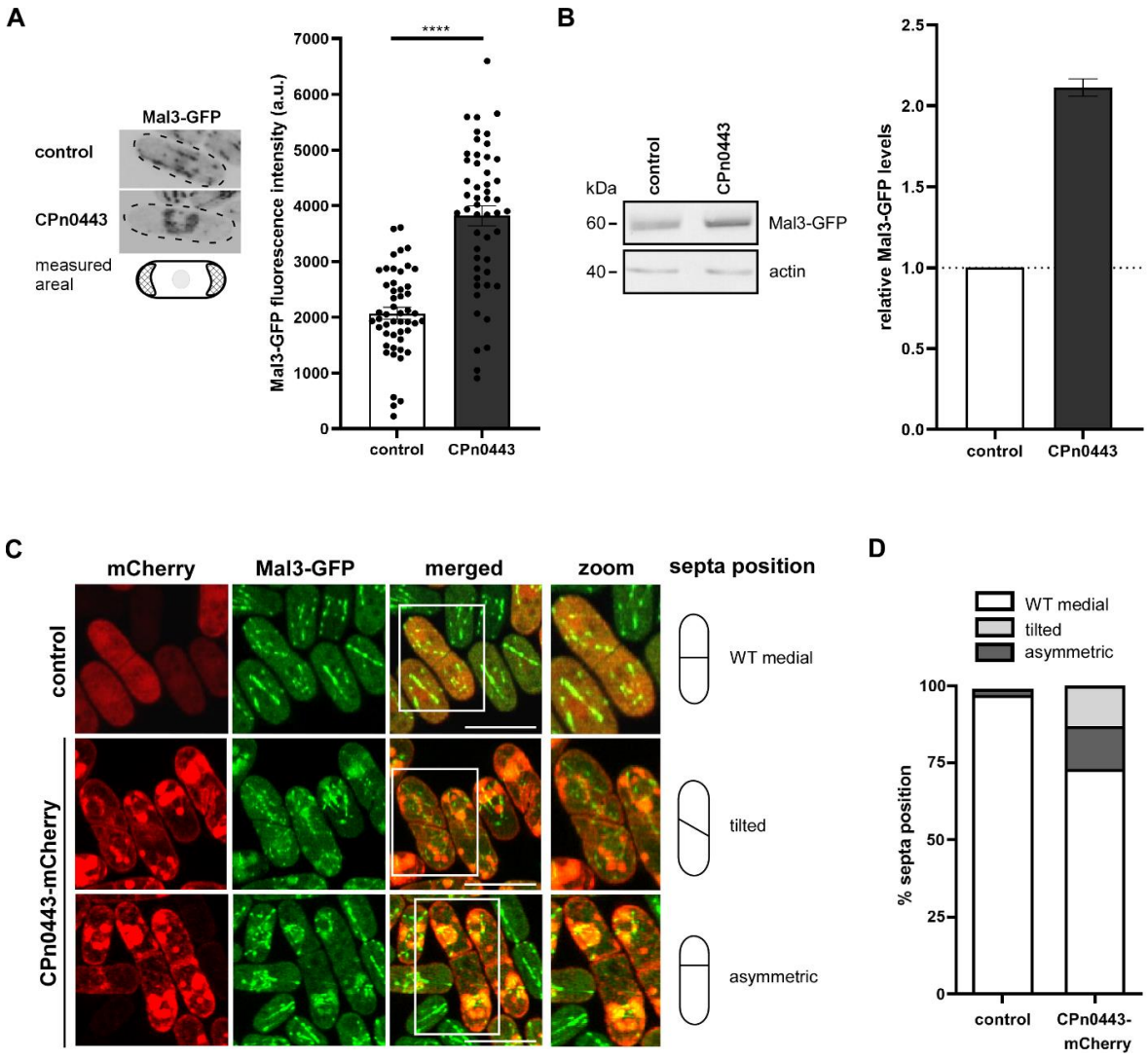

Supplementary Figure 10: Expression of *cpn0443-mCherry* affects Mal3-GFP levels and caused abnormal septa positioning in the *mal3*$^{+}$*-gfp* strain.

A *S. pombe* cells expressing the endogenous *mal3*$^{+}$*-gfp* (*mal3-pk-gfp,* green) were transformed with a control plasmid (pJR2-3XL *LEU2*) or a plasmid carrying the *cpn0443* and highly expressed from the *nmt1*$^{+}$ promoter under plasmid selective conditions at 25 °C. Quantification of Mal3-GFP fluorescence signals from lectin labeled *cpn0443* expressing cells or lectin-untreated control cells. Schematic cells show the measured area of Mal3-GFP fluorescence signals normalized against the background. Two-tailed student's t-test was used to determine statistical significance p <0.0001 (****). 50 cells from one experiment were analyzed. Error bars represent ± SEM. a.u. arbitrary fluorescence unit. **B** Western blot analysis of whole-cell lysates of the samples shown in **A**. Top: detection of Mal3-GFP (63 kDa) visualized with an anti-GFP antibody. Bottom: detection of the actin (42 kDa) with an anti-actin antibody. The band intensity of Mal3-GFP was normalized against the actin bands. The measurement from the control transformant was set to 1. Error bars represent ± SEM. **C** Photomicrographs and schematic illustration of abnormal septa positioning caused by *cpn0443-mCherry* (red) expression in the

mal3^{+}*-gfp* (green) expressing strain. White boxes show enlargements (zoom). Scale bars, 10 µm. **D** Quantification of wild-type (WT) medial, tilted, or asymmetric septa positioning caused by *cpn0443-mCherry* expression. WT medial septa positioning: located at the midpoint of the long axis of the cell, aligned at a 90° angle to the long side of the cell that separates the cell into two equal parts. Tilted septa positioning: located at the midpoint of the long axis of the cell. Asymmetric septa positioning: strongly shifted from the midpoint of the long axis of the cell that causes cell division into two unequal parts (ratio >60:<40). From each of the two individual experiments, 50 cells were analyzed.

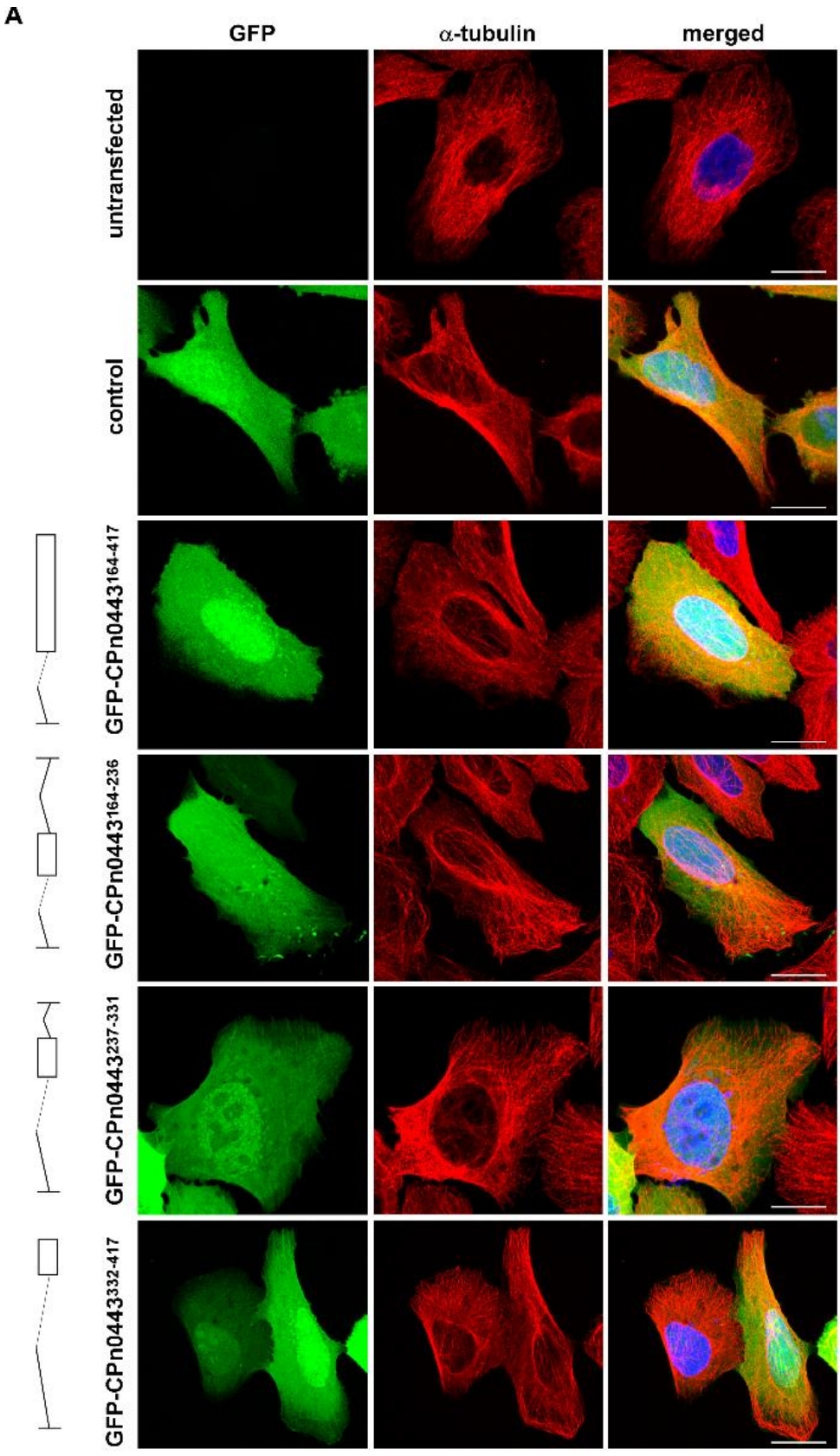
A
GFP
α-tubulin
merged
untransfected
control
GFP-CPn0443164-417
GFP-CPn0443164-236
GFP-CPn0443237-331
GFP-CPn0443332-417

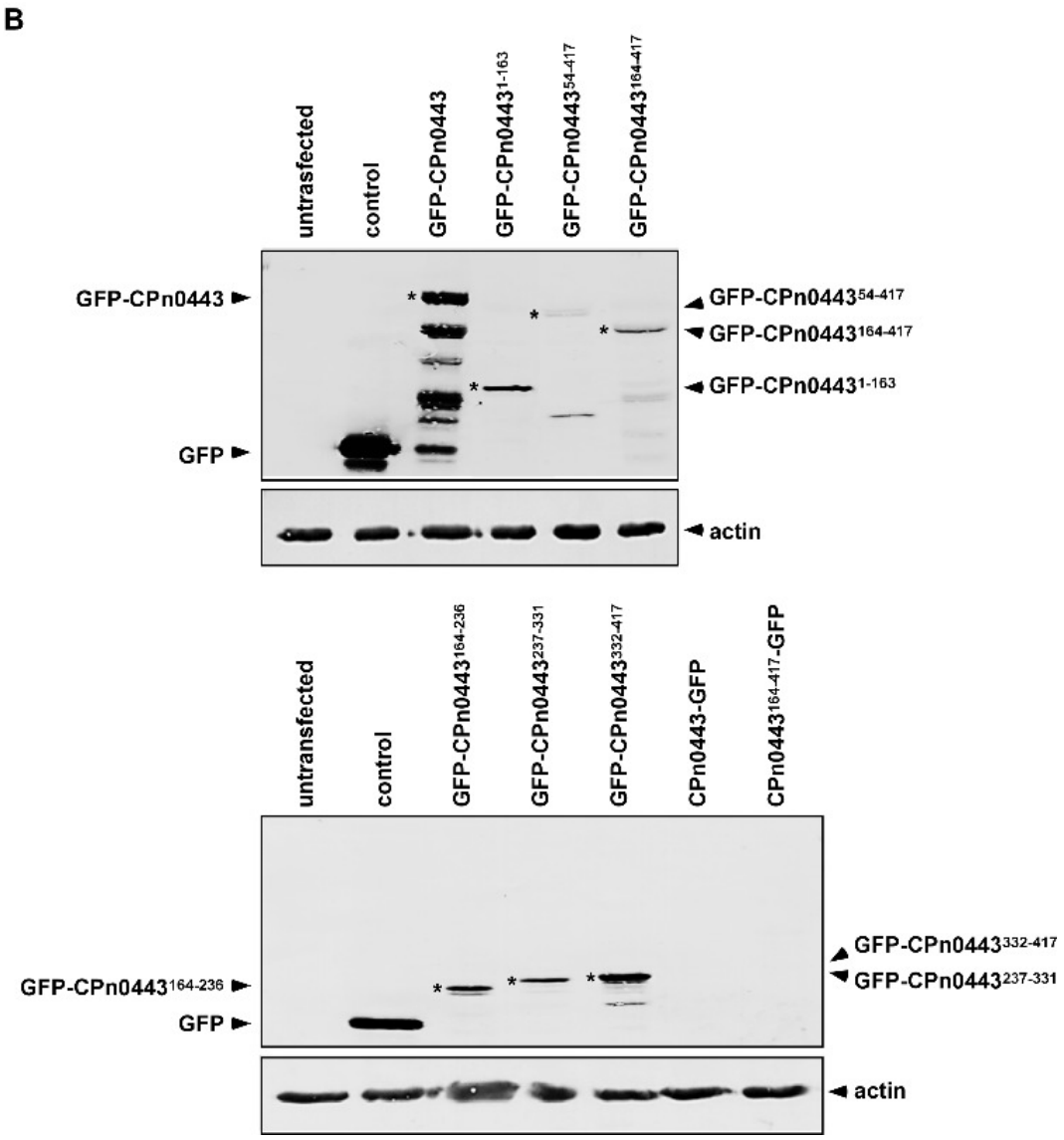

Supplementary Figure 11: Localization of transfected CPn0443 variants in human U2OS cells. **A** Confocal fluorescence images of human U2OS cells were transfected for 18 hours with plasmids expressing GFP (control) or different GFP-CPn0443 variants. MTs were visualized with anti-α-tubulin antibody (red) and DNA with DAPI (blue). Scale bars, 10 µm. Untransfected cells were used as a negative control. **B** Western blot analysis of whole-cell lysates isolated from transfected cells shown in **A**. Top blots: detection of GFP-fused proteins were visualized with anti-GFP antibody and marked with asterisks. Protein bands are shown for GFP (27 kDa), GFP-CPn0443 (73 kDa), GFP-CPn0443$^{1-63}$ (44 kDa), GFP-CPn0443$^{54-417}$ (67 kDa), and GFP-CPn0443$^{164-417}$ (56 kDa); GFP-CPn0443$^{164-236}$ (35 kDa), GFP-CPn0443$^{237-331}$ (38 kDa), GFP-CPn0443$^{332-417}$ (37 kDa), CPn0443-GFP (73 kDa), and CPn0443$^{164-417}$-GFP (56 kDa). Bottom blots: detection of the actin (42 kDa) visualized with anti-actin antibody as an internal control. **A-B** Two individual experiments were analyzed.

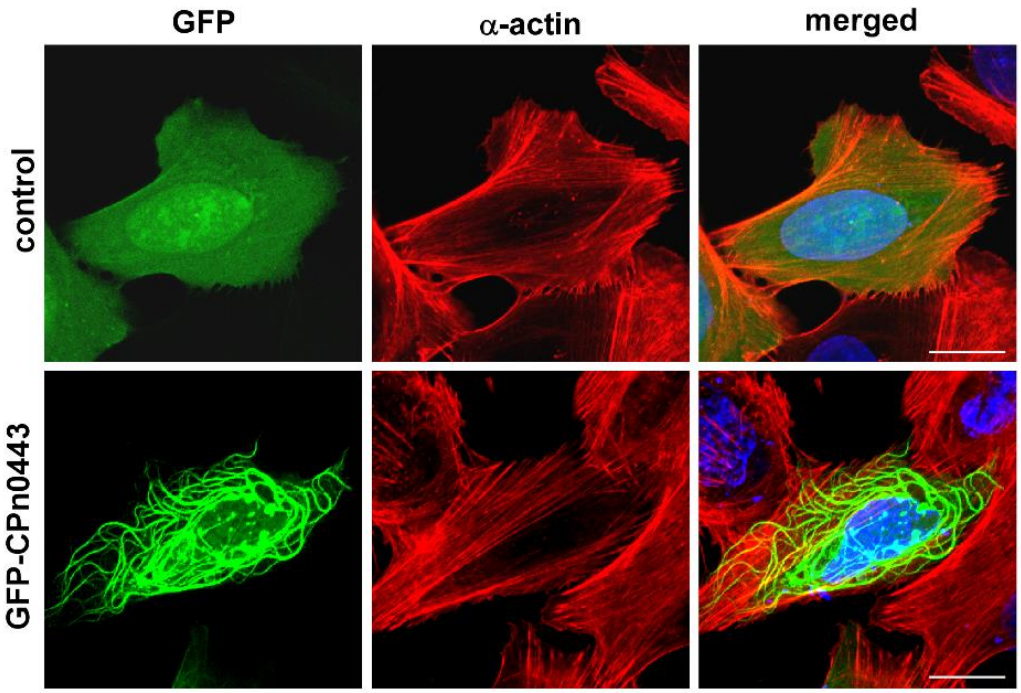

Supplementary Figure 12: GFP-CPn0443 does not co-localize with actin or modulate the actin structure. Confocal fluorescence images of human U2OS cells were transfected for 18 hours with plasmids expressing GFP (control) or GFP-CPn0443. Actin was visualized with anti-α-actin antibody (red) and DNA with DAPI (blue). Scale bars, 10 µm. Two individual experiments were analyzed.

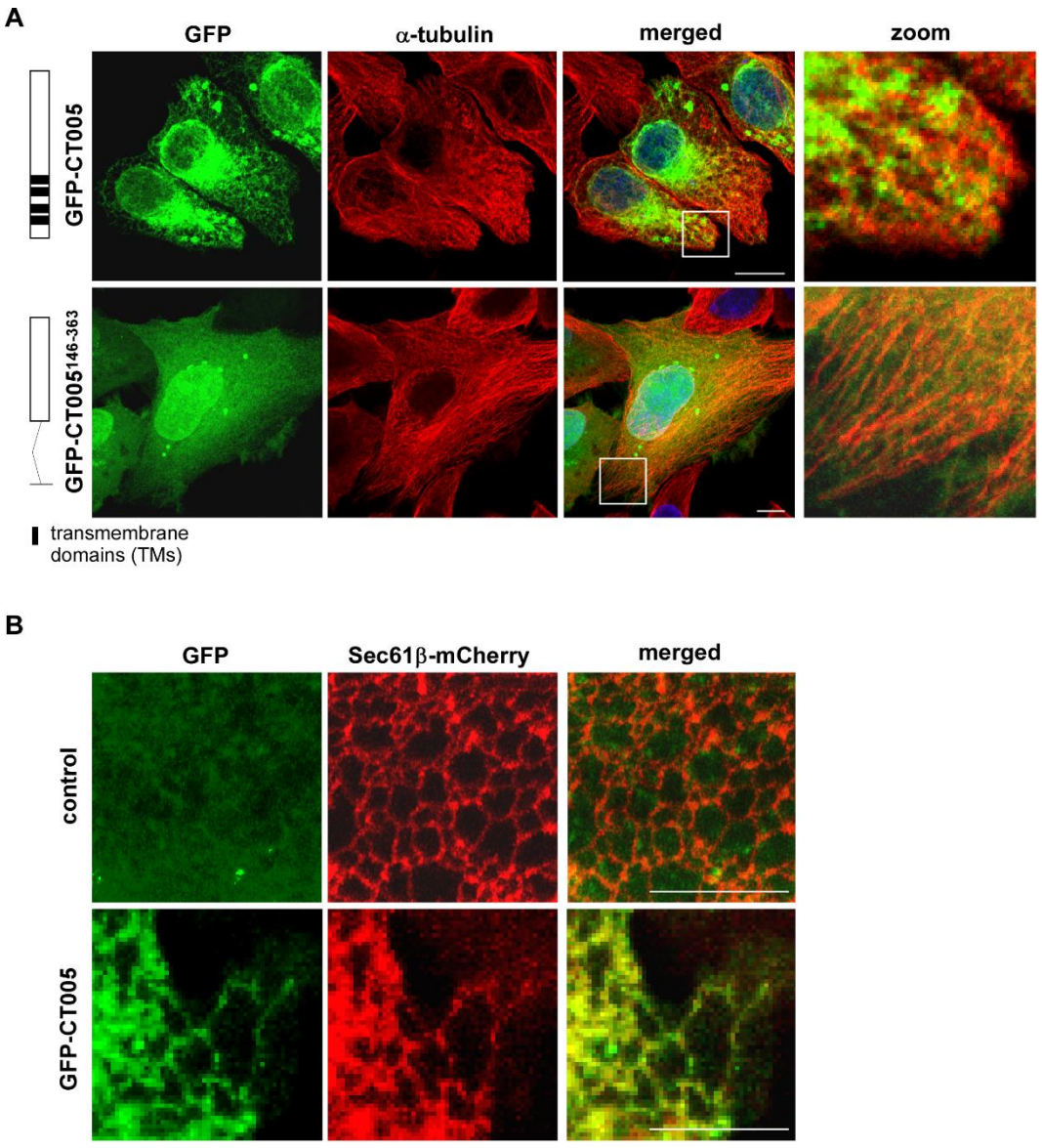

Supplementary Figure 13: GFP-CT005 lokalizes to an ER-like strukture.

Confocal fluorescence images of human U2OS cells were transfected for 18 hours with plasmids expressing GFP-CT005 (green), or GFP-CT005$^{146-363}$. Two individual experiments were analyzed. **A** MTs were visualized with anti-α-tubulin antibody (red) and DNA with DAPI (blue). **B** In addition, cells were co-transfected with a plasmid expressing Sec61β-mCherry (red, ER marker). One experiment was analyzed. Scale bars, 10 µm.

Acknowledgments

At this point, I would like to take this opportunity to express my sincere thanks to everyone who contributed to the completion of this PhD thesis and to everyone who was affected by it. Those who know me, know that I am not a person who sings long hymns of praise, so I will be brief.

First of all, I am indebted to my supervisor Prof. Dr. Ursula Fleig for allowing me to conduct my PhD project in her Institute of Eukaryotic Microbiology. I am grateful that you gave me the opportunity to be part of the MOI III family.
In addition, I am also indebted to Prof. Dr. Johannes Hegemann, head of the Institute Functional Genomics of Microorganisms and supported me in practical work with chlamydial material and fresh ideas for my project.
I express my thanks to Prof. Dr. Klaus Pfeffer, head of the Institute of Medical Microbiology and Hospital Hygiene, who agreed to be my third supervisor.

Personally, special thanks to my fellow sufferer Quynh (HBQ) and Rosi alias Anna-Lene for your Excellent support, for quietly accepting my dynamic moods, and also for celebrating the most Notable successes with me.
I already miss the after-work beer and the extraordinary office decorations.... which often Surprised me;)

Furthermore, my special thanks go to all members of the Institute for Functional Genomics of Microorganisms and Eukaryotic Microbiology for their helpful advice and practical training. Through your efforts, I have grown personally and professionally.

Another thank you goes to my former boss, Prof. Dr. Hansen. Without her permission to study parallel to my work as a BTA, I would not be in the position I am now: at the end of my PhD. I do not take this opportunity for granted and therefore I would like to express my appreciation at this point. So, thank you very much for your support Wiebke.

Last, but not least to my family.

Liebe Familie, ihr kennt mich, ich bin kein Mensch der lange Lobgesänge, daher halt ich es kurz.

Ich möchte mich bei meine Eltern für deren immer offenes Ohr, all die Unterstützung und Durchfütterung mit leckerer Speisen an stressreichen Wochentagen/-enden bedanken. Dadurch wurden meine Nahrungsbeschaffungsmaßnahmen erheblich erleichtert, da die beiden für einen vollen Magen und brechend vollen Taschen für den Heimweg gesorgt haben. Zugleich möchte ich mich auch für meine emotional Fluch-Eskapaden entschuldigen, es war mit Sicherheit nicht immer amüsant mit mir… aber wie Dad immer so gerne sagt: man erntet was man säht. Also eine erfreuliche Ernte ihr Lieben ;)

Einen besonderen Dank gilt meinem Dad, weil er mir und meinen Kollegen im Labor die Erstellung der Mikroskopie Slides enorm erleichtert hat durch die patentwürdigen Objektträgerrahmen. Ein echter Segen! Auf diesem Weg sage ich Danke im Namen des ganzen Labors!

Auch meinem Bruder möchte ich danken, dass er mich das ein oder andere Mal abgeholt und nach Hause gefahren hat. Die Erwähnung der angefallenen Gegenleistungen spare ich mir an dieser Stelle…

Schlussendlich bin ich auch meinem Opi sehr dankbar, da er mich während meines Studiums nicht nur mit Zucker, sondern auch finanziell unterstützet hat. Demnach vielen Dank Opi!

Statutory Declaration

I declare under oath that I have compiled my dissertation independently and without any undue assistance by third parties under consideration of the 'Principles for the Safeguarding of Good Scientific Practice at Heinrich Heine University Düsseldorf'.

I declare that I have not used sources or means without declaration in the text. All the passages taken from other works in the wording or in the meaning have been clearly indicated with sources. This thesis has not been used in the same or similar version to achieve an academic grading or is being published elsewhere.

Düsseldorf, May 4th, 2023

Carolin Wevers